JSCSEN 78(6)759–907(2013)

ISSN 1820-7421(Online)

Journal of the Serbian Chemical Society

Electronic Version

VOLUME 78

No 6

BELGRADE 2013

Available on line at

www.shd.org.rs/JSCS/

The full search of JSCS is available through

DOAJ DIRECTORY OF OPEN ACCESS JOURNALS

www.doaj.org

Journal of the Serbian Chemical Society
JSCS-info@shd.org.rs • www.shd.org.rs/JSCS

J. Serb. Chem. Soc. Vol. 78, No. 6 (2013)

CONTENTS

Published by the Serbian Chemical Society
Karnegijeva 4/III, 11000 Belgrade, Serbia
Printed by the Faculty of Technology and Metallurgy
Karnegijeva 4, P.O. Box 35-03, 11120 Belgrade, Serbia

Journal of the Serbian Chemical Society
JSCS-info@shd.org.rs • www.shd.org.rs/JSCS
J. Serb. Chem. Soc. 78 (6) 759–768 (2013)
JSCS–4455
UDC 547.21.024+547.313+547.53.024:
66.095.253.094.48:66.095.11
Original scientific paper

Synthesis of five- and six-membered 1,3,3-trimethyl-2--(trimethylsilyl)cycloalkenes: a novel preparation of alkyl/alkenyl/aryl 2,5,5-trimethyl-1-cyclopentenyl ketones

MANJUNATHA A. VENKATESHA and HARIPRASAD SURESH*

Department of Chemistry, Central College Campus, Palace Road, Bangalore University, Bangalore – 560001, India

(Received 1 May, revised 1 December 2012)

Abstract: 1,3,3-trimethyl-2-(trimethylsilyl)cyclopentene and 1,3,3-trimethyl-2--(trimethylsilyl)cyclohexene were prepared in good yields by the Wurtz–Fittig coupling reaction of the corresponding 2-iodo-1,3,3-trimethylcyclopentene and 2-chloro-1,3,3-trimethylcyclohexene with metallic sodium and chlorotrimethylsilane in anhydrous ether solvent. The Friedel–Crafts acylation reaction of 1,3,3-trimethyl-2-(trimethylsilyl)cyclopentene with six different acid chlorides and the novel preparation of six alkyl/alkenyl/aryl 2,5,5-trimethyl-1-cyclopentenyl ketones are reported.

Keywords: cyclic vinylsilanes; anionic synthons; Wurtz–Fittig reaction; Friedel–Crafts acylation; *β*-silyl effect.

INTRODUCTION

Cyclic vinylsilanes are an important class of compounds in synthetic organic chemistry.[1] The compounds are anionic synthons with the trimethylsilyl group behaving as a masking agent.[2] The silicon in these compounds is capable of directing a reaction in a highly regio- and stereo-specific manner. Several methods have been reported in the literature for the preparation of cyclic vinylsilanes.[3]

Our laboratory is primarily involved in the preparation of cyclic vinylsilanes by employing the Wurtz–Fittig-type coupling reaction of cyclic vinyl halides with sodium and chlorotrimethylsilane in a suitable anhydrous solvent. The method is simple, and employing this reaction, a number of simple and substituted cyclic vinylsilanes have been successfully prepared. Various novel reactions of the prepared simple and substituted cyclic vinylsilanes have also been reported.[4]

* Corresponding author. E-mail: hariprasad@bub.ernet.in
doi: 10.2298/JSC120501015A

In further studies and in attempts to prepare some important substituted cyclic vinylsilanes, the synthesis of 1,3,3-trimethyl-2-(trimethylsilyl)cyclopentene (**1**) and 1,3,3-trimethyl-2-(trimethylsilyl)cyclohexene (**2**) were chosen. Compounds **1** and **2** would serve as potential synthons to several terpenes, vitamin A and related compounds.[5] In particular, it may be noted that the 1,3,3-trimethylcycloalkanyl- group is a common functionality present in capnellane,[6a] taiwaniaquinoid,[6b] actinidiolide,[6c] hedychenone[6d] and labdane diterpene[6e] group of compounds. Paquette reported the preparation of **1** by the tosyl hydrazone route, and isolation using preparative vapour-phase chromatography (VPC).[7] To the best of our knowledge, compound **2** has not been reported, but its corresponding vinyl stannane has been synthesized.[8]

In this article, the successful preparation of **1** and **2** by the Wurtz–Fittig coupling reaction are reported. The Friedel–Crafts acylation of **1** with six different acid chlorides gave some novel alkyl/alkenyl/aryl 2,5,5-trimethyl-1-cyclopentenyl ketones.

RESULTS AND DISCUSSION

Chemistry

Preparation of five- and six-membered α,α,α′-trimethylcycloalkanones. Hereby a new route for the synthesis of 2,5,5-trimethylcyclopentanone is reported.[9a] Diethyl adipate (**3**) upon Dieckmann cyclisation with sodium/toluene afforded ethyl 2-oxocyclopentanecarboxylate (**4**).[9b] Total methylation of **4** using methyl iodide (6 equivalents) and sodium hydride (4 equivalents) gave ethyl 1,3,3-trimethyl-2-oxocyclopentanecarboxylate (**5**) in 71 % yield. Subsequent hydrochloric acid catalyzed hydrolysis and decarboxylation gave the pure five-membered 2,2,5-trimethylcyclopentanone (**6**) in 58 % isolated yield from **5**.

2,2,6-Trimethylcyclohexanone was prepared according to a reported literature procedure.[10] Reaction of cyclohexanone (**7**) with diethyl oxalate in presence of sodium ethoxide followed by pyrolysis with a catalytic amount of ground iron powder/glass-wool at 175 °C gave ethyl 2-oxocyclohexanecarboxylate (**8**) in 45 % yield. Total methylation of **8** using 4 equivalents of sodium hydride and 6 equivalents of methyl iodide gave 1,3,3-trimethyl-2-oxocyclohexanecarboxylate (**9**) in 78 % yield. Hydrochloric acid catalyzed hydrolysis and decarboxylation yielded pure 2,2,6-trimethylcyclohexanone (**10**) in 77 % yield (Scheme 1).

Conversion to cyclic vinyl halides. A number of procedures have been developed for the conversion of ketones to vinyl halides. This is due to the growing use of metal-catalyzed coupling reactions of alky/alkenyl/aryl halides in organic synthesis. Some of the recently developed reagents used to perform the transformation include $(PhO)_3P/X_2$,[11a] CH_3COX/CF_3COOH,[11b] WCl_6,[11c] $(EtO)_2P(O)Cl$/

/P(Ph$_3$)/X$_2$,[11d] along with traditional halogenating agents such as thionyl chloride and phosphorus pentachloride.[11e–g]

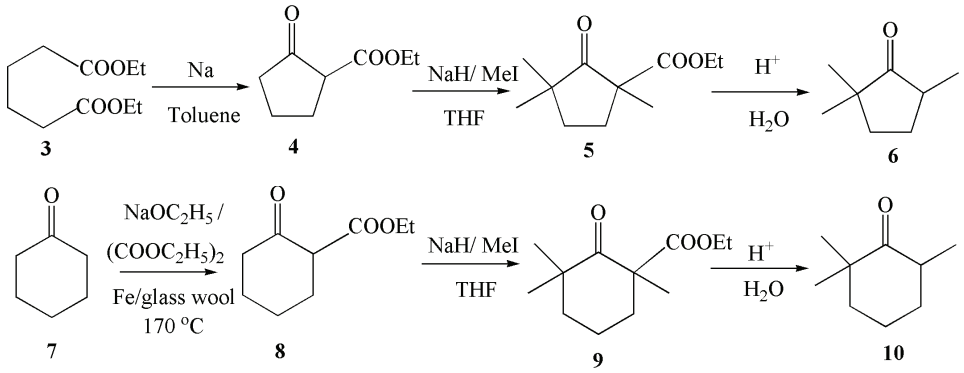

Scheme 1. Synthesis of five- and six-membered *α,α,α′*-trimethylcycloalkanones (**6** and **10**).

Some of the reagents reported for the conversion of cyclic ketones to cycloalkenyl halides were explored in the present study. The investigations showed that the Takeda general method for preparation of *gem*-halides was most useful.[12] The method involves the conversion of the carbonyl compounds to their corresponding hydrazones, followed by reaction with cupric halide/Et$_3$N.

The compounds **6** and **10** were converted to their corresponding hydrazones 2,2,5-trimethylcyclopentanone hydrazone (**11**) in 75 % yield and 2,2,6-trimethylcyclohexanone hydrazone (**12**)[6d] in 78 % yield, respectively.

Treatment of the hydrazones **11** and **12** with 6 equivalents of copper(II) chloride and 3 equivalents of triethylamine gave 1,1-dichloro-2,2,5-trimethylcyclopentane (**13**) in 33 % yield and 1,1-dichloro-2,2,6-trimethylcyclohexane (**14**) in 42 % yield, respectively. Subsequent dehydrochlorination of **13** and **14** employing morpholine/DMSO and benzene[13] gave 2-chloro-1,3,3-trimethylcyclopentene (**17**) in 31 % yield and 2-chloro-1,3,3-trimethylcyclohexene (**18**)[5c] in 40 % yield, respectively.

Similar bromination of **11** and **12** with 6 equivalents of copper(II) bromide and 3 equivalents of triethylamine gave a mixture of *gem*-dibromides **15** and **16** and vinyl bromides **19** and **20** in a 1:1 ratio due to the elimination of HBr under the employed reaction conditions. Without isolation of the mixture of *gem*-dibromide and vinyl bromide, the mixture was subjected to dehydrobromination using morpholine/DMSO/benzene to isolate 2-bromo-1,3,3-trimethylcyclopentene (**19**) in 64 % yield and 2-bromo-1,3,3-trimethylcyclohexene (**20**) in 69 % yield.

The cyclic vinyl iodides 2-iodo-1,3,3-trimethylcyclopentene (**21**) and 2-iodo-1,3,3-trimethylcyclohexene (**22**)[6d] were prepared by adopting the Barton vinyl iodination procedure. Reaction of **11** and **12** with iodine and 2,3,4,6,7,8-hexahydropyrrolo[1,2-*a*]pyrimidine (DBN)[6d,14] gave **21** in 79 % yield and **22** in 82 %

yield (Scheme 2). The results for the preparation of the cyclic vinyl halides **17**–**22** are summarized in Table I.

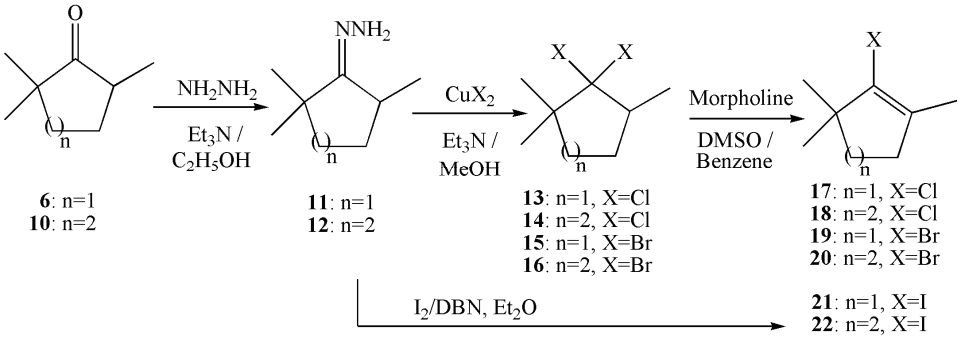

Scheme 2. Synthesis of five- and six-membered 2-halo-1,3,3-trimethylcycloalkenes (**17**–**22**).

TABLE I. Synthesis of five- and six-membered 2-halo-1,3,3-trimethylcycloalkenes **17**–**22**

Entry	Substrate	Reagent/base/solvent	Ring size	Product	Yield, %
1	**11**	$CuCl_2/Et_3N$/MeOH	5	**17**	31
2	**12**	$CuCl_2/Et_3N$/MeOH	6	**18**	40
3	**11**	$CuBr_2/Et_3N$/MeOH	5	**19**	64
4	**12**	$CuBr_2/Et_3N$/MeOH	6	**20**	69
5	**11**	I_2/DBN/Et_2O	5	**21**	79
6	**12**[6d]	I_2/DBN/Et_2O	6	**22**[6d]	82

Wurtz–Fittig coupling reaction to the five- and six-membered 1,3,3-trimethyl-2--(trimethylsilyl)cycloalkenes

The cyclic vinyl halides **17**–**22** were subjected to the Wurtz–Fittig coupling reaction with sodium and chlorotrimethylsilane in anhydrous ether solvent, using well established protocols.[4] The reactions were followed using gas chromatography. After completion of reaction, as indicated by the chromatograms of aliquot samples, the mixtures were worked up and distilled to isolate pure **1** and **2** (Scheme 3).

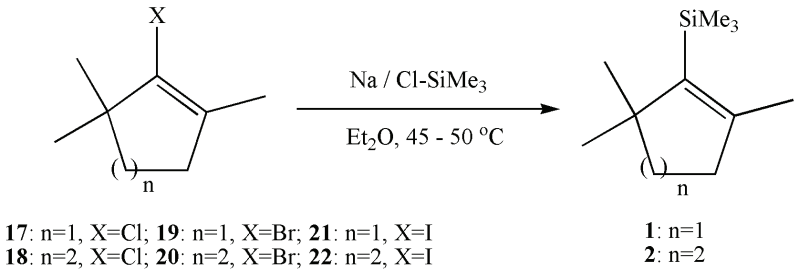

Scheme 3. Wurtz–Fittig coupling to 1,3,3-trimethyl-2-(trimethylsilyl)cycloalkenes (**1** and **2**).

Each reaction was performed a minimum of five times for each cyclic vinyl halide substrate (**17**–**22**) and the yields of the products **1** and **2** were averaged and are given in Table II.

TABLE II. Synthesis of 1,3,3-trimethyl-2-(trimethylsilyl)cycloalkenes **1** and **2** by Wurtz–Fittig coupling of **17**–**22** with sodium and chlorotrimethylsilane in anhydrous diethyl ether as solvent

Entry	Substrate	Halogen	Ring size	Product	Yield, %
1	**17**	Cl	5	**1**	73–76
2	**18**[5c]	Cl	6	**2**	75–77
3	**19**	Br	5	**1**	72–74
4	**20**	Br	6	**2**	<10
5	**21**	I	5	**1**	81–83
6	**22**[6d]	I	6	**2**	<10

The hindered cyclic vinyl halides **17**–**22** exhibited different reactivity with sodium metal in the Wurtz–Fittig reaction. The five membered cyclic vinyl halides 2-chloro-1,3,3-trimethylcyclopentene (**17**), 2-bromo-1,3,3-trimethylcyclopentene (**19**) and 2-iodo-1,3,3-trimethylcyclopentene (**21**) reacted with sodium smoothly to form **1** in > 70 % yields (Table II). Among all the five-membered cyclic vinyl halides, the 2-iodo-1,3,3-trimethylcyclopentene (**21**) was found to be the best substrate for the preparation of 1,3,3-trimethyl-2-(trimethylsilyl)cyclopentene (**1**), with the highest isolated yield of 81–83 %.

In case of the six-membered ring system, the 1,3,3-trimethyl-2-(trimethylsilyl)cyclohexene (**18**)[5c] was found to be the best substrate with isolated yields of 2-trimethylsilyl-1,3,3-trimethylcyclohexene (**2**) in the range of 75–77 % (Table II). The other six-membered cyclic vinyl halides **20** and **22** did not give satisfactory yields under the employed reaction conditions. Change of metal to potassium, magnesium or lithium and use of solvents: THF, benzene or hexamethylphosphoramide (HMPA) gave **2** in less than 10 % yields.

It was not possible to prepare **2** in large quantities (1 g scale). Although the vinyl halides **20** and **22** could be prepared in large quantities, their Wurtz–Fittig couplings proceeded to give low and inconsistent yields. On the other hand, although the Wurtz–Fittig reaction of the vinyl chloride **18** occurred in good yields, the preparation of **18** proved difficult because of low yields[5c] in both the *gem*--chlorination (42 % yield) and dehydrochlorination steps (40 % yield).

In the light of the preparation of the five-membered cyclic vinyl silane **1** in sufficient quantities (2 g scale), Friedel–Crafts acylation reactions of the five-membered cyclic vinyl silane **1** with six different acid chlorides were performed.

Conversion to novel alkyl/alkenyl/aryl 2,5,5-trimethyl-1-cyclopentenyl ketones. The Friedel–Crafts acylation reactions are some of the most widely studied

and used reactions in organosilicon chemistry.[1–3] The reaction has been extended to several classes of organosilicon compounds, such as allylsilanes, arylsilanes, vinylsilanes, *etc*., to obtain a wide variety of carbonyl moiety-containing products. The conversions employ the β-silyl effect.[15] Using the Friedel–Crafts acylation reaction and employing standardized procedures, the synthesis of a wide variety of novel products from cyclic vinylsilanes was previously reported.[4]

The Friedel–Crafts reaction of **1** was performed on the 0.2 g scale with 3 molar equivalents each of anhydrous aluminium chloride and six different acid chlorides in dichloromethane as solvent.

The reactions were found to be clean and afforded the novel alkyl/alkenyl/aryl 2,5,5-trimethyl-1-cyclopentenyl ketones **23a**–**f** (Scheme 4) in isolated yields ranging between 65–87 % in five trials for each substrate (Table III).

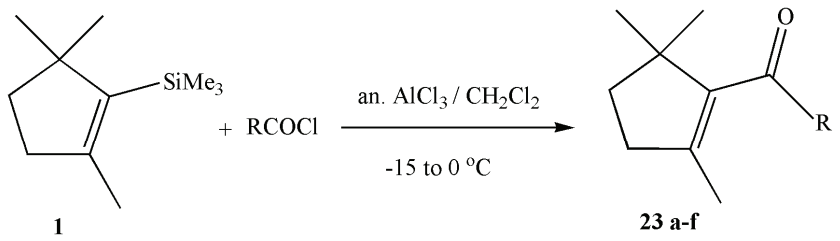

(a) R: -CH_3 (b) R: -CH_2CH_3 (c) R: *trans*-CH=CH-CH_3 (d) R: n-C_4H_9 (e) R: n-C_5H_{11} (f) R: -C_6H_5

Scheme 4. Facile route for the synthesis of alkyl/alkenyl/aryl 2,5,5-trimethyl-1-cyclopentenyl ketones (**23a**–**f**).

TABLE III. Synthesis of some novel alkyl/alkenyl/aryl 2,5,5-trimethyl-1-cyclopentenyl ketones (**23a–f**)

Entry	Product	R	Yield, %	B.p. / °C (1 mm)
1	**23a**[16]	–CH_3	65	53–57
2	**23b**	–C_2H_5	71	64–67
3	**23c**	–(*E*)-C_3H_5	78	69–73
4	**23d**	*n*-C_4H_9	83	68–72
5	**23e**	*n*-C_5H_{11}	87	71–74
6	**23f**	–C_6H_5	86	82–84

The compound **23a** is a known compound prepared earlier by Stille in the palladium-catalysed coupling of (α-ethoxyvinyl)trimethylstannane with 2,5,5-trimethyl-1-cyclopenten-1-yl trifluoromethanesulfonate.[16] All the other (2,5,5-trimethyl-1-cyclopentenyl)ketones **23b**–**f** are not reported in the literature and are reported herein for the first time. The procedure employs the Friedel–Crafts acylation reaction of **1** and utilizes the β-silyl effect. Compound **23c** is the lower analogue of the naturally occurring β-damascone.[17] Compounds **23a**–**f** may be useful in the aroma and perfume industries.[18]

EXPERIMENTAL

All reactions were monitored using GC or TLC. The TLC was run on Merck TLC Silicagel 60 F_{254} pre-coated plates with elution solvent 1:20 ethyl acetate/hexane (60–80 °C fraction). The GC was run on an SE-30 SS 2 m×1/8″ column in a Mayura 9800 gas chromatograph. The IR spectra were recorded on Shimadzu FT-IR 8400S on NaCl plates as neat thin liquid film samples. The NMR spectra were recorded in $CDCl_3$ on a Bruker AMX 400 spectrometer using tetramethylsilane (TMS) as an internal standard. The GC–MS spectra were obtained using a Shimadzu GC–MS QP 5050A instrument equipped with a 30 m×0.32 mm BP-5 capillary column. Elemental Analysis were realised using an Elementar Vario Microcube-15106062 instrument. All yields refer to the isolated yields of the products.

The spectral data of the products are given in the Supplementary material to this paper.

*General procedure for the synthesis of five- and six-membered 2-chloro/bromo-1,3,3-trimethylcycloalkenes (**17**–**20**)*

To a solution of copper(II) halide (6 molar equivalents) in 80 mL methanol was added triethylamine (3 molar equivalents) at 20 °C. The reaction mixture was stirred for 10 min and cooled to 0 °C. A methanolic solution of *α,α,α′*-trimethylcycloalkanone hydrazones **11** and **12** (3 g in 30 mL MeOH) was added dropwise over 20 min, and the mixture was further stirred for 2 h, simultaneously allowing the reaction mixture to attain ambient temperature. TLC indicated complete conversion of the hydrazone. The mixture was quenched by the addition of 50 mL of a 3.5 % aqueous NH_3 solution, and extracted with diethyl ether (3×30 mL). The combined organic extracts were washed with saturated $NaHCO_3$ (2×30 mL), water (2×30 mL), saturated NaCl (2×30 mL) and dried over anhydrous $MgSO_4$. The solvent was removed on a rotavapor and the residue distilled under reduced pressure to isolate the halogenated products.

The mixture of halogenated products (2 g) was added to morpholine (10 molar equivalents)/DMSO (10 molar equivalents)/8 mL of benzene and refluxed at 100 °C for 24 h. Gas chromatography indicated complete conversion to the cyclic vinyl halides **17**–**20**. The mixture was cooled, added to ice cold 2M HCl (50 mL) and extracted with diethyl ether (3×40 mL). The combined organic extracts were washed with saturated $NaHCO_3$ (2×30 mL), water (2×30 mL), saturated NaCl (2×30 mL) and dried over anhydrous $MgSO_4$. The solvent was removed on a rotavapor and the residue distilled under reduced pressure to isolate the pure 2-chloro/ /bromo-1,3,3-trimethylcycloalkenes (**17**–**20**).

*General procedure for the synthesis of five- and six-membered 2-iodo-1,3,3-trimethylcycloalkenes (**21** and **22**)*

To a suspension of 4 g of *α,α,α′*-trimethylcycloalkanone hydrazones **11** and **12** and 6 molar equivalents of 1,5-diazabicyclo[4.3.0]non-5-ene in 50 mL anhydrous diethyl ether was added dropwise a solution of 2.2 molar equivalents iodine in 100 mL anhydrous diethyl ether. The reaction mixture was stirred for 3.5 h, when the GC indicated completion of the reaction. The reaction mixture was washed with saturated sodium bicarbonate solution (20 mL). The ethereal layer was separated and the aqueous layer re-extracted with diethyl ether (3×40 mL). The organic layers were combined, dried over anhydrous sodium sulphate, and evaporated *in vacuo*. The residue was chromatographed through silica gel using hexane as the solvent to afford the cyclic vinyl iodides **21** and **22**.

*General procedure for the synthesis of 1,3,3-trimethyl-2-(trimethylsilyl)cycloalkenes (**1** and **2**)*

To a suspension of finely cut sodium pieces (5 molar equivalents) and chlorotrimethylsilane (3 molar equivalents) in 10 mL of dry diethyl ether was added 2-halo-1,3,3-trimethylcycloalkene (3.2 g (13.5 mmol) of **21**, or 0.22 g (1.3 mmol) of **18**) in 10 mL of anhydrous

diethyl ether. The mixture was refluxed with efficient stirring on an oil bath at 45–50 °C, whereby a deep navy blue colouration developed. Monitoring the reaction by GC indicated that the reactants required 6 h for complete conversion to the products. The mixture was cooled; the precipitated solids and remaining sodium removed by filtration through a plug of glass wool and washed with diethyl ether (2×5 mL). Saturated sodium bicarbonate (15 mL) was added to the combined filtrate, the layers were separated, and the organic layer was successively washed with water (3×10 mL), saturated sodium chloride (15 mL), dried over anhydrous Na_2CO_3, concentrated and distilled under reduce pressure to isolate **1** and **2**. The yields of the isolated products are given in Table II.

*General procedure for the synthesis of alkyl/alkenyl/aryl 2,5,5-trimethyl-1-cyclopentenyl ketones (**23a–f**)*

To a magnetically stirred mixture of anhydrous $AlCl_3$ (3 molar equivalents) and acid chloride (3 molar equivalents) in dry CH_2Cl_2 (20 mL), cooled to –15 °C on an ice–salt bath, was added dropwise 0.2 g of **1** in 5 ml of dry CH_2Cl_2 over a period of 5 min. After stirring for 3 h, the gas chromatogram of an aliquot indicated complete disappearance of the reactant **1**. Saturated $NaHCO_3$ solution (20 mL) was added to the mixture and stirred for 30 min, simultaneously allowing the reaction mixture to attain room temperature. The organic layer was separated, washed with $NaHCO_3$ solution (2×20 mL), water (25 mL) and saturated NaCl solution (20 mL). The pale yellow organic extract was dried over anhydrous Na_2SO_4, concentrated and finally subjected to bulb-to-bulb distillation under reduced pressure to isolate individually the alkyl/alkenyl/aryl 2,5,5-trimethyl-1-cyclopentenyl ketones (**23a–f**).

CONCLUSIONS

The simple synthesis of 1,3,3-trimethyl-2-(trimethylsilyl)cyclopentene and 1,3,3-trimethyl-2-(trimethylsilyl)cyclohexene is reported. The Friedel–Crafts acylations of 1,3,3-trimethyl-2-(trimethylsilyl)cyclopentene gave a series of six alkyl/alkenyl/aryl 2,5,5-trimethyl-1-cyclopentenyl ketones.

SUPPLEMENTARY MATERIAL

Spectral data of the products are available electronically from http://www.shd.org.rs/ /JSCS/, or from the corresponding author on request.

*Acknowledgment*s. Grateful thanks are due to the Bangalore University Internal Research Fund; University Grants Commission and Department of Science and Technology of the Government of India, New Delhi, India, for financial assistance. M. A. V. thanks the Council for Scientific and Industrial Research for a Research Fellowship. We are also thankful to the NMR Department, Indian Institute of Science – Bangalore, India.

ИЗВОД

СИНТЕЗА ПЕТО- И ШЕСТОЧЛАНИХ 2-(ТРИМЕТИЛСИЛИЛ)-1,3,3-ТРИМЕТИЛ-ЦИКЛОАЛКАНА: НОВ ПОСТУПАК СИНТЕЗЕ АЛКИЛ/АЛКЕНИЛ/АРИЛ-(2,5,5-ТРИМЕТИЛЦИКЛОПЕНТЕНИЛ)-КЕТОНА

VENKATESHA M. ACHANNA и HARIPRASAD SURESH

Department of Chemistry, Central College Campus, Palace Road, Bangalore University, Bangalore – 560001, India

1,3,3-Триметил-2-(триметилсилил)-циклопентен и 1,3,3-триметил-2-(триметилсилил)-циклохексен добијени су, у добром приносу, Вурц–Фитиговим куповањем пола-

зећи од одговарајућих 2-јод-1,3,3-триметилциклопентена и 2-хлор-1,3,3-триметилциклохексена са металним натријумом и хлортриметилсиланом у анхидрованом етру као растварачу. Приказано је Фридел–Крафтсово ацеловање 1,3,3-триметил-2-(триметилсилил)-циклопентена са шест различитих алканоилхлорида и нова синтеза шест алкил/алкенил/арил-(2,5,5-триметил-1-циклопентенил)-кетона.

(Примљено 1. маја, ревидирано 1. децембра 2012)

REFERENCES

1. a) M. A. Brook, *Silicon in Organic, Organometallic and Polymer Chemistry*, Wiley: New York, 2000; b) B. Marciniec, *Hydrosilylation: A Comprehensive Review on Recent Advances*, Springer, Berlin, 2009
2. E. Langkopf, D. Schinzer, *Chem. Rev.* **95** (1995) 1375
3. a) W. P. Weber, *Silicon Reagents for Organic Synthesis*, Springer, Berlin, 1983, p. 103; b) E. W. Colvin, *Silicon Reagents in Organic Synthesis*, Academic Press, New York, 1988, p. 12; c) R. L. Danheiser, D. J. Carini, D. M. Fink, A. Basak, *Tetrahedron* **39** (1983) 935; d) W. Adam, M. J. Richter *Synthesis* (1994) 176; e) P. F. Hudrlik, A. K. Kulkarni, S. Jain, A. M. Hudrlik, *Tetrahedron* **39** (1983) 877
4. a) G. Nagendrappa, *Synthesis* (1980) 704; b) B. S. Bandodakar, G. Nagendrappa, *Tetrahedron Lett.* (1989) 7461; c) S. HariPrasad, G. Nagendrappa, *Tetrahedron* (1993) 3387; d) S. HariPrasad, G. Nagendrappa, *Indian J. Chem., Sect. B* **36** (1997) 1016; e) G. S. Patil, G. Nagendrappa, *Indian J. Chem., B* **41** (2002) 1019; f) S. HariPrasad, G. Nagendrappa, *Indian J. Chem., B* **36** (1997) 691; g) D. Jyothi, S. HariPrasad, *Synth. Commun.* **39** (2009) 875; h) D. Jyothi, S. HariPrasad, *ARKIVOC* (2012) 194
5. a) *Vitamin A: Vitamins and Hormones* Vol. 75, G. Litwack, Ed., Elsevier, London, 2007; b) *The Retinoids: Biology, Chemistry and Medicine*, 2nd ed. M. B. Sporn, A. B. Roberts, D. S. Goodman, Eds., Wiley, New York, 1993; c) G. Kobrich, W. E. Breckoff, W. Drischel, *Liebigs Ann. Chem.* **704** (1967) 51
6. a) C. H. Chang, Z.-H. Wen, S.-K. Wang, C.-Y. Duh, *J. Nat. Prod.* **71** (2008) 619; b) G. Majetich, J. M. Shimkus, *J. Nat. Prod.* **73** (2010) 284; c) K. F. Eidman, B. S. MacDougall, *J. Org. Chem.* **71** (2006) 9513; d) M. E. Jung, M. Murakami, *Org. Lett.* **8** (2006) 5857; e) A. Cyr, P. R. Wilderman, M. Determan, R. J. Peters, *J. Am. Chem. Soc.* **129** (2007) 6684
7. L. A. Paquette, W. E. Fristad, D. S. Dime, T. R. Bailey, *J. Org. Chem.* **45** (1980) 3017
8. W. D. Wulff, G. A. Peterson, W. E. Bauta, K.-S. Chan, K. L. Faron, S. R. Gilbertson, R. W. Kaesler, D. C. Yang, C. K. Murray, *J. Org. Chem.* **51** (1986) 279
9. a) J. B. Dubois, J. F. Fort, *Tetrahedron* **28** (1972) 1653; b) P. S. Pinkney, *Org. Synth. Coll. Vol.* **2** (1943) 116
10. C. L. Stevens, A. J. Weinheimer, *J. Am. Chem. Soc.* **80** (1958) 4072
11. a) F. Prati, *J. Org. Chem.* **72** (2007) 2216; b) K. Moughamir, B. Mezgueldi, A. Atmani, H. Mestdagh, C. Rolando, *Tetrahedron Lett.* **39** (1998) 59; c) M. E. Jung, J. I. Wasserman, *Tetrahedron Lett.* **44** (2003) 7273; d) K. Kamei, N. Maeda, T. Tatsuoka, *Tetrahedron Lett.* **46** (2005) 229; e) J. Burkhard, J. Janku, L. Vodička, *Coll. Czech. Chem. Commun.* **53** (1988) 110; f) Y. Eszenyi, T. Timar, P. Sebok, *Tetrahedron Lett.* **32** (1991) 827; g) A. J. Fry, R. H. Moore, *J. Org. Chem.* **33** (1968) 425
12. T. Takeda, R. Sasaka, S. Yamuchi, T. Fujiwara, *Tetrahedron* **53** (1997) 557
13. B. S. Bandodkar, G. Nagendrappa, *Synthesis* (1990) 843
14. D. H. R. Barton, R. E. O'Brien, S. Sternhell, *J. Chem. Soc.* (1962) 470

15. a) J. B. Lambert, *Tetrahedron* **46** (1990) 2677; b) Z. N. Parnes, G. I. Bolestova, *Synthesis* (1984) 991; c) M. Ramaiah, *Synthesis* (1984) 529; d) L. A. Paquette, *Science* **217** (1982) 793; e) I. Fleming, A. Pearce, *J. Chem. Soc. Perkin Trans. 1* (1980) 2485; f) T. H. Chan, I. Fleming, *Synthesis* (1979) 761
16. H. B. Kwon, B. H. McKee, J. K. Stille, *J. Org. Chem.* **55** (1990) 3114
17. R. R. Calkin, J. S. Jellinek, *Perfumery: Practice and Principles*, Wiley, New York, (1994)
18. a) P. Kraft, K. Popaj, *Eur. J. Org. Chem.* (2008) 4806; b) P. Kraft, J. A. Bajgrowicz, C. Denis, G. Frater, *Angew. Chem. Int. Ed.* **39** (2000) 2980.

Journal of the Serbian Chemical Society
JSCS@tmf.bg.ac.rs • www.shd.org.rs/JSCS
J. Serb. Chem. Soc. 78 (6) S57–S61 (2013) *Supplementary material*

SUPPLEMENTARY MATERIAL TO

Synthesis of five- and six-membered 1,3,3-trimethyl-2--(trimethylsilyl)cycloalkenes: a novel preparation of alkyl/alkenyl/aryl 2,5,5-trimethyl-1-cyclopentenyl ketones

VENKATESHA M. ACHANNA and HARIPRASAD SURESH*

Department of Chemistry, Central College Campus, Palace Road, Bangalore University, Bangalore – 560001, India

J. Serb. Chem. Soc. 78 (6) (2013) 759–768

SPECTRAL DATA OF THE PRODUCTS

1,3,3-Trimethyl-2-(trimethylsilyl)cyclopentene (***1***).[1] Light yellow oil; yield: 81–83 %; b.p.: 65–70 °C/4 mm. IR (film, cm^{-1}): 2958, 2866, 1647, 1458, 1377, 1261, 1095, 1016, 802. ^{1}H-NMR (400 MHz, $CDCl_3$, δ / ppm): 0.08 (9H, *s*, $–SiMe_3$), 0.98 (6H, *s*, $[–CH_3]_2$), 1.48–1.51 (2H, *t*, *J* = 7.2 Hz, $–CH_2–$), 1.70 (3H, *s*, $–CH_3$), 2.17–2.21 (2H, *t*, *J* = 7.2 Hz, $–CH_2–$). ^{13}C-NMR (100, MHz, $CDCl_3$, δ / / ppm): 1.5 ($–SiMe_3$), 17.9, 28.7, 28.8, 39.0, 41.8, 51.7, 142.7 [C (sp^2)], 149.6 [C (sp^2)]. GC–MS (*m*/*z* (relative intensity)): 182 (13, M^+), 167 (72), 108 (28), 93 (25), 73 (100 %, base peak), 74 (46), 59 (58), 45 (62).

1,3,3-Trimethyl-2-(trimethylsilyl)cyclohexene (***2***). New compound. Light yellow oil; yield: 75–77 %; b.p.: 77–80 °C/2 mm; Anal. Calcd. for $C_{12}H_{24}Si$: C, 73.38; H, 12.32 %. Found: C, 73.58; H, 12.42 %; IR (film, cm^{-1}): 2950, 2866, 1649, 1581, 1452, 1456, 1255, 1095, 1051, 840, 808, 761; ^{1}H-NMR (400 MHz, $CDCl_3$, δ / ppm): 0.22 (9H, *s*, $–SiMe_3$), 1.05 (6H, *s*, $[–CH_3]_2$), 1.33–1.36 (2H, *m*, $–CH_2–$), 1.53–1.59 (2H, *m*, $–CH_2–$), 1.75 (3H, *s*, $–CH_3$), 1.90–1.94 (2H, *t*, *J* = = 8Hz, $–CH_2–$). ^{13}C-NMR (100, MHz, $CDCl_3$, δ / ppm): 3.8, 19.3, 24.7, 29.5, 34.6, 35.5, 41.3, 139.1 [C (sp^2)], 142.8 [C (sp^2)]. GC–MS (*m*/*z* (relative intensity)): 196 (3, M^+), 181(8), 123 (10), 122 (31), 107 (25), 73 (100 %, base peak), 59 (15), 45 (24), 43 (15).

2,2,5-Trimethylcyclopentanone hydrazone (***11***). New compound. White needles; yield: 75 %; Anal. Calcd. for $C_8H_{16}N_2$: C, 68.52; H, 11.5; N, 19.98 %. Found: C, 68.34; H, 11.65; N, 20.30 %; IR (film, cm^{-1}): 3357, 3211, 2962, 2871, 1737, 1461, 1380, 1361, 1255, 1080, 1006. ^{1}H-NMR (400 MHz, $CDCl_3$, δ / ppm): 1.07 (3H, *s*, $–CH_3$), 1.13 (3H, *s*, $–CH_3$), 1.16–1.18 (3H, *d*, *J* = 8Hz, $–CH_3$), 1.46–

* Corresponding author. E-mail: hariprasad@bub.ernet.in

–1.56 (2H, *m*, –CH–), 1.68–1.75 (1H, *m*), 1.93–2.00 (1H, *m*), 2.76–2.81 (1H, *m*), 4.8 (2H, *s*, $–NH_2$). ^{13}C-NMR (100, MHz, $CDCl_3$, δ / ppm): 15.9, 27.2, 27.6, 30.2, 32.8, 38.2, 42.1, 168.6 [C (sp^2)]. GC–MS (*m*/*z* (relative intensity)):140 (35, M^+), 125 (46), 124 (54), 109 (10), 108 (17), 95 (21), 81 (26), 69 (28), 67 (29), 55 (63), 41 (100 %, base peak).

*2,2,6-Trimethylcyclohexanone hydrazone (**12**)*.[2] White needles; yield: 78 %; ^{1}H-NMR (400 MHz, $CDCl_3$, δ / ppm): 1.12 (6H, *s*, $[–CH_3]_2$), 1.16 (3H, *d*, *J* = 8 Hz, $–CH_3$), 1.53–1.58(2H, *m*, $–CH_2–$), 1.59–1.63 (2H, *m*, $–CH_2–$), 1.72–1.77(2H, m, $–CH_2–$), 2.95-2.99 (1H, *m*, –CH–), 4.69 (2H, *s*, $–NH_2$). ^{13}C-NMR (100, MHz, $CDCl_3$, δ / ppm): 17.6, 17.8, 26.9, 29.3, 29.9, 32.1, 38.06, 40.8, 163.02 [C (sp^2)]. GC–MS (*m*/*z* (relative intensity)):154 (5, M^+), 139 (3), 122 (5), 109 (4), 95 (5), 81 (10), 67 (14), 56 (31), 41 (100 %, base peak).

*1,1-Dichloro-2,2,5-trimethylcyclopentane (**13**)*. New compound. Yellow oil; yield: 33 %; b.p.: 60–63 °C/4 mm. Anal. Calcd. for $C_8H_{14}Cl_2$: C, 53.06; H, 7.79 %. Found: C, 53.47; H, 7.29 %; IR (film, cm^{-1}): 2966, 2939, 2875, 1506, 1455, 1371, 1217, 1105, 1002, 973, 914, 848, 784, and 761. ^{1}H-NMR (400 MHz, $CDCl_3$, δ / ppm): 1.17 (3H, *s*, $–CH_3$), 1.22–1.24 (3H, *d*, *J* = 8 Hz, $–CH_3$), 1.27 (3H, *s*, $–CH_3$), 1.36–1.43 (1H, *m*), 1.55–1.62 (1H, *m*), 1.73–1.78 (1H, *m*), 1.81––1.93 (1H, *m*), 2.65–2.71 (1H, *m*, –CH–). ^{13}C-NMR (100, MHz, $CDCl_3$, δ / ppm): 15.0, 24.0, 27.0, 27.3, 35.0, 46.8, 50.5, 106.9 ($–CCl_2$). GC–MS (*m*/*z* (relative intensity)): 184 (1, M+4), 182 (3, M+2), 180 (1, M^+), 144 (1), 131 (2), 129 (7), 109 (29), 104 (16), 97 (22), 77 (9), 70 (23), 69 (100 %, base peak), 56 (19), 55 (9), 42 (14), 41 (30).

*1,1-Dichloro-2,2,6-trimethylcyclohexane (**14**)*. New compound. Yellow oil; yield: 42 %; b.p.: 72–75 °C/4 mm; Anal. Calcd. for $C_9H_{16}Cl_2$: C, 55.40; H, 8.26 %. Found: C, 55.12; H, 8.45 %; IR (film, cm^{-1}): 2987, 2937, 2864, 1456, 1373, 1326, 1278, 1242, 1215, 1175, 1122, 1058, 989; ^{1}H-NMR (400 MHz, $CDCl_3$, δ / ppm): 1.21–1.23 (3H, *d*, *J* = 8 Hz, $–CH_3$), 1.24 (3H, *s*, $–CH_3$), 1.28 (3H, *s*, $–CH_3$), 1.36–1.41 (1H, *m*), 1.46–1.61 (4H, *m*), 1.82–1.85 (1H, *m*), 2.36–2.37 (1H, *m*, –CH–) ^{13}C-NMR (100, MHz, $CDCl_3$, δ / ppm): 18.0, 20.6, 24.8, 27.3, 32.0, 36.5, 42.6, 44.8, 108.6 ($–CCl_2$). GC–MS (*m*/*z* (relative intensity)): 198 (1, M+4), 196 (3, M+2), 194 (1, M^+), 145 (4), 143 (2), 123 (20), 109 (6), 107 (21), 93 (6), 91 (16), 81 (32), 69 (34), 53 (39), 41 (100, base peak).

*2-Chloro-1,3,3-trimethylcyclopentene (**17**)*. New compound. Yellow oil; yield: 31 %; b.p.: 60–63 °C/4 mm. Anal. Calcd. for $C_8H_{13}Cl$: C, 66.43; H, 9.06 %. Found: C, 66.23; H, 9.27 %; IR (film, cm^{-1}): 2960, 2867, 1664, 1461, 1363, 1259, 1006, 939; ^{1}H-NMR (400 MHz, $CDCl_3$, δ / ppm): 1.04 (6H, *s*, $[–CH_3]_2$), 1.69 (3H, *s*, $–CH_3$), 1.76 (2H, *t*, *J* = 4.4 Hz, $–CH_2–$), 2.26 (2H, *t*, *J* = 6 Hz, $–CH_2–$). ^{13}C-NMR (100, MHz, $CDCl_3$, δ / ppm): 14.2, 24.9, 26.4, 33.0, 34.8, 37.3, 130.9 [C (sp^2)], 134.9 [C (sp^2)]. GC–MS (*m*/*z* (relative intensity)): 146 (5, M+2), 144

(17, M^+), 131 (31), 129 (100 %, base peak), 93 (59), 91 (31), 78 (43), 63 (67), 53 (14), 45 (30), 41 (22).

2-Chloro-1,3,3-trimethylcyclohexene (***18***).[3] Yellow oil; yield: 40 %; b.p.: 72–75 °C/4 mm; Anal. Calcd. for $C_9H_{15}Cl$: C, 68.13; H, 9.53 %. Found: C, 68.23; H, 9.27 %; IR (film, cm^{-1}): 2964, 2933, 2870, 1654, 1458, 1361, 1161, 964. ^{1}H-NMR (400 MHz, $CDCl_3$, δ / ppm): 1.06 (6H, *s*, $[-CH_3]_2$), 1.55–1.58 (4H, *m*), 1.70 (3H, *s*, $-CH_3$), 2.03–2.04 (2H, *m*, $-CH_2-$). ^{13}C-NMR (100, MHz, $CDCl_3$, δ / ppm): 18.5, 20.4, 27.8, 32.5, 36.9, 38.8, 128.9 [C(sp^2)], 135.1 [C (sp^2)]. GC–MS (*m*/*z* (relative intensity)): 160 (4, M+2), 158 (12, M^+), 145 (12), 143 (41), 123 (12), 109 (10), 107 (100, base peak), 91 (41), 81 (25), 79 (34), 77 (28), 53 (23), 41 (51).

2-Bromo-1,3,3-trimethylcyclopentene ***(19)***. New compound. Brown oil; yield: 64 %; b.p.: 69–71 °C/4 mm; Anal. Calcd. for $C_8H_{13}Br$: C, 50.81; H, 6.93 %. Found: C, 51.2; H, 7.23 %; IR (film, cm^{-1}): 2956, 2925, 2854, 1656, 1504, 1467, 1441, 1375, 1259, 1080, 1020, 860, 796. ^{1}H-NMR (400 MHz, $CDCl_3$, δ / ppm): 1.06 (6H, *s*, $[-CH_3]_2$), 1.70 (3H, *s*, $-CH_3$), 1.79–1.82 (2H, *m*, $-CH_2-$), 2.23–2.27 (2H, *m*, $-CH_2-$). ^{13}C-NMR (100, MHz, $CDCl_3$, δ / ppm): 16.1, 27.1, 28.2, 34.1, 37.3, 128.3 [C (sp^2)], 139.3 [C (sp^2)]. GC–MS (*m*/*z* (relative intensity)): 190 (18, M+2), 188 (18, M^+), 175 (83), 173 (86), 94 (100 %, base peak), 79 (44), 64 (14), 53 (16), 41 (20).

2-Bromo-1,3,3-trimethylcyclohexene ***(20)***. New compound. Brown oil; yield: 69 %; b.p.: 76–78 °C/4 mm; Anal. Calcd. for $C_9H_{15}Br$: C, 53.22; H, 7.44 %. Found: C, 53.42; H, 7.13 %; IR (film, cm^{-1}): 2960, 2927, 2866, 1650, 1456, 1361, 1338, 1280, 1211, 1049, 939, 803, 815, 761; ^{1}H-NMR (400 MHz, $CDCl_3$, δ / ppm): 1.05 (6H, *s*, $[-CH_3]_2$), 1.53–1.58 (4H, *m*), 1.72 (3H, *s*, $-CH_3$), 1.98–2.01 (2H, *m*, $-CH_2-$). ^{13}C-NMR (100, MHz, $CDCl_3$, δ / ppm): 19.2, 24.4, 29.3, 29.7, 33.8, 39.5, 131.8 [C (sp^2)], 131.9 [C (sp^2)]. GC–MS (*m*/*z* (relative intensity)): 204 (26, M+2), 202 (24, M^+), 188 (79), 186 (77), 123 (53), 107 (100), 91 (49), 81 (42), 67 (21), 52 (25), 41 (44).

2-Iodo-1,3,3-trimethylcyclopentene ***(21)***. New compound. Brown oil; yield: 79 %; b.p.: 82–85 °C/4 mm. Anal. Calcd. for $C_8H_{13}I$: C, 40.70; H, 5.55 %. Found: C, 40.31; H, 5.71 %; IR (film, cm^{-1}): 2954, 2923, 2866, 1677, 1589, 1446, 1308, 1261, 1018, 802; ^{1}H-NMR (400 MHz, $CDCl_3$, δ / ppm): 0.99 (6H, *s*, $[-CH_3]_2$), 1.75 (3H, *s*, $-CH_3$), 1.85 (2H, *t*, J = 6.96 Hz, $-CH_2-$), 2.35 (2H, *t*, J = = 7.44 Hz, $-CH_2-$). ^{13}C-NMR (100, MHz, $CDCl_3$, δ / ppm): 19.5, 28.1, 35.6, 36.7, 49.3, 51.8, 109.4 [C (sp^2)], 141.7 [C (sp^2)]. GC–MS (*m*/*z* (relative intensity)): 236 (31, M^+), 221 (100, base peak), 127(20), 109 (5), 94 (87), 79 (70), 65 (19), 53 (24), 41 (31).

2-Iodo-1,3,3-trimethylcyclohexene ***(22)***.[2] Brown oil; yield: 82 %; ^{1}H-NMR (400 MHz, $CDCl_3$, δ / ppm): 1.02 (6H, *s*, $[-CH_3]_2$), 1.54–1.67 (*m*, 4H), 1.79 (3H, *s*, $-CH_3$), 2.07–2.11 (2H, *t*, J = 7.76 Hz, $-CH_2-$). ^{13}C-NMR (100, MHz, $CDCl_3$, δ /

/ ppm): 19.4, 31.0, 31.5, 33.7, 37.9, 39.5, 117.3 [C (sp^2)], 137.7 [C (sp^2)]. GC–MS (*m*/*z* (relative intensity)): 250 (52, M^+), 235 (21), 123(86), 108 (41), 93 (58), 81 (100), 67 (28), 53 (26), 41 (56).

1-(2,5,5-Trimethylcyclopent-1-enyl)-1-ethanone ***(23a)***.[4] Light yellow oil; yield: 65 %; 53–57 °C/1 mm; GC–MS (*m*/*z* (relative intensity)): 152 (27, M^+), 109 (100 %, base peak), 91 (15), 81(28), 67 (82), 55 (17), 40 (92).

1-(2,5,5-Trimethylcyclopent-1-enyl)-1-propanone ***(23b)***. New compound. Light yellow oil; yield: 71 %; b.p.: 64–67 °C/1 mm; Anal. Calcd. for $C_{11}H_{18}O$: C, 79.46; H, 10.91 %. Found: C, 78.98; H, 10.67 %; IR (film, cm^{-1}): 2881, 2857, 2830, 1718,1450, 1360, 1248, 1017; ^{1}H-NMR (400 MHz, $CDCl_3$, δ / ppm): 0.96 (3H, *t*, J = 3.08 Hz, $–CH_3$), 0.96 (3H, *s*, $–CH_3$), 1.27 (3H, *s*, $–CH_3$), 1.26–1.38 (2H, *m*, $–CH_2–$), 1.54–1.59 (2H, *m*, $–CH_2–$), 1.67 (3H, *s*, $–CH_3$), 2.09–2.13 (2H, *m*, $–CH_2–$), 2.14–2.35 (2H, *m*, $–CH_2–$). ^{13}C-NMR (100, MHz, $CDCl_3$, δ / ppm): 15.2, 23.9, 28.8, 31.0, 35.6, 42.2, 46.6, 71.3, 126.5 [C (sp^2)], 137.0 [C (sp^2)], 212.0 (C=O). GC–MS (*m*/*z* (relative intensity)): 166 (22, M^+), 151 (2), 137 (4), 123 (10), 109 (100 %, base peak), 95 (7), 91 (14), 81 (20), 67 (59), 57 (43), 55 (19), 40 (73).

*(*E*)-1-(2,5,5-Trimethylcyclopent-1-enyl)but-2-en-1-one* ***(23c)***. New compound. Light yellow oil; yield: 78 %; b.p.: 69–73 °C/1 mm; Anal. Calcd. for $C_{12}H_{18}O$: C, 80.85; H, 10.18 %. Found: C, 80.36; H, 10.43 %; IR (film, cm^{-1}): 2950, 2890, 1755, 1708, 1635, 1442, 1301, 1075, 950; ^{1}H-NMR (400 MHz, $CDCl_3$, δ / ppm): 1.08 (6H, *s*, $[–CH_3]_2$), 1.48 (3H, *s*, $–CH_3$), 1.75–1.85 (5H, *m*), 1.95–2.15 (2H, *m*, $–CH_2–$), 6.18–6.23(1H, *m*, =CH–), 6.84–6.93 (1H, *m*, =CH–). ^{13}C-NMR (100, MHz, $CDCl_3$, δ / ppm): 15.2, 17.2, 24.2, 31.1, 42.2, 46.9, 126.5, 130.2, 137.2, 138.6 [C (sp^2)], 141.6 [C (sp^2)], 200.2 (C=O). GC–MS (*m*/*z* (relative intensity)): 178 (9, M+), 163 (6), 135 (3), 122 (4), 109 (33), 91 (9), 79 (14), 69 (100, base peak), 55 (12), 41 (55).

1-(2,5,5-Trimethylcyclopent-1-enyl)-1-pentanone ***(23d)***. New compound. Light yellow oil; yield: 83 %; b.p.: 68–72 °C/1 mm. Anal. Calcd. for $C_{13}H_{22}O$: C, 80.35; H, 11.41 %. Found: C, 80.56; H, 11.13 %; IR (film, cm^{-1}): 2880, 2855, 2830, 1720,1450, 1340, 1250, 1020; ^{1}H-NMR (400 MHz, $CDCl_3$, δ / ppm): 0.93(3H, *t*, J = 3.08 Hz, $–CH_3$), 0.99 (3H, *s*, $–CH_3$), 1.28 (3H, *s*, $–CH_3$), 1.29––1.36 (4H, *m*), 1.51–1.58 (2H, *m*, $–CH_2–$), 1.65 (3H, *s*, $–CH_3$), 2.07–2.11 (2H, *m*), 2.1–2.39 (3H, *m*). ^{13}C-NMR (100, MHz, $CDCl_3$, δ / ppm): 12.9, 15.3, 21.4, 24.36, 24.5, 31.0, 42.3, 46.7, 71.3, 126.4 [C (sp^2)], 137.1 [C (sp^2)], 211.5 (C=O). GC–MS (*m*/*z* (relative intensity)): 194 (26, M^+), 179 (1), 151 (4), 137 (4), 109 (100 %, base peak), 91 (10), 85 (74), 67 (52), 57 (70), 41 (43).

1-(2,5,5-Trimethylcyclopent-1-enyl)-1-hexanone ***(23e)***. New compound. Light yellow oil; yield: 87 %; b.p.: 71–74 °C/1 mm; Anal. Calcd. for $C_{14}H_{24}O$: C, 80.71; H, 11.61 %. Found: C, 80.34; H, 11.45 %; IR (film, cm^{-1}): 2958, 2931, 1710, 1465, 1335, 1265, 1073; ^{1}H-NMR (400 MHz, $CDCl_3$, δ / ppm): 0.87 (3H,

m, $-CH_3$), 0.97 (3H, *s*, $-CH_3$), 1.25 (3H, *s*, $-CH_3$), 1.28–1.35 (6H, *m*), 1.53–1.68 (5H, *m*), 2.11–2.38 (4H, *m*). ^{13}C-NMR (100, MHz, $CDCl_3$, δ / ppm): 13.9, 16.3, 22.5, 23.1, 25.0, 29.7, 31.5, 32.1, 43.5, 47.7, 72.3, 127.4 [C (sp^2)], 138.1 [C (sp^2)]. GC–MS (*m*/*z* (relative intensity)): 208 (24, M^+), 193 (2), 165 (2), 137 (4), 109 (100 %, base peak), 99 (68), 81 (20), 71 (56), 67 (49), 55 (19), 43 (73).

(2,5,5-Trimethylcyclopent-1-enyl)phenylmethanone ***(23f)***. New compound. Yellow oil; yield: 86 %; b.p.: 82–84 °C /1 mm; Anal. Calcd. for $C_{15}H_{18}O$: C, 84.07; H, 8.47 %. Found: C, 84.74; H, 8.45 %; IR (film, cm^{-1}): 2846, 1681, 1600, 1454, 1415, 1323, 1026; ^{1}H-NMR (400 MHz, $CDCl_3$, δ / ppm): 1.22 (6H, *s*, $[-CH_3]_2$), 1.48 (3H, *s*, $-CH_3$), 1.80 (2H, *t*, J = 6.8 Hz, $-CH_2-$), 2.41–2.48 (2H, *m*, $-CH_2-$), 7.41–7.45 (3H, *m*, aromatic), 7.80–7.87 (2H, *m*, aromatic). ^{13}C-NMR (100, MHz, $CDCl_3$, δ / ppm): 16.0, 26.1, 29.3, 35.7, 39.1, 48.3, 124.4, 127.0, 127.2, 131.1, 138.5, 142.3, 143.5, 197.6 (C=O). GC–MS (*m*/*z* (relative intensity)): 214 (16, M^+), 199 (38), 158 (9), 137 (1), 105 (100 %, base peak), 91 (7), 77 (52), 67 (6), 51 (12), 41 (9).

REFERENCES

1. L. A. Paquette, W. E. Fristad, D. S. Dime, T. R. Bailey, *J. Org. Chem.* **45** (1980) 3017
2. M. E. Jung, M. Murakami, *Org. Lett.* **8** (2006) 5857
3. G. Kobrich, W. E. Breckoff, W. Drischel, *Liebigs Ann. Chem.* **704** (1967) 51
4. H. B. Kwon, B. H. McKee, J. K. Stille, *J. Org. Chem.* **55** (1990) 3114

Journal of the Serbian Chemical Society
JSCS-info@shd.org.rs • www.shd.org.rs/JSCS
J. Serb. Chem. Soc. 78 (6) 769–779 (2013)
JSCS–4456
UDC 547.815+539.12:546.723'722+542.913+544.351–145.82
Original scientific paper

Fe_3O_4 nanoparticles: a highly efficient and easily reusable catalyst for the one-pot synthesis of xanthene derivatives under solvent-free conditions

MOHAMMAD ALI GHASEMZADEH[1], JAVAD SAFAEI-GHOMI[1]* and SAFURA ZAHEDI[2]

[1]*Department of Chemistry, Qom Branch, Islamic Azad University, Qom, I. R. Iran and* [2]*Department of Organic Chemistry, Faculty of Chemistry, University of Kashan, 51167-Kashan, I. R. Iran*

(Received 24 June, revised 9 December 2012)

Abstract: Magnetically separable Fe_3O_4 nanoparticles supply an environmentally friendly procedure for the synthesis of 14-aryl-14*H*-dibenzo[*a*,*j*]xanthene and 1,8-dioxooctahydroxanthene derivatives. These compounds were obtained in high yields and short reaction times by the reaction of dimedone and 2-naphthol with various aromatic aldehydes under solvent-free conditions. The catalyst could be easily recovered using an external magnet and reused for six cycles with almost consistent activity.

Keywords: xanthenes, nanoparticles, solvent-free condition, magnetic catalyst, Fe_3O_4.

INTRODUCTION

Nanotechnology has been one of the most active research areas in recent years. The reactivity of catalytic nanoparticles is largely determined by the energy of surface atoms, which can be easily gauged by the number of neighboring atoms and by the bonding modes and accompanying energies of small molecules to be transformed on the surfaces of nanoparticles.[1,2] Magnetic nanoparticles are a class of nanostructured materials of current interest, due to the largely advanced technology and medical applications, envisioned or realized. Among the various magnetic nanoparticles under investigation, Fe_3O_4 nanoparticles (Fe_3O_4 NPs) are arguably the most extensively studied.[3] The main characteristic of these nanoparticles is the simple and convenient separation from a reaction media by magnetic separation.[4–7] Recently, magnetite nanoparticles were used as an efficient catalyst in many organic transformations.[8–12]

* Corresponding author. E-mail: safaei@kashanu.ac.ir
doi: 10.2298/JSC120624156G

Xanthene and its derivatives are an important class of organic compounds because of their wide range of biological and pharmaceutical properties.[13–15] In addition, these compounds are widely used in dyes,[16] laser technologies[17] and as pH-sensitive fluorescent materials.[18] There are several methods for the synthesis of xanthene derivatives, such as in the reaction of aryloxymagnesium halides with triethyl orthoformate,[19] cyclodehydration,[20] trapping of benzynes by phenols,[21] intramolecular reactions of benzaldehyde and acetophenones,[22] cyclization of polycyclic aryl triflate esters,[23] cyclocondensation of 2-hydroxy aromatic aldehydes[24] and the reaction of aldehydes, 2-naphthol and dimedone.[25] The preparation of xanthenes has been achieved *via* reaction of aldehydes and 2-naphthol by cyclodehydration using diverse catalysts, such as $H_4[SiW_{12}O_{40}]$,[26] PEG–SO_3H,[27] WCl_6,[28] poly(4-vinylpyridinium) hydrogen sulfate,[29] silica sulfuric acid,[30] $Cu(CH_3CN)_4PF_6$,[31] bismuth(III) chloride,[32] sulfonic acid functionalized silica (SiO_2–Pr-SO_3H),[33] $Sc[N(SO_2C_8F_{17})_2]_3$,[34] silica-supported ferric hydrogen sulfate,[35] P_2O_5 or $InCl_3$,[36] polystyrene-supported aluminum chloride,[37] nano TiO_2,[38] AgI nanoparticles,[39] organocatalysts[40] and functionalized SBA-15.[41]

The classical method for the synthesis of 1,8-dioxooctahydroxanthenes involves the condensation of two equivalent of 1,3-diketones, such as dimedone (5,5-dimethyl-1,3-cyclohexanedione) with various aldehydes,[42] catalyzed using different catalysts including *p*-dodecylbenzenesulfonic acid,[43] $InCl_3$/ionic liquid,[44] Fe^{3+}–montmorillonite,[45] $NaHSO_4$–SiO_2 or silica chloride,[46] amberlyst 15,[47] silica sulfuric acid[48] and 1-(carboxymethyl)-3-methylimidazolium tetrafluoroborate ([cmmim][BF_4]).[49]

In accordance to the above-mentioned importance of magnetite nanoparticles and the significant importance of xanthenes derivatives, it was thought that there is scope for further innovation towards milder reaction conditions, short reaction time and improvement of yield in the synthesis of xanthene derivatives. Herein a highly efficient and clean method for the synthesis of 14-aryl-14*H*-dibenzo[*a*,*j*]-xanthene and 1,8-dioxooctahydroxanthene derivatives using Fe_3O_4 nanoparticles as a green and robust catalyst under thermal and solvent-free conditions is reported (Scheme 1).

EXPERIMENTAL

The employed high purity commercial reagent grade chemicals were purchased from Merck and Fluka. Fe_3O_4 nanoparticles were prepared according to the procedure reported by Zhang *et al.*[9] The IR spectra were recorded as KBr pellet on a Perkin-Elmer 781 spectrophotometer and an Impact 400 Nicolet FT-IR spectrophotometer. The ^{1}H- and ^{13}C-NMR spectra were recorded in $CDCl_3$ solvent on a Bruker DRX-400 spectrometer (400 MHz) using TMS as an internal reference. The mass spectra were recorded on a Joel D-30 instrument at an ionization potential of 70 eV. All melting points are uncorrected and were determined in a capillary tube on Boetius melting point microscope. The purity determination of the substrates and reactions monitoring were accomplished by TLC on silica gel polygram SILG/UV 254 plates. The elemental analyses (C, H, N) were realized using a Carlo Erba Model EA 1108

analyzer. Powder X-ray diffraction (XRD) patterns were obtained on a Philips diffractometer of the X'pert Company using mono chromatized Cu K_α radiation (λ = 1.5406 Å). The microscopic morphology of the products was visualized by SEM (LEO 1455VP).

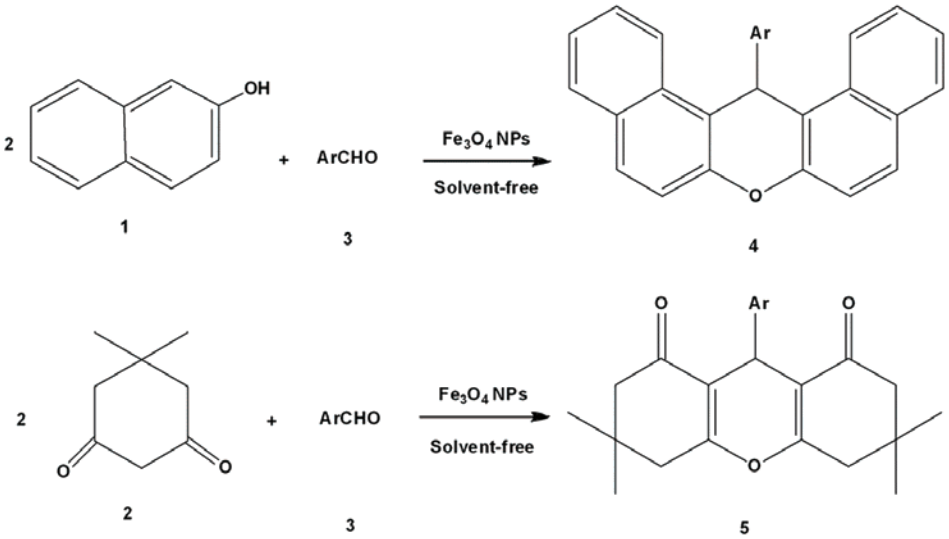

Scheme 1. One-pot synthesis of 14-aryl-14*H*-dibenzo[*a*,*j*]xanthenes and 1,8-dioxo-octahydroxanthenes.

Preparation of magnetic Fe_3O_4 nanoparticles

To a solution of $FeCl_2 \cdot 4H_2O$ (2.5 g) and $FeCl_3 \cdot 6H_2O$ (6 g) in 30 ml deionized water was added dropwise 1.0 mL of concentrated hydrochloric acid at room temperature. The solution was added in to 300 mL of 1.5 mol L^{-1} NaOH and then the solution was stirred vigorously at 70 °C until precipitation. Afterwards, the prepared magnetic nanoparticles were separated magnetically, washed with deionized water and then dried at 70 °C for 8 h.

*General procedure for the preparation of 14-aryl-14*H*-dibenzo[*a,j*]xanthene derivatives (**4a–o**)*

A mixture of 2-naphthol (0.14 g, 1 mmol), various aldehydes (0.5 mmol) and Fe_3O_4 NPs (0.02 g, 0.1 mmol, 10 mol %) was heated at 100 °C for 20–40 min. Progress of the reaction was continuously monitored by TLC. On completion of the reaction, the reaction mixture was cooled to room temperature and dissolved in 10 mL of dichloromethane. The catalyst is insoluble in CH_2Cl_2 and was separated magnetically.[4–7] The solvent was evaporated and the obtained solid was recrystallized from ethanol to afford the pure 14-aryl-14*H*-dibenzo[*a*,*j*]-xanthenes.

*General procedure for the preparation of 1,8-dioxooctahydroxanthene derivatives (**5a–o**)*

A mixture of 5,5-dimethyl-1,3-cyclohexanedione (0.14 g, 1 mmol), various aldehydes (0.5 mmol) and Fe_3O_4 NPs (0.02 g, 0.1 mmol, 10 mol %) was heated at 100 °C for 15–40 min. During the procedure, the reaction was monitored by TLC. Upon completion, the reaction mixture was cooled to room temperature and then dichloromethane was added. The catalyst is insoluble in CH_2Cl_2 and was separated magnetically. The solvent was evaporated and the

obtained solid was recrystallized from ethanol to afford the pure 1,8-dioxooctahydroxanthenes.

Spectral data for all of the compounds are reported in the Supplementary material to this paper.

Recycling and reuse of the catalyst

After completion of the reaction, the reaction mixture was dissolved in dichloromethane and then the catalyst was separated magnetically. The magnetic Fe_3O_4 nanoparticles were washed three to four times with CH_2Cl_2 (3 ml) and then dried at 100 °C for 5 h. The separated catalyst was used in six cycles with only a slight decrease in activity, as shown in Fig. 1.

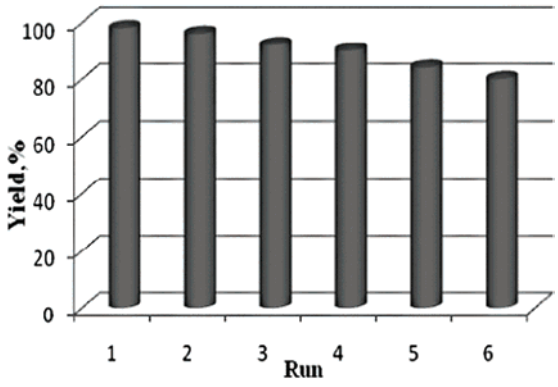

Fig. 1. Recoverability of Fe_3O_4 nanoparticles.

RESULTS AND DISCUSSION

In order to optimize the reaction conditions, the reaction of 4-nitrobenzaldehyde and 2-naphthol was selected as a model system (Scheme 2).

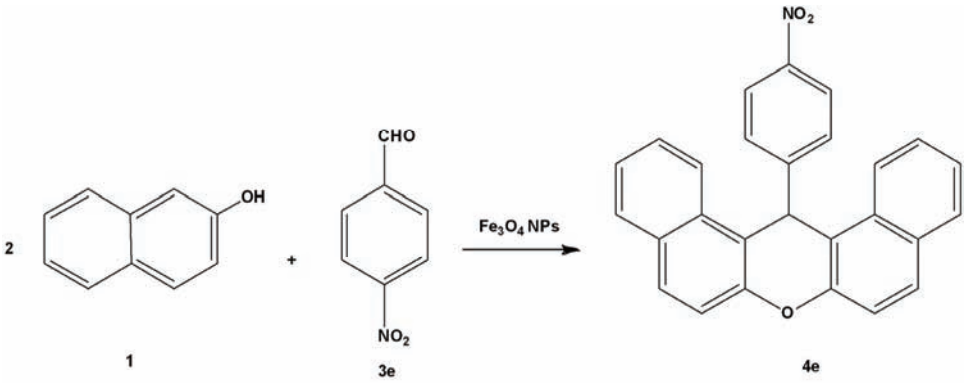

Scheme 2. The model study for the one-pot synthesis of corresponding xanthene.

Initially, to show the merit of the present approach in comparison with other catalysts, the model reaction was performed in the presence of various catalysts, such as CuO, MgO, SiO_2 and Fe_3O_4, for the synthesis of the 14-aryl-14*H*-dibenzo[*a*,*j*]xanthene derivative. As shown in Table I, the magnetite nanoparticles

were the best catalysts with respect to reaction time and yield of the obtained product.

TABLE I. The model reaction catalyzed by various catalysts; yields refer to the isolated products

Entry	Catalyst	Time, min	Yield, %
1	CuO	80	60
2	MgO	87	50
3	Fe_3O_4	60	80
4	SiO_2	90	65

Three types of catalysts were examined, *i.e.*, Fe_3O_4, Fe_3O_4 nanoparticles and recovered Fe_3O_4 nanoparticles. The highest yield of the product was obtained using Fe_3O_4 NPs, which may be due to the better diffusion of nano Fe_3O_4 in the reaction mixture. Astonishingly, the recovered catalyst acted almost the same as the fresh Fe_3O_4 NPs. The results are shown in Fig. 2.

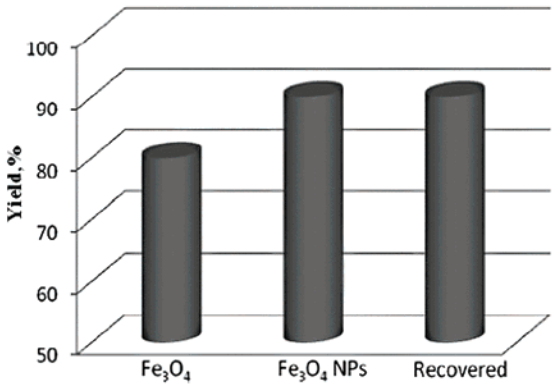

Fig. 2. The effect of different types of Fe_3O_4 in the model reaction.

In order to investigate the morphology and particle size of the Fe_3O_4 nanoparticles, SEM images of the magnetic nanoparticles were taken and the images are presented in Figs. 3a and 3b. These results show that spherical Fe_3O_4 nanoparticles were obtained with an average size between 40–50 nm.

The XRD pattern of the Fe_3O_4 nanoparticles is shown in Fig. 4. All reflection peaks can be readily indexed to pure cubic crystal phase of Fe_3O_4 with F-33m space group (JCDPS No. 75-0449). In addition, no specific peaks due to any impurities were observed. The broad peaks indicate that the particles are in nanoscale size range. The crystallite diameter (D) of the magnetic nanoparticles was calculated by Debye–Scherrer Equation ($D = K\lambda/\beta\cos\theta$), where β, the FWHM (full-width at half-maximum or half-width), is in radians and θ is the position of the maximum of the diffraction peak, K is the so-called shape factor, which usually takes a value of about 0.9, and λ is the X-ray wavelength (1.5406

Å for Cu K_α). The average crystallite size of the prepared nano-Fe_3O_4 was found by SEM analysis to be 45 nm.

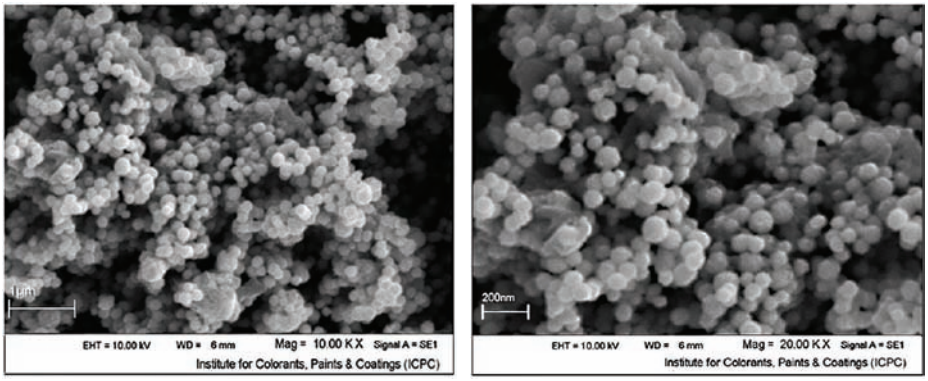

(a) (b)

Fig. 3. SEM images of Fe_3O_4 nanoparticles; magnification: a) 10000×, b) 20000×.

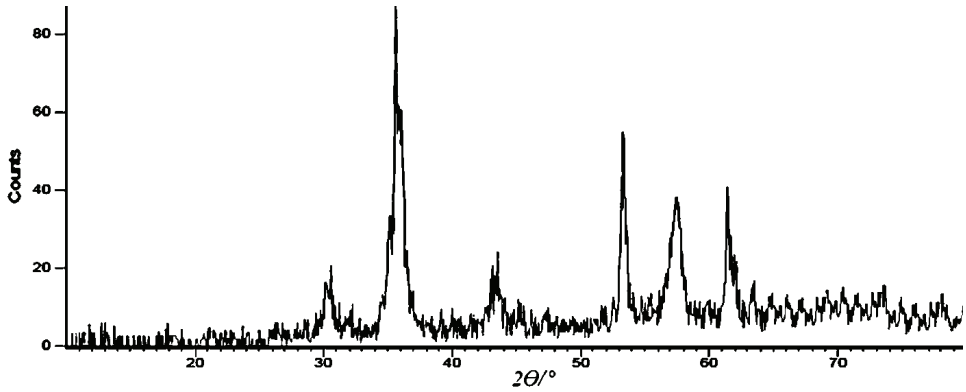

Fig. 4. The XRD pattern of the Fe_3O_4 nanoparticles.

The experimental research was continued using different amounts of nano-catalyst in the reaction involving 4-nitrobenzaldehyde (1 mmol) and 2-naphthol (2 mmol) to afford the product 14-(4-nitrophenyl)-14*H*-dibenzo[*a*,*j*]xanthene under solvent-free conditions at 100 °C. From these experiments, the optimum amount of this catalyst was found to be 10 mol %. Increasing this amount did not result in any significant changes in the yield and time of reaction (Table II).

Then, the effect of solvent was investigated. Thus, the model reaction in the presence of magnetite nanoparticles was run using different solvents and under solvent-free conditions. As shown in Table III, it is noteworthy that the solvent-free conditions afforded the product in excellent yield and shorter reaction time than under solvent conditions.

TABLE II. The effect of the amount of Fe_3O_4 nanoparticles on the model reaction; reaction conditions: 2-naphthol, 2 mmol, 4-nitrobenzaldehyde, 1 mmol, at 100 °C

Entry	Catalyst amount, mol %	Time, min	Yield[a], %
1	–	180	15
2	4	45	55
3	7	30	70
4	10	20	92
5	15	20	92

[b]Isolated yields

In continuations of on-going research using nanoparticles in organic reactions,[50–52] the test reactions of aldehydes with dimedone were encouraging. Thus, the optimized reaction conditions in the presence of Fe_3O_4 NPs were employed to produce 1,8-dioxooctahydroxanthene derivatives. A series of experiments were performed in which a number of 1,8-dioxooctahydroxanthenes were prepared in high yields and short reaction times.

TABLE III. The model reaction in various solvents catalyzed by Fe_3O_4 nanoparticles; yields refer to the isolated products

Entry	Solvent	Time, min	Yield, %
1	CH_2Cl_2	180	60
2	THF	120	70
3	toluene	210	45
4	ethanol	90	75
5	No solvent	20	92

In the present work, magnetic Fe_3O_4 nanoparticles were successfully prepared and then used for the synthesis of 14-aryl-14*H*-dibenzo[*a*,*j*]xanthene and 1,8-dioxooctahydroxanthene derivatives. Application of this catalytic system effectively gives the desired products in excellent yields (Table IV). As seen from Table IV, aromatic aldehydes with electron-withdrawing groups as expected reacted faster than those with electron-releasing groups. Sterically hindered aromatic aldehydes required longer reaction times.

A plausible mechanism for the synthesis of 1,8-dioxooctahydroxanthene derivatives using magnetite nanoparticles as catalyst is shown in Scheme 3. Based on the present experimental results together with some literature data,[54–57] it is supposed that catalytically active site of Fe_3O_4 NPs is Fe^{3+} that behaves as a Lewis acid and coordinates to the carbonyl groups of dimedone and the aldehyde. This interaction accelerates the conjugation and directs the additions of the nucleophiles to the corresponding substrates. Finally, product **5** was obtained and the Fe_3O_4 nanoparticles were released for further reactions. Moreover, the effect of the catalytic behavior of Fe_3O_4 NPs in the synthesis of 14-aryl-14*H*-dibenzo[*a*,*j*]xanthenes was the same as the above-mentioned mechanism for the preparation of 1,8-dioxooctahydroxanthenes.

TABLE IV. Synthesis of 14-aryl-14*H*-dibenzo[*a*,*j*]xanthenes (**4**) and 1,8-dioxooctahydroxanthenes (**5**) by Fe_3O_4 nanoparticles

Entry	Ar	Products **4a–o** Time, min/Yield[a], %	M.p. / °C	Products **5a–o** Time, min/Yield, %	M.p. / °C
a	C_6H_5	30/88	184–185[26]	30/89	203–205[43]
b	4-$MeOC_6H_4$	35/85	203–205[26]	35/85	242–245[43]
c	4-ClC_6H_4	20/90	289–290[26]	20/88	230–233[43]
d	4-BrC_6H_4	20/90	297–298[26]	20/88	226–229[43]
e	4-$NO_2C_6H_4$	20/92	311–312[26]	15/90	225–226[43]
f	4-MeC_6H_4	35/86	227–229[26]	35/87	212–214[43]
g	2-$NO_2C_6H_4$	25/89	215–217[28]	30/89	246–248[43]
h	4-FC_6H_4	20/91	239–240[26]	20/90	225–227[49]
i	3-ClC_6H_4	35/85	210–212[28]	35/86	184–185[49]
j	4-OHC_6H_4	40/85	135–136[26]	40/85	244–246[43]
k	3-$NO_2C_6H_4$	20/90	210–211[26]	20/89	165–167[49]
l	4-$(CH_3)_2CHC_6H_4$	35/85	152–154[36]	40/80	203–206[b]
m	4-NCC_6H_4	30/92	209–211[53]	25/90	216–217[53]
n	4-$MeSC_6H_4$	35/85	264–266[39]	35/86	256–257[b]
o	4-$CHOC_6H_4$	30/90	252–254[39]	30/89	211–213[b]

[a]Isolated yield; [b]new compounds

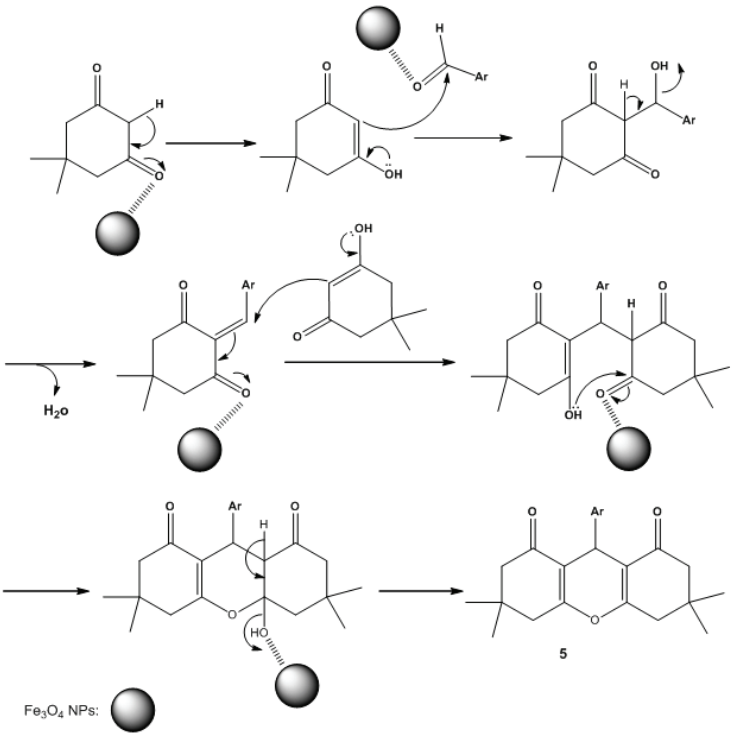

Scheme 3. Proposed reaction pathway for the synthesis of 1,8-dioxooctahydroxanthenes by Fe_3O_4 nanoparticles.

CONCLUSIONS

In conclusion, the efficient one-pot syntheses of 14-aryl-14*H*-dibenzo[*a*,*j*]-xanthenes and 1,8-dioxooctahydroxanthene derivatives from 2-naphthol, dimedone with various aldehydes using magnetically separable Fe_3O_4 nanoparticles, found to be an eco-environmentally friendly catalyst under solvent-free conditions, was demonstrated. The simplicity, easy workup, as well as safety and reusability of the catalyst are the advantages of this procedure over previously reported ones.

SUPPLEMENTARY MATERIAL

Spectral data for all of the compounds are available electronically from http://www.shd.org.rs/JSCS/, or from the corresponding author on request.

Acknowledgements. The authors gratefully acknowledge the financial support of this work by the Research Affairs Office of the Islamic Azad University, Qom Branch, Qom, I. R. Iran.

ИЗВОД

Fe_3O_4 НАНОЧЕСТИЦЕ: ВИСОКО ЕФИКАСАН КАТАЛИЗАТОР ЗА СИНТЕЗУ ДЕРИВАТА КСАНТЕНА У ЈЕДНОМ РЕАКЦИОНОМ КОРАКУ, БЕЗ УПОТРЕБЕ РАСТВАРАЧА

MOHAMMAD ALI GHASEMZADEH[1], JAVAD SAFAEI-GHOMI[1] и SAFURA ZAHEDI[2]

[1] *Department of Chemistry, Qom Branch, Islamic Azad University, Qom, I. R. Iran и* [2] *Department of Organic Chemistry, Faculty of Chemistry, University of Kashan, 51167-Kashan, I. R. Iran*

Наночестице Fe_3O_4, погодне за издвајање магнетом, омогућавају еколошки прихватљив поступак за синтезу деривата 14-арил-14*H*-дибензо[*a*,*j*]ксантена и 1,8-диоксооктахидроксантена. Једињења су добијена из димедона и 2-нафтола са различитим ароматичним алдехидима, без растварача у високом приносу и кратком реакционом времену. Катализатор се може изоловати уз помоћ екстерног магнета и поново користити у шест реакционих циклуса без већег губитка активности.

(Примљено 24. јуна, ревидирано 9. децембра 2012)

REFERENCES

1. Z. Bing, H. Scott, R. Raja, G. A. Somorjai, *Nanotechnology in Catalysis*, Vol. 3, Springer, Ottawa, 2007
2. H. Jiang, L. Gai, Y. Tian, *J. Serb. Chem. Soc.* **76** (2011) 923
3. A. H. Lu, E. L. Salabas, F. Schuth, *Angew. Chem., Int. Ed.* **46** (2007) 1222
4. A. H. Latham, M. E. Williams, *Acc. Chem. Res.* **41** (2008) 411
5. S. Laurent, D. Forge, M. Port, A. Roch, C. Robic, L. V. Elst. R. N. Muller, *Chem. Rev.* **108** (2008) 2064
6. C. T. Yavuz, J. T. Mayo, W. W. Yu, A. Prakash, J. C. Falkner, S. Yean, L. Cong, H. J. Shipley, A. Kan, M. Tomson, D. Natelson, V. L. Colvin, *Science* **314** (2006) 964
7. L. M. Rossi, F. P. Silva, L. L. R. Vono, P. K. Kiyohara, E. L. Duarte, R. Itri, R. Landers, G. Machado, *Green Chem.* **9** (2007) 379
8. P. D. Stevens, J. Fan, H. M. R. Gardimalla, M. Yen, Y. Gao, *Org. Lett.* **7** (2005) 2085
9. H. Y. Lü, S. H. Yang, J. Deng, Z. H. Zhang, *Aust. J. Chem.* **63** (2010) 1290

10. S. M. Roopan, F. R. Nawaz-Khan, B. K. Mandal, *Tetrahedron Lett.* **51** (2010) 2309
11. T. Zeng, W. Chen, C. M. Cirtiu, A. Moores, G. Song, C. Li, *Green Chem.* **12** (2010) 570
12. V. Polshettiwar, R. S. Varma, *Tetrahedron* **66** (2010) 1091
13. R. W. Lambert, J. A. Martin, J. H. Merrett, K. E. B. Parkes, G. J. Thomas, PCT Int. Appl., WO 9706178, 1997; *CA* **126** (1997) 212377y
14. T. Hideo, J. Teruomi, Jpn. Tokkyo Koho, JP 56005480, 1981; *CA* **95** (1981) 80922b
15. H. N. Hafez, M. I. Hegab, I. S. Ahmed-Farag, A. B. A. El-Gazzar, *Bioorg. Med. Chem. Lett.* **18** (2008) 4538
16. S. M. Menchen, S. C. Benson, J. Y. L. Lam, W. Zhen, D. Sun, B. B. Rosenblum, S. H. Khan, M. Taing, U. S. Patent, US 6583168, 2003; *CA* **139** (2003) 54287f
17. M. Ahmad, T. A. King, K. Do-Kyeong, B. H. Cha, J. Lee, *J. Phys., D* **35** (2002) 1473
18. C. G. Knight, T. Stephens, *Biochem. J.* **258** (1989) 683
19. G. Casiraghi, G. Casnati, M. Cornia, *Tetrahedron Lett.* **14** (1973) 679
20. A. Bekaert, J. Andrieux, M. Plat, *Tetrahedron Lett.* **33** (1992) 2805
21. D. W. Knight, P. B. Little, *J. Chem. Soc., Perkin Trans. 1* (2001) 1771
22. C. W. Kuo, J. M. Fang, *Synth. Commun.* **31** (2001) 877
23. J. Q. Wang, R. G. Harvey, *Tetrahedron* **58** (2002) 5927
24. A. Jha, J. Beal, *Tetrahedron Lett.* **45** (2004) 8999
25. Z. Karimi-Jaberi, S. Z. Abbasi, B. Pooladian, M. E. Jokar, *E-J. Chem.* **8** (2011) 1895
26. S. Allameh, A. Davoodnia, A. Khojastehnezhad, *Chin. Chem. Lett.* **23 (**2012) 17
27. D. Prasd, M. Nath, *Catal. Sci. Technol.* **2** (2012) 93
28. M. A. Zolfigol, A. R. Moosavi-Zare, P. Arghavani-Hadi, A. Zare, V. Arghavani-Hadi, G. Arghavani-Hadi, *RSC Advances* **2** (2012) 3618
29. N. G. Khaligh, *Ultrason. Sonochem.* **19** (2012) 736
30. R. K. FischerHunnur, B. Sunilkumar, P. S. Kumar, N. Srinivasulu, R. H. Udupi, V. Himabindu, *Chem. Heterocycl. Compd.* **44** (2008) 143
31. E. Soleimani, M. Zainal, S. Lotfi, *Lett. Org. Chem.* **8** (2011) 573
32. E. Soleimani, M. H. Khodei, A. T. Kal Koshvandi, *Chin. Chem. Lett.* **22** (2011) 927
33. G. Mohammadi Ziarani, A.-R. Badiei, M. Azizi, *Scientia Iranica, C* **18** (2011) 453
34. M. Hong, C. Cai, *J. Fluorine Chem.* **130** (2009) 989
35. H. Eshghi, M. Bakavoli, H. Moradi, *Org. Prep. Proced. Int.* **43** (2011) 302
36. R. Kumar, G. C. Nandi, R. K. Verma, M. S. Singh, *Tetrahedron Lett.* **5** (2010) 442
37. A. Rahmatpour, J. Aalaie, *Heteroat. Chem.* **22** (2011) 51
38. B. F. Mirjalili, A. Bamoniri, A. Akbari, N. Taghavinia, *J. Iran. Chem. Soc.* **8** (2011) S129
39. J. Safaei-Ghomi, M. A. Ghasemzadeh, *J. Saud. Chem. Soc*, in Press, http:// //dx.doi.org/10.1016/j.jscs.2012.05.007
40. J. Mondala, M. Nandia, A. Modaka, A. Bhaumik, *J. Mol. Catal., A* **363**–**364** (2012) 254
41. M. Nandi, J. Mondal, K. Sarkar, Y. Yamauchi, A. Bhaumik. *Chem. Commun.* **47** (2011) 6677
42. T. S. Jin, J. S. Zhang, A. Q. Wang, T. S. Li, *Synth. Commun.* **35** (2005) 2339
43. T. S. Jin, J. S. Zhang, J. C. Xiao, A. Q. Wang, T. S. Li, *Synlett.* **5** (2004) 866
44. X. Fan, X. Hu, X. Zhang, J. Wang, *Can. J. Chem.* **83** (2005) 16
45. G. Song, B. Wang, H. Luo, L. Yang, *Catal. Commun.* **8** (2007) 673
46. B. Das, P. Thirupathi, I. Mahender, K. R. Reddy, B. Ravikanth, L. Nagarapu, *Catal. Commun.* **8** (2007) 535

47. B. Das, P. Thirupathi, I. Mahender, V. S. Reddy, Y. K. Rao, *J. Mol. Catal., A* **247** (2006) 233
48. M. Seyyedhamzeh, P. Mirzaei, A. Bazgir, *Dyes Pigm.* **76** (2008) 836
49. A. N. Dadhania, V. K. Patel, D. K. Raval, *C. R. Chim.* **15** (2012) 378
50. M. A. Ghasemzadeh, J. Safaei-Ghomi, H. Molaei, *C. R. Chim.* **15** (2012) 696
51. J. Safaei-Ghomi, A. Ziarati, S. Zahedi, *J. Chem. Sci.* **124** (2012) 933
52. J. Safaei-G., M. A.Ghasemzadeh, S. Zahedi, *S. Afr. J. Chem.* **65** (2012) 191
53. a) W. Su, D. Yang, C. Jin, B. Zhang, *Tetrahedron Lett.* **21** (2008) 3391; b) F. Darviche, S. Balalaie, F. Chadegani, P. Salehi, *Synth. Commun.* **37** (2007) 1059
54. Y. Joseph, C. Kuhrs, W. Ranke, M. Ritter, W. Weiss, *Chem. Phys. Lett.* **314** (1999) 195
55. R. Martnez, D. J. Ram, M. Yusa, *Adv. Synth. Catal*. **350** (2008) 1235
56. B. Sreedhar, A. S. Kumar, P. S. Reddy, *Tetrahedron Lett.* **51** (2010) 1891
57. M. M. Mojtahedi, M. S. Abaee, T. Alishiri, *Tetrahedron Lett.* **50** (2009) 2322.

Journal of the Serbian Chemical Society
JSCS@tmf.bg.ac.rs • www.shd.org.rs/JSCS
J. Serb. Chem. Soc. 78 (6) S62–S74 (2013) *Supplementary material*

SUPPLEMENTARY MATERIAL TO

Fe_3O_4 nanoparticles: a highly efficient and easily reusable catalyst for the one-pot synthesis of xanthene derivatives under solvent-free conditions

MOHAMMAD ALI GHASEMZADEH[1], JAVAD SAFAEI-GHOMI[1]* and SAFURA ZAHEDI[2]

[1]*Department of Chemistry, Qom Branch, Islamic Azad University, Qom, I. R. Iran and* [2]*Department of Organic Chemistry, Faculty of Chemistry, University of Kashan, 51167-Kashan, I. R. Iran*

J. Serb. Chem. Soc. 78 (6) (2013) 769–779

SPECTRAL DATA FOR KNOWN COMPOUNDS

*14-Phenyl-14*H*-dibenzo[*a,j*]xanthene (**4a**).* White crystals; yield: 88 %; m.p.: 181–183 °C; Anal. Calcd. for $C_{27}H_{18}O$ (FW: 358.14): C, 90.47; H 5.06 %. Found: C, 90.22; H, 5.21 %; FT-IR (KBr, cm^{-1}): 3052 (=C–H stretching of aromatic ring), 1625 (C=C– stretching of aromatic ring), 1575, 1253 (C–O stretching), 814; ^{1}H-NMR (400 MHz, $CDCl_3$, δ / ppm): 6.44 (1H, *s*, CH), 7.16 (2H, *d*, *J* = 8.0 Hz, Ar-H), 7.25–7.33 (4H, *m*, Ar-H), 7.37–7.41 (5H, *m*, Ar-H), 7.46 (4H, *t*, *J* = 7.8 Hz, Ar-H), 7.72 (2H, *d*, *J* = 8.0 Hz, Ar-H); ^{13}C-NMR (100 MHz, $CDCl_3$, δ / ppm): 31.9 (CH), 115.8,116.5, 119.2, 123.1, 124.9, 126.6, 128.2, 129.5, 130.2, 132.2, 136.9, 141.5, 148.1, 149.9 (Ar–C).

*14-(4-Methoxyphenyl)-14*H*-dibenzo[*a,j*]xanthene (**4b**).* Yellow crystals; yield: 85 %; m.p.: 202–204 °C; Anal. Calcd. for $C_{28}H_{20}O_2$ (FW: 388.15): C, 86.57; H, 5.19 %. Found: C, 86.72; H, 5.06 %; FT-IR (KBr, cm^{-1}): 3042 (=C–H stretching of aromatic ring), 1625 (C=C– stretching of aromatic ring), 1594, 1251 (C–O stretching), 1236 (C–O stretching), 811; ^{1}H-NMR (400 MHz, $CDCl_3$, δ / / ppm): 3.62 (3H, *s*, OCH_3), 6.45 (1H, *s*, CH), 6.68 (2H, *d*, *J* = 7.9 Hz, Ar-H), 7.27–7.40 (4H, *m*, Ar-H), 7.42–7.46 (4H, *m*, Ar-H), 7.79 (2H, *d*, *J* = 8.0 Hz, Ar-H), 8.83 (2H, *d*, *J* = 8.0 Hz, Ar-H), 8.39 (2H, *d*, *J* = 7.9 Hz, Ar-H); ^{13}C-NMR (100 MHz, $CDCl_3$, δ / ppm): 37.1 (CH), 55.1 (OCH_3), 113.8, 117.5, 118.0, 122.7, 124.7, 126.7, 128.7, 128.8, 129.2, 131.1, 131.4, 137.4, 148.6, 157.8 (Ar–C).

*14-(4-Chlorophenyl)-14*H*-dibenzo[*a,j*]xanthene (**4c**).* Yellow crystals; yield: 90 %; m.p.: 289–290 °C; Anal. Calcd. for $C_{27}H_{17}ClO$ (FW: 392.10): C, 82.54; H, 4.36 %. Found: C, 86.27; H, 4.52 %; FT-IR (KBr, cm^{-1}): 3044 (=C–H

* Corresponding author. E-mail: safaei@kashanu.ac.ir

stretching of aromatic ring), 1621 (C=C– stretching of aromatic ring), 1588, 1246 (C–O stretching), 814; ^{1}H-NMR (400 MHz, $CDCl_3$, δ / ppm): 6.46 (1H, *s*, CH), 7.11 (2H, *d*, *J* = 8.1 Hz, Ar-H), 7.26–7.45 (6H, *m*, Ar-H), 7.48 (2H, *t*, *J* = 7.6 Hz, Ar-H), 7.57–7.82 (4H, *m*, Ar-H), 8.32 (2H, *d*, *J* = 8.1 Hz, Ar-H); ^{13}C-NMR (100 MHz, $CDCl_3$, δ / ppm): 36.9 (CH), 115.8, 116.9, 118.1, 121.3, 124.2, 125.8, 127.5, 128.1, 129.5, 131.3, 132.2, 136.3, 148.5, 158.7 (Ar–C).

*14-(4-Bromophenyl)-14*H-*dibenzo[*a,j*]xanthene* (***4d***). Yellow crystals; yield: 90 %; m.p.: 296–297 °C; Anal. Calcd. for $C_{27}H_{17}BrO$ (FW: 436.05): C, 74.15; H, 3.92 %. Found: C, 74.31; H, 3.71 %; FT-IR (KBr, cm^{-1}): 3042 (=C–H stretching of aromatic ring), 1624 (C=C– stretching of aromatic ring), 1521, 1244 (C–O stretching), 812; ^{1}H-NMR (400 MHz, $CDCl_3$, δ / ppm): 6.45 (1H, *s*, CH), 7.18 (2H, *d*, *J* = 8.1 Hz, Ar-H), 7.23–7.31 (4H, *m*, Ar-H), 7.40 (2H, *t*, *J* = 7.8 Hz, Ar-H), 7.44–7.49 (6H, *m*, Ar-H), 8.17 (2H, *d*, *J* = 8.1 Hz, Ar-H); ^{13}C-NMR (100 MHz, $CDCl_3$, δ / ppm): 37.1 (CH), 116.1, 116.9, 117.8, 121.3, 123.1, 125.4, 127.2, 127.9, 130.1, 132.2, 133.7, 136.9, 146.5, 155.9 (Ar–C).

*14-(4-Nitrophenyl)-14*H-*dibenzo[*a,j*]xanthene* (***4e***). Yellow crystals; Yield: 92 %; m.p.: 311–312 °C; Anal. Calcd. for $C_{27}H_{17}NO_3$ (FW: 403.12): C, 80.38; H, 4.25; N, 3.47 %. Found: C, 80.54; H, 4.31; N, 3.28 %; FT-IR (KBr, cm^{-1}): 3041 (=C–H stretching of aromatic ring), 1622 (C=C– stretching of aromatic ring), 1583, 1548 (NO_2), 1348 (NO_2), 1242 (C–O stretching), 809; ^{1}H-NMR (400 MHz, $CDCl_3$, δ / ppm): 6.61 (1H, *s*, CH), 7.44 (2H, *t*, *J* = 8.0 Hz, Ar-H), 7.52 (2H, *d*, *J* = 8.1 Hz, Ar-H), 7.60 (2H, *t*, *J* = 8.0 Hz, Ar-H), 7.69 (2H, *d*, *J* = = 8.1 Hz, Ar-H), 7.84–7.87 (4H, *m*, Ar-H), 8.01 (2H, *d*, *J* = 8.0 Hz, Ar-H), 8.29 (2H, *d*, *J* = 8.0 Hz, Ar-H); ^{13}C-NMR (100 MHz, $CDCl_3$, δ / ppm): 36.9 (CH), 115.9, 116.2, 117.1, 120.2, 122.5, 124.8, 126.1, 128.1, 129.7, 132.6, 134.1, 135.9, 148.3, 159.1 (Ar–C).

*14-(*p-*Tolyl)-14*H-*dibenzo[*a,j*]xanthene* (***4f***). Yellow crystals; yield: 86 %; m.p.: 228–230 °C; Anal. Calcd. for $C_{28}H_{20}O$ (FW: 372.15): C, 90.29; H, 5.41 %. Found: C, 90.52; H, 5.25 %; FT-IR (KBr, cm^{-1}): 3047 (=C–H stretching of aromatic ring), 1619 (C=C– stretching of aromatic ring), 1515, 1249 (C–O stretching), 809; ^{1}H-NMR (400 MHz, $CDCl_3$, δ / ppm): 2.16 (3H, *s*, CH_3), 6.46 (1H, *s*, CH), 6.96 (2H, *d*, *J* = 7.9 Hz, Ar-H), 7.39–7.43 (4H, *m*, Ar-H), 7.49 (2H, *d*, *J* = 8.1 Hz, Ar-H), 7.57 (2H, *d*, *J* = 7.9 Hz, Ar-H), 7.78–7.84 (4H, *m*, Ar-H), 8.41 (2H, *d*, *J* = 8.1 Hz, Ar-H); ^{13}C-NMR (100 MHz, $CDCl_3$, δ / ppm): 20.9 (CH_3), 37.7 (CH), 116.3, 117.5, 118.1, 122.8, 124.2, 126.8, 128.1, 128.8, 129.2, 131.1, 135.9, 142.2, 148.7, 149.8 (Ar–C).

*14-(2-Nitrophenyl)-14*H-*dibenzo[*a,j*]xanthene* (***4g***). White crystals; yield: 89 %; m.p.: 214–216 °C; Anal. Calcd. for $C_{27}H_{17}NO_3$ (FW: 403.12): C, 80.38; H, 4.25; N, 3.47 %. Found: C, 80.21; H, 4.33; N, 3.58 %; FT-IR (KBr, cm^{-1}): 3067 (=C–H stretching of aromatic ring), 2925, 1548 (NO_2), 1481 (C=C– stretching of aromatic ring), 1357 (NO_2), 1243 (C–O stretching), 749; ^{1}H-NMR (400 MHz,

$CDCl_3$, δ / ppm): 6.81 (1H, *s*, CH), 6.84–7.27 (4H, *m*, Ar-H), 7.41–7.50 (4H, *m*, Ar-H), 7.61 (2H, *t*, *J* = 7.9 Hz, Ar-H), 7.80–7.84 (4H, *m*, Ar-H), 8.42 (2H, *t*, *J* = = 7.8 Hz, Ar-H); ^{13}C-NMR (100 MHz, $CDCl_3$, δ / ppm): 30.2 (CH), 115.1, 115.2, 116.7, 117.9, 122.3, 124.4, 125.1, 127.1, 128.2, 128.6, 129.1, 130.9, 131.1, 131.5, 132.4 (Ar–C).

*14-(4-Fluorophenyl)-14*H-*dibenzo[*a,j*]xanthene* (***4h***). Yellow crystals; yield: 91 %; m.p.: 238–240 °C; Anal. Calcd. for $C_{27}H_{17}FO$ (FW: 376.13): C, 86.15; H, 4.55 %. Found: C, 86.28; H, 4.41 %; FT-IR (KBr, cm^{-1}): 3052 (=C–H stretching of aromatic ring), 1618 (C=C– stretching of aromatic ring), 1581, 1223 (C–O stretching), 812; ^{1}H-NMR (400 MHz, $CDCl_3$, δ / ppm): 6.41 (1H, *s*, CH), 7.07 (2H, *d*, *J* = 8.0 Hz, Ar-H), 7.17–7.24 (4H, *m*, Ar-H), 7.38 (2H, *d*, *J* = 7.9 Hz, Ar-H), 7.51–7.54 (6H, *m*, Ar-H), 8.12 (2H, *d*, *J* = 8.0 Hz, Ar-H); ^{13}C-NMR (100 MHz, $CDCl_3$, δ / ppm): 36.8 (CH), 115.8, 117.1, 117.7, 122.1, 124.5, 125.2, 127.7, 127.9, 131.6, 132.1, 133.8, 137.1, 146.5, 156.1 (Ar–C).

*14-(3-Chlorophenyl)-14*H-*dibenzo[*a,j*]xanthene* (***4i***). White crystals; yield: 85 %; m.p.: 211–212 °C; Anal. Calcd. for $C_{27}H_{17}ClO$ (FW: 392.10): C, 82.54; H, 4.36 %. Found: C, 82.41; H, 4.48 %; FT-IR (KBr, cm^{-1}): 3045 (=C–H stretching of aromatic ring), 1592, 1513 (C=C– stretching of aromatic ring), 1247 (C–O stretching), 808; ^{1}H-NMR (400 MHz, $CDCl_3$, δ / ppm): 6.46 (1H, *s*, CH), 7.12 (2H, *d*, *J* = 7.9 Hz, Ar-H), 7.26 (2H, *d*, *J* = 8.1 Hz, Ar-H), 7.54–7.62 (5H, *m*, Ar-H), 7.79–7.84 (4H, *m*, Ar-H), 8.22 (1H, *s*, Ar-H), 8.27 (2H, *d*, *J* = 7.9 Hz, Ar-H); ^{13}C-NMR (100 MHz, $CDCl_3$, δ / ppm): 35.9 (CH), 117.1, 117.8, 118.5, 123.1, 125.1, 126.4, 127.1, 128.3, 129.5, 130.1, 132.3, 136.1, 138.1, 147.4, 152.2, 159.9, 163.1 (Ar–C).

*14-(4-Hydroxyphenyl)-14*H-*dibenzo[*a,j*]xanthene* (***4j***). White crystals; Yield: 85 %; m.p.: 135–136 °C; Anal. Calcd. for $C_{27}H_{18}O_2$ (FW: 374.13): C, 86.61; H, 4.85 %. Found: C, 86.42; H, 4.98 %; FT-IR (KBr, cm^{-1}): 3441 (OH stretching), 3060 (=C–H stretching of aromatic ring), 1623 (C=C– stretching of aromatic ring), 1581, 1244 (C–O stretching), 819; ^{1}H-NMR (400 MHz, $CDCl_3$, δ / ppm): 5.54 (1H, *bs*, OH), 6.44 (1H, *s*, CH), 6.87–6.91 (4H, *m*, Ar-H), 7.12 (2H, *d*, *J* = = 7.8 Hz, Ar-H), 7.22–7.26 (4H, *m*, Ar-H), 7.39 (4H, *d*, *J* = 8.0 Hz, Ar-H), 7.52 (2H, *d*, *J* = 7.8 Hz, Ar-H); ^{13}C-NMR (100 MHz, $CDCl_3$, δ / ppm): 36.8 (CH), 114.9, 116.8, 118.3, 121.5, 123.8, 125.2, 126.1, 127.2, 128.9, 130.5, 132.5, 135.1, 144.2, 152.7.

*14-(3-Nitrophenyl)-14*H-*dibenzo[*a,j*]xanthene* (***4k***). Yellow crystals; yield: 90 %; m.p.: 208–210 °C; Anal. Calcd. for $C_{27}H_{17}NO_3$ (FW: 403.12): C, 80.38; H, 4.25; N, 3.47 %. Found: C, 80.61; H, 4.38; N, 3.20 %; FT-IR (KBr, cm^{-1}): 3045 (=C–H stretching of aromatic ring), 1626 (C=C– stretching of aromatic ring), 1551 (NO_2), 1344 (NO_2), 1241 (C–O stretching), 811; ^{1}H-NMR (400 MHz, $CDCl_3$, δ / ppm): 6.60 (1H, *s*, CH), 6.65 (1H, *s*, Ar-H) 7.41–7.44 (3H, *m*, Ar-H), 7.48 (2H, *d*, *J* = 7.9 Hz, Ar-H), 7.51–7.54 (4H, *m*, Ar-H), 7.64 (2H, *d*, *J* =

= 7.9 Hz, Ar-H), 7.83–7.87 (4H, *m*, Ar-H); ^{13}C-NMR (100 MHz, $CDCl_3$, δ / ppm): 37.3 (CH), 116.3, 116.8, 117.4, 121.1, 122.3, 125.4, 126.9, 128.2, 129.1, 134.7, 136.3, 137.1, 138.2, 146.5, 147.9, 158.3.

*14-(4-Isopropylphenyl)-14*H-*dibenzo[*a,j*]xanthene* (***4l***). Yellow crystals; yield: 85 %; m.p.: 152–154 °C; Anal. Calcd. for $C_{30}H_{24}O$ (FW: 400.18): C, 89.97; H, 6.04 %. Found: C, 89.73; H, 6.18 %; FT-IR (KBr, cm^{-1}): 3048 (=C–H stretching of aromatic ring), 1578 (C=C– stretching of aromatic ring), 1510, 1244 (C–O stretching), 806; ^{1}H-NMR (400 MHz, $CDCl_3$, δ / ppm): 2.22 (6H, *d*, 2×CH_3), 3.1 (1H, *m*, C**H**(CH_3)$_2$), 6.46 (1H, *s*, CH), 6.85 (2H, *d*, *J* = 8.0 Hz, Ar-H), 7.12–7.41 (4H, *m*, Ar-H), 7.48–7.53 (4H, *m*, Ar-H), 7.68–7.71 (4H, *m*, Ar-H), 7.87 (2H, *d*, *J* = 8.0 Hz, Ar-H); ^{13}C-NMR (100 MHz, $CDCl_3$, δ / ppm): 23.8 (2×CH_3), 33.5 (CH), 37.6 (CH), 117.6, 118.1, 122.8, 124.2, 126.4, 126.5, 126.7, 128.0, 128.8, 131.1, 131.5, 142.3, 146.6, 148.8 (Ar–C).

*4-(14*H-*dibenzo[a,j]xanthen-14-yl)benzonitrile* (***4m***). White crystals; yield: 92 %; m.p.: 209–211 °C; Anal. Calcd. for $C_{28}H_{17}NO$ (FW: 383.13): C, 87.71; H, 4.47; N, 3.65 %. Found: C, 87.58; H, 4.59; N, 3.78 %. FT-IR (KBr, cm^{-1}): 3041 (=C–H stretching of aromatic ring), 2218 (C≡N stretching), 1622, 1583 (C=C– stretching of aromatic ring), 1242 (C–O stretching), 809; ^{1}H-NMR (400 MHz, $CDCl_3$, δ / / ppm): 6.55 (1H, *s*, CH), 7.45 (4H, *t*, Ar-H), 7.50 (2H, *d*, *J* = 8.8 Hz, Ar-H), 7.61 (4H, *q*, Ar-H), 7.85 (4H, *t*, *J* = 8.4 Hz, Ar-H), 8.28 (2H, *d*, *J* = 8.2 Hz, Ar-H); ^{13}C-NMR (100 MHz, $CDCl_3$, δ / ppm): 38.0 (CH), 110.3 (Ar–C), 115.9 (C≡N), 118.0, 118.6, 122.0, 124.5, 127.1, 128.8, 129.0, 129.5, 131.0, 131.1, 132.5, 148.7, 150.0 (Ar–C); MS-EI (m/z): 383.13 (M^+).

*14-(4-(Methylthio)phenyl)-14*H-*dibenzo[*a,j*]xanthene* (***4n***). Yellow crystals; yield: 85 %; m.p.: 263–265 °C; Anal. Calcd. for $C_{28}H_{20}OS$ (FW: 404.54): C, 83.14; H, 4.98 %. Found: C, 83.27; H, 4.86 %; FT-IR (KBr, cm^{-1}): 3046 (=C–H stretching of aromatic ring), 1621 (C=C– stretching of aromatic ring), 1592, 1228 (C–O stretching), 1156 (C–S), 815; ^{1}H-NMR (400 MHz, $CDCl_3$, δ / ppm): 2.81 (3H, *s*, SCH_3), 6.42 (1H, *s*, CH), 6.83 (2H, *d*, *J* = 8.1 Hz, Ar-H), 7.34–7.42 (4H, *m*, Ar-H), 7.51–7.56 (4H, *m*, Ar-H), 7.66–7.74 (4H, *m*, Ar-H), 8.25 (2H, *d*, *J* = 8.1 Hz, Ar-H); ^{13}C-NMR (100 MHz, $CDCl_3$, δ / ppm): 21.2 (SCH_3), 34.2 (CH), 112.1, 116.9, 117.1, 121.9, 123.9, 126.5, 127.1, 128.8, 129.1, 130.9, 131.5, 138.1, 147.5, 156.1 (Ar–C).

*4-(14*H-*Dibenzo[*a,j*]xanthen-14-yl)benzaldehyde* (***4o***). Pink crystals; yield: 90 %; m.p.: 252–254 °C; Anal. Calcd. for $C_{28}H_{18}O_2$ (FW: 386.13): C, 87.03; H, 4.69 % Found: C, 87.26; H, 4.51 %; FT-IR (KBr, cm^{-1}): 3060 (=C–H stretching of aromatic ring), 2923, 2765 (–CHO), 1691 (–C=O stretching of –CHO), 1595 (C=C– stretching of aromatic ring), 1513, 1243 (C–O stretching), 819; ^{1}H-NMR (400 MHz, $CDCl_3$, δ / ppm): 6.58 (1H, *s*, CH), 7.18 (2H, *d*, *J* = 8.0 Hz, Ar-H), 7.43 (2H, *t*, *J* = 7.8 Hz, Ar-H), 7.50–7.68 (4H, *m*, Ar-H), 7.70–7.78 (4H, *m*, Ar-H),

7.84 (2H, *t*, *J* = 7.6 Hz, Ar-H), 8.34 (2H, *d*, *J* = 8.0 Hz, Ar-H), 9.79 (1H, *s*, CHO); ^{13}C-NMR (100 MHz, $CDCl_3$, δ / ppm): 33.5 (CH), 117.6, 118.1, 122.8, 124.2, 126.4, 126.5, 126.7, 128.7, 128.8, 131.1, 131.5, 142.3, 146.6, 148.8 (Ar-C), 192.3 (–C=O).

*3,4,6,7-Tetrahydro-3,3,6,6-tetramethyl-9-phenyl-2*H*-xanthene-1,8(*5H,9H*)-dione (**5a**)*. White solid; yield: 89 %; m.p.: 203–205 °C; Anal. Calcd. for $C_{23}H_{26}O_3$ (FW: 350.19): C, 78.83; H, 7.48 %. Found: C, 78.72; H, 7.59 %; FT-IR (KBr, cm^{-1}): 3052 (=C–H stretching of aromatic ring), 2942, 1661 (C=O), 1618 (C=C– stretching of aromatic ring), 1362, 1199 (C–O stretching); ^{1}H-NMR (400 MHz, $CDCl_3$, δ / ppm): 0.99 (6H, *s*, 2×CH_3), 1.10 (6H, *s*, 2×CH_3), 1.99––2.12 (4H, *m*, 2×CH_2), 2.46 (4H, *s*, 2×CH_2), 4.67 (1H, *s*, CH), 7.24–7.28 (5H, *m*, Ar-H); ^{13}C-NMR (100 MHz, $CDCl_3$, δ / ppm): 27.6 (2×CH_3), 28.2 (2×CH_3), 32.1 (2×**C**$(CH_3)_2$), 32.5 (CH), 40.8 (2×CH_2), 50.8 (2×CH_2), 110.2, 119.0, 129.2, 132.0, 149.4, 162.9 (Ar–C), 196.3 (C=O).

*9-(4-Methoxyphenyl)-3,3,6,6-tetramethyl-3,4,5,6,7,9-hexahydro-1*H*-xanthene-1,8(2*H*)-dione (**5b**)*. White solid; yield: 85 %; m.p.: 242–245 °C; Anal. Calcd. for $C_{24}H_{28}O_4$ (FW: 383.20): C, 75.76; H, 7.42 %. Found: C, 75.62; H, 7.57 %; FT-IR (KBr, cm^{-1}): 3042 (=C–H stretching of aromatic ring), 2955, 1667 (C=O), 1623 (C=C– stretching of aromatic ring), 1249 (C–O), 1198 (C–O stretching); ^{1}H-NMR (400 MHz, $CDCl_3$, δ / ppm): 0.99 (6H, *s*, 2×CH_3), 1.10 (6H, *s*, 2×CH_3), 2.14–2.25 (4H, *m*, 2×CH_2), 2.45 (4H, *s*, 2×CH_2), 3.73 (3H, *s*, OCH_3), 4.70 (1H, *s*, CH), 6.75 (2H, *d*, *J* = 8.1 Hz, Ar-H), 7.20 (2H, *d*, *J* = 8.1 Hz, Ar-H); ^{13}C-NMR (100 MHz, $CDCl_3$, δ / ppm): 27.3 (2×CH_3), 29.2 (2×CH_3), 30.9 (2×**C**$(CH_3)_2$), 32.3 (CH), 40.7 (2×CH_2), 50.6 (2×CH_2), 55.7 (OCH_3), 113.1, 115.5, 129.2, 136.5, 155.8, 168.1 (Ar–C), 196.6 (C=O).

*9-(4-Chlorophenyl)-3,3,6,6-tetramethyl-3,4,5,6,7,9-hexahydro-1*H*-xanthene-1,8(2*H*)-dione (**5c**)*. White solid; Yield: 88 %; m.p.: 230–233 °C; Anal. Calcd. for $C_{23}H_{25}ClO_3$ (FW: 384.15): C, 71.77; H, 6.55 %. Found: C, 71.62; H, 6.66 %; FT-IR (KBr, cm^{-1}): 3054 (=C–H stretching of aromatic ring), 2963, 1666 (C=O), 1617 (C=C– stretching of aromatic ring), 1364, 1211 (C–O stretching); ^{1}H-NMR (400 MHz, $CDCl_3$, δ / ppm): 1.01 (6H, *s*, 2×CH_3), 1.11 (6H, *s*, 2×CH_3), 2.14––2.25 (4H, *m*, 2×CH_2), 2.45 (4H, *s*, 2×CH_2), 4.95 (1H, *s*, CH), 7.15 (2H, *d*, *J* = = 8.1 Hz, Ar-H), 7.38 (2H, *d*, *J* = 8.1 Hz, Ar-H); ^{13}C-NMR (100 MHz, $CDCl_3$, δ / ppm): 27.2 (2×CH_3), 29.2 (2×CH_3), 32.1 (2×**C**$(CH_3)_2$), 32.2 (CH), 40.8 (2×CH_2), 50.9 (2×CH_2), 110.1, 119.2, 129.5, 132.1, 149.4, 162.8 (Ar–C), 196.6 (C=O).

*9-(4-Bromophenyl)-3,3,6,6-tetramethyl-3,4,5,6,7,9-hexahydro-1*H*-xanthene--1,8(2*H*)-dione (**5d**)*. White solid; yield: 88 %; m.p.: 226–229 °C; Anal. Calcd. for $C_{23}H_{25}BrO_3$ (FW: 428.10): C, 64.34; H, 5.87 %. Found: C, 64.42; H, 8.77 %; FT-IR (KBr, cm^{-1}): 3061 (=C–H stretching of aromatic ring), 2963, 1663 (C=O), 1619 (C=C– stretching of aromatic ring), 1358, 1218 (C–O stretching); ^{1}H-NMR

(400 MHz, $CDCl_3$, δ / ppm): 0.99 (6H, *s*, 2×CH_3), 1.12 (6H, *s*, 2×CH_3), 2.14–2.26 (4H, *m*, 2×CH_2), 2.46 (4H, *s*, 2×CH_2), 4.69 (1H, *s*, CH), 7.17 (2H, *d*, *J* = 8.0 Hz, Ar-H), 7.33 (2H, *d*, *J* = 8.0 Hz, Ar-H); ^{13}C-NMR (100 MHz, $CDCl_3$, δ / ppm): 27.1 (2×CH_3), 29.2 (2×CH_3), 32.2 (2×**C**$(CH_3)_2$), 32.3 (CH), 40.7 (2×CH_2), 50.9 (2×CH_2), 111.1, 119.1, 129.5, 132.2, 149.5, 162.6 (Ar–C), 196.4 (C=O).

*3,3,6,6-Tetramethyl-9-(4-nitrophenyl)-3,4,5,6,7,9-hexahydro-1*H*-xanthene-1,8(2*H*)-dione (**5e**)*. Yellow solid; Yield: 90 %; m.p.: 225–226 °C; Anal. Calcd. for $C_{23}H_{25}NO_5$ (FW: 395.17): C, 69.86; H, 6.37; N, 3.54 %. Found: C, 69.97; H, 6.26; N, 3.43 %; FT-IR (KBr, cm^{-1}): 3064 (=C–H stretching of aromatic ring), 1667 (C=O), 1611 (C=C– stretching of aromatic ring), 1538 (NO_2), 1344 (NO_2), 1214 (C–O stretching); ^{1}H-NMR (400 MHz, $CDCl_3$, δ / ppm): 1.00 (6H, *s*, 2×CH_3), 1.12 (6H, *s*, 2×CH_3), 2.12–2.24 (4H, *m*, 2×CH_2), 2.41–2.44 (4H, *m*, 2×CH_2), 4.86 (1H, *s*, CH), 7.38 (2H, *d*, *J* = 8.0 Hz, Ar-H), 7.98 (2H, *d*, *J* = 8.0 Hz, Ar-H); ^{13}C-NMR (100 MHz, $CDCl_3$, δ/ ppm): 27.2 (2×CH_3), 29.2 (2×CH_3), 32.1 (2×**C**$(CH_3)_2$), 32.2 (CH), 40.8 (2×CH_2), 50.9 (2×CH_2), 109.2, 118.8, 129.5, 132.2, 149.4, 163.1 (Ar–C), 196.9 (C=O).

*3,3,6,6-Tetramethyl-9-(*p*-tolyl)-3,4,5,6,7,9-hexahydro-1*H*-xanthene-1,8(2*H*)-dione (**5f**)*. Yellow solid; yield: 87 %; m.p.: 212–214 °C; Anal. Calcd. for $C_{24}H_{28}O_3$ (FW: 364.20): C, 79.09; H, 7.74 %. Found: C, 78.92; H, 7.89; %; FT-IR (KBr, cm^{-1}): 3022 (=C–H stretching of aromatic ring), 2956, 1666 (C=O), 1625 (C=C– stretching of aromatic ring), 1365, 1197 (C–O stretching); ^{1}H-NMR (400 MHz, $CDCl_3$, δ / ppm): 1.00 (6H, *s*, 2×CH_3), 1.10 (6H, *s*, 2×CH_3), 2.15––2.25 (4H, *m*, 2×CH_2), 2.28 (3H, CH_3), 2.47 (4H, *s*, 2×CH_2), 4.71 (1H, *s*, CH), 6.91 (2H, *d*, *J* = 7.9 Hz, Ar-H), 7.08 (2H, *d*, *J* = 7.9 Hz, Ar-H); ^{13}C-NMR (100 MHz, $CDCl_3$, δ / ppm): 22.1 (Ar–CH_3), 27.5 (2×CH_3), 28.2 (2×CH_3), 32.2 (2×**C**$(CH_3)_2$), 32.4 (CH), 40.8 (2×CH_2), 50.9 (2×CH_2), 109.1, 119.1, 129.2, 132.2, 148.1, 161.8 (Ar–C), 196.7 (C=O).

*3,3,6,6-Tetramethyl-9-(2-nitrophenyl)-3,4,5,6,7,9-hexahydro-1*H*-xanthene--1,8(2*H*)-dione (**5g**)*. Yellow solid; yield: 89 %; m.p.: 246–248 °C; Anal. Calcd. for $C_{23}H_{25}NO_5$ (FW: 395.17): C, 69.86; H, 6.37; N, 3.54 %. Found: C, 69.72; H, 6.49; N, 3.66 %; FT-IR (KBr, cm^{-1}): 3043 (=C–H stretching of aromatic ring), 1663 (C=O), 1618 (C=C– stretching of aromatic ring), 1544 (NO_2), 1347 (NO_2), 1197 (C–O stretching); ^{1}H-NMR (400 MHz, $CDCl_3$, δ / ppm): 0.95 (6H, *s*, 2×CH_3), 1.09 (6H, *s*, 2×CH_3), 2.10–2.23 (4H, *m*, 2×CH_2), 2.35–2.49 (4H, *s*, 2×CH_2), 4.86 (1H, *s*, CH), 7.11 (1H, *d*, *J* = 8.0 Hz, Ar-H), 7.17 (1H, *t*, *J* = 7.9 Hz, Ar-H), 7.38 (1H, *t*, *J* = 7.9 Hz, Ar-H), 7.79 (1H, *d*, *J* = 8.0 Hz, Ar-H); ^{13}C--NMR (100 MHz, $CDCl_3$, δ / ppm): 27.3 (2×CH_3), 28.2 (2×CH_3), 32.1 (2×**C**$(CH_3)_2$), 32.5 (CH), 40.7 (2×CH_2), 50.9 (2×CH_2), 109.1, 119.1, 122.2, 129.2, 132.2, 148.1, 158.1, 161.8 (Ar–C), 196.2 (C=O).

*9-(4-Fluorophenyl)-3,3,6,6-tetramethyl-3,4,5,6,7,9-hexahydro-1*H-*xanthene-1,8(2*H)*-dione (**5h**)*. White solid; yield: 90 %; m.p.: 225–227 °C; Anal. Calcd. for $C_{23}H_{25}FO_3$ (FW: 368.18): C, 74.98; H, 6.84 %. Found: 74.88; H, 6.73 %; FT-IR (KBr, cm^{-1}): 3068 (=C–H stretching of aromatic ring), 2953, 1666 (C=O), 1612 (C=C– stretching of aromatic ring), 1355, 1222 (C–O stretching); ^{1}H-NMR (400 MHz, $CDCl_3$, δ / ppm): 1.03 (6H, *s*, 2×CH_3), 1.12 (6H, *s*, 2×CH_3), 2.14––2.25 (4H, *m*, 2×CH_2), 2.45 (4H, *m*, 2×CH_2), 4.95 (1H, *s*, CH), 7.15 (2H, *d*, *J* = = 8.1 Hz, Ar-H), 7.38 (2H, *d*, *J* = 8.1Hz, Ar-H); ^{13}C-NMR (100 MHz, $CDCl_3$, δ / ppm): 28.1 (2×CH_3), 29.2 (2×CH_3), 32.2 (2×**C**$(CH_3)_2$), 32.2 (CH), 40.6 (2×CH_2), 50.7 (2×CH_2), 111.5, 118.9, 123.7, 136.2, 141.1, 161.9 (Ar–C), 195.9 (C=O).

*9-(3-Chlorophenyl)-3,3,6,6-tetramethyl-3,4,5,6,7,9-hexahydro-1*H-*xanthene--1,8(2*H)*-dione (**5i**)*. White solid; Yield: 86 %; m.p.: 184–185 °C; Anal. Calcd. for $C_{23}H_{25}ClO_3$ (FW: 384.15): C, 71.77; H, 6.55 %. Found: C, 71.88; H, 6.44 %; FT-IR (KBr, cm^{-1}): 3051 (=C–H stretching of aromatic ring), 2966, 1667 (C=O), 1621 (C=C– stretching of aromatic ring), 1354, 1216 (C–O stretching); ^{1}H-NMR (400 MHz, $CDCl_3$, δ / ppm): 1.06 (6H, *s*, 2×CH_3), 1.17 (6H, *s*, 2×CH_3), 2.12–2.21 (4H, *m*, 2×CH_2), 2.46 (4H, *s*, 2×CH_2), 4.86 (1H, *s*, CH), 7.42–7.45 (3H, *m*, Ar-H), 7.72 (1H, *s*, Ar-H); ^{13}C-NMR (100 MHz, $CDCl_3$, δ / / ppm): 27.9 (2×CH_3), 28.8 (2×CH_3), 32.2 (2×**C**$(CH_3)_2$), 32.3 (CH), 40.7 (2×CH_2), 50.9 (2×CH_2), 110.1, 119.2, 129.5, 132.1, 149.4, 152.7, 157.6, 162.8 (Ar–C), 196.6 (C=O).

*9-(4-Hydroxyphenyl)-3,3,6,6-tetramethyl-3,4,5,6,7,9-hexahydro-1*H-*xanthene-1,8(2*H)*-dione (**5j**)*. White solid; yield: 85 %; m.p.: 244–246 °C; Anal. Calcd. for $C_{24}H_{26}O_4$ (FW: 366.18): C, 75.38; H, 7.15 %. Found: C, 75.49; H, 7.07 %; FT-IR (KBr, cm^{-1}): 3448 (OH stretching), 3052 (=C–H stretching of aromatic ring), 2955, 1666 (C=O), 1611 (C=C– stretching of aromatic ring), 1208 (C–O stretching); ^{1}H-NMR (400 MHz, $CDCl_3$, δ / ppm): 1.01 (6H, *s*, 2×CH_3), 1.12 (6H, *s*, 2×CH_3), 2.13–2.23 (4H, *m*, 2×CH_2), 2.46 (4H, *s*, 2×CH_2), 4.70 (1H, *s*, CH), 5.48 (1H, *bs*, OH), 6.85 (2H, *d*, *J* = 8.0 Hz, Ar-H), 7.24 (2H, *d*, *J* = 8.0 Hz, Ar-H); ^{13}C-NMR (100 MHz, $CDCl_3$, δ / ppm): 27.7 (2×CH_3), 29.1 (2×CH_3), 30.9 (2×**C**$(CH_3)_2$), 32.2 (CH), 40.7 (2×CH_2), 50.9 (2×CH_2), 111.2, 115.4, 129.1, 133.1, 154.5, 168.2 (Ar–C), 196.9 (C=O).

*3,3,6,6-Tetramethyl-9-(3-nitrophenyl)-3,4,5,6,7,9-hexahydro-1*H-*xanthene--1,8(2*H)*-dione (**5k**)*. Yellow solid; yield: 89 %; m.p.: 165–167 °C; Anal. Calcd. for $C_{23}H_{25}NO_5$ (FW: 384.15): C, 71.77; H, 6.55 %. Found: C, 71.88; H, 6.44 %; FT-IR (KBr, cm^{-1}): 3042 (=C–H stretching of aromatic ring), 2966, 1663 (C=O), 1623 (C=C– stretching of aromatic ring), 1541 (NO_2), 1364 (NO_2), 1218 (C–O stretching); ^{1}H-NMR (400 MHz, $CDCl_3$, δ / ppm): 1.01 (6H, *s*, 2×CH_3), 1.12 (6H, *s*, 2×CH_3), 2.14–2.26 (4H, *m*, 2×CH_2), 2.46 (4H, *s*, 2×CH_2), 4.81 (1H, *s*, CH), 7.55–7.57 (3H, *m*, Ar-H), 7.92 (1H, *s*, Ar-H); ^{13}C-NMR (100 MHz, $CDCl_3$,

δ / ppm): 27.6 (2×CH_3), 28.9 (2×CH_3), 32.2 (2×**C**(CH_3)$_2$), 32.1 (CH), 40.8 (2×CH_2), 50.8 (2×CH_2), 110.2, 120.1, 130.4, 134.1, 150.5, 154.5, 158.1, 161.9 (Ar–C), 195.8 (C=O).

*4-(2,3,4,5,6,7,8,9-Octahydro-3,3,6,6-tetramethyl-1,8-dioxo-1*H*-xanthen-9-yl)-benzonitrile (**5m**).* Yellow solid; Yield: 90 %; m.p.: 216–217 °C; Anal. Calcd. for $C_{24}H_{25}NO_3$ (FW: 375.18): C, 76.77; H, 6.71; N, 3.73 %. Found: C, 76.92; H, 6.86; N, 3.82 %; FT-IR (KBr, cm^{-1}): 3065 (=C–H stretching of aromatic ring), 2960, 2225 (C≡N), 1663 (C=O), 1620 (C=C– stretching of aromatic ring), 1362, 1199 (C–O); ^{1}H-NMR (400 MHz, $CDCl_3$, δ / ppm): 0.99 (6H, *s*, 2×CH_3), 1.12 (6H, *s*, 2×CH_3), 2.15–2.28 (4H, *m*, 2×CH_2), 2.49 (4H, *s*, 2×CH_2), 4.77 (1H, *s*, CH), 7.42 (2H, *d*, *J* = 8.0 Hz, Ar-H), 7.53 (2H, *d*, *J* = 8.0 Hz, Ar-H); ^{13}C-NMR (100 MHz, $CDCl_3$, δ / ppm): 27.3 (2×CH_3), 29.2 (2×CH_3), 32.2 (2×**C**(CH_3)$_2$), 32.4 (CH), 40.8 (2×CH_2), 50.6 (2×CH_2), 110.2, 114.6 (C≡N), 119.0, 129.2, 132.0, 149.4, 162.9 (Ar–C), 196.3 (C=O); MS-EI (m/z): 375.18 (M^+).

SUPPLEMENTARY INFORMATION FOR NEW COMPOUNDS

*9-(4-Isopropylphenyl)-3,3,6,6-tetramethyl-3,4,5,6,7,9-hexahydro-1*H*-xanthene--1,8(2*H*)-dione (**5l**)*

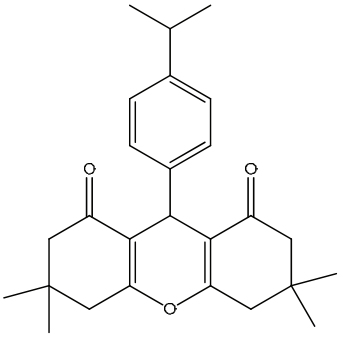

Yellow solid; Yield: 80 %; m.p.: 203–206 °C; Anal. Calcd. for $C_{26}H_{32}O_3$ (FW: 392.24): C, 79.56; H, 8.22 %. Found: C, 79.39; H, 8.36 %; FT-IR (KBr, cm^{-1}): 3071 (=C–H stretching of aromatic ring), 2961, 1665 (C=O), 1624 (C=C– stretching of aromatic ring), 1359, 1198 (C–O); ^{1}H-NMR (400 MHz, $CDCl_3$, δ / / ppm): 1.00 (6H, *s*, 2×CH_3), 1.10 (6H, *s*, 2×CH_3), 1.18 (6H, *d*, 2×CH_3), 2.16––2.26 (4H, *m*, 2×CH_2), 2.46 (4H, *s*, 2×CH_2), 2.78–2.81 (1H, *m*, C**H**(CH_3)$_2$), 4.73 (1H, *s*, CH), 7.05 (2H, *d*, *J* = 8.0 Hz, Ar-H), 7.18 (2H, *d*, *J* = 8.0 Hz, Ar-H); ^{13}C--NMR (100 MHz, $CDCl_3$, δ / ppm): 23.9 (2×CH_3), 27.4 (2×CH_3), 29.2 (2×CH_3), 31.3 (C**H**(CH_3)$_2$), 32.2 (2×**C**(CH_3)$_2$), 33.6 (CH), 40.8 (2×CH_2), 50.8 (2×CH_2), 115.8, 126.1, 128.1, 141.3, 146.5, 162.1 (Ar–C), 196.4 (C=O); MS-EI (*m/z*): 392.24 (M^+).

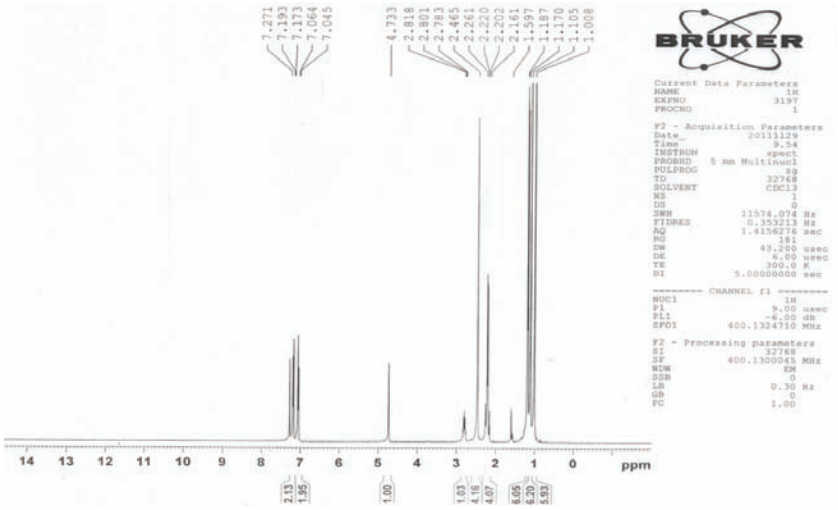

Fig. S-1. ^{1}H-NMR (400 MHz, $CDCl_3$) spectrum of **5l**.

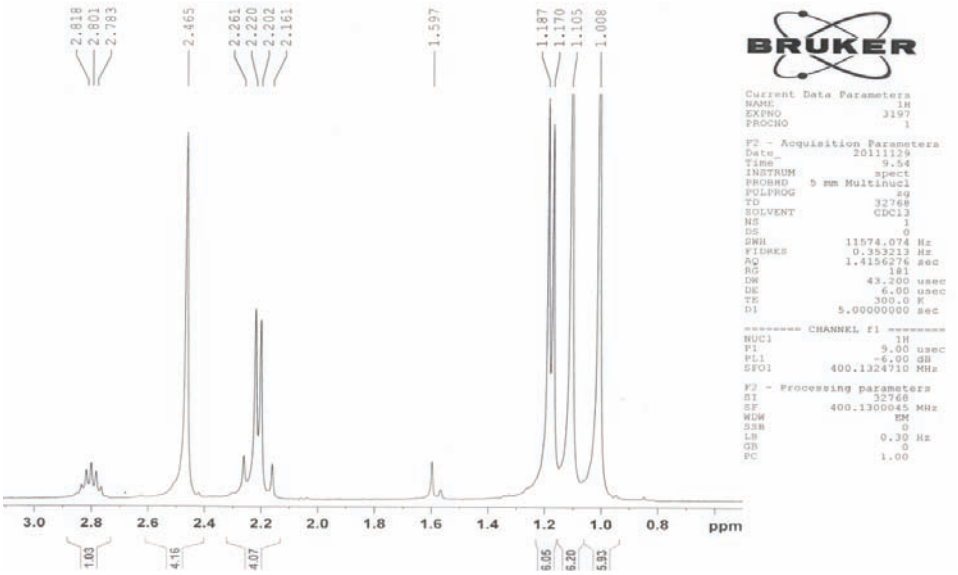

Fig. S-2. ^{1}H-NMR (400 MHz, $CDCl_3$) expanded spectrum of **5l**.

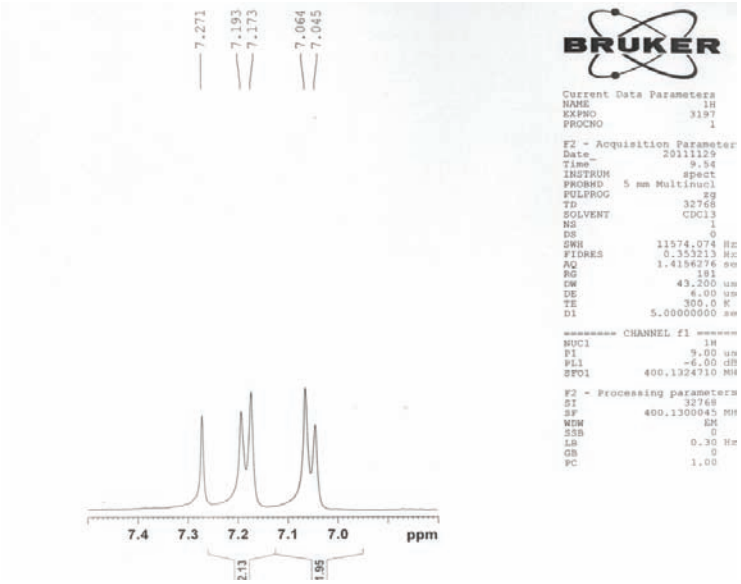

Fig. S-3. ^{1}H-NMR (400 MHz, $CDCl_3$) expanded spectrum of **5l**.

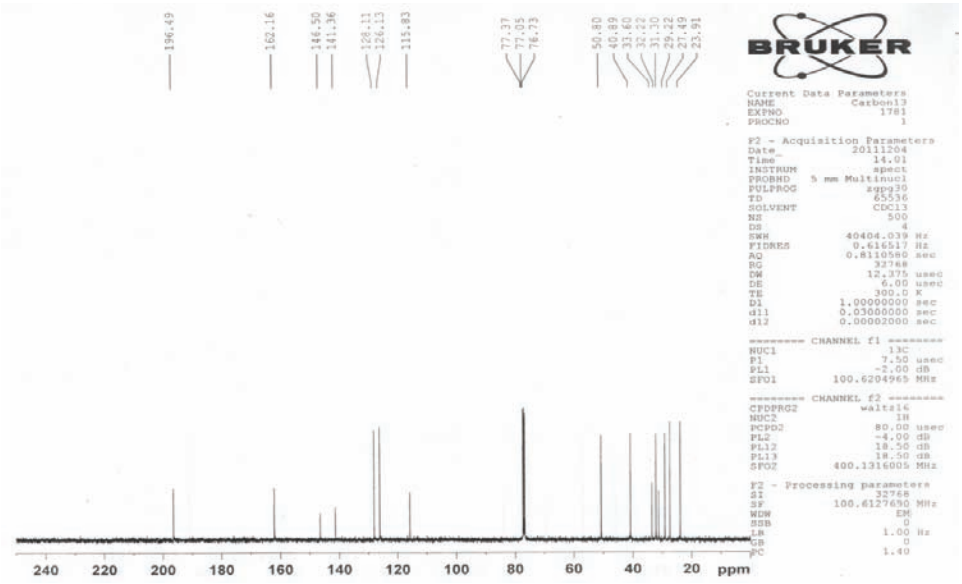

Fig. S-4. ^{13}C-NMR (100 MHz, $CDCl_3$) spectrum of **5l**.

*3,3,6,6-Tetramethyl-9-[4-(methylthio)-phenyl]-3,4,5,6,7,9-hexahydro-1*H*-xanthene-1,8(2*H*)-dione (**5n**)*

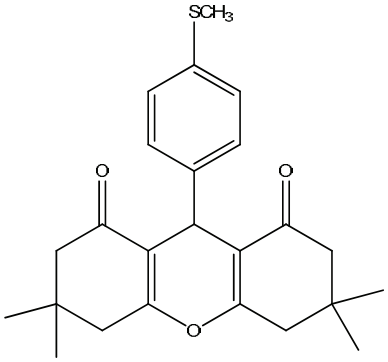

White solid; Yield: 86 %; m.p.: 256–257 °C; Anal. Calcd. for $C_{24}H_{28}O_3S$ (FW: 396.18): C, 72.69; H, 7.12 %. Found: C, 72.82; H, 6.99 %; FT-IR (KBr, cm^{-1}): 3045 (=C–H stretching of aromatic ring), 2963, 1661 (C=O), 1621 (C=C– stretching of aromatic ring), 1226 (C–O), 1152 (C–S); ^{1}H-NMR (400 MHz, $CDCl_3$, δ / ppm): 1.00 (6H, *s*, 2×CH_3), 1.10 (6H, *s*, 2×CH_3), 2.14–2.21 (4H, *m*, 2×CH_2), 2.24 (3H, *s*, SCH_3), 2.46 (4H, *s*, 2×CH_2), 4.71 (1H, *s*, CH), 7.02 (2H, *d*, *J* = 7.9 Hz, Ar-H), 7.18 (2H, *d*, *J* = 7.9 Hz, Ar-H); ^{13}C-NMR (100 MHz, $CDCl_3$, δ / ppm): 21.4 (SCH_3), 27.3 (2×CH_3), 29.2 (2×CH_3), 30.9 (2×**C**$(CH_3)_2$), 32.1 (CH), 40.8 (2×CH_2), 50.7 (2×CH_2), 113.4, 115.7, 129.3, 136.5, 157.9, 162.1 (Ar–C), 196.4 (C=O); MS-EI (*m/z*): 396.18 (M^+).

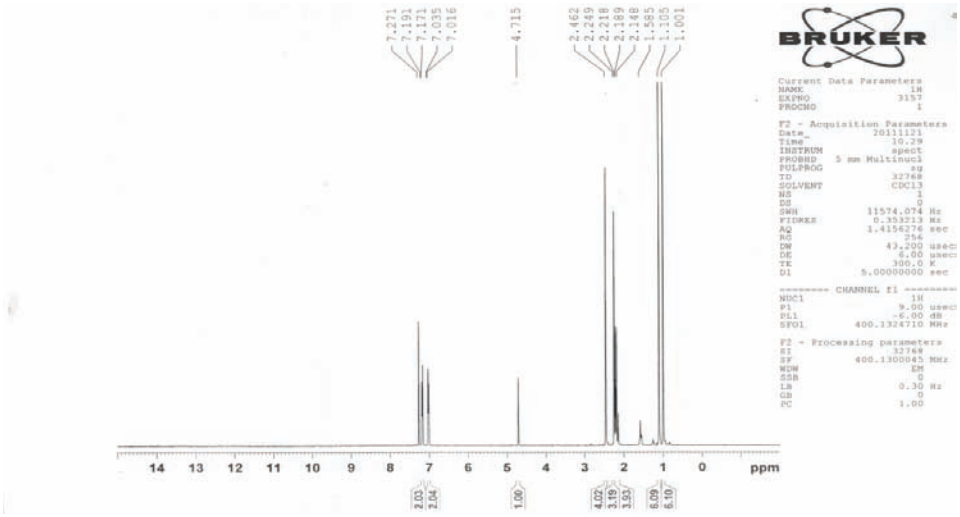

Fig. S-5. ^{1}H-NMR (400 MHz, $CDCl_3$) spectrum of **5n**.

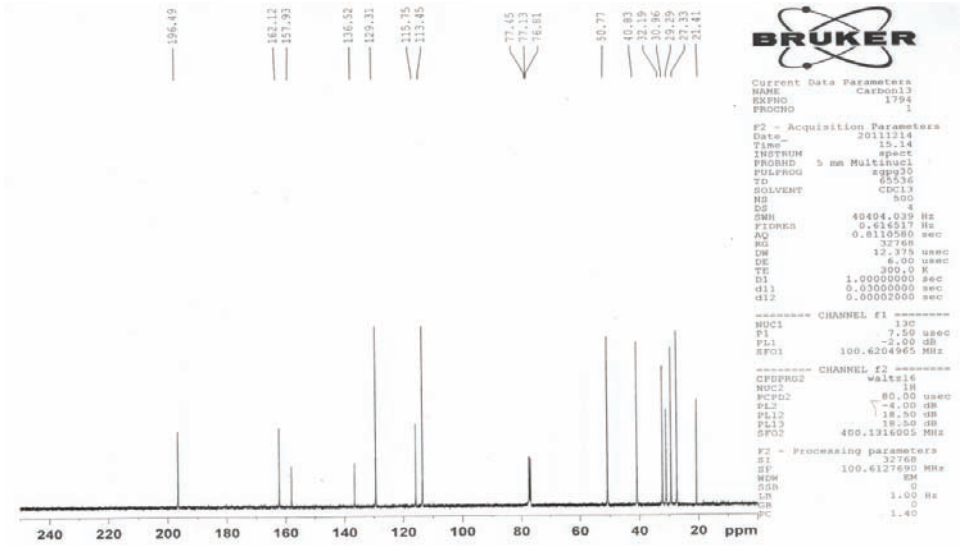

Fig. S-6. ^{13}C-NMR (100 MHz, $CDCl_3$) spectrum of **5n**.

*4-(2,3,4,5,6,7,8,9-Octahydro-3,3,6,6-tetramethyl-1,8-dioxo-1*H*-xanthen-9-yl)-benzaldehyde (**5o**)*

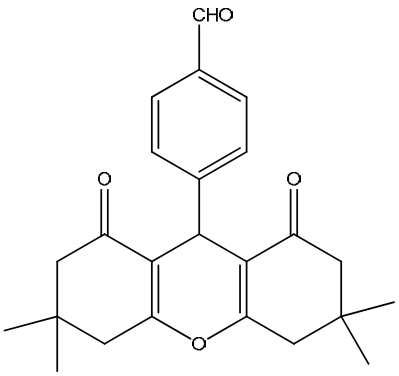

White solid; Yield: 89 %; m.p.: 211–213 °C; Anal. Calcd. for $C_{24}H_{26}O_4$ (FW: 378.18): C, 76.17; H, 6.92 %. Found: C, 76.05; H, 7.09 %; FT-IR (KBr, cm^{-1}): 3063 (=C–H stretching of aromatic ring), 2873 (=C–H aldehyde), 1728 (–C=O stretching of –CHO), 1663 (C=O), 1618, 1517 (C=C– stretching of aromatic ring), 1358, 1200 (C–O); ^{1}H-NMR ($CDCl_3$): 1.01 (6H, *s*, 2×CH_3), 1.10 (6H, *s*, 2×CH_3), 2.13–2.22 (4H, *m*, 2×CH_2), 2.47 (4H, *s*, 2×CH_2), 4.70 (1H, *s*, CH), 7.39 (2H, *d*, *J* = 8.0 Hz, Ar-H), 7.51 (2H, *d*, *J* = 8.0 Hz, Ar-H), 9.72 (1H, *s*, CHO); ^{13}C-NMR ($CDCl_3$): 27.3 (2×CH_3) , 29.2 (2×CH_3), 31.5 (CH), 32.2 (2×**C**$(CH_3)_2$), 40.8 (2×CH_2), 50.6 (2×CH_2), 115.1, 120.2, 130.1, 131.1, 143.2,

162.4 (Ar–C), 196.3 (–C=O), 204.8 (–C=O, aldehyde). MS-EI (*m/z*): 378.18 (M^+).

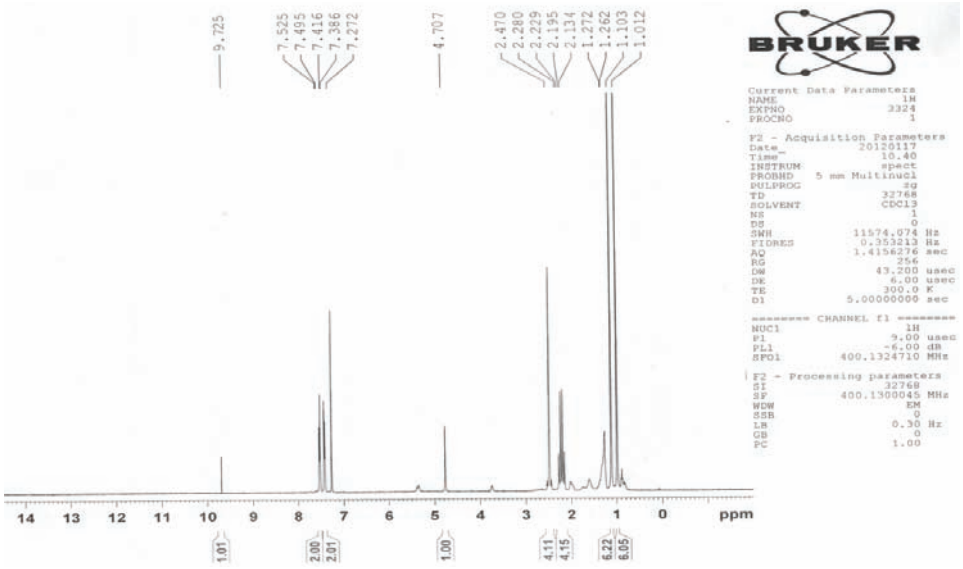

Fig. S-12. ^{1}H-NMR (400 MHz, $CDCl_3$) spectrum of **5o**.

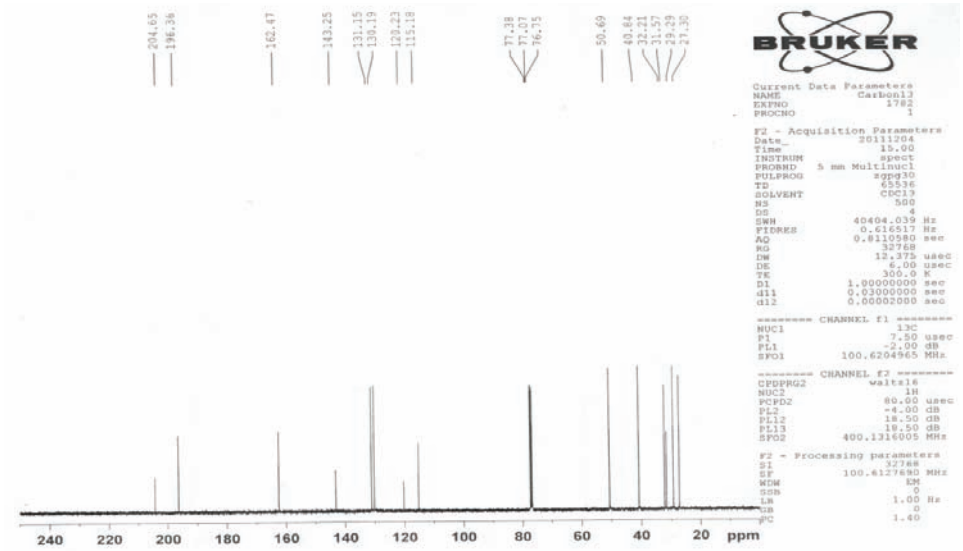

Fig. S-13. ^{13}C-NMR (100 MHz, $CDCl_3$) spectrum of **5o**.

Journal of the Serbian Chemical Society
JSCS-info@shd.org.rs • www.shd.org.rs/JSCS
J. Serb. Chem. Soc. 78 (6) 781–794 (2013)
JSCS–4457
UDC **Yarrowia lipolytica*+577.15:665.327.3:628.4.038
Original scientific paper

Lipase production by *Yarrowia lipolytica* using olive oil processing wastes as substrates

OMAR A. S. MOFTAH[1], SANJA Ž. GRBAVČIĆ[2], WALID A. S. MOFTAH[3], NEVENA D. LUKOVIĆ[1], OLIVERA L. PRODANOVIĆ[4#], SONJA M. JAKOVETIĆ[1#] and ZORICA D. KNEŽEVIĆ-JUGOVIĆ[1*#]

[1]Department of Biochemical Engineering and Biotechnology, Faculty of Technology and Metallurgy, University of Belgrade, Karnegijeva 4, 11000 Belgrade, Serbia, [2]Innovation Center, Faculty of Technology and Metallurgy, University of Belgrade, Karnegijeva 4, 11000 Belgrade, Serbia, [3]Department of Environmental Management, Faculty of Applied Ecology, Singidunum University, Belgrade, Serbia and [4]Institute for Multidisciplinary Research, University of Belgrade, Kneza Višeslava 1, 11030 Belgrade, Serbia

(Received 5 September 2012, revised 11 January 2013)

Abstract: In this study, the solid and liquid wastes from the olive oil processing industry were evaluated as substrates for *Yarrowia lipolytica* growth with the aim of lipase production. Olive mill wastewater and olive oil cake seemed to provide the necessary nutrients and physical support for yeast growth and enzyme production. The highest lipolytic activity of 850 IU dm^{-3} was achieved after 4 days of submerged cultivation in supplemented olive mill wastewater. In addition, olive oil cake appeared to be a convenient substrate for lipase production under a solid-state fermentation mode. Lipase production was further improved by media supplementation and/or change in the physical settings of the experiment. However, the most significant improvement of lipase production under solid-state fermentation was achieved by an alkaline treatment of the substrate (more than 10-fold), when the amount of produced lipase reached up to ≈40 IU g^{-1} of substrate.

Keywords: olive oil cake; olive mill wastewater; *Yarrowia lipolytica*; solid-state fermentation; lipase production.

INTRODUCTION

Olive oil is considered one of the best edible oil in terms of tastiness, stability and lipid profile. It is very rich in oleic acid and contains omega-6 and omega-3 essential fatty acids in a favorable ratio, making it one of the healthiest cooking oils. In addition, olive oil contains large amounts of plant-derived anti-

* Corresponding author. E-mail: zknez@tmf.bg.ac.rs
# Serbian Chemical Society member.
doi: 10.2298/JSC120905005M

oxidants (such as hydroxytyrosol, oleocanthal and oleuropein), phyto-sterols and vitamins.[1] The growing awareness of the importance of a proper diet rich in essential fatty acids and antioxidants on human health, as well as its distinct taste, has resulted in a worldwide increase in olive oil consumption.

Almost all of the produced olive oil (estimated at over 2.5 million tonnes per year) originates from the Mediterranean region.[2] Libya, as a Mediterranean country, has millions of olive trees, which are native to the region. According to the Food and Agriculture Organization of the United Nations, Libya produced 15000 tonnes of olive oil in 2009.

The olive oil production industry generates large amounts of waste, of which olive mill wastewater (OMW) and crude olive oil cake (solid waste – OOC) have the highest organic load and therefore present the largest pollutants of the oil processing industry. The quality and quantity of the constituents of these wastes are dependent of many factors, such as type and maturity of the olives, climatic conditions and region of origin, cultivation methods, and the technology used for oil extraction.[3] Traditional pressing and the three-phase system are relatively obsolete technologies for oil extraction that are being replaced by a new centrifugation two-phase system labeled as ecological due to the reduced generation of OMW. The processing of 1 t of fresh olives by the most frequently employed three-phase system yields about 210 kg of olive oil, 550 kg of crude olive cake, and 1–1.6 m^3 of OMW.[3] The phytotoxic and antimicrobial nature of these wastes are credited to their high phenolic and residual lipid contents.

Although several methods for olive oil processing waste have been proposed, *i.e.*, anaerobic digestion, ultrafiltration, precipitation/flocculation and electrocoagulation, olive oil processing waste is mostly improperly managed.[3,4] In most cases, olive mill wastewater is spread on ground or collected in vaporization ponds, causing pollution of the underlying soil. Solid residues (OOC) are sometimes used as fuel due to their high-energy content. Several pyrolysis methods were developed for the production of fuel from this waste.[5,6] Due to its content and unfavorable effects on plants and animals, its use as a component of fertilizers or animal feed is limited.[7,8] Thus, very little of the large quantity of olive oil processing wastes is being valorized.

However, as with the wastes of other agricultural processing industries that are difficult to treat and valorize, these substances can be used as starting materials for biotechnological applications, in particular for the synthesis of high value metabolites, such as single cell proteins, microbial lipids, organic acids, bio-surfactants and enzymes.[9] The use of these substrates for fermentation processes aimed at enzyme production decreases the final cost of the enzyme, making industrial enzymatic processes cost-competitive with chemical ones.[10]

Yarrowia lipolytica is strictly an aerobic yeast widely used in industrial applications due to its ability to produce a wide spectrum of products, such as

organic acids and/or extracellular enzymes, in adequate amounts. Several processes in which this strain is employed were classified as generally recognized as safe (GRAS) by the Food and Drug Administration (USA).[11] The yeast is also widely used in bioremediation processes due to its specific metabolic pathways and the ability to alter its cell surface, thereby enabling the efficient degradation of hydrophobic substrates, such as *n*-alkanes, fatty acids, fats, and oils.[12] Of a total of 300 yeast isolates obtained from samples of agro-industrial wastes, two strains, identified as *Y. lipolytica* species, have been proven to be the most capable to produce valuable products, such as lipase and citric acid, when grown on different waste substances.[9]

A variety of wastes have been studied as substrates for the growth of different strains of *Y. lipolytica* as a means of waste disposal and/or upgradation by additionally generating value-added products.[13] However, only few reports were focused on the production of lipase by the yeast when grown on olive oil processing wastes. For example, De Felice *et al*. investigated lipase production as well as OMW degradation in batch cultures of *Y. lipolytica* W29 (ATCC 20255), showing that the yeast was capable of metabolizing the waste and, under optimum conditions, a lipase activity of 770 U dm^{-3} was obtained.[14] Gonçalves *et al*. also cultivated *Y. lipolytica* W29 on OMW for lipase production under batch and fed-batch culture conditions, finding that the enzyme yields were higher in the former.[15,16] Although a few other reports considering lipase production by *Y. lipolytica* using OMW as a substrate have been published,[17–19] to the best of our knowledge, no attempts have hitherto been made to use the olive oil cake as a substrate for the production of lipase by this yeast using solid state fermentation (SSF).

The present study was aimed to valorize olive oil processing wastes (OMW and OOC) as substrate mediums for the cultivation of the yeast *Y. lipolytica* in order to facilitate the production of lipases. Some of the factors affecting the growth and the production of extracelluar lipase by the yeast strain were studied. To the best of our knowledge, this is the first report on a more complete assessment of lipase production by the yeast using different olive oil processing wastes.

EXPERIMENTAL

Organism

The microorganism used in this study, *Yarrowia lipolytica* NRRL Y-1095, was donated by the Agricultural Research Centre (USA) to the Microbiological Laboratory of the Faculty of Technology and Metallurgy, Belgrade, Serbia. The employed yeast strain was maintained on malt agar slants at 4 °C. A one-day-old culture grown in malt broth was used as the inoculum (approximately 5×10^7 cells cm^{-3}).

Characterization of the substrates

The OMW samples were collected from various traditional olive oil mills in Lasaba and Gharian, Libya, and used as fermentation medium for the submerged yeast cultivation. The

substrate samples were characterized before fermentation for total solids, chemical oxygen demand (*COD*), pH, crude protein, phenols, reducing sugars and total lipids. The total phenols were determined photometrically at 765 nm using the Folin–Ciocalteu method and are expressed as gallic acid equivalents.[20] The crude protein content was determined by the Kjeldahl method and multiplying the nitrogen content by 6.25.[21] The lipid content was determined gravimetrically after lyophilization of the sample and subsequent extraction of the samples with *n*-hexane at 60 °C for 20 h using a Soxhlet extraction apparatus.[21] The DNS (3,5-dinitrosalicylic acid) method was used for carbohydrate detection.[22] The *COD* was assessed using the standard method of titration.[23]

Samples of OOC were also obtained from various traditional olive oil mills (Libya) and used as a natural substrate for the SSF. They were packed in vacuum-sealed packages and stored at 4 °C until use. The moisture content of the cake was determined gravimetrically as described in detail elsewhere.[21] The ash and crude fiber contents were determined as previously described.[21] The total nitrogen of the substrate was determined following the standard Kjeldahl method while the oil content of the OOC was determined gravimetrically after extraction of the samples with *n*-hexane using a Soxhlet extraction apparatus.[21]

Submerged fermentation using olive mill wastewater as the substrate

The submerged fermentation was performed by transferring 100 cm^3 of undiluted samples of OMW to Erlenmeyer flasks and sterilizing them at 121 °C (at 1.2 bar pressure) for 30 min prior to inoculation with 1 % (v/v) of the yeast culture in malt broth. The fermentation was performed in thermostat shaker at 30 °C at 150 rpm. Samples were withdrawn at 24 h intervals and tested for lipase activity.

Optimization of the substrate

Composition of the OMW was optimized by the addition of ammonium sulfate (0.6 % w/v), yeast extract (0.1 % w/v), maltose (0.5 % w/v), olive oil (0.3 % w/v) and peptone I (0.1 % w/v).

Solid-state fermentation (SSF) on olive oil cake

The substrate was dried at 105±5 °C for 1 h, and sieved to provide particles of size between 0.2 and 0.5 mm. The experiments were performed in 150 cm^3 Erlenmeyer flask with 5 g of well ground dry substrate supplemented with 0.15 g of yeast extract. Then, 1 cm^3 of distilled water was added and the contents of the flask were mixed and autoclaved at 121 °C for 20 min. Unless otherwise stated, SSF was realized by inoculating olive oil cake (initial moisture content adjusted to 50 %) with 500 μL of inoculum followed by incubation at 30 °C. The water added with the inoculums was also considered in the moisture content. Optimization studies were performed by varying the moisture content of the substrate and amount of inoculum. The effect of the addition of various carbon and nitrogen supplements was also studied for optimal lipase production.[21] Carbon (maltose, oleic acid and starch) and an inorganic nitrogen source (NH_4NO_3) were used at the 1 % level, while organic nitrogen sources (peptone and yeast extract) were used at the 3 % level to investigate their effect on lipase production.

Alkaline treatment of OOC

The alkaline treatment has been performed by mixing dried OOC with 3 % (w/v) NaOH and holding overnight at 20–22 °C. The pretreated substrate was then washed with distilled water until pH 7, dried, autoclaved at 121 °C for 20 min and used for fermentation. The pH of the substrate was not followed during fermentation due to the non-homogeneity of the fermen-

tation mixture. After 5 days of fermentation, the pH of a homogenized suspension of 1 g of fermented cake in 10 cm^3 of deionized water was measured using a pH meter.

Extraction of the enzymes

The crude enzymes were extracted by mixing a known quantity of fermented substrate with sterilized distilled water (1:5, w/w) following incubation in a KS 4000 orbital shaker (Ika-Werke, Germany) at 30 °C and 180 rpm for 30 min. A part of the liquid phase was used for the determination of yeast cell growth, while the rest was centrifuged at 12,000 rpm for 10 min. The supernatant was used for the determination of the lipase activity.

Lipase activity assay

Lipase activity was determined by hydrolysis of *p*-NPP (*p*-nitrophenyl palmitate) substrate by lipases according to a previously described method.[24] The amount of liberated *p*-nitrophenol was measured photometrically (410 nm) during the first 3 min of reaction. One unit of enzyme activity (IU) is defined as the amount of enzyme that formed 1 μmol of *p*-nitrophenol per minute (ε =1500 dm^3 mol^{-1} cm^{-1}) under the assay conditions.

Growth studies

Determination of yeast cell growth was performed by spreading suitably diluted cell suspensions on malt agar plates and counting the yeast cell colonies after incubation for 48 h at 30 °C.

RESULTS AND DISCUSSION

Characteristics of the substrates

Although composition of OMW can vary, this waste was a dark, acidic liquid (pH 4.8±0.6) with a characteristic odor and high organic load (*COD* 220±35 g dm^{-3}). The solid content was 127.5 g dm^{-3}. The OMW samples contained 11.9 g dm^{-3} of reducing sugars (expressed as the glucose equivalent) and 18.9 g dm^{-3} of lipids. The organic fraction of OMW also included phenols (6.9 g dm^{-3}) and proteins (195 mg dm^{-3}). Almost all phenolic matter of the olive fruit was reported to remain in the OMW (53 %) and OOC (45 %).[16] Since phenols were reported to act as enzymatic inhibitors, they could prevent spontaneous microbial processes, making these wastes serious pollution threats.[17] The mean moisture content of the olive oil cake was 51.4±1.5 mass%, while the composition of the cake on a dry-weight basis, except moisture, was 4.1±0.4 mass% proteins, 11.1±0.5 mass% lipids, 20.6±0.9 mass% carbohydrates, 60.1±1.3 mass% fibers and 4.1±0.4 mass% ash.[21]

Submerged fermentation using olive mill wastewater as the substrate

In this study, the yeast *Y. lipolytica* was tested for its ability to grow and produce lipase in such a medium. The OMW was inoculated with the strain for a preliminary study to estimate the suitability of olive oil wastewater as a substrate for growth and lipase production.

Y. lipolytica demonstrated the ability to grow in unsupplemented OMW, yielding up to ≈160 IU dm^{-3} lipolytic activity on the fifth day of fermentation

(Fig. 1). Suitability of the OMW medium for growth of various *Y. lipolytica* strains was already demonstrated by many researchers.[12,25] Lopes *et al*. studied two *Y. lipolytica* strains, ATCC20460 and IMUFRJ 50 682, which produced up to 30 IU dm^{-3} lipolytic activity in unsupplemented OMW.[2] Additionally, Gonçalves *et al*. studied three *Y. lipolytica* strains in OMW from different stages of olive processing, achieving 317-1041 IU dm^{-3} lipolytic activity while simultaneously reducing the *COD* and phenolic content by up to 51 % and 35 %, respectively.[16] In addition, almost all of the 62 *Y. lipolytica* strains studied by Lanciotti *et al.* were able to grow and produce lipase in OMW.[19] Papanikolaou *et al.* examined the capability of this yeast to produce citric acid in an OMW-based medium. These fermentation processes resulted in significant reductions in the phenolic content and *COD*.[26]

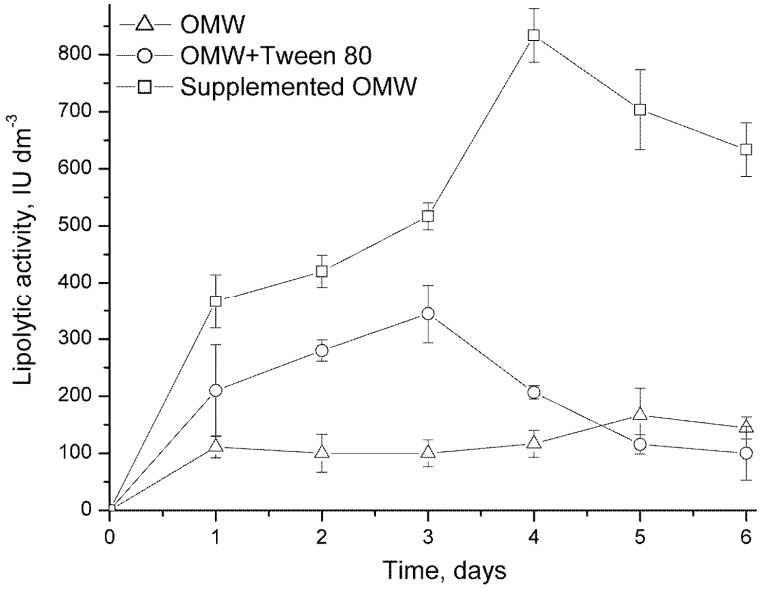

Fig. 1. Lipase production by *Y. lipolytica* in olive mill wastewater. The OMW was supplemented by the addition of ammonium sulfate (0.6 % w/v), yeast extract (0.1 % w/v), maltose (0.5 % w/v), olive oil (0.3 % w/v) and peptone I (0.1 % w/v).

Since the OMW contained a relatively large amount of residual fat, studies aimed at determining the influence of the addition of Tween 80 were undertaken with the intention to increase the oil dispersion in the medium. The addition of Tween 80 was shown to improve lipase secretion significantly (Fig. 1). Such a phenomenon of increased lipase production could be credited to changes in the permeability of cell membranes, facilitating the release of various metabolites, including enzymes, out of the cell. The literature review particularly confirmed this indicating that *Y. lipolytica* produced various lipases (extracellular Lip2p,

cell-bound lipases I and II, as well as intracellular lipolytic enzymes).[27] Surfactant supplementation seemed to lead to a 2-fold increase in lipase production, shifting the maximum of the enzyme production to the third day of fermentation. However, this effect of surfactant addition to the medium was not always registered and literature data showed significant variations in the influence of surfactant, even among the same species. Although the addition of surfactant appeared to stimulate biomass production of several *Y. lipolytica* strains, lipase production was inhibited in such media.[2,28] On the other hand, the addition of Tween 80 led to a 3-fold increase in lipase production by *Y. lipolytica* 681.[29]

Since a literature survey showed that OMW lacked some basic nutrients, the effect of substrate supplementation on lipase production was investigated. It seemed that the supplementation led to a 5-fold increase in lipase production in comparison to enzyme production in non-supplemented media. The level of produced enzyme reached up to ≈850 IU dm^{-3}, which is comparable to or higher than data found in literature related to OMW treatment with *Y. lipolytica* spp., as well as with other microorganisms.[2,16,30]

Solid-state fermentation (SSF) on olive oil cake

Although submerged fermentation is the most commonly used method for lipase production,[31] recently production by SSF has been gaining significant attention.[32–34] The advantages of SSF are low total capital investment and low production costs, relatively high productivity and better product characteristics. It was reported that for a production scale of 100 m^3 lipase concentrate per year, the total capital investment needed for the submerged fermentation technology was 78 % higher than that needed for SSF.[35] Despite all the advantages of SSF over submerged fermentation, the use of this technique for the lipase production is still far from being applied on the industrial scale.

The suitability of OOC as a substrate for lipase production in the SSF cultivation mode was verified by inoculating 5 g of previously moistened OOC (moisture content 50 mass%) with 500 µL of a one-day-old culture in malt broth. Growth and lipase production curves are given in Fig. 2.

The studied yeast strain seemed to effectively grow and produce lipase in such a medium, achieving the maximum yield of produced lipase (3.8 IU g^{-1} of substrate) on the second day of fermentation and decreasing thereafter. Generally, these results corresponded to the literature data suggesting similar pattern of lipase production by *Y. lipolytica* in which lipase production occurred during the intensive cell growth.[27,36] The decrease in the lipolytic activity in the later phases of growth was usually accredited to nitrogen and carbon utilization and pH decrease as a result of the production of organic acids, such as citric acid.[28,29] However, this growth to lipase production ratio was not a common pattern for other microorganisms, particularly in the SSF mode of culture. For instance,

Candida utilis growth in the same medium reached maximum lipase activity on the 4th day of fermentation, which was followed by cessation of yeast growth.[21] The abrupt decrease in viable cell counts on the 5th day could be due to a decrease in pH and sugar consumption.

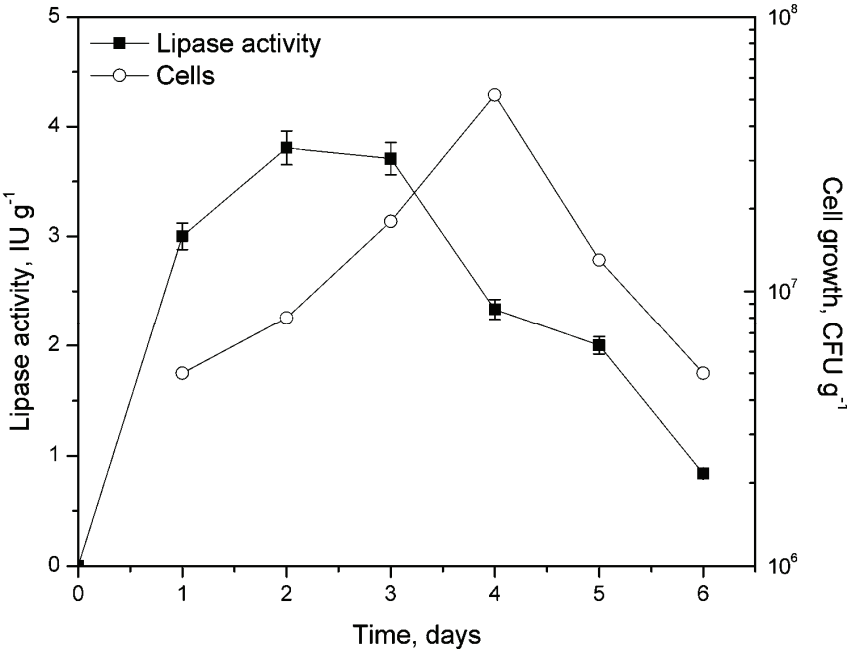

Fig. 2. The kinetics of growth and lipase production by *Y. lipolytica* in unsupplemented olive oil cake under solid-state fermentation conditions (30 °C, moisture content: 50 %). CFU g^{-1} – colony forming units per g.

Effect of moisture content and inoculum size

Since the capability of *Y. lipolytica* growth and lipase production were confirmed, studies were undertaken to optimize lipase production in this medium. In view of the fact that the moisture content and inoculum size could be critical factors in solid-state fermentations, the effect of both different initial moisture levels and inoculum size on lipase production and cell growth were evaluated. The optimal moisture content for lipase production appeared to be at 55 % initial moisture content of substrate, as shown in Fig. 3, similar to previous results considering lipase production by *C. utilis* on the same medium, where the optimal moisture content was found to be 55–60 %.[21] According to a literature survey on SSF lipase production on various food and agricultural wastes, it was suggested that an excessive moisture content has a negative effect on the physical properties of the substrate, causing agglutination of substrate particles that led to retarded oxygen transfer and over-intrusion of the substrate particles. However, sub-optimal

moisture levels adversely affected microbial growth due to insufficient particle swelling, which had a negative impact on the enzymatic activity.[21] The optimum substrate moisture content corresponded well to most of the literature data. For instance, Imandi *et al*. found the maximum lipase activity was achieved when *Y. lipolytica* was grown in seed oil cake at 60 % initial moisture.[34] In general, the differences in moisture requirements in SSF depend not only on the microorganism employed, but also greatly on the type of substrate, especially in terms of the water-holding capacity of the substrate.

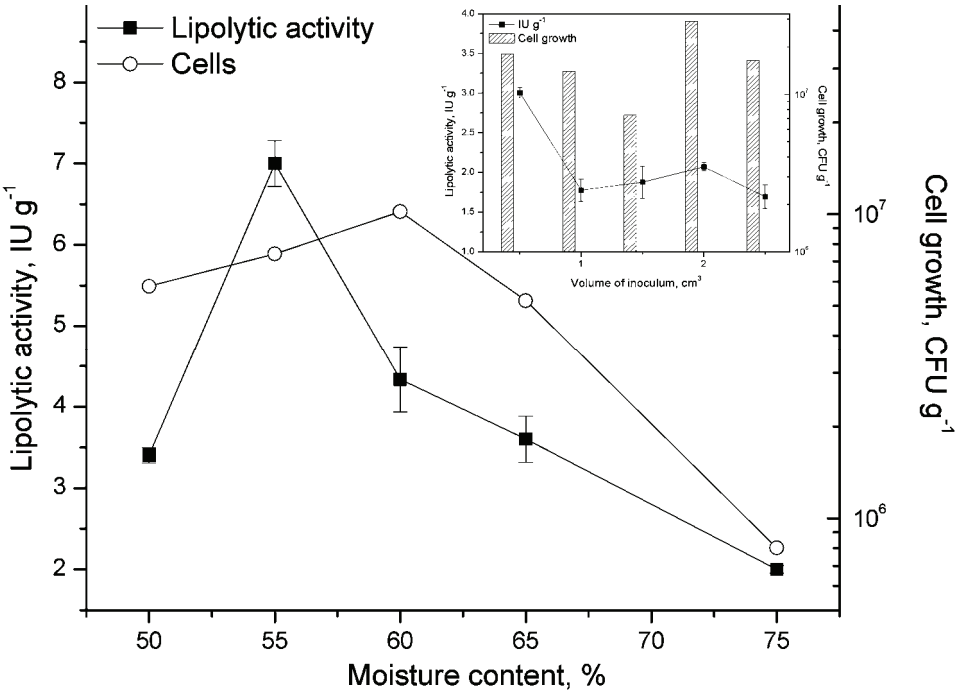

Fig. 3. Effect of moisture content and inoculum size on lipase production and growth of *Y. lipolytica* on olive oil cake (30 °C, 3rd day of fermentation).

The highest yield of produced lipase was achieved in OOC inoculated with 0.5 cm^3 of yeast culture in malt broth (approximately 5×10^7 cells cm^{-3}). It was interesting that higher cell concentrations did not result in higher lipase activity under the same culture conditions. The inhibition of the biosynthesis of lipase at higher cell concentrations might be related to inferior oxygen transfer into the culture media. It is known that low oxygen transfer negatively affects the metabolism of several microorganisms.[37] At higher cell concentrations, the oxygen transfer appeared to be lower, altering the yeast metabolism and, consequently, the production of lipase. The other possible explanation might be related to sugar consumption and pH decrease because of the production of organic acids, result-

ing in lipase deactivation. In addition, the decrease of lipase production could be due to the action of proteases.

Although microbial growth seemed to be influenced strongly by the level of inoculum employed, a significant impact of this factor on lipase production was not detected. Contrary to the present results, other researchers using the same range of inoculum volumes found that this factor had a major impact on lipase production by *Y. lipolytica* on seed oil cake in SSF, with the maximum activity being obtained when 2 cm^3 of inoculum was used.[34] However, the inoculum concentrations were not specified.

Effect of medium supplementation

To increase lipase production by the yeast and considering that the choice of the carbon source could be of crucial importance for the reduction of catabolite repression and induction of lipase biosynthesis, the basal medium (OOC) was supplemented with various carbon sources. For comparison, the yeast strain was also grown with OOC as the sole carbon source. Additionally, the medium was supplemented with several nitrogen sources. The achieved lipolytic activities in the control and enriched mediums are presented in Fig. 4.

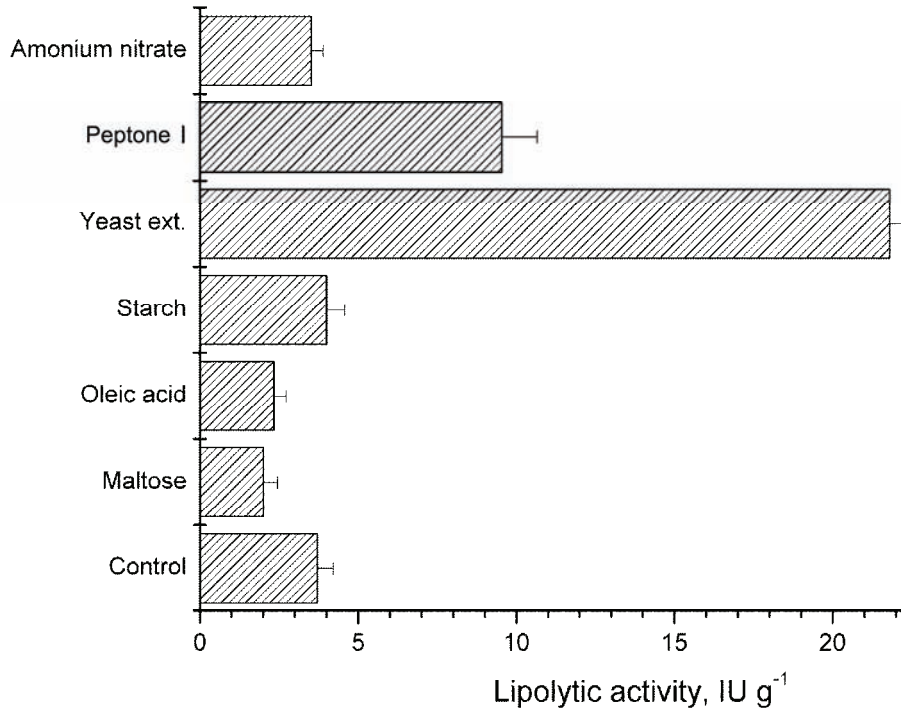

Fig. 4. Effect of supplementation of olive oil cake on lipase production by *Y. lipolytica* (30 °C, 3rd day of fermentation).

As can be seen in Fig. 4, additional oil and maltose supplementation inhibited the production of lipase. Among investigated carbon sources, starch appeared to enhance lipase production. However, the effect of starch addition was negligible as the increase in produced amounts of enzyme was only to 10 % with the respect to the control. These results differed significantly from those obtained with *C. utilis* on the same medium. A previous study on lipase production with this yeast strain showed a significant influence on lipase production on OOC supplemented with maltose, while starch inhibited enzyme secretion.[21]

On the other hand, lipase production seemed to be strongly influenced by the addition of nitrogen sources. The addition of organic nitrogen sources to the basal medium was found to be effective in enhancing the production of lipase by *Y. lipolytica*, while addition of inorganic nitrogen did not affect the enzyme production. Yeast extract addition caused a 6-fold increase in the secreted lipase unlike in a previous study with *C. utilis*, which showed that nitrogen addition had a negligible effect on lipase production. Moreover, all the employed nitrogen sources, except the yeast extract, inhibited lipase production by *C. utilis* on the same medium.[21]

In accord with the present results, a study of *Y. lipolytica* growth on seed oil cake showed a major positive impact of medium supplementation with nitrogen sources such as urea, peptone or yeast extract on the yield of the produced lipase, while NH_4NO_3 also had a negligible effect on enzyme production.[34]

Effect of alkaline treatment of the substrate

Since alkaline treatment of the OOC caused significantly better utilization of the substrate in a previous study on lipase production by *C. utilis* on the same media,[21] the same preparation method was employed to verify the possibility of improving the consumption of the substrate by *Y. lipolytica* and subsequently enhancing lipase production. The treatment was conducted based on the assumption that it could cause swelling and disruption of the structure of the substrate cell wall, facilitating thereby the access of degradative enzymes.[38] Namely, studies showed that alkaline treatment of olive oil pomace led to a significant reduction in the contents of cellulose, hemicellulose and lignin.[39] In addition, literature data showed that alkaline pretreatment of other substrates, such as bagasse, coir pith and rice husks, had tremendous effects on the physical properties of the substrates, leading to significant improvement of cellulase production by several microorganisms under SSF conditions.[39–41] The effects of this treatment on both lipase production and cell growth are shown in Fig. 5.

The biomass concentration gradually increased with fermentation period when the strain grew in alkali-treated OOC. A different pattern of cell growth was obtained for untreated OOC when the biomass concentration reached a maximum after 4 days and then decreased. This result is possibly related to the differences in the pH profile during fermentation in treated and untreated sub-

strates, although the pH was not controlled during the fermentation because of the non-homogeneity of the fermentation systems. Specifically, the measured pH after fermentation was 6.3 and 4.5 for treated and untreated substrates, respectively.

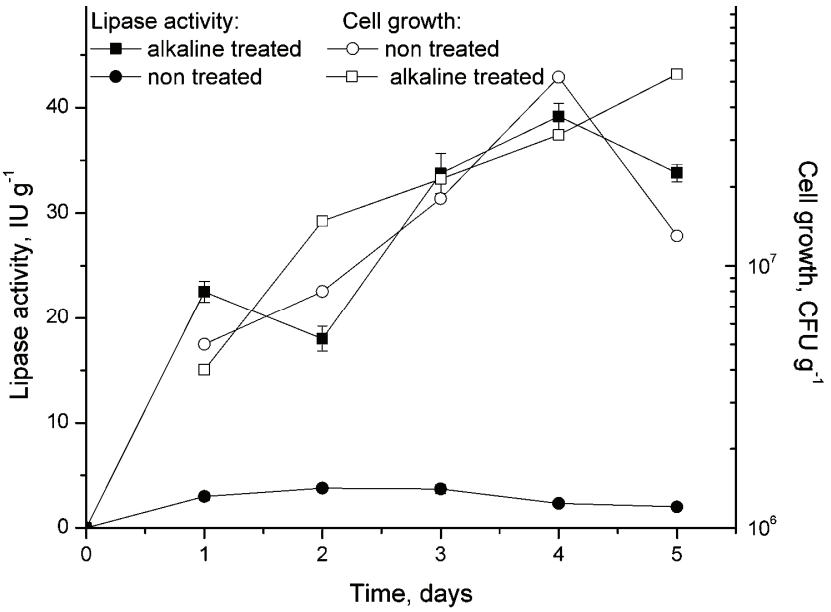

Fig. 5. Kinetics of *Y. lipolytica* growth and lipase production on alkaline-treated and non-treated OOC.

The treatment resulted in a more than a 10-fold increase in the yield of produced lipases, although it seemed that the level of produced biomass was unaffected. The amount of produced lipase reached up to ≈40 IU g^{-1} of substrate, exceeding numerous reported values considering lipase production in the SSF mode with different strains and substrates.[30]

CONCLUSIONS

This study showed that the *Y. lipolytica* NRRL Y-1095 strain could be successfully utilized for treatment and valorization of olive oil processing waste. OMW and OOC seemed to provide the necessary nutrients and physical support for yeast growth and enzyme production but this production could be further optimized by media supplementation and/or change in the physical settings of the experiment. Additionally, alkaline treatment of OOC appeared to improve remarkably lipase production by *Y. lipolytica* in SSF production. The amount of lipase in this initial study is promising and it could be of interest to attempt the production of other industrial enzymes from different microbes.

Acknowledgements. This research was realized with the financial support from the Ministry of Education, Science and Technological Development of the Republic of Serbia (Eureka project E!6750 and Project No. III 46010). The authors would also like to express their gratitude to the Agricultural Research Center (USA) for their kind donation of the *Yarrowia lipolytica* NRRL Y-1095 strain.

ИЗВОД

ПРОИЗВОДЊА ЛИПАЗЕ ИЗ *Yarrowia lipolytica* КОРИШЋЕЊЕМ ОТПАДНИХ СИРОВИНА ИНДУСТРИЈЕ ПРЕРАДЕ МАСЛИНА КАО СУПСТРАТА

OMAR A. S. MOFTAH[1], САЊА Ж. ГРБАВЧИЋ[2], WALID A. S. MOFTAH[3], НЕВЕНА Д. ЛУКОВИЋ[1], ОЛИВЕРА Л. ПРОДАНОВИЋ[4], СОЊА М. ЈАКОВЕТИЋ[1] и ЗОРИЦА Д. КНЕЖЕВИЋ-ЈУГОВИЋ[1]

[1]Катедра за биохемијско инжењерство и биотехнологију, Технолошко–металуршки факултет, Универзитет у Београду, Карнегијева 4, 11000 Београд, [2]Иновациони центар Технолошко–металуршког факултета, Универзитет у Београду, Карнегијева 4, 11000 Београд, [3]Факултет за примењену екологију, Универзитет Синергидунум, 11000 Београд и [4]Институт за мултидисциплинарна истраживања, Универзитет у Београду, Кнеза Вишеслава 1, 11030 Београд

У овом раду, течне и чврсте отпадне сировине које заостају приликом прераде маслина испитане су као потенцијални супстрати за раст квасца *Yarrowia lipolytica* са циљем производње липаза. Отпадна вода из млина, као и погача која заостаје након цеђења уља из маслина, показали су се као добри извори нутријената за раст овог квасца и производњу ензима. У оптимизованој течној подлози, принос липаза достиже и до 850 IU dm^{-3}. Поред тога, погача која заостаје након цеђења уља из маслина се показала као погодан чврсти супстрат за гајење производног микроорганизма. Продукција липаза на овом медијуму је додатно оптимизована суплементацијом различитим изворима азота и угљеника, као и променом осталих параметара ферментације. Утврђено је да се најзначајније побољшање продукције липазе остварује алкалним предтретманом супстрата (више од 10 пута).

(Примљено 5. септембра 2012, ревидирано 11. јануара 2013)

REFERENCES

1. G. Cioffi, M. S. Pesca, P. De Caprariis, A. Braca, L. Severino, N. De Tommasi, *Food Chem.* **121** (2010) 105
2. M. Lopes, C. Araújo, M. Aguedo, N. Gomes, C. Gonçalves, J. A. Teixeira, I. Belo, *J. Chem. Technol. Biotechnol*. **84** (2009) 533
3. A. Roig, M. L. Cayuela, M. A. Sánchez-Monedero, *Waste Manage.* **26** (2006) 960
4. A. S. E. Yay, H. V. Oral, T. T. Onay, O. Yenigün, *Resour. Conserv. Recycl.* **60** (2012) 64
5. J. M. Encinar, J. F. González, G. Martínez, J. M. González, *Fuel Process. Technol.* **89** (2008) 1448
6. J. M. Encinar, J. F. Gonzalez, G. Martínez, S. Roman, *J. Anal. Appl. Pyrolysis* **85** (2009) 197
7. Y. Kavdir, D. Killi, *Bioresour. Technol.* **99** (2008) 2326
8. B. Aliakbarian, A. A. Casazza, P. Perego, *Food Chem.* **128** (2011) 704
9. L. Mafakher, M. Mirbagheri, F. Darvishi, I. Nahvi, H. Zarvesh-Esfahani, G. Emtiazi, *New Biotechnol.* **27** (2010) 337
10. A. D'Annibale, G. G. Sermanni, F. Federici, M. Petruccioli, *Bioresour. Technol.* **97** (2006) 1828
11. P. F. F. Amaral, M. Lehocky, A. M. V. Timmons, M. H. M. Rocha-Leao, M. A. Z. Coelho, J. A. P. Coutinho, *Yeast* **23** (2006) 867

12. A. V. Bankar, A. R. Kumar, S. S. Zinjarde, *Appl. Microbiol. Biotechnol.* **84** (2009) 847
13. F. Darvishi, I. Nahvi, H. Zarvesh-Esfahani, F. Momenbeik, *J. Biomed. Biotechnol.* **2009** (2009) 562943
14. B. De Felice, G. Pontecorvo, M. Carfagna, *Acta Biotechnol*. **17** (1997) 231
15. C. Gonçalves, F. Oliveira, C. Pereira, I. Belo, *J. Chem. Technol. Biotechnol.* **87** (2012) 1215
16. C. Gonçalves, M. Lopes, J. P. Ferreira, I. Belo, *Bioresour. Technol.* **100** (2009) 3759
17. C. Scioli, L. Vollaro, *Water Res.* **31** (1997) 2520
18. C. Araújo, M. Aguedo, N. Gomes, J. A. Teixeira, I. Belo, in *Proceedings of International Chemical Engineering Conference: CHEMPOR 9*, 2005, Coimbra, Portugal, 2005
19. R. Lanciotti, A. Gianotti, D. Baldi, R. Angrisani, G. Suzzi, D. Mastrocola, M. E. Guerzoni, *Bioresour. Technol.* **96** (2005) 317
20. A. L. Waterhouse, in *Current Protocols in Food Analytical Chemistry*, R. E. Wrolstad, Ed., John Wiley & Sons, New York, 2002, p. 1
21. O. A. S. Moftah, S. Grbavčić, M. Žuža, N. Luković, D. Bezbradica, Z. Knežević-Jugović, *Appl. Biochem. Biotechnol.* **166** (2012) 348
22. G. L. Miller, *Anal. Chem.* **31** (1959) 426
23. APHA, *Standard Methods for the Examination of Water and Wastewater*, 18th ed., Washington, DC, 1992
24. S. Grbavčić, D. Bezbradica, L. Izrael-Živkovic, N. Avramović, N. Milosavić, I. Karadžić, Z. Knežević-Jugović, *Bioresour. Technol.* **102** (2011) 11226
25. P. Fickers, A. Marty, J. M. Nicaud, *Biotechnol. Adv.* **29** (2011) 632
26. S. Papanikolaou, M. Galiotou-Panayotou, S. Fakas, M. Komaitis, G. Aggelis, *Bioresour. Technol.* **99** (2008) 2419
27. S. V. Kamzolova, J. N. Lunina, I. G. Morgunov, *J. Am. Oil. Chem. Soc.* **88** (2011) 1965
28. A. Domínguez, F. J. Deive, M. A. Sanromán, M. A Longo, *J. Chem. Technol. Biotechnol.* **78** (2003) 1166
29. G. Corzo, S. Revah, *Bioresour. Technol.* **70** (1999) 173
30. A. Salihua, Md. Z. Alam, M. I. AbdulKarim, H. M. Salleh, *Resour. Conserv. Recycl.* **58** (2012) 36
31. S. Grbavčić, S. Dimitrijević-Branković, D. Bezbradica, S. Šiler-Marinković, Z. Knežević--Jugović, *J. Serb. Chem. Soc.* **72** (2007) 757
32. A. Domínguez, M. Costas, M.A. Longo, A. Sanromán, *Biotechnol. Lett.* **25** (2003) 1225
33. Y. Yano, H. Oikawa, M. Satomi, *Int. J. Food Microbiol.* **121** (2008) 302
34. S. B. Imandi, S. K. Karanam, H. R. Garapati, *J. Microbial. Biochem. Technol.* **2** (2010) 28
35. L. R. Castilho, T. L. M. Alves, R. A. Medronho, *Bioresour. Technol*, **71** (2000) 45
36. S. V. Kamzolova, I. G. Morgunov, A. Aurich, O. A. Perevoznikova, N. V. Shishkanova, U. Stottmeister, T. V. Finogenova, *Food Technol. Biotechnol.* **43** (2005) 113
37. M. Elibol, D. Ozer, *Process Biochem.* **36** (2000) 325
38. M. S. Haddadin, S. M. Abdulrahim, G. Y. Al-Khawaldeh, R. K. Robinson, *J. Chem. Technol. Biotechnol.* **74** (1999) 613
39. X. Zhao, Y. Zhou, G. Zheng, D. Liu, *Appl. Biochem. Biotechnol.* **160** (2010) 1557
40. S. Anuradha Jabasingha, C. Valli Nachiyar, *Ind. Crops Prod.* **34** (2011) 1564
41. C. Aiello, A. Ferrer, A. Ledesma, *Bioresour. Technol.* **57** (1996) 13.

Journal of the Serbian Chemical Society
JSCS-info@shd.org.rs • www.shd.org.rs/JSCS
J. Serb. Chem. Soc. 78 (6) 795–804 (2013)
JSCS–4458
UDC 542.9+547.571+547.551:547.864+
547.821+546.13:543.552:543.42
Original scientific paper

Synthesis, spectroscopic studies and electrochemical properties of Schiff bases derived from 2-hydroxy aromatic aldehydes and phenazopyridine hydrochloride

SULTAN YAGMUR[1], SELEHATTIN YILMAZ[1]*, GULSEN SAGLIKOGLU[1], MURAT SADIKOGLU[2], MUSTAFA YILDIZ[1] and KAMRAN POLAT[3]

[1]*Canakkale Onsekiz Mart University, Faculty of Science and Arts, Department of Chemistry, 17020, Canakkale, Turkey,* [2]*Gaziosmanpasa University, Faculty of Education, Department of Science Education, 60100, Tokat, Turkey and* [3]*Ankara University, Faculty of Science, Department of Chemistry, 06100, Ankara, Turkey*

(Received 24 May, revised 13 December 2012)

Abstract: Novel Schiff bases **1**–**4** were synthesized by the reaction of 2-hydroxybenzaldehyde, 2-hydroxy-5-methoxybenzaldehyde, 2-hydroxy-5-nitrobenzaldehyde and 2-hydroxy-1-naphthaldehyde with phenazopypridine hydrochloride (PAP), respectively, and their structures were elucidated by means of spectroscopic techniques. The electrochemical reduction of PAP and its Schiff bases (**1**–**4**) were realized on a glassy carbon electrode (GCE) in dimethyl sulfoxide (DMSO) using the cyclic voltammetric (CV) technique. The effect of functional groups on reduction potential of the Schiff bases was investigated. A general electrochemical reduction mechanism of the compounds is suggested.

Keywords: phenazopyridine hydrochloride; Schiff base; spectroscopy; voltammetry.

INTRODUCTION

Phenazopyridine hydrochloride (PAP) is an analgesic drug used to provide symptomatic pain relief in conditions such as cystitis and urethritis.[1–5] The electrochemical reduction and determination of phenazopyridine hydrochloride were realized on a carbon paste electrode by Osteryoung square wave voltammetry.[5] The electrochemical properties of PAP were also investigated by the adsorptive stripping voltammetric technique.[6] In addition, differential pulse polarography is a convenient method for the analysis of nitrofurantoin and phenazopyridine in tablet form.[7]

Schiff bases are used extensively as ligands in coordination chemistry.[8,9] They have thermochromic and photochromic properties in their solid state.[10]

* Corresponding author. E-mail: seletyilmaz@hotmail.com
doi: 10.2298/JSC120524151Y

They are also used as model systems for biological macromolecules and catalytic reactions.[11,12] There are relatively few studies on the electrochemical behavior of imines or Schiff bases in aprotic media.[13] A different mechanism was proposed in non-aqueous media where hydrolysis does not pose problems.

In Schiff bases, the reduction potential is dependent on the size of the aromatic groups on either side of the –C=N– group,[14–17] the types of substituent attached to the aromatic ring[15–19] and intra-molecular hydrogen bonds.[20,21] It has also been claimed that the presence of electron withdrawing groups and hydrogen bonding facilitate the reduction. Schiff base ligands consist of a variety of substituents with different electron-donating and electron-withdrawing groups, and therefore may have interesting electrochemical properties.

Although the electrochemical reduction reactions of Schiff bases containing –N=N– and –C=N– groups in aqueous medium[22–25] have been studied, insufficient studies have been directed to the electrochemical reduction of PAP and its Schiff bases in aqueous and non-aqueous media. In the present study, the Schiff bases **1**–**4** were synthesized and investigated by elemental analysis, FT-IR, ^{1}H-NMR, ^{13}C-NMR, UV–Vis and MS spectroscopic techniques in order to study their electrochemical properties in dimethyl sulfoxide (Scheme 1).

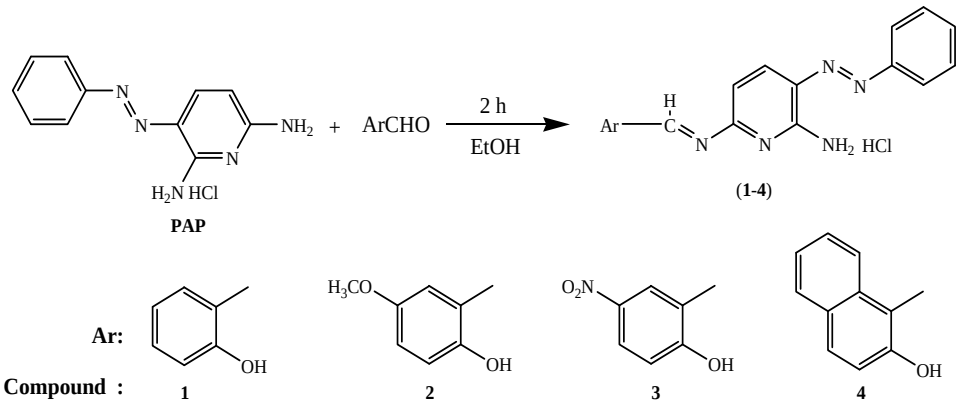

Scheme 1. The synthesis of Schiff bases **1**–**4**.

EXPERIMENTAL

Instrumentation

The ^{1}H- and ^{13}C-NMR spectra were recorded on a Bruker Avance DPX NMR spectrometer operating at 400 and 101.6 MHz, respectively. The infrared absorption spectra were recorded on a Perkin Elmer BX II spectrometer in KBr discs and are reported in cm^{-1}. The UV–Vis spectra were measured using a Shimadzu 1208 series spectrometer. Carbon, nitrogen and hydrogen analyses were performed with a Leco CHNS-932 analyzer. Melting points were measured on an Electro Thermal IA 9100 apparatus using a capillary tube. LC mass spectra were recorded on an Agilent 1100 MSD spectrometer with an ion source temperature of 240 °C. A Model Metrohm 757 VA trace analyzer (Herisau, Switzerland) was employed for the

voltammetric measurements, with a three-electrode system consisting of a GCE (surface size, φ = 7 mm, disc diameter, R = 2 mm Metrohm) working electrode, a platinum wire auxiliary electrode and a Ag/Ag^+ (0.01 M $AgNO_3$/DMSO) reference electrode. Before each measurement the working electrode was polished manually with polishing alumina (prepared from 0.01 μm aluminum oxide) on an alumina polish pad, then rinsed with ultra pure deionized water and ethanol and DMSO. All measurements were performed after deoxygenating the supporting electrolyte with argon gas for 5 min and 60 s for the sample prior to each measurement.

Reagents

PAP was kindly supplied by Faco Inc. (Istanbul, Turkey). 2-Hydroxybenzaldehyde, 2-hydroxy-5-methoxybenzaldehyde, 2-hydroxy-5-nitrobenzaldehyde, 2-hydroxy-1-naphthaldehyde, EtOH, DMSO and tetrabutylammonium iodide (TBAI, 98 %) were obtained from BDH Chemicals and alumina and silver nitrate were purchased from Merck (Germany).

Synthesis of the Schiff bases

*2-({[6-Amino-5-(2-phenyldiazenyl)pyridin-2-yl]imino}methyl)phenol hydrochloride (**1**).* PAP (0.1 g; 4.0×10^{-4} mol) was added to a dry EtOH (100 mL) solution of 2-hydroxybenzaldehyde (0.049 g; 4.0×10^{-4} mol). The mixture was stirred and heated for 2 h. Compound **1** was obtained after EtOH evaporation and crystallization from chloroform/*n*-heptane.

*2-({[6-Amino-5-(2-phenyldiazenyl)pyridin-2-yl]imino}methyl)-4-methoxyphenol hydrochloride (**2**).* Compound **2** was obtained in a similar manner to **1** but using a dry EtOH (100 mL) solution of 2-hydroxy-5-methoxybenzaldehyde (0.0608 g; 4.0×10^{-4} mol).

*2-({[6-Amino-5-(2-phenyldiazenyl)pyridin-2-yl]imino}methyl)-4-nitrophenol hydrochloride (**3**).* Compound **3** was obtained in a similar manner to **1** but using a dry EtOH (100 mL) solution of 2-hydroxy-5-nitrobenzaldehyde (0.0668 g; 4.0×10^{-4} mol).

*1-({[6-Amino-5-(2-phenyldiazenyl)pyridin-2-yl]imino}methyl)-2-naphthol hydrochloride (**4**).* Compound **4** was obtained in a similar manner to **1** but using a dry EtOH (100 mL) solution of 2-hydroxy-1-naphthaldehyde (0.0688 g; 4.0×10^{-4} mol).

RESULTS AND DISCUSSION

Schiff bases are important in diverse fields of chemistry due to their biological activities. In addition to their biological activities, their photochromic characteristics have led to their usage in various areas, such as the control and measurement of radiation intensity, display systems and optical computers. In the field of coordination chemistry, the *ortho* hydroxylated type of Schiff bases has received overwhelming attention, particularly in the study of complex formation. Recently, it was found that the introduction of lateral polar hydroxyl groups enhanced the molecular polarizability and stabilized the liquid crystalline compounds. These compounds also contain interesting groups, such as (–N=N– and –C=N–), for electrochemical studies.

Analytic and spectral data of the synthesized Schiff bases

*2-({[6-Amino-5-(2-phenyldiazenyl)pyridin-2-yl]imino}methyl)phenol hydrochloride (**1**).* Brown crystals; yield: 0.12 g, 86 %; m.p.: 227 °C; Anal. Calcd. for $C_{18}H_{16}ClN_5O$: C, 61.10; H, 4.53; N, 19.80 %. Found: C, 61.10; H, 4.56; N,

19.79 %; IR (KBr, cm^{-1}): 3306 (*m*, O–H); 3071 (*m*, Ar–H); 1631 (*m*, C=N); 1450 (*s*, C=C); 1264 (*m*, C–O); ^{1}H-NMR (400 MHz, DMSO, δ / ppm): 14.86 (1H, *s*, Ar–OH); 8.59 (1H, *s*, Ar–CH=N–); 6.29 (2H, *s*, Ar–NH_2–); 6.61–7.90 (11H, *m*, Ar-H); ^{13}C-NMR (100.6 MHz, DMSO, δ / ppm): 192.0, 162.3, 155.2, 146.8, 139.1, 137.5, 136.8, 129.9, 129.6, 128.3, 119.9, 118.9, 117.7, 117.1, 117.1, 116.2.

*2-({[6-Amino-5-(2-phenyldiazenyl)pyridin-2-yl]imino}methyl)-4-methoxyphenol hydrochloride (**2**).* Brown crystals; yield: 0.130 g, 85 %; m.p.: 195 °C; Anal. Calcd. for $C_{19}H_{18}ClN_5O_2$: C, 59.45; H, 4.69; N, 18.25 %. Found: C, 59.45; H, 4.73; N, 18.25 %; IR (KBr, cm^{-1}): 3298 (*m*, O–H); 3079 (*m*, Ar-H); 1623 (*m*, C=N); 1451 (*s*, C=C); 1266 (*m*, C–O); ^{1}H-NMR (400 Hz, DMSO, δ / ppm): 15.85 (1H, *s*, Ar–OH); 8.63 (1H, *s*, Ar–CH=N–); 6.32 (2H, *s*, Ar–NH_2–); 6.64––7.92 (10H, *m*, Ar-H); 3.79 (3H, *s*, Ar–OCH_3); ^{13}C-NMR (101.6 MHz, DMSO, δ / ppm): 191.2, 155.9, 152.6, 150.1, 142.3, 130.1, 129.7, 126.6, 126.5, 122.5, 119.2, 118.8, 117.8, 116.8, 114.5, 110.3, 55.92.

*2-({[6-Amino-5-(2-phenyldiazenyl)pyridin-2-yl]imino}methyl)-4-nitrophenol hydrochloride (**3**).* Brown crystals; yield: 0.136 g, 86 %; m.p.: 167 °C; Anal. Calcd. for $C_{18}H_{15}ClN_6O_3$: C, 54.20; H, 3.79; N, 21.08 %. Found: C, 54.21; H, 3.79; N, 21.07 %; IR (KBr, cm^{-1}): 3306 (*m*, O–H); 3063 (*m*, Ar-H); 1619 (*m*, C=N); 1451 (*s*, C=C); 1336 (*m*, C–O); ^{1}H-NMR (400 MHz, DMSO, δ / ppm): 12.21 (1H, *s*, Ar–OH); 8.90 (1H, *s*, Ar–CH=N–); 8.44 (2H, *s*, Ar–NH_2–); 6.21–8.51 (10H, *m*, Ar-H); ^{13}C-NMR (101.6 MHz, DMSO, δ / ppm): 192.2, 166.1, 142.3, 139.3, 130.1, 129.2, 128.8, 127.3, 125.2, 124.3, 123.1, 121.1, 119.3, 118.2, 116.4, 115.2.

*1-({[6-Amino-5-(2-phenyldiazenyl)pyridin-2-yl]imino}methyl)-2-naphthol hydrochloride (**4**).* Brown crystals; Yield: 0.133 g, 83 %; m.p.: 237 °C; Anal. Calcd. for $C_{22}H_{18}ClN_5O$: C, 65.43; H, 4.46; N, 17.35 %. Found: C, 65.43; H, 4.49; N, 17.34 %; IR (KBr, cm^{-1}): 3282 (*m*, O–H); 3062 (*m*, Ar-H); 1633 (*m*, C=N); 1455 (*s*, C=C); 1365 (*m*, C–O); ^{1}H-NMR (400 MHz, DMSO, δ / ppm): 15.34 (1H, *s*, Ar–OH); 8.61 (1H, *s*, Ar–CH=N–); 6.60 (2H, *s*, Ar–NH_2–); 7.58––8.96 (13H, *m*, Ar-H); ^{13}C-NMR (101.6 MHz, DMSO, δ / ppm): 193.2, 164.5, 155.1, 138.8, 130.5, 130.1, 129.8, 129.7, 129.6, 128.2, 128.0, 124.6, 122.8, 121.7, 119.7, 112.9, 109.9, 108.9, 108.3, 106.4.

FT-IR, ^{1}H-NMR, ^{13}C-NMR and UV spectroscopy

The vibration bands with the wave numbers 3306, 3298, 3306 and 3282 cm^{-1} (O–H); 3071, 3079, 3063 and 3062 cm^{-1} (C–H, Ar–H); 1450, 1451, 1451 and 1455 cm^{-1} (C=C) and 1264, 1266, 1336 and 1365 cm^{-1} (C–O, Ar–O) were observed for compounds **1**–**4**, respectively. The C=N bond was observed at 1631, 1623, 1619 and 1633 cm^{-1} for **1**–**4**, respectively. The stretching frequency observed at 2875–2745 cm^{-1} in compounds **1**–**4** showed the presence of O–H···N

intramolecular hydrogen bonds.[26,27] The C=N bond, which is partially accountable for the existence of enol–imine form, can also be inferred from the IR spectra of compounds **1**–**4**. Compounds **1**–**4** with strong bands at 1278, 1280, 1282 and 1284 cm^{-1}, respectively, possessed high percentages of the enol–imine tautomer due to stabilization of the phenolic C–O bond.[28]

The ^{1}H-NMR data for compounds **1**–**4** show that the tautomeric equilibrium favors the enol–imine in DMSO. The OH protons were observed as singlets at 14.86, 15.85, 12.21 and 15.34 ppm for compounds **1**–**4**, respectively. The azomethine protons were observed as singlets at 8.59, 8.63, 8.90 and 8.61 ppm for compounds **1**–**4**, respectively. The amine protons were found as singlets at 6.29, 6.32, 8.44 and 6.60 ppm for compounds **1**–**4**. The phenyl protons resonated as multiplets at 6.61–7.90, 6.64–7.92, 6.21–8.51 and 7.58–8.96 ppm for compounds **1**–**4**, respectively. The singlet of the Ar–OCH_3 protons was observed at 3.79 ppm for compound **2**. The ^{13}C-NMR spectra of compounds **1**–**4** have 16, 17, 16 and 20 signals, respectively.

The UV–Vis spectra of the compounds were studied in DMSO. The Schiff bases exhibited absorptions in the range greater than 400 nm in polar and non-polar solvents.[26,27] The UV–Vis spectrum of *ortho* hydroxylated Schiff-bases that exist mainly as the enol–imine structure is indicated by the presence of a band at <400 nm, while compounds existing either as keto–amine or as mixture of enol–imine/keto–amine forms show a new band, especially in polar and non-polar solvents in both acidic and basic media, at >400 nm.[26–29] Compounds **1**–**4** showed absorption above 400 nm in DMSO. The enol–imine⇆keto–amine tautomerisms of the compounds **1**–**4** are found to be 40, 38, 48 and 49 % in DMSO, respectively.

In conclusion, UV–Vis, ^{1}H-NMR and ^{13}C-NMR results showed that the compounds existed in the enol–imine form in DMSO.

Electrochemical studies

The reduction properties of PAP and its Schiff bases were investigated using a GCE by cyclic voltammetry in the potential range 0 to –3 V. The cyclic voltammetry (CV) curves of these compounds are given in Fig. 1. The curves were recorded in DMSO solution containing 0.1 M tetrabutylammonium iodide (TBAI) as a supporting electrolyte at a scan rate of 3 V s^{-1}. Three cathodic peaks were observed for PAP and compounds **1**, **2** and **4** and four peaks for compound **3**. A new reduction peak, which was thought to belong to the reduction of the NO_2 group, appeared at –2.7 V on the CV curve for compound **3**.

Since the –N=N– group (all compounds) is more susceptible to reduction than the –C=N– (compound **1**–**4**) and NO_2 (compound **3**), the –N=N– group is reduced at less negative potential than the other groups.[22–25] As could be seen from Fig. 1, the first peak (about –1.0 V) can, therefore, be attributed to the

reduction of the –N=N– (azo) group. The second peak (about –1.5 V) may most probably be due to the reduction of –C=N– (azomethine) group of the adsorbed molecule and the third peak (about –2.0 V) was thought to be due to the reduction of –C=N– group of the molecule in solution.[30] The NO_2 group is reduced at a more negative potential than the others. The fourth peak (about –2.7 V) can conveniently be attributed to reduction of the NO_2 group. Electrochemical data of these compounds are given in Table I.

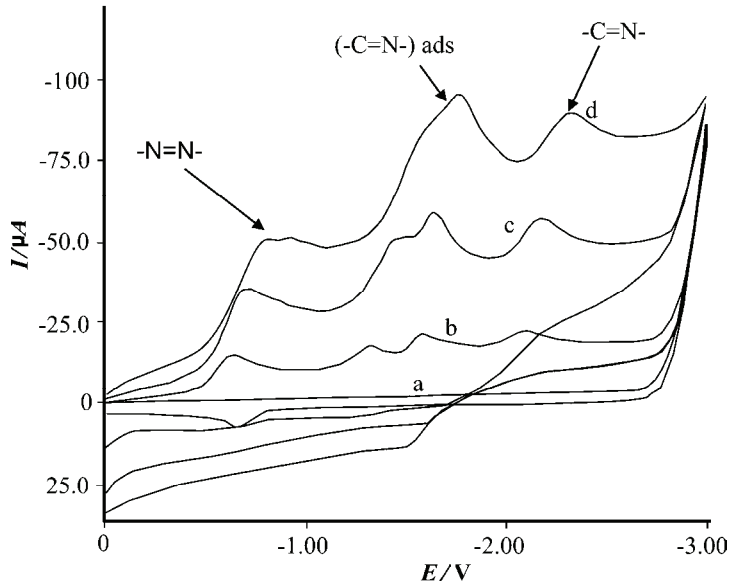

Fig. 1. The cyclic voltammograms of 2×10^{-3} M PAP and its Schiff bases in 0.1 M TBAI/DMSO at a GCE. Scan rate = 3.0 V s^{-1}.

TABLE I. Peak potential and peak current values of 2×10^{-3} M PAP and its novel Schiff bases in 0.1 M TBAI/DMSO at a GCE from CV. Scan rate = 3 V s^{-1}

Compound	Peak 1		Peak 2		Peak 3		Peak 4	
	E_{p1} / V	I_{p1} / μA	E_{p2} / V	I_{p2} / μA	E_{p3} / V	I_{p3} / μA	E_{p4} / V	I_{p4} / μA
PAP	–0.73	20.70	–1.68	31.00	–2.22	12.80	–	–
1	–0.78	22.50	–1.76	33.50	–2.30	20.30	–	–
2	–0.79	23.70	–1.77	34.90	–2.33	20.60	–	–
3	–0.61	13.60	–1.26	14.30	–1.69	26.60	–2.77	14.50
4	–0.76	23.90	–1.71	35.30	–2.26	24.50	–	–

As can be seen from Table I, the current values of the two –C=N– groups of the Schiff bases were found to be nearly twice that of the single –C=N– group of PAP. The reduction potentials depend on the electronegativity of the groups in Schiff bases.[14–21] While the reduction potential had a negative value for compound **3**, it was observed that compound **2** had a more negative potential value.

The observed reduction potentials of the Schiff bases were –0.78, –0.79, –0.61 and –0.76 V (–N=N–), –1.76, –1.77, –1.26 and –1.71 V $(–C=N–)_{ads}$ and –2.30, –2.33, –1.69, –2.26 V (–C=N–) for compounds **1**–**4**, respectively. The effects of various scan rates between 0.1–10 V $s^{–1}$ on the peak potential and the peak current of $2×10^{–3}$ M PAP and its Schiff bases were evaluated. Scan rate studies were performed to assess whether the processes on the GCE were under diffusion- or adsorption control.[31–40]

The cyclic voltammograms of $2×10^{–3}$ M PAP and its Schiff bases were obtained in 0.1 M TBAI/DMSO on a GCE. A linear relationship existed between the peak current and square root of the scan rate between 0.1–10 V $s^{–1}$ (correlation coefficient about 0.99), which showed that the reduction process was predominantly under diffusion-control over the complete scan rate range studied. In addition, a plot of the logarithm of the peak current *vs*. the logarithm of the scan rate gave a straight line (correlation coefficient about 0.99) with a slope of about 0.5, which is the expected value for an ideal reaction of solution species.[33–43] Therefore, a diffusion component must be taken into account. Other studies were conducted in line with this phenomenon.

Mechanism of the electrochemical reduction of the compounds

When describing electrochemical reactions, an "*E*" and "*C*" formalism is often employed.[32,33] *E* represents an electron transfer; sometimes E_O and E_R are used to represent oxidations and reductions, respectively. *C* represents a chemical reaction, which can be any elementary reaction step, and is often called a "following" reaction.

The electrochemical reduction mechanisms are given in Scheme 2 for PAP **1**–**4**. The electrochemical reduction occurred in three steps. The –N=N– and the –C=N– groups were reduced in the first and the second step in compounds PAP and compounds **1**–**4** and in the last step, the $–NO_2$ group was reduced in compound **3**. Both the –C=N– groups in PAP and the Schiff bases were reduced at the same potential.

As can be seen from the mechanism given in Scheme 2, the first step is the 2e reduction of the diazenyl group of PAP, in which the –N=N– bond opens resulting $–N–N^{2–}–$ dianion. Then, the hydrazine anion binds $2H^+$, resulting in the formation of a hydrazine compound (–NH–NH–). In the second step, the imine groups of PAP and its Schiff bases form a radical anion ($C–N^–$) with a 1e electron transfer. Then, the negatively charged nitrogen atom binds to a proton resulting in C–NH. This radical carbon atom takes one more electron giving a carbanion $C^–$–NH. Finally, the carbanion reacts with a proton from the solution, resulting in an amine (CHNH). In the third stage, the NO_2 group in compound **3** is reduced. According to these data, it can conveniently be claimed that the reactions occur according to an EC mechanism.[32]

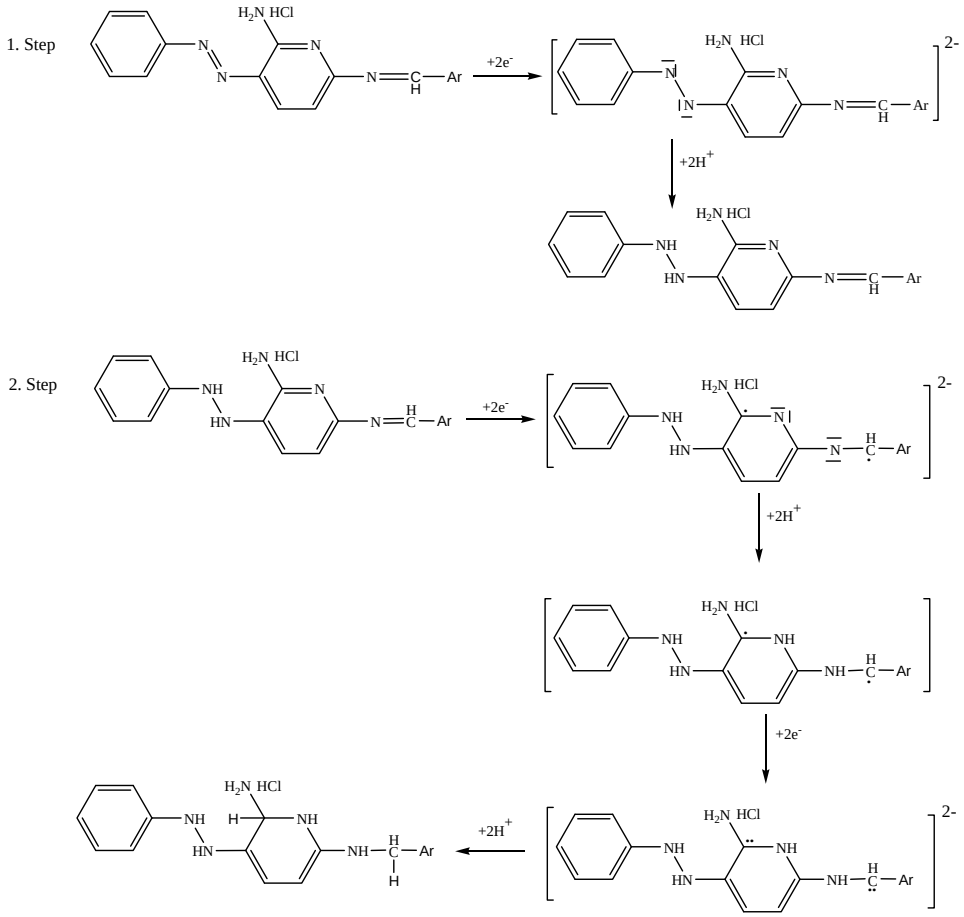

Scheme 2. Electrochemical reduction mechanism of PAP and the Schiff bases **1**–**4**.

CONCLUSIONS

In the present work, the Schiff bases **1**–**4** were synthesized and characterized, and the electrochemical properties of PAP and its Schiff bases were investigated by cyclic voltammetry. A simple, sensitive and selective CV technique was developed for the examination of the electrochemical reduction behavior of PAP and its Schiff bases **1**–**4** on a GCE. While the electrochemical reduction occurred over three steps for PAP and compounds **1**, **2** and **4**, compound **3** had a fourth step. As could be seen from the cyclic voltammograms, the first, second and third peaks belong to the –N=N–, –C=N– and –C=N–(ads) groups, respectively, and the fourth peak belongs to the NO_2 group.

It could also be concluded that the reduction potentials and currents depended on the electron withdrawing groups and hydrogen bonding on either side of the –N=N– and –C=N– groups.[14–17]

ИЗВОД

СИНТЕЗА, СПЕКТРОСКОПСКО ИСПИТИВАЊЕ И ЕЛЕКТРОХЕМИЈСКЕ ОСОБИНЕ ШИФОВИХ БАЗА ДОБИЈЕНИХ ОД 2-ХИДРОКСИ АРОМАТИЧНИХ АЛДЕХИДА И ФЕНАЗОПИРИДИН-ХИДРОХЛОРИДА

SULTAN YAGMUR[1], SELEHATTIN YILMAZ[1], GULSEN SAGLIKOGLU[1], MURAT SADIKOGLU[2], MUSTAFA YILDIZ[1] и KAMRAN POLAT[3]

[1]Canakkale Onsekiz Mart University, Faculty of Science and Arts, Department of Chemistry, 17020, Canakkale, Turkey, [2]Gaziosmanpasa University, Faculty of Education, Department of Science Education, 60100, Tokat, Turkey и [3]Ankara University, Faculty of Science, Department of Chemistry, 06100, Ankara, Turkey

У реакцијама између 2-хидроксибензалдехида, 2-хидрокси-5-метоксибензалдехида, 2-хидрокси-5-нитробензалдехида, 2-хидрокси-1-нафталдехида и феназопиридин-хидрохлорида (PAP) синтетизоване су нове Шифове базе (**1**–**4**), које су окарактерисане применом спектроскопских метода. Електрохемијска редукција феназопиридин-хидрохлорида (PAP) и одговарајућих Шифових база (**1**–**4**) је извођена на електроди од стакластог угљеника (GCE) у диметил-сулфоксиду (DMSO) применом цикличне волтаметрије (CV). Испитиван је утицај функционалних група на потенцијал редукције Шифових база. Поред тога, предложен је механизам електрохемијске редукције испитиваних једињења.

(Примљено 24. маја, ревидирано 13. децембра 2012)

REFERENCES

1. R. J. Cornwall, J. K. Bartek, *Digital Urology Journal*, Urology Nurses Online, http://www.duj.com/Pyridium.html (last accessed in 2006)
2. Medlineplus, A Service of the U.S. National Library of Medicine and The National Institutes of Health, http://www.nlm.nih.gov/medlineplus/druginfo/meds/a682231.html (last accessed on 25 June, 2013)
3. J. A. Squella, G. Valencia, I. Lemus, Lj. J. Nunez-Vergara. *J. Assoc. Anal. Chem.* **4** (1989) 72
4. V. Mirceski, B. Jordanoski, S. Komorsky-Lovric, *Portugaliae Electrochim. Acta* **16** (1998) 43
5. M. Cıtak, S. Yilmaz, Y. Dilgin, G. Türker, S. Yagmur, H. Erdugan, N. Erdugan, *Curr. Pharm. Anal.* **3** (2007) 141
6. S. M. Sabry, *Talanta* **50** (1999) 133
7. P. Surmann, P. Aswakun, *Arch. Pharm.* **318** (2006) 14
8. H. Unver, D. M. Zengin, T. N. Durlu, *Anal. Sci.* **17** (2001) 1021
9. H. Unver, D. M. Zengin, K. Güven, *J. Chem. Crystallogr.* **30** (2000) 359
10. M. D. Cohen, G. M. Schmidt, S. J. Flavian, *J. Chem. Soc., B* (1964) 2041
11. D. Chen, A. E. Martel, *Inorg. Chem.* **26** (1987*)* 1026
12. D. E. Hamilton, R. S. Dragu, A. Zonbeck, *J. Am. Chem. Soc.* **109** (1987) 374
13. M. J. Peover, A. J. Bard, *Electroanalytical Chemistry*, Marcel Dekker, New York, 1967
14. J. M. V. Scott, W. H. Jura, *Can. J. Chem.* **45** (1967) 2375
15. L. V. Kononenko, V. D. Bezuglyi, V. N. Dmitrieva, *Zh. Obshch. Khim.* **38** (1968) 2153
16. P. Martinet, J. Simonet, J. Tendil, *C. R. Acad. Sci., C* **268** (1969) 303
17. V. N. Dmitrieva, L. V. Kononenko, V. D. Bezuglyi, *Teor. Eksp. Khim.* **1** (1965) 456
18. V. D. Bezuglyi, L. V. Kononenko, A. F. Forunova, V. N. Dmitrieva, B. L. Timan, *Zh. Obshch. Khim.* **39** (1969) 1680

19. V. N. Dmitrieva, N. A. Rozanel'skaya, B. M. Krasovitskii, B. I. Stepanov, V. D. Bezuglyi, *Zh. Obshch. Khim.* **41** (1971) 60
20. V. N. Dmitrieva, V. B. Smelyakova, B. M. Krasovitskii, V. D. Bezulglyi, *Zh. Obshch. Khim.* **36** (1966) 405
21. N. F. Levchenko, L. S. Afanasiadi, V. D. Bezuglyi, *Zh. Obshch. Khim.* **37** (1967) 666
22. S. Cakir, E. Bicer, M. Odabasoglu, Ç. Albayrak, *J. Braz. Chem. Soc.* **16** (2005) 711
23. O. Çakir, E. Biçer, *Portugaliae Electrochim. Acta* **16** (1998) 11
24. E. Ispir, *Dyes Pigm.* **82** (2009) 13
25. S. Yagmur, *PhD Thesis*, Çanakkale Onsekiz Mart University, Graduate School of Science and Engineering Chair for Chemistry, Çanakkale, 2010 (in Turkish)
26. H. Nazir, M. Yildiz, H. Yilmaz, M. N. Tahir, D. Ulku, *J. Mol. Struct.* **524** (2000) 241
27. G. Y. Yeap, S. T. Ha, N. Ishizawa, K. Suda, P. L. Boey, W. A. K. Mahmood, *J. Mol. Struct.* **658** (2003) 87
28. H. Unver, M. Yildiz, N. Ocak, T. N. Durlu, *J. Chem. Crystallogr.* **38** (2008) 103
29. M. Pamuk, *M.Sc. Thesis*, Çanakkale Onsekiz Mart University, Canakkale, 2008 (in Turkish)
30. R. H. Wopschall, I. Shain, *Anal. Chem.* **39** (1967) 1535
31. M. Sadikoglu, *Ph.D. Thesis*, Ankara University, Ankara, 2005 (in Turkish)
32. R. A. Marcus, *J. Phys. Chem.* **67** (1963) 853
33. S. Yilmaz, *Analytic Voltammetry*, Canakkale Onsekiz Mart University Publication, Çanakkale, 2008 (in Turkish)
34. S. Yilmaz, *Electranalytic Chemistry*, Kriter Publication, Istanbul, 2012
35. S. Yilmaz, B. Uslu, S. A. Ozkan, *Talanta* **54** (2001) 351
36. B. Uslu, S. Yilmaz, S. A. Ozkan, *Pharmazie* **56** (2001) 629
37. B. T. Demircigil, S. A. Ozkan, O. Coruh, S. Yilmaz, *Electroanalysis* **14** (2002) 122
38. S. A. Ozkan, B. Uslu, *Anal. Bioanal. Chem.* **372** (2002) 582
39. S. Skrzypek, W. Ciesielski, S. Yilmaz, *Chem. Anal.(Warsaw)* **52** (2007) 1071
40. S. Yilmaz, S. Skrzypek, Y. Dilgin, S. Yagmur, M. Coskun, *Curr. Anal. Chem.* **3** (2007) 41
41. S. Yilmaz, M. Sadikoglu, G. Saglikoglu, S. Yagmur, G. Askin, *Int. J. Electrochem. Sci.* **3** (2008) 534
42. S. Yilmaz, *Colloids Surfaaces, B* **71** (2009) 79
43. M. Sadikoglu, G. Saglikoglu, S. Yagmur, E. Orta, S. Yilmaz, *Curr. Anal. Chem.* **7** (2010) 30.

Journal of the Serbian Chemical Society
JSCS-info@shd.org.rs • www.shd.org.rs/JSCS
J. Serb. Chem. Soc. *78* (6) 805–810 (2013)
JSCS–4459
UDC 532.74:515.12:519.17:54
Original scientific paper

Testing the quality of molecular structure descriptors. Vertex–degree-based topological indices

IVAN GUTMAN*# and JELENA TOŠOVIĆ

Faculty of Science, University of Kragujevac, P. O. Box 60, 34000 Kragujevac, Serbia

(Received 2 October 2012)

Abstract: The correlation abilities of 20 vertex–degree-based topological indices occurring in the chemical literature were tested for the case of standard heats of formation and normal boiling points of octane isomers. It is found that the correlation ability of many of these indices is either rather weak or nil. The augmented Zagreb index and the atom-bond connectivity index yield the best results.

Keywords: topological index; molecular structure descriptor; vertex–degree-based topological index; molecular graph; chemical graph theory.

INTRODUCTION

According to the IUPAC definition,[1] a *topological index* (or molecular structure descriptor) is a numerical value associated with chemical constitution for the correlation of chemical structure with various physical properties, chemical reactivity or biological activity. In the current literature, countless "structure descriptors" have been and are being proposed,[2,3] in many cases without any examination of whether these correlate with any of the "various physical properties, chemical reactivity or biological activity". Especially numerous are the molecular-graph-based structure descriptors. To use a mild expression, today there are far too many such descriptors and a firm criterion to stop or slow down their proliferation seems to be lacking.

In order to contribute towards a reduction in the number of molecular-graph-based structure descriptors and, at the same time, to single out those that deserve to be used in chemical applications, a comparative testing thereof was undertaken. In this paper, the considerations are restricted to a family of descriptors that all have the general form:[4]

* Corresponding author. E-mail: gutman@kg.ac.rs; jaca_90@live.com
# Serbian Chemical Society member.
doi: 10.2298/JSC121002134G

$$D = D(G) = \sum_{u \approx v} F(d_u, d_v) \quad (1)$$

where the summation goes over all pairs of adjacent vertices u,v of the molecular graph G and d_u denotes the degree (= number of first neighbors) of the vertex u. Hitherto, in the chemical literature, the following special cases of the function $F = F(x, y)$ in Eq. (1) have been considered:

[a] $F(x,y) = \frac{1}{\sqrt{xy}}$, for the Randić (or connectivity) index;[5,6]

[b] $F(x,y) = (x,y)^{\lambda}$, for the general Randić index,[6] where λ is an adjustable parameter;

[c] $F(x,y) = x + y$, for the first Zagreb index;[7–9]

[d] $F(x,y) = xy$, for the second Zagreb index;[7–9]

[e] $F(x,y) = \sqrt{\frac{x+y-2}{xy}}$, for the atom-bond connectivity (ABC) index;[10,11]

[f] $F(x,y) = \frac{1}{\sqrt{x+y}}$, for the sum-connectivity index;[12]

[g] $F(x,y) = (x+y)^{\lambda}$, for the general sum-connectivity index,[13] where λ is an adjustable parameter;

[h] $F(x,y) = \frac{2\sqrt{xy}}{(x+y)}$, for the geometric-arithmetic index;[14–16]

[i] $F(x,y) = \left(\frac{xy}{x+y-2}\right)^3$, for the augmented Zagreb index;[17–19]

[j] $F(x,y) = \frac{2}{x+y}$, for the harmonic index.[20]

Three more vertex-degree-based topological indices were recently proposed, in which Eq. (1) was modified, so that the summation was replaced by multiplication:

$$D^{\otimes} = D^{\otimes}(G) = \prod_{u \approx v} F(f(u), d(v))$$

These indices are the first multiplicative Zagreb index,[21–23] (Π_1), the modified first multiplicative Zagreb index[24] (Π_1^*) and the second multiplicative Zagreb index[23] (Π_2), defined as:

$$\Pi_1 = \prod_v (d_v)^2, \quad \Pi_1^* = \prod_{u \approx v} (d_u + d_v), \quad \Pi_2 = \prod_{u \approx v} d_u d_v$$

The logarithms of the above expressions are then of the form (1), and pertain to the following choices of the function $F(x, y)$:

[k] $F(x, y) = \frac{\ln x}{x} + \frac{\ln y}{y}$, for the logarithm of first multiplicative Zagreb index;[25]

[l] $F(x, y) = \ln(x + y)$, for the logarithm of the modified first multiplicative Zagreb index;

[m] $F(x, y) = \ln x + \ln y$, for the logarithm of second multiplicative Zagreb index.

NUMERICAL WORK

How well the above-specified topological indices are correlated with two simple physico-chemical parameters were tested. The parameters chosen were the standard heats of formation (representative for thermochemical properties) and the normal boiling points (representative for intermolecular, van der Waals-type, interactions). In order to avoid size-dependency problems, a class of isomers was considered. In order to minimize problems caused by steric effects, polar functional groups, hydrogen bonding, and similar, the tests were made on a class of alkanes. The octanes were chosen as they are particularly convenient for such studies, because the number of their structural isomers (18) is large enough to make statistical inferences reliable, and because experimental data are available for all isomers.

From the formulas displayed in the preceding section, it is evident that for $\lambda = -1/2$, the general Randić index and the general sum-connectivity index are equal to the ordinary Randić index and the ordinary sum-connectivity index, respectively. For $\lambda = 1$, the general Randić index and the general sum-connectivity index coincide with the second and first Zagreb indices, respectively. In addition, for $\lambda = -1$, the general sum-connectivity index reduces to the harmonic index. In view of this, the variable Randić index for $\lambda = -3, -2, -1, 2, 3$ and the variable sum-connectivity index for $\lambda = -3, -2, 2, 3$ were tested. Thus, a total of 20 different vertex-degree-based topological indices of the form (1) were tested.

Experimental data for the heats of formations and boiling points of all octane isomers were taken from standard reference databases[26] (for details see Ref. 11). The topological indices were evaluated by an in-house computer program. Correlations between experimental data and topological indices were analyzed by a standard statistical software package.

In each particular case, the possibility of a curvilinear correlation was tested. In not a single case, could the existence of such a correlation be established. Therefore, the quality of the examined correlations could be assessed and compared by their correlation coefficients. These are collected in Table I.

TABLE I. Correlation coefficients $R(\Delta H_f^0)$ and $R(b.p.)$ for the correlations between the vertex-degree-based topological indices and the standard heats of formation (ΔH_f^0) and normal boiling points ($b.p.$) of isomeric octanes. The considered topological indices are defined *via* Eq. (1), in which the function $F(x,y)$ is given by the formulas [a]–[m]

Index	$R(\Delta H_f^0)$	$R(b.p.)$
[a]	–0.846	0.816
[b], $\lambda = -3$	–0.827	0.791
[b], $\lambda = -2$	–0.869	0.832
[b], $\lambda = -1$	–0.886	0.853

TABLE I. Continued

Index	$R(\Delta H_f^0)$	$R(b.p.)$
[b], $\lambda = 2$	0.447	–0.372
[b], $\lambda = 3$	0.437	–0.335
[c]	0.757	–0.713
[d]	0.536	–0.491
[e]	0.890	–0.860
[f]	–0.827	0.797
[g], $\lambda = -3$	–0.870	0.851
[g], $\lambda = -2$	–0.865	0.844
[g], $\lambda = 2$	0.705	–0.649
[g], $\lambda = 3$	0.655	–0.587
[h]	–0.854	0.818
[i]	–0.921	0.922
[j]	–0.844	0.817
[k]	–0.745	0.728
[l]	0.806	–0.772
[m]	0.752	–0.723

From Table I, it can be see that for each topological index, the two correlation coefficients were nearly equal, thus implying almost identical conclusions concerning the quality of the index. This detail confirms that the choice of the two test parameters (the physicochemical nature of which were quite different) was a reasonable one, and that the results of the comparison were indeed representative for the general quality of the topological indices considered.

DISCUSSION AND CONCLUDING REMARKS

By inspection of the data given in Table I, it is possible to draw a number of conclusions, some quite unfavorable for several well-established topological indices.

First, the famous and much studied Zagreb indices ([c] and [d]) were found to be completely inadequate for any structure–property correlation. This important detail seems to have been ignored in recent comprehensive surveys[27,28] on Zagreb indices.

In addition, the results for [k], [l] and [m] revealed that the recently advocated idea of using the multiplicative Zagreb indices[22–24] did not pass the test. Consequently, it may be justified to halt any further elaboration of the theory of these multiplicative indices.

The Randić index ([a]) is one of the most often applied molecular-graph-based structure descriptors. It is therefore remarkable to realize that its modification [b] with exponent $\lambda = -1$ (and to a lesser extent with exponent $\lambda = -2$) performs significantly better than the ordinary variant (with exponent $\lambda = -0.5$). This fact was mentioned neither in a recent review[29] by Randić himself, nor in some books.[2,6]

From a practical point of view, topological indices for which the absolute value of the correlation coefficients is less than 0.8 can be characterized as useless. This especially applies to the variable Randić index [b] and the variable sum-connectivity index [g] with exponents $\lambda > 1$.

The newly proposed sum-connectivity index [f][12] and harmonic index [j],[20] although having reasonably good correlation abilities, are outperformed by several older indices. Therefore, the justification of their use in structure–property correlations is questionable.

The only vertex-degree-based topological index that has correlation coefficients over 0.9 is the augmented Zagreb index [i], recently invented by Furtula *et al*.[17] It may be stated that only this index successfully passed the tests applied in the present study. Consequently, this index should be preferred in designing quantitative structure–property relations.

The second-best vertex-degree-based molecular structure-descriptor appears to be the Estrada atom-bond connectivity (ABC) index [e].

Acknowledgement. The authors thank the Ministry of Education, Science and Technological Development of the Republic of Serbia for support (Grant No. 174033).

И З В О Д

ТЕСТИРАЊЕ КВАЛИТЕТА МОЛЕКУЛСКИХ СТРУКТУРНИХ ДЕСКРИПТОРА. ТОПОЛОШКИ ИНДЕКСИ ЗАСНОВАНИ НА СТЕПЕНИМА ЧВОРОВА

ИВАН ГУТМАН и ЈЕЛЕНА ТОШОВИЋ

Природно–математички факултет Универзитета у Крагујевцу

За 20 тополошких индекса заснованих на степенима чворова, а који су разматрани у хемијској литератури, тестирана је корелација са стандардним топлотама образовања и нормалним тачкама кључана изомерних октана. Показано је да су за већину ових индекса ове корелације или веома слабе или непостојеће. Најбоље резултате дају "појачани индекс Загреб" (*augmented Zagreb index*) и ABC индекс.

(Примљено 2. октобра 2012)

REFERENCES

1. H. Van de Waterbeemd, R. E. Carter, G. Grassy, H. Kubiny, Y. C. Martin, M. S. Tutte, P. Willet, *Pure Appl. Chem.* **69** (1997) 1137
2. R. Todeschini, V. Consonni, *Molecular Descriptors for Chemoinformatics*, Vols. 1 & 2, Wiley-VCH, Weinheim, Germany, 2009
3. I. Gutman, B. Furtula, Eds., *Novel Molecular Structure Descriptors – Theory and Applications*, Vols. 1 & 2, Univ. Kragujevac, Kragujevac, 2010
4. I. Gutman, B. Furtula, *J. Serb. Chem. Soc.* **77** (2012) 1031
5. M. Randić, *J. Am. Chem. Soc.* **97** (1975) 6609
6. X. Li, I. Gutman, *Mathematical Aspects of Randić-Type Molecular Structure Descriptors*, Univ. Kragujevac, Kragujevac, Serbia, 2006
7. B. Liu, Z. You, *MATCH Commun. Math. Comput. Chem.* **65** (2011) 581

8. T. Došlić, B. Furtula, A. Graovac, I. Gutman, S. Moradi, Z. Yarahmadi, *MATCH Commun. Math. Comput. Chem.* **66** (2011) 613
9. T. Réti, *MATCH Commun. Math. Comput. Chem.* **68** (2012) 169
10. E. Estrada, L. Torres, L. Rodríguez, I. Gutman, *Indian J. Chem., A* **37** (1998) 849
11. I. Gutman, J. Tošović, S. Radenković, S. Marković, *Indian J. Chem., A* **51** (2012) 690
12. B. Zhou, N. Trinajstić, *J. Math. Chem.* **46** (2009) 1252
13. B. Zhou, N. Trinajstić, *J. Math. Chem.* **47** (2010) 210
14. D. Vukičević, B. Furtula, *J. Math. Chem.* **46** (2010) 1369
15. M. Mogharrab, G. H. Fath-Tabar, *MATCH Commun. Math. Comput. Chem.* **65** (2011) 33
16. K. C. Das, I. Gutman, B. Furtula, *MATCH Commun. Math. Comput. Chem.* **65** (2011) 595
17. B. Furtula, A. Graovac, D. Vukičević, *J. Math. Chem.* **48** (2010) 370
18. Y. Huang, B. Liu, L. Gan, *MATCH Commun. Math. Comput. Chem.* **66** (2011) 483
19. D. Wang, Y. Huang, B. Liu, *Commun. Math. Comput. Chem.* **68** (2012) 209
20. L. Zhong, *Appl. Math. Lett.* **25** (2012) 561
21. H. Narumi, M. Katayama, *Mem. Fac. Engin. Hokkaido Univ.* **16** (1984) 209
22. D. J. Klein, V. R. Rosenfeld, *MATCH Commun. MATCH. Comput. Chem.* **64** (2010) 607
23. I. Gutman, M. Ghorbani, *Appl. Math. Lett.* **25** (2012) 1435
24. M. Eliasi, A. Iranmanesh, I. Gutman, *MATCH Commun. Math. Comput. Chem.* **68** (2012) 217
25. T. Došlić, T. Réti, D. Vukičević, *Chem. Phys. Lett.* **512** (2011) 283
26. NIST Standard Reference Database, http://webbook.gov/chemistry
27. S. Nikolić, G. Kovačević, A. Miličević, N. Trinajstić, *Croat. Chim. Acta* **76** (2003) 113
28. N. Trinajstić, S. Nikolić, A. Miličević, I. Gutman, *Kem. Ind.* **59** (2010) 577
29. M. Randić, *J. Mol. Graphics Modell.* **20** (2001) 19.

Journal of the Serbian Chemical Society
JSCS-info@shd.org.rs • www.shd.org.rs/JSCS
J. Serb. Chem. Soc. 78 (6) 811–826 (2013)
JSCS–4460
UDC 546.92+544.723+544.4:536–33
Original scientific paper

Comparison of the adsorption by rice hulls and Lewatit TP 214 of platinum from chloroplatinic solution

MEHMET HAKAN MORCALI*, BIHTER ZEYTUNCU and ONURALP YUCEL

Istanbul Technical University, Faculty of Chemical and Metallurgical Engineering, Maslak, 34469, Istanbul, Turkey

(Received 12 September, revised 1 December 2012)

Abstract: Rice hulls, a biomass waste product, and Lewatit TP 214, a thiosemicarbazide sorbent, were investigated as adsorbents for the adsorption of platinum(IV) ions from synthetically prepared dilute chloroplatinic acid solutions. The rice hulls were characterized by attenuated total reflection-Fourier transform infrared spectroscopy (ATR-FTIR). The effects of the different adsorption parameters, sorbent dosage, contact time, temperature and pH of the solution on the percent adsorption were studied in detail for batch sorption. The adsorption equilibrium data were best fitted with the Langmuir isotherm model. The maximum monolayer adsorption capacities, Q_{max}, at 25 °C were found to be 42.02 and 33.22 mg g^{-1} for the rice hulls and Lewatit TP 214, respectively. Thermodynamic calculations using the measured $\Delta H°$, $\Delta S°$ and $\Delta G°$ values indicated that the adsorption process was spontaneous and endothermic. The pseudo-first-order and pseudo-second-order rate equations were investigated; the adsorption of platinum ions for both sorbents was found to be described by the pseudo-second-order kinetic model. The kinetic rate, k_2, using 30 mg sorbent at 25 °C was found to be 0.0289 and 0.0039 g min^{-1} mg^{-1} for the rice hulls and Lewatit TP 214, respectively. The results indicated that the rice hulls could be effectively used for the removal of platinum from aqueous solution.

Keywords: adsorption; platinum; rice hulls; kinetics; isotherm.

INTRODUCTION

Platinum is one of the most important precious metals as it is widely used worldwide in many industrial applications, such as in catalytic converters, thermocouples, the jewelry sector, platinum electroplating solutions, and laboratory equipments, *etc*. The diminishing availability of mineral sources and the increasing demand for platinum make its recovery from waste solutions and scrap materials important.[1] Platinum recovery from secondary sources, such as catalytic converters, thermocouples, waste electroplating solutions and leaching solutions

* Corresponding author. E-mail: hakanmorcali@gmail.com
doi: 10.2298/JSC120912150M

stemming from primary resources, is of paramount importance.[1] Recently, platinum adsorption from aqueous solutions via resins or waste materials has received considerable attention because platinum is appreciably present in electronic parts and plating materials due to its high resistance to oxidation.[2]

Worldwide, adsorption is commonly applied in waste treatment applications. Liquid–solid adsorption systems are based on the ability of certain solids to concentrate preferentially specific substances from solutions onto their surfaces. This ability can be used for the removal of pollutants, such as heavy metal ions and chemical compounds, from wastewater.[3–6]

Over the past decade, significant research effort has been directed to find low cost, high capacity adsorbents for the removal of metal ions. A wide range of adsorbents have been developed and tested, including several activated carbons.[7–10] In addition, a number of low cost agricultural wastes, such as peat coal, rice hulls, tree fern and chitosan, have been used for the removal of a range of metal ions. In particular, several natural resources have been studied for platinum recovery, including activated carbon,[2] chitosan[11] and ion exchange resins.[12]

Adsorption methods are widely used and are very effective at low metal concentrations. Among the different types of sorbents, synthetic ion-exchange resins offer substantial advantages, such as high selectivity, good kinetic properties, and the following convenient forms for use: granules, powders, fibers, and filters. The majority of these resins are based on organic matrices with chemically bound functional groups that coordinate to or chelate metal ions. Lewatit TP-214 is a chelating resin with thiourea groups that exhibit a high affinity for platinum and other precious metals, such as silver and gold. The resin possesses a matrix of cross-linked polystyrene. Lewatit TP 214 is one of the most commonly used resins that consist of polystyrene-containing thiourea groups.[13]

Rice hulls, the hard protective covering of rice grains, are an agricultural waste material. Recently, rice hulls have been employed as building materials, fertilizers, insulation materials and fuel. In the majority of rice-producing countries (*e.g.*, Japan, China, Turkey and India) most of the hulls generated from rice processing are either burned or discarded as waste.[13,14]

In Turkey, agricultural by-products and waste materials that are available in large quantities may have the potential to be used as low-cost adsorbents. The conversion of agricultural waste materials into activated carbon would add considerable economic value, help to reduce the cost of waste disposal and, most importantly, provide a potentially inexpensive alternative to the existing commercial activated carbons.

There are many studies in the literature on the preparation of activated carbons from agricultural wastes, such as sunflower seed hulls, peanut hulls, almond shells, wheat bran, coir pith, banana pith, date pits, cotton stalks, palm tree,

orange peel, corncob, barley husk, palm kernel shells, rice husk, pinewood and soy hulls.[15–27]

In this work, rice hulls, an agricultural by-product, and Lewatit TP 214 were used to adsorb platinum from dilute platinum chloride solutions. The objective of the study was to describe an effective adsorption process using either Lewatit TP 214 or rice hulls and to compare the two sorbents by describing the optimal conditions and parameters for the adsorption of platinum, including the adsorption isotherms of platinum ions and the kinetics and thermodynamics of the adsorption process. For these reasons, the following parameters were studied to investigate their effect on the percentage of platinum adsorbed: amount of sorbent, contact time, temperature and solution pH.

EXPERIMENTAL

The Lewatit TP 214 (with a density of approximately 1.1 g ml^{-1}) was obtained from the Lanxess Company, Germany. The rice hulls were obtained from the Gokbayrak Company, Turkey. The rice hull material of ≈250 μm was used for all experiments.

The platinum-containing solutions for the experiments were prepared from chloroplatinic acid (H_2PtCl_6) standard solution (Merck, Germany). Distilled water was used for the wet chemical analyses.

This study was conducted using a batch system by varying one parameter at a time. For each experiment, 5 ml of a platinum solution was brought into contact with the sorbent (Lewatit TP 214 or rice hulls) in a Falcon tube to avoid exposure to air. The Falcon tubes were shaken in a temperature-controlled water bath at a manually adjusted shaking rate of 100 rpm. The initial platinum ion concentrations were 100, 150, 200 and 250 mg L^{-1}.

The first experimental series examined the effect of varying the sorbent dosage. The second experimental series investigated the effect of varying the contact time from 15 to 120 min. The third experimental series explored the influence of temperature, which ranged from 25 to 45 °C. In the fourth experimental series, the effect of solution pH was evaluated. For this purpose, hydrochloric acid and sodium hydroxide were employed to adjust the pH level of the solution. The final experimental series investigated the adsorption kinetics, isotherm and thermodynamics.

Solid–liquid separation was performed following each run. For the ICP-OES analysis, each filtered solution was introduced into the instrument following an appropriate dilution.

The adsorption percentage, A, was calculated using the following equation:[28,29]

$$A = 100(c_0 - c_t)/c_0 \quad (1)$$

The adsorption capacity of the platinum ion was calculated using the following general equation:[28,29]

$$q_e = (c_0 - c_t)V/m \quad (2)$$

in which q_e is the amount of metal ions adsorbed at equilibrium per unit weight of sorbent (mg g^{-1}), c_0 and c_t (mg L^{-1}) are the platinum ion concentrations present in the solution before and after adsorption, respectively, V is the volume of the solution (in L), and m is the amount of sorbent (in g) used in the adsorption experiment.

Preparation and characterization of the rice hulls

The dry rice hulls were crushed using a crushing mill. The resulting recovered product was washed several times with distilled water to eliminate water-soluble impurities and then dried in an oven at 105 °C. The sample was then removed from the oven and cooled in a desiccator. After cooling, the rice hull material was subsequently subjected to a homogenization treatment using a three-dimensional shaker for 1 h.

The identification of some characteristic functional groups was performed using FTIR spectroscopy. The IR spectrum of the rice hulls is displayed in Fig. 1.

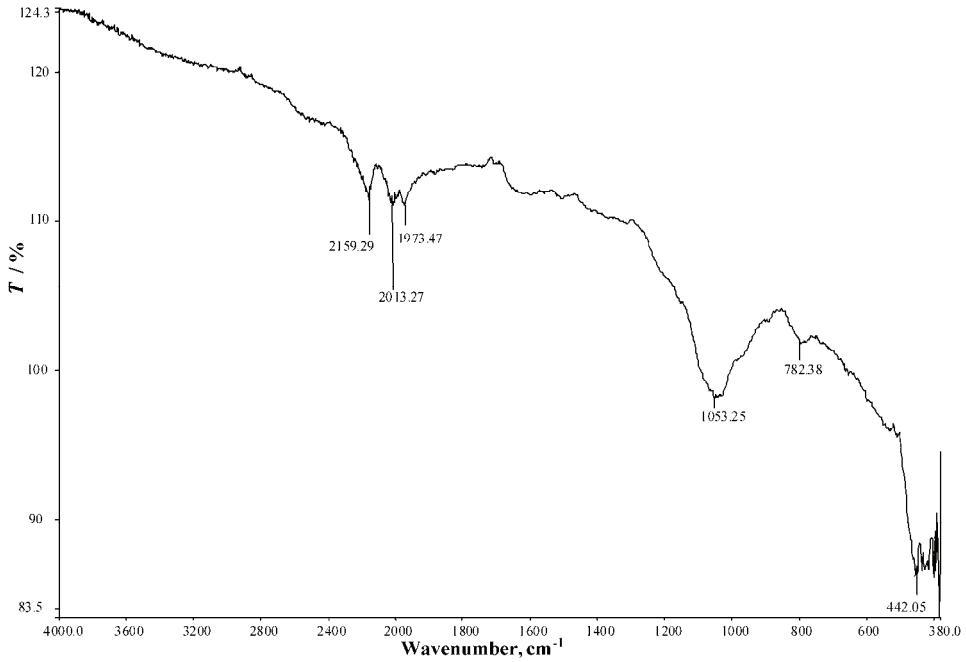

Fig. 1. FTIR absorption spectrum of rice hulls.

The IR bands of rice hulls in the region 1200–1000 cm^{-1} were considered to result from the superposition of vibrations of the C–OH bonds and Si–O bonds in the siloxane (Si–O–Si) groups. The intense band at 1053 cm^{-1} corresponds to the stretching vibrations of silicon–oxygen tetrahedrons (SiO_4). The high intensity of this peak was probably due to the superposition of the stretching vibrations of the C–OH bonds in the interval 1200–1000 cm^{-1} and the stretching vibrations of the Si–O bonds. The absorbance peak at 442 cm^{-1} was due to the bending vibration of siloxane bonds.[13]

RESULTS AND DISCUSSION

The following results outline the factors that play a role in platinum adsorption and the conditions for attaining maximum adsorption percentage of platinum.

Effect of sorbent dosage on platinum adsorption

The dosages of the rice hulls and Lewatit TP 214 material were varied, ranging from 10 to 100 mg in the first experimental series. The adsorptions of platinum with increasing sorbent dosages are presented in Fig. 2.

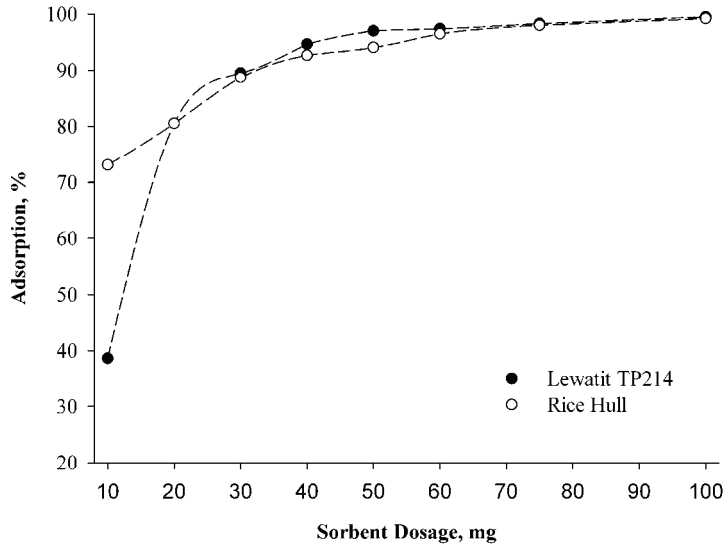

Fig. 2. The effect of increasing sorbent dosage on platinum adsorption (60 min, 25 °C, 100 rpm, pH 1.5 and 5 mL of 100 ppm solution).

The platinum adsorption was found to increase with increasing sorbent dosage because adsorption reactions are thermodynamically more favorable when the sorbent-to-metal ion ratio is high.[13,30] This is an expected result because as the amount of adsorbent increased, the available surface area increased, thereby exposing more active sites for the binding of metal ions. A similar trend for the effect of adsorbent concentration was observed in a study by Aktas and Morcali.[13]

The rice hull material was equally successful as Lewatit TP 214 at adsorbing platinum ions. For a 60 min contact time with the platinum-containing solution, Lewatit TP 214 (20 mg) exhibited a platinum adsorption of 80 %; with 50 mg of the Lewatit TP 214, 95 % of the platinum was adsorbed. Similarly, for a 60 min contact time, 95 % of the platinum was adsorbed using 60 mg of the rice hull material.

Effect of time on the platinum adsorption

In this experimental series, the effect of contact time on the percent platinum adsorption was studied in the range of 15 to 120 min. The platinum adsorption as a function of contact time is presented in Fig. 3.

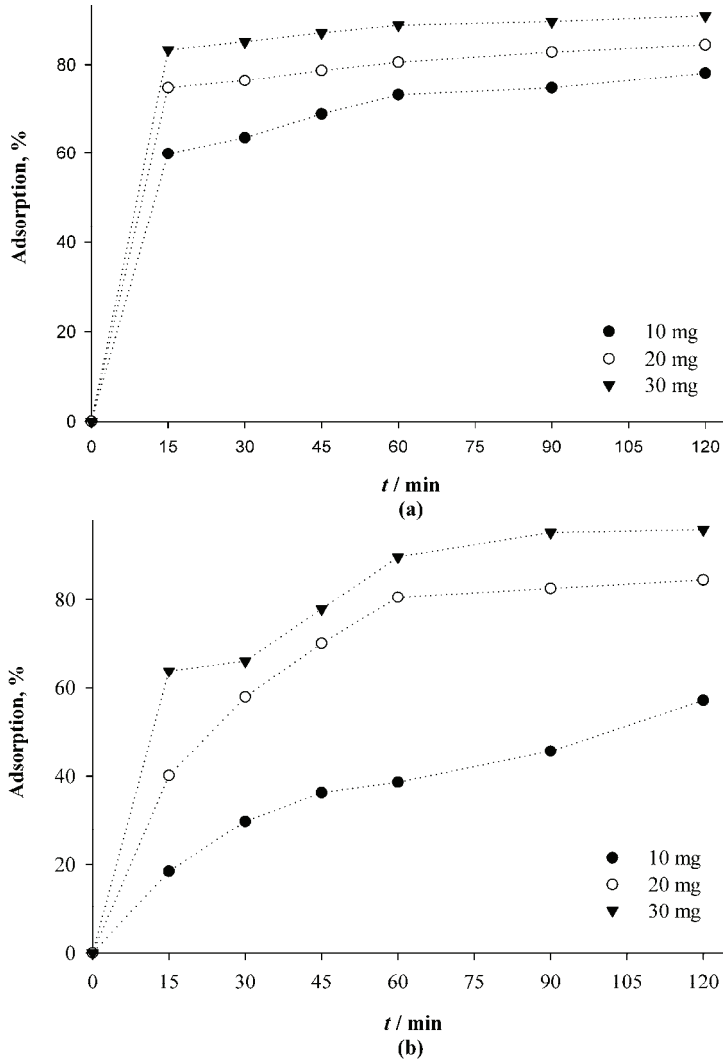

Fig. 3. Platinum adsorption as a function of contact time by a) rice hulls and b) Lewatit TP 214 (25 °C, 100 rpm, pH 1.5 and 5 mL of 100 ppm solution).

Figure 3 demonstrates that increasing the contact time had a positive effect on the platinum adsorption (*i.e.*, the platinum adsorption increased with increasing time). Figure 3a shows that the adsorption of platinum reached equilibrium after 15 min, *i.e.*, there was no significant increase in adsorption percentage after 15 min. Initially, the rate of adsorption was higher because all the adsorption sites on the rice hull material were vacant and the concentration was high, but after 15 min, all the adsorption sites were filled with platinum ions, resulting in unchanged adsorption percentages. Figure 3b indicates that the adsorption of pla-

tinum by Lewatit TP 214 reached equilibrium after 90 min. This is an expected result because the adsorption rate of Lewatit TP 214 was stable. Thus, the adsorption rate of the rice hull material is faster than that of Lewatit TP 214.

To analyze the adsorption rates of platinum ions onto the rice hull material and Lewatit TP 214, two different kinetic models were applied.

Adsorption kinetics

To investigate the controlling mechanism of the adsorption process, *i.e.*, mass transfer or chemical reaction, the pseudo-first-order and pseudo-second-order rate equations were studied for the adsorption of platinum ions by the rice hull material and Lewatit TP 214.

Pseudo-first-order rate equation. The pseudo-first-order rate expression, popularly known as the Lagergren Equation, is generally described by the following equation:[31,32]

$$\mathrm{d}q/\mathrm{d}t = k_{\mathrm{ad}}(q_{\mathrm{e}} - q_t) \quad (3)$$

where q_{e} is the amount of metal ions adsorbed at equilibrium per unit weight of sorbent (mg g^{-1}), q_t is the amount of metal ions adsorbed at any time t (mg g^{-1}), and k_{ad} is the rate constant (min^{-1}). Integrating and applying the boundary conditions from $t = 0$ and $q = 0$ to $t = t$ and $q = q_t$, Eq. (3) takes the form:

$$\ln (q_{\mathrm{e}} - q_t) = \ln q_{\mathrm{e}} - k_{\mathrm{ad}}t \quad (4)$$

To determine the rate constants, plots of $\ln (q_{\mathrm{e}} - q_t)$ *vs.* t (time) were made (not presented). These plots exhibited straight lines for the rice hull material and for Lewatit TP 214. The intercept of these plots results in $\ln q_{\mathrm{e}}$.

Pseudo-second-order rate equation. The adsorption data were also analyzed in terms of a pseudo-second-order mechanism given by:[33]

$$\mathrm{d}q/\mathrm{d}t = k_2(q_{\mathrm{e}} - q_t)^2 \quad (5)$$

where k_2 is the rate constant (g min^{-1} mg^{-1}). Integrating the above equation and applying the boundary conditions, *i.e.*, $t = 0$ for $q = 0$ and $t = t$ for $q = q_t$, gives:

$$t/q_t = 1/(k_2 q_{\mathrm{e}}^2) + 1/(q_{\mathrm{e}}t) \quad (6)$$

The plots of t/q_t *vs.* t yielded straight lines, as shown in Fig. 4, which enabled the calculation of k_2. The linear model exhibited a good fit for the two sorbents.

The application of the different kinetic models revealed interesting features regarding the mechanism and the rate-controlling step in the overall sorption process. The kinetic parameters of both the rice hulls and Lewatit TP 214 under different conditions were calculated and the results are given in Table I. To quantify the applicability of each model, the correlation coefficient (R^2) was calculated from these plots. The fits showed that the pseudo-second-order rate equation, an indication of a chemisorptions mechanism, is a better fit ($R^2 \geq 0.99$) than the pseudo-first-order rate equation ($R^2 << 0.99$) (Table I).

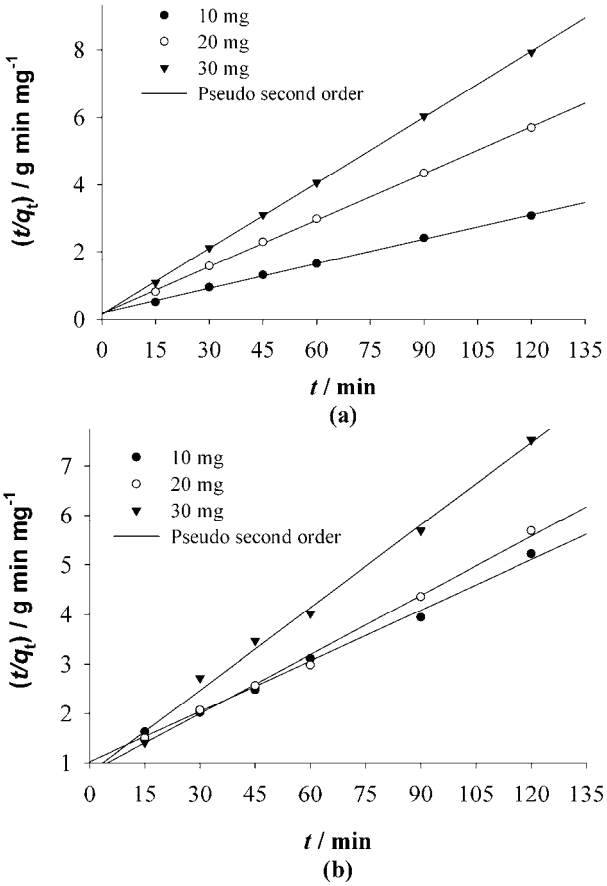

Fig. 4. a) The pseudo-second-order rate equation plots for platinum adsorbed onto rice hulls and b) the pseudo-second-order rate equation plots for platinum adsorbed onto Lewatit TP 214 (25 °C, 100 rpm, pH 1.5 and 5 mL of 100 ppm solution).

TABLE I. Constants for the pseudo-first-order and pseudo-second-order rate equations for platinum ion adsorption onto rice hulls and Lewatit TP 214

	Rice hulls			Lewatit TP 214		
Constants for the pseudo first-order rate equation (Lagergren rate constants)						
Sorbent, mg	k_{ad} / min^{-1}	q_e / mg g^{-1}	R^2	k_{ad} / min^{-1}	q_e / mg g^{-1}	R^2
10	0.0438	29.02	0.8562	0.0436	32.08	0.9574
20	0.0291	5.09	0.9549	0.0451	23.63	0.9796
30	0.0268	2.23	0.9632	0.0462	16.10	0.9685
Constants for the pseudo second-order rate equation						
Sorbent, mg	k_2 / g min^{-1} mg^{-1}	q_e / mg g^{-1}	R^2	k_2 / g min^{-1} mg^{-1}	q_e / mg g^{-1}	R^2
10	0.0032	41.15	0.9986	0.0011	29.41	0.9944
20	0.0127	21.60	0.9995	0.0020	25.19	0.9941
30	0.0289	15.36	0.9999	0.0039	17.99	0.9927

Effect of temperature on platinum adsorption

In this experimental series, the effect of temperature on platinum adsorption was studied in the range of 25 to 45 °C. The percentage adsorption of platinum as a function of temperature is presented in Fig. 5.

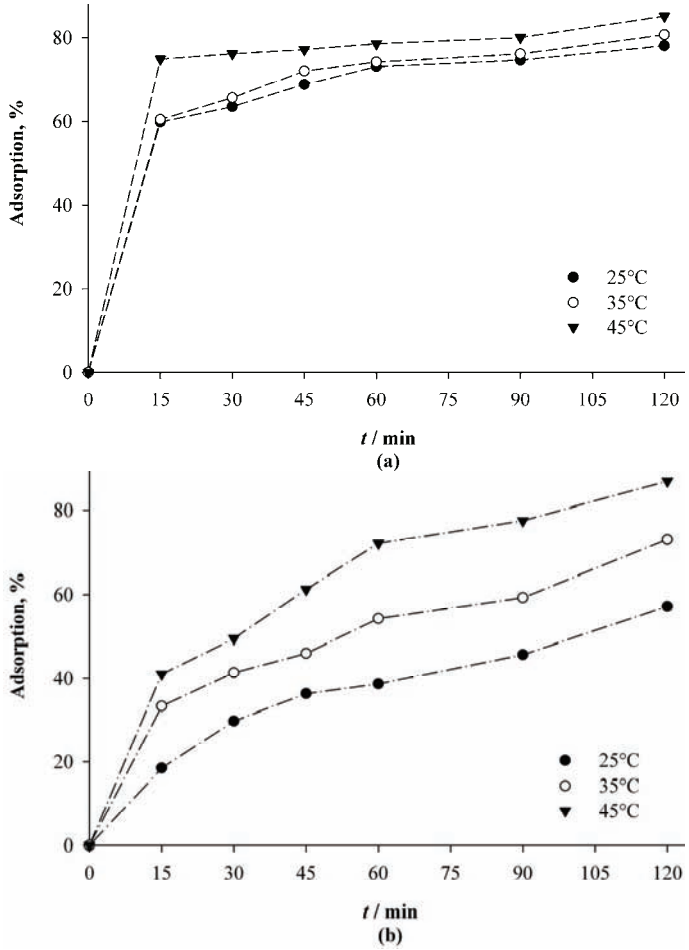

Fig. 5. Platinum adsorption as a function of temperature by a) rice hulls; b) Lewatit TP 214 (10 mg, 100 ppm, 100 rpm, pH 1.5 and 5 mL of 100 ppm solution).

Figure 5a shows that the temperature had little influence on the adsorption percentage for the rice hulls. After 120 min, only an approximately 10 % increment was obtained when the temperature was increased from 25 °C to 45 °C. The platinum adsorption *vs.* time curves at different temperatures were smooth and continuous, gradually leading to saturation, which indicates a monolayer coverage of metal ions on the surface of the adsorbent.[34] However, as evident from

Fig. 5b, increasing the temperature had a noticeable effect on platinum adsorption onto Lewatit TP214. After 120 min, an approximately 35 % increment was obtained when the temperature was increased from 25 to 45 °C. Thus, the temperature clearly had a greater effect for Lewatit TP 214 than for the rice hulls.

Effect of solution pH on platinum adsorption

In this experimental series, the effect of solution pH on platinum adsorption was studied using sorbent dosage of 20 and 30 mg at room temperature for 1 h. The influences of solution pH on platinum adsorption are presented in Fig. 6.

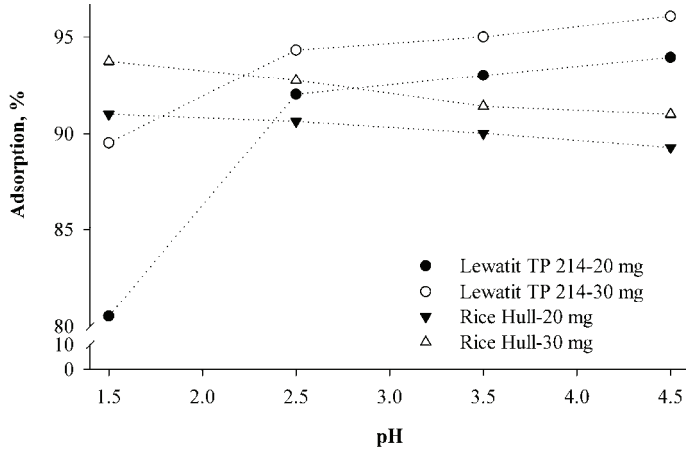

Fig. 6. Platinum adsorption as a function of solution pH by rice hulls and Lewatit TP 214 (25 °C, 60 min, 100 rpm, 5 mL of 100 ppm solution).

From Fig. 6, it can be seen that increasing the solution pH resulted in higher platinum adsorption by Lewatit TP 214. However, on increasing the solution pH, slightly lower adsorption percentages were obtained with the rice hulls. It could be concluded that platinum adsorption should be performed using acidic media of pH ≈2.5.[35]

Investigation of the adsorption isotherms

The adsorption isotherms of platinum ions on these sorbents were studied at three different temperatures, specifically 25, 35 and 45 °C, by varying the initial concentrations of the solutions from 100 to 250 ppm while keeping all other parameters constant.

The equilibrium data obtained were analyzed with respect to the Langmuir and Freundlich isotherms.

Freundlich isotherms. The data obtained for the adsorption of platinum ions onto the sorbents at equilibrium concentration, c_e, ranging from 100 to 250 ppm,

were fitted to the Freundlich Equation. The following linearized form was used:[36,37]

$$\log q_e = \log K_F + (1/n)\log c_e \quad (7)$$

in which, q_e is the amount of metal ions adsorbed at equilibrium per unit weight of sorbent (mg g^{-1}), c_e is the equilibrium ion concentration present in the solution after adsorption, K_F is the empirical Freundlich constant or the capacity factor (mg g^{-1}), and $1/n$ is the Freundlich isotherm constant. The constants K_F and n are empirical constants that are characteristic of the system and depend on the nature of the sorbent, the nature of the sorbate, the temperature and the pressure.

Plots of log q_e *vs.* log c_e for the adsorption of platinum ions onto the rice hulls and the Lewatit TP 214 yielded straight lines with positive slopes, given by $1/n$, and intercepts at log K_F (not shown).

Langmuir isotherms. The following linearized form of the Langmuir Equation was used to analyze the adsorption data for the adsorption of platinum ion on the rice hulls and the Lewatit TP 214, respectively:[37,38]

$$c_e/q_e = 1/(Q_{max}K_L) + (1/Q_{max})c_e \quad (8)$$

where q_e is the amount of metal ions adsorbed at equilibrium per unit weight of sorbent (mg g^{-1}), c_e is the equilibrium concentration of the sorbate in solution following adsorption, Q_{max} is the maximum adsorption capacity (mg g^{-1}) (which is generally called the monolayer capacity), and K_L is the Langmuir equilibrium constant (L mg^{-1}). Figure 7 shows the Langmuir adsorption isotherm plot of c_e/q_e *versus* c_e.

The adsorption isotherms of both rice hulls and Lewatit TP 214 under different conditions were calculated and the results are given in Table II. The values of each model and the correlation coefficient, R^2, were calculated from these plots. The linearity of these plots indicates the applicability of the two models. The correlation coefficients, R^2, showed that the Langmuir isotherm ($R^2 \geq \geq 0.99$) fits the data better than the Freundlich isotherm ($R^2 < 0.99$). This result indicates that the adsorption process of platinum ions onto the surfaces of Lewatit TP 214 and rice hulls is a monolayer adsorption process.

Investigation of adsorption thermodynamics

The temperature range chosen in this study was 298 to 318 K. The adsorption percentage increases with increasing temperature. The thermodynamic parameters for these adsorption processes, such as enthalpy change, $\Delta H°$, entropy change, $\Delta S°$, and the free energy of specific adsorption, $\Delta G°$, were calculated using the following equations:[34,39,40]

$$K_c = c_{Ac}/c_e \quad (9)$$

where K_c is the equilibrium constant, c_{Ac} and c_e are the equilibrium concentrations (in mg L^{-1}) of the platinum ion adsorbed and remaining in solution,

respectively. The free energy of adsorption, $\Delta G°$, was calculated from the following relationship:

$$\Delta G = \Delta G° + RT\ln K_C \quad (10)$$

At equilibrium, $\Delta G = 0$, thus:

$$\Delta G° = -RT \ln K_C \quad (11)$$

where T is absolute temperature in Kelvin and R is the gas constant.

$\Delta H°$ was calculated from the following equations:

$$\Delta G° = \Delta H° - T\Delta S° \quad (12)$$

$$\ln K_C = \Delta S°/R - \Delta H°/RT \quad (13)$$

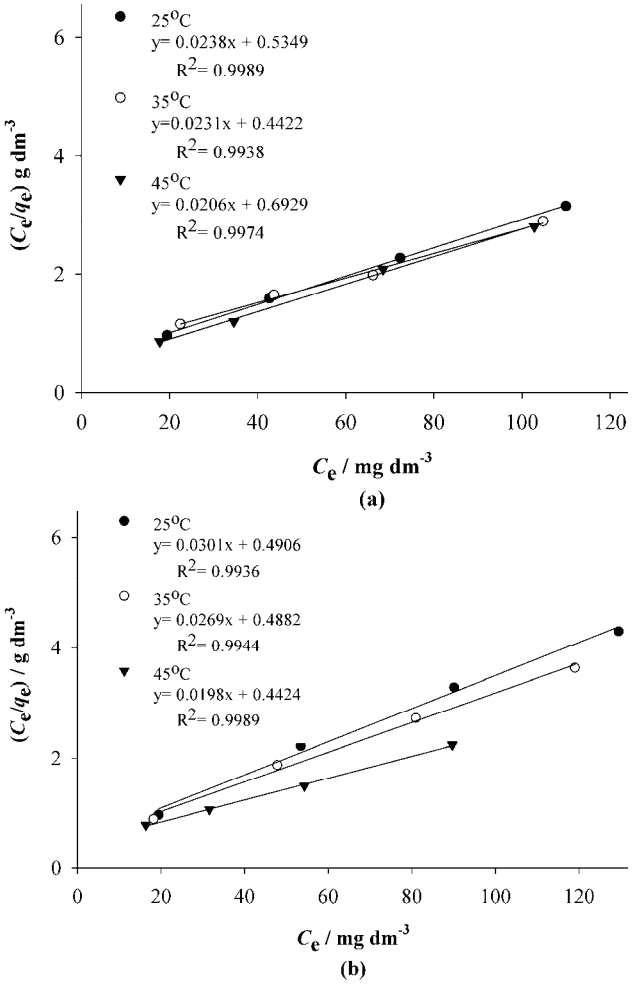

Fig. 7. The Langmuir isotherm of platinum adsorbed onto a) rice hulls and b) Lewatit TP 214 (20 mg sorbent, 60 min, 100 rpm, pH 1.5, and 5 mL solution of concentration 100–250 ppm).

TABLE II. Langmuir constants for the adsorption of platinum ions at various temperatures

T / °C	Rice hulls			Lewatit TP 214		
	K_L / dm^3 mg^{-1}	Q_{max} / mg g^{-1}	R^2	K_L / dm^3 mg^{-1}	Q_{max} / mg g^{-1}	R^2
25	0.04	42.02	0.9989	0.06	33.22	0.9936
35	0.05	43.29	0.9938	0.06	37.17	0.9944
45	0.03	48.54	0.9974	0.05	50.51	0.9989

The enthalpy change, $\Delta H°$, and the entropy change, $\Delta S°$, were calculated from the slope and from the intercept in linear plots of ln K_c *vs.* T^{-1} and are as shown in Fig. 8.

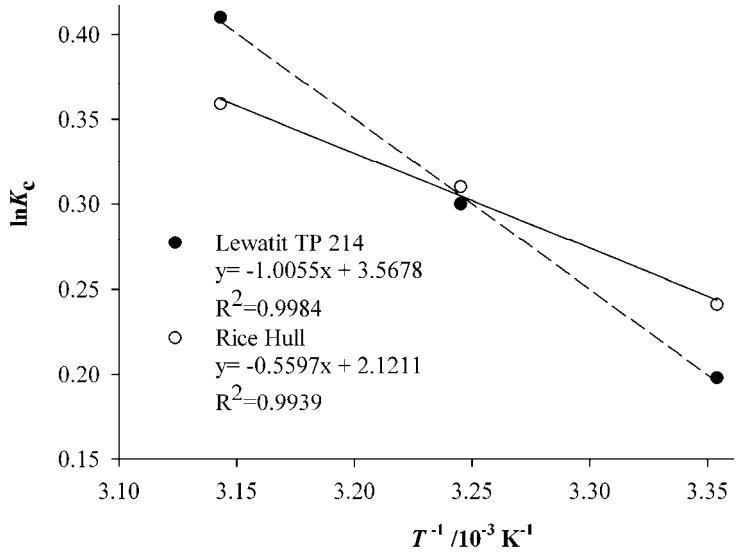

Fig. 8. ln K_c *vs.* 1000/T for platinum on Lewatit TP 214 and rice hulls (30 mg sorbent, 60 min, 100 rpm, pH 1.5 and 5 mL of 200 ppm solution).

The values of the thermodynamic parameters, $\Delta H°$, $\Delta S°$ and $\Delta G°$, for the platinum adsorption onto Lewatit TP 214 and the rice hulls were calculated using Eqs. (9)–(13) and are given in Table III.

TABLE III. Thermodynamic constants for the adsorption of platinum ions at various temperatures

T / K	Rice hulls			Lewatit TP 214		
	$\Delta G°$ kJ mol^{-1}	$\Delta H°$ kJ mol^{-1}	$\Delta S°$ J mol^{-1} K^{-1}	$\Delta G°$ kJ mol^{-1}	$\Delta H°$ kJ mol^{-1}	$\Delta S°$ J mol^{-1} K^{-1}
298	–0.60	4.65	17.6	–0.49	8.36	29.7
308	–0.79			–0.77		
318	–0.95			–1.08		

As shown in Fig. 5, an increase in the value of the adsorption percentage with increasing temperature indicates the endothermic character of platinum adsorption onto the sorbents. The value of $\Delta H°_{298\ K}$ for the platinum adsorption onto the rice hulls and Lewatit TP 214 were calculated to be 4.65 and 8.36 kJ mol^{-1}, respectively. The negative values of the free energy of specific adsorption $\Delta G°$ for the adsorption of platinum onto the sorbents, as shown in Table III, indicate that the process is spontaneous.[34] The value of $\Delta G°$ becomes more negative as the temperature increases, indicating an increasing driving force toward equilibrium, thereby resulting in a greater adsorption percentage at higher temperatures. The increase in the adsorption capacity of platinum onto the sorbents at higher temperature may be attributed to an enlargement of the pore size or to increased activation of the adsorbent surface. The greater extent of platinum adsorption at higher temperatures becomes apparent in an increase in the monolayer capacity. The process can only occur spontaneously if the entropy of the system increases and the value of $T\Delta S°$ become greater than the value of $\Delta H°$, yielding a negative value for the free energy of specific adsorption, $\Delta G°$. The adsorption of platinum onto the sorbents is accompanied by an increase in the entropy of the overall system. The positive value of $\Delta S°$ indicates an increase in the randomness at the solid/solution interface during the adsorption of the metal ions onto the rice hulls and Lewatit TP 214. The results are in good agreement with those of other base metal ions adsorbed onto Lewatit TP 214[41] and rice hulls.[42]

CONCLUSIONS

This study demonstrated that both the commercially available rice hulls, an agricultural waste by-product, and Lewatit TP 214 can be effective for the adsorption of platinum ions from aqueous solutions. Equilibrium adsorption data were well fitted by the Langmuir model. The maximum monolayer adsorption capacities, Q_{max}, at 25 °C of platinum ions onto rice hulls and Lewatit TP 214 were found to be 42.02 and 33.22 mg g^{-1}, respectively. Adsorption of platinum ions followed the pseudo-second-order rate equation, with a correlation coefficient of 0.99, rather than the pseudo-first-order rate equation. The kinetic rate of pseudo-second-order, k_2, using 30 mg sorbent at 25 °C was found to be 0.0289 and 0.0039 g min^{-1} mg^{-1} for the rice hulls and Lewatit TP 214, respectively**.** The enthalpy change $\Delta H°_{298\ K}$ and the entropy change $\Delta S°_{298\ K}$ for this adsorption process for the rice hulls were calculated to be 4.65 kJ mol^{-1} and 17.6 J mol^{-1} K^{-1}, respectively, and the same quantities were calculated for Lewatit TP 214 to be 8.36 kJ mol^{-1} and 29.7 J mol^{-1} K^{-1}, respectively. Thus, the adsorption process was found to be endothermic.

This study demonstrates that platinum adsorption can successfully be achieved using rice hulls, which are abundantly available in Turkey, as an alternative to

more costly materials for the treatment of waste solutions containing heavy metal ions. These promising results suggest that platinum containing waste solutions, such as catalytic converter leach solutions, seasoned platinum plating solutions, anode slime solutions, *etc*. can be successfully treated with rice hulls. Best of all, this method does not involve the using of any chemicals; hence it does not generate any hazardous byproducts.

Acknowledgement. The authors thank the Istanbul Technical University, Turkey, for their financial support.

ИЗВОД

АДСОРПЦИЈА ПЛАТИНЕ НА ЉУСКАМА ПИРИНЧА И LEWATIT-У TP 214 ИЗ РАСТВОРА ХЛОРОПЛАТИНСКЕ КИСЕЛИНЕ

M. H. MORCALI, B. ZEYTUNCU и O. YUCEL

Istanbul Technical University, Faculty of Chemical and Metallurgical Engineering, Maslak, 34469, Istanbul, Turkey

Љуске пиринча, отпадна биомаса, и Lewatit TP 214, тиосемикарбазидни сорбент, испитивани су као адсорбенти за адсорпцију платине(IV) из разблаженог растовара хлороплатинске киселине. Љуске пиринча су окарактерисане методом ометене тоталне рефлексије са Фуријеовом трансформацијом (ATR-FTIR). Испитивани су детаљно утицаји различитих адсорпционих параметара: дозе сорбента, времена контакта, температуре и pH раствора на проценат адсорпције. Подаци добијени при адсорпционој равнотежи су најбоље фитовани Лангмировим моделом изотерме. Максимални капацитети монослоја, Q_{max}, на 25 °C су били 42,02 и 33,22 mg g^{-1} за љуске пиринча и Lewatit TP 214, редом. Термодинамички прорачуни у којима су коришћене измерене вредности за $\Delta H°$, $\Delta S°$ и $\Delta G°$ указују да је адсорпциони процес спонтан и егзотерман. Испитиване су једначине за брзине псеудо-првог реда и псеудо-другог реда; адсорпција јона платине на оба адсорбента је описана кинетичким моделом псеудо-другог реда. Константа брзине, k_2, при коришћењу 30 mg сорбента на 25 °C је била 0,0289 и 0,0039 g min^{-1} mg^{-1} за љуске пиринча и Lewatit TP 214, редом. Резултати указују да се љуске пиринча могу успешно користити за уклањање платине из водених раствора.

(Примљено 12. септембра, ревидирано 1. децембра 2012)

REFERENCES

1. A. Wolowicz, Z. Hubicki, *Chem. Eng. J*. **197** (2012) 439
2. S. Aktas, M. H. Morcali, *Trans. Nonferrous Met. Soc. China* **21** (2011) 2554
3. A. Netzer, D. E. Hughes, *Water Res.* **18** (1984) 927
4. W. S. W. Ngah, C. S. Endud, R. Mayanar, *React. Funct. Polym.* **50** (2002) 181
5. K. Wang, B. Xing, *Chemosphere* **48** (2001) 665
6. K. H. C. Keith, M. Gordon, *Chemosphere* **60** (2005) 1141
7. K. C. Cheung, T. H. Venkitachalam, *Chemosphere* **41** (2000) 243
8. M. Rao, A. V. Parwate, A. G. Bhole, *Waste Manag.* **22** (2002) 821
9. E. Yildiz, *Sep. Purif. Technol.* **35** (2004) 241
10. C. A. Gray, A. P. Schwab, *Water, Air, Soil Pollut.* **69** (1993) 309
11. E. Guibal, T. Vincent, A. Larkin, J. M. Tobin, *Ind. Eng. Chem. Res.* **38** (1999) 4011

12. O. N. Kononova, T. A. Leyman, A. M. Melnikov, D. M. Kashirin, M. M. Tselukovskaya, *Hydrometallurgy* **100** (2010) 161
13. S. Aktas, M. H. Morcali, *Int. J. Miner. Process.* **101** (2011) 63
14. R. Chand, T. Watari, K. Inoue, H. Kawakita, H. N. Luitel, D. Parajuli, T. Torikai, M. Yada, *Miner. Eng.* **22** (2009) 1277
15. N. Thinakaran, P. Baskaralingam, M. Pulikesi, P. Panneerselvam, S. Sivanesan, *J. Hazard. Mater.***151** (2008) 316
16. L. C. Romero, A. Bonomo, E. E. Gonzo, *Adsorpt. Sci. Technol.* **21** (2001) 617
17. Y. Bulut, Z. Tez, *J. Hazard. Mater.***139** (2007) 35
18. A. Ozer, G. Dursun, *J. Hazard. Mater.***146** (2007) 262
19. M. Valix, W. H. Cheung, G. McKay, *Chemosphere* **56** (2006) 493
20. C. Namasivayam, R. Radhika, S. Suba, *Waste Manag.* **21** (2001) 381
21. F. Banat, S. Al-Asheh, L. Al-Makhadmeh, *Process Biochem.* **39** (2003) 193
22. A. Hashem, A. A. Aly, A. S. Aly, A. Hebeish, *Polym.-Plast. Technol. Eng.* **45** (2006) 389
23. S. Rajeshwari, C. Namasivayam, K. Kadirvelu, *Waste Manag.* **21** (2001) 105
24. T. Robinson, B. Chandran, P. Nigam, *Environ. Int.* **28** (2002) 29
25. M. M. Mohamed, *J. Colloid Interface Sci.* **272** (2004) 28
26. R. L. Tseng, F. C. Wu, R. S. Juang, *Carbon* **41** (2003) 487
27. A. Mokhtar, Y. L. Nargess, M. M. Niyaz, S. T. Nooshin, *J. Hazard. Mater.***135** (2006) 171
28. J. Tóth, *Adsorption: Theory, Modeling and Analysis*, Marcel Dekker, New York, USA, 2001, p. 251
29. D. M. Ruthven, *Principles of Adsorption and Adsorption Processes*, Wiley–Interscience, New York, USA, 1984, p. 177
30. C. Tasdelen, S. Aktas, E. Acma, Y. Guvenilir, *Hydrometallurgy* **96** (2009) 253
31. D. Ozcimen, A. Ersoy-Meriçboyu, *Adsorpt. Sci. Technol.* **28** (2010) 327
32. Y. S. Ho, G. McKay, *Chem. Eng. J.* **70** (1998) 115
33. R. G. Pearson, *Chemical Hardness*, Wiley–VCH, Weinheim, Germany, 1997, p. 43
34. G. Hussain, M. A. Khan, *J. Chem. Soc. Pak.* **33** (2011) 317
35. L. Zhou, J. Xua, X. Lianga, Z. Liub, *J. Hazard. Mater.* **182** (2010) 518
36. H. M. F. Freundlich, *J. Phys. Chem.* **57** (1906) 385
37. S. Y. Liu, J. Gao, Y. J. Yang, Y. C. Yang, Z. X. Ye, *J. Hazard. Mater.* **173** (2010) 558
38. I. Langmuir, *J. Am. Chem. Soc.* **40** (1918) 1361
39. H. Jaman, D. Chakraborty, P. Saha, *Clean: Soil, Air, Water* **37** (2009) 704
40. I. Kula, M. Ugurlu, H. Kaleaoglu, A. Celik, *Bioresour. Technol.* **99** (2008) 492
41. S. W. Won, J. Park, J. Mao, Y. S. Yun, *Bioresour. Technol.* **102** (2011) 3888
42. S. Naeem, U. Zafar, A. Altaf, A. Inayat, *J. Chem. Soc. Pak.* **31** (2009) 379.

Journal of the Serbian Chemical Society
JSCS-info@shd.org.rs • www.shd.org.rs/JSCS
J. Serb. Chem. Soc. 78 (6) 827–838 (2013)
JSCS–4461
UDC 547.756:66.095.252.091.7:543.552
Original scientific paper

Synthesis and electrochemical characterization of substituted indolizine carboxylates

MARIA-LAURA SOARE[1], ELEONORA-MIHAELA UNGUREANU[1]*, EMILIAN GEORGESCU[2] and LIVIU BIRZAN[3]**

[1]*Faculty of Applied Chemistry and Material Sciences, University "Politehnica" of Bucharest, 1–7 Polizu Str., 011061, Bucharest, Romania,* [2]*Research Center Oltchim, Uzinei Street 1, 240050, Ramnicu Valcea, Romania and* [3]*Institute of Organic Chemistry "C. D. Nenitzescu" of the Romanian Academy, Splaiul Independentei 202B, P. O. Box 15-258, 71141 Bucharest, Romania*

(Received 10 August, revised 15 October 2012)

Abstract: This work was devoted to the synthesis and characterization of new indolizine derivatives. Particular attention was paid to electrochemical investigations by cyclic voltammetry and differential pulse voltammetry. The redox processes for each compound were established, analyzed and assigned to the particular functional groups at which they occur. This assignment was based on detailed comparisons between the electrochemical behaviour of the compounds, the similarities in their structure, as well as substituent effects.

Keywords: indolizine derivatives; cycloaddition; cyclic voltammetry; differential pulse voltammetry.

INTRODUCTION

Indolizine is a π-rich system that can be easily oxidized to the radical cation.[1,2] For this reason, many indolizine derivatives showed valuable biological activity; thus they have found application in medicine and pharmacology (antimicrobial activity,[3] antioxidants,[4] cancer treatment,[5] ischemic heart disease and hypertension treatment[6]). Hence, the necessity to design new and convenient synthetic routes for compounds belonging to this class resulted in considerable efforts in the past few decades.[7–11] Indolizine derivatives are also highly luminescent,[12] this property enabling the design of fluorescent markers and sensors.[13,14] Indolizine derivatives could also find application in the design of new sensors for modern technologies,[15] due to their capacity to form surface films.[1,2] In this context, their electrochemical behaviour is, therefore, of crucial importance.

Corresponding authors. E-mail: (*)em_ungureanu2000@yahoo.com; (**)lbirzan@yahoo.com
doi: 10.2298/JSC120810117S

The present work is part of a series of studies related to the electrochemical characterization of indolizine derivatives.[16] It is focused on the synthesis of new, structurally related, indolizine derivatives **IVa–e** (Table I, Scheme 1) and the study of their electrochemical behaviour. This study concerns an assessment of the electrochemical peaks related to specific redox processes that occur at the functional groups grafted on the indolizine skeleton based on their redox potentials, which are governed by their structures.

TABLE I. Structure of the studied indolizine derivatives

Compound	R_1	R_2	R_3	R_4
IVa	7-CH_3	H	C_6H_4Cl (*p*)	CH_3
IVb	7-CH_3	H	C_6H_4F (*p*)	C_2H_5
IVc	7-COC_6H_5	H	C_6H_4F (*p*)	C_2H_5
IVd	5-CH_3	8-C_2H_5	$C_6H_4NO_2$ (*m*)	C_2H_5
IVe	7-COC_6H_5	H	OC_2H_5	C_2H_5
IVf[a]	H	H	C_6H_4Cl (*p*)	C_2H_5

[a]Previously published[16]

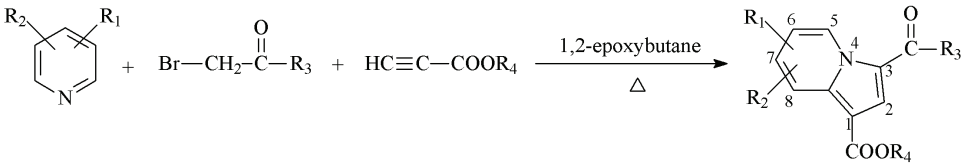

I **II** **III** **IVa-e**

Scheme 1. General scheme for the synthesis of the indolizine derivatives.

EXPERIMENTAL

All compounds in Scheme 1, pyridine derivatives (**I**), substituted phenacyl bromides or ethyl bromoacetates (**II**), propiolic esters (**III**) and 1,2-epoxybutane were purchased from Aldrich and used without further purification. Acetonitrile and tetrabutylammonium perchlorate (TBAP), from Fluka, were used as received as the solvent and supporting electrolyte, respectively.

As a general procedure for the synthesis of indolizine derivatives, a solution of 2.5 mmol of pyridine derivative (**I**), 2.5 mmol substituted phenacyl bromide or ethyl bromoacetate (**II**), and 3 mmol of propiolic ester (**III**) in 25 mL of 1,2-epoxybutane was heated at reflux temperature for 24 h. The solvent was partly removed under vacuum, the mixture was left over night at 5–10 °C and the formed solid was filtered off and crystallized from $CHCl_3/Et_2O$.

The melting points of compounds **IVa–e** were determined on a Boetius hot plate microscope. The elemental analysis was realized on a Costech Instruments EAS 32 apparatus. The IR spectra were recorded on a Nicolet Impact 410 spectrometer in KBr pellets. The ^{1}H- and ^{13}C-NMR spectra were recorded on a Varian Gemini 300 BB instrument. Supplementary evidence was given by COSY (H–H) experiments. The mass spectra were obtained using a Varian 1200L Triple Quadrupole LC/MS/MS spectrometer by direct injection in ESI. Silica gel 60 and alumina (II–III Brockmann grade, 70–230 mesh ASTM) were used for the column chromatography.

Cyclic voltammetry (CV) and differential pulse voltammetry (DPV) were employed for the electrochemical experiments using a PGSTAT12 Autolab potentiostat connected to a three-compartment cell. The CV curves were generally recorded at 0.1 V s^{-1} except when studying the influence of the scan rate in the range 0.1–1 V s^{-1}. DPV curves were recorded at 0.01 V s^{-1} with a pulse height of 0.025 V and a step time of 0.2 s. The working electrode was a glassy carbon disk (diameter 3 mm). The active surface was polished before each determination with diamond paste (200 μm). The Ag/10 mM $AgNO_3$ in 0.1 M TBAP, CH_3CN, was used as the reference electrode. The potential was referred to the potential of the ferrocene/ferricinium redox couple (Fc/Fc^+), which under the employed experimental conditions was +0.07 V. A platinum wire was used as the auxiliary electrode. The determinations were performed at 25 °C under an argon atmosphere.

RESULTS AND DISCUSSION

Synthesis of indolizine derivatives

Indolizine derivatives **IVa**–**e** have been prepared by one-pot, three-component procedure, developed and applied for other indolizine and azaindolizine derivatives,[17,18] starting from pyridine derivatives **I**, α-bromocarbonyl compounds **II** and electron deficient alkynes **III** in 1,2-epoxybutane, used as both reaction medium and proton scavenger (the synthetic route is shown in Scheme 1). This cycloaddition is a regiospecific process, requiring simple reaction conditions and all the final products were easily recovered by crystallization.

The reaction mechanism implies the intermediate formation of the pyridinium salts **V** from pyridine derivatives **I** and α-bromocarbonyl compounds **II** (Scheme 2). Subsequently, the bromine ion of the pyridinium salt attacks the oxirane ring of 1,2-epoxybutane, resulting in epoxide ring opening and the generation of pyridinium-*N*-ylides **VI**. The pyridinium-*N*-ylides **VI** react with the activated alkyne **III** to give the corresponding dihydroindolizines **VII** as the primary cycloadducts. Finally, by rearrangement and spontaneous *in situ* dehydrogenation of the primary cycloadduct, the indolizine derivatives **IV** are obtained.

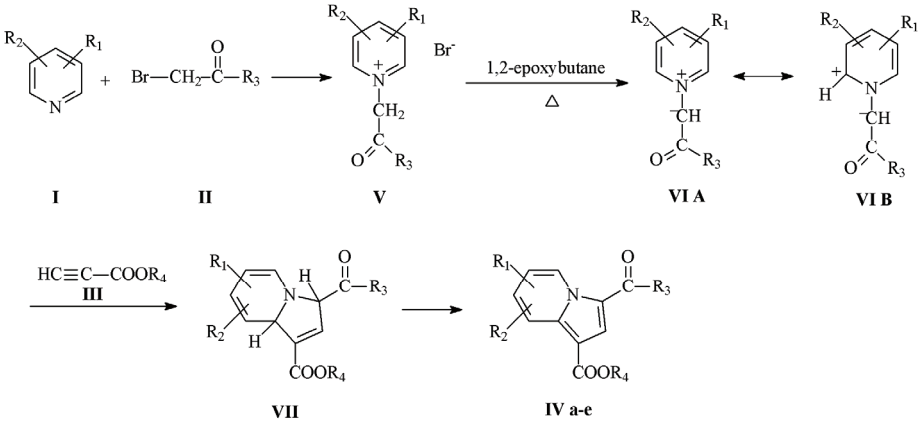

Scheme 2. Mechanism of synthesis.

Analytic and spectral data

The structures of all the indolizine derivatives **IVa**–**e** (Table I) were confirmed by chemical and spectral analysis. The data are given in the Supplementary material to this paper.

Electrochemical studies

CV and DPV anodic and cathodic curves were recorded individually, starting from the stationary potential, for various concentrations (0–3 mM) of the studied compounds in 0.1 M TBAP/CH_3CN.

The DPV and CV curves obtained for different concentrations of **IVa** are presented in Fig. 1. Several anodic (a) and cathodic (c) processes were observed, denoted in the order in which they appeared in the voltammograms. The DPV and CV curves for increasing concentrations of **IVb**–**e** are shown in Figs. 1S–8S of the Supplementary material to this paper, respectively. The influences of the scan domain and scan rate on the CV curves are illustrated in Figs. 2 and 1S–8S. The insets in these figures show the dependences of the CV peak currents (1a, 1c and 1c′) on the square root of the scan rate. The data from all figures allow the character of each peak for **IVa**–**e** to be established (Tables II–VI, respectively).

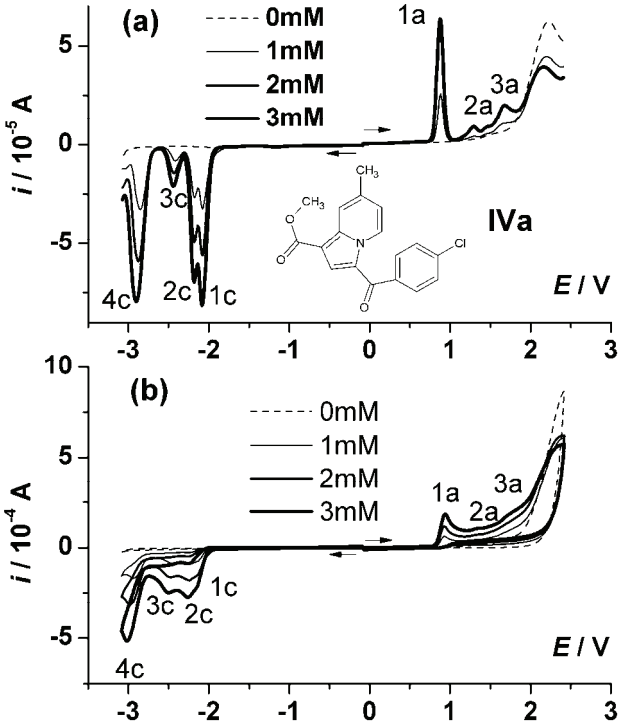

Fig. 1. a) DPV and b) CV curves for different concentrations of **IVa** in 0.1 M TBAP, CH_3CN.

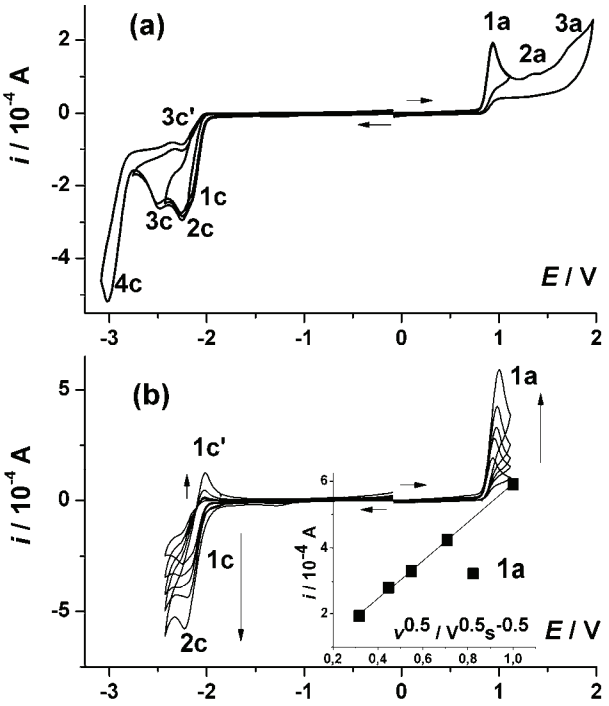

Fig. 2. CV curves for various scan domains at 0.1 V s^{-1} (a) and at different scan rates: 0.1, 0.2, 0.3, 0.5 and 1 V s^{-1} in the domains of peaks 1c and 1a (b) for **IVa** (3 mM) in 0.1 M TBAP, CH_3CN.

In order to assess the peaks obtained for **IVa**, they were compared to those of a very similar compound, ethyl 3-(4-chlorobenzoyl)indolizine-1-carboxylate, previously reported[16] and denoted **IVf**. Taking into account both the structural similarity between **IVa** and **IVf** and the specific activity potential for each functional group,[19–21] the assignments given in Table II were made for the peaks of **IVa** and **IVf** (detailed discussion further). Similarly, the redox processes for **IVb–IVe** were established using the comparison between the corresponding CV and DPV curves for: **IVa** and **IVb**, **IVb** and **IVc**, **IVb** and **IVd**, **IVe** and **IVc**, respectively. These assignments are summarized in Tables II–VI, respectively.

TABLE II. Potential (in V) and characteristics of the peaks from CV (r – reversible; i – irreversible; q – quasi-reversible) and their assignment for **IVa** and **IVf**[16]

Peak	**IVa**		**IVf**		Functional group involved / process
	DPV	CV	DPV	CV	
1a	0.873	0.941 (i)	0.951	1.008 (i)	Indolizine nitrogen / oxidation
2a	1.294	1.366 (i)	–	–	Methyl / oxidation
3a	1.673	1.746 (i)	1.733	1.800 (i)	Ketone / oxidation
1c	–2.086	–2.148 (r)	–2.065	–2.122 (r)	Ketone / reduction
2c	–2.181	–2.263 (i)	–2.164	–2.235 (i)	Halogen (Cl^-) / reduction[a]
3c	–2.444	–2.502 (q)	–2.395	–2.485 (q)	Ester / reduction
4c	–2.897	–3.015 (i)	–2.852	–2.921 (i)	Indolizine system / reduction

[a]Reductive elimination mechanism[19,20]

TABLE III. Potential (in V) and characteristics of the peaks from CV (r – reversible; i – irreversible; q – quasi-reversible) and their assignment for **IVb**

Peak	DPV	CV	Functional group involved / process
1a	0.860	0.921 (i)	Indolizine nitrogen / oxidation
2a	1.081	1.107 (i)	Methyl / oxidation
3a	1.681	1.806 (i)	Ketone / oxidation
1c	–2.183	–2.256 (r)	Ketone / reduction
2c	–2.531	–2.584 (q)	Ester / reduction
3c	–2.941	–3.035 (i)	Indolizine system / reduction

TABLE IV. Potential (in V) and characteristics of the peaks from CV (r – reversible; i – irreversible; q – quasi-reversible) and their assignment for **IVc**

Peak	DPV	CV	Functional group involved / process
1a	1.095	1.147 (i)	Indolizine nitrogen / oxidation
2a	1.768	1.935 (i)	Ketone (position 3) / oxidation
3a	2.126	2.236 (i)	Ketone (position 7) / oxidation
1c	–1.685	–1.747 (r)	Ketone (position 7) / reduction
2c	–2.043	–2.101 (q)	Ketone (position 7) / reduction-dianion
3c	–2.211	–2.287 (r)	Ketone (position 3) / reduction
4c	–2.517	–2.570 (q)	Ester / reduction
5c	–2.906	–2.995 (i)	Indolizine system / reduction

TABLE V. Potential (in V) and characteristics of the peaks from CV (r – reversible; i – irreversible; q – quasi-reversible) and their assignment for **IVd**

Peak	DPV	CV	Functional group involved / process
1a	0.816	0.862 (i)	Indolizine nitrogen / oxidation
2a	1.542	1.588 (i)	Methyl / oxidation
3a	1.721	1.765 (i)	Ketone (position 3) / oxidation
1c	–1.395	–1.447 (r)	Nitro / reduction (to NO)
2c	–1.922	–1.996 (i)	Nitro / reduction (to hydroxylamine)
3c	–2.258	–2.332 (r)	Ketone (position 3) / reduction
4c	–2.637	–2.695 (q)	Ester / reduction
5c	–2.953	–3.040 (i)	Indolizine system / reduction

TABLE VI. Potential (in V) and characteristics of the peaks from CV (r – reversible; i – irreversible; q – quasi-reversible) and their assignment for **IVe**

Peak	DPV	CV	Functional group involved / process
1a	1.084	1.133 (i)	Indolizine nitrogen / oxidation
2a	1.779	1.894 (i)	Ketone(position 3) / oxidation
3a	2.042	2.204 (i)	Esters / oxidation
1c	–1.780	–1.841 (r)	Ketone (position 7) / reduction
2c	–2.148	–2.204 (q)	Ester(position 3) / reduction
3c	–2.717	–2.797 (q)	Ester(position 1) / reduction
4c	–2.948	–3.053 (i)	Pyrrole / reduction to pyridinium salt
5c	–3.043	–3.159 (i)	Pyridinium salt / final reduction

The differences between the oxidation and reduction potentials of the two ketone groups in **IVc** could be explained by the fact that the six-membered cycle behaves as a pyridine, decreasing the electron density on the connected CO group, while the five-membered cycle, being richer in electrons, increases the electron density on the connected carbonyl group. For **IVe,** the reduction and oxidation potentials of the ester groups were established using the comparison between the DPV data for compounds **IVe** and **IVf**. The ester group in position 1 is much more conjugated than that in position 3, and was therefore harder to reduce and easier to oxidize.

It is known that indolizines are more stable when they are substituted with an electron withdrawing group at C1 (COOMe or COOEt) and they decay faster when this group is removed by reduction. However, the monoreduction to a pyridinium salt becomes possible, which generates an extra cathodic peak (5c for **IVe**) when the indolizine moiety is relatively symmetrically substituted.

The diffusion coefficients (D_0) of the new indolizines were calculated (Table VII) from the dependence of the values of currents of the first oxidation peak (**1a**) on the square root of the scan rate in CV.[22] The highest value was obtained for **IVa**, probably because this compound is less bulky as it has the lowest number of substituents.

TABLE VII. Diffusion coefficients for **IVa–e**

Compound	D_0 / 10^{-5} cm^2 s^{-1}
IVa	17
IVb	5.1
IVc	6.5
IVd	2.7
IVe	5.1

Comparison between substrates

Indolizine is an aromatic system due to its 8 π-electrons and 2 nonbonding electrons from the nitrogen atom. Therefore, the nonbonding electrons are strongly retained by the system, inducing a much higher first oxidation potential than in the cases of normal enamines. The first anodic process (1a) that is seen in the DPV and CV anodic curves is indolizine oxidation. Several remarks can be made concerning the influence of substituents (the peak potential values were taken here from the DPV experiments) on the potential of 1a. It occurs at 0.951 V in case of ethyl 3-(4-chlorobenzoyl)indolizine-1-carboxylate (**IVf**) and decreases on substitution of the indolizine ring with electron releasing groups. For instance, when Me is situated at position 7, it becomes 0.873 V in **IVa** and 0.860 V in **IVb**, while, when two alkyl substituents are present, the oxidation potential decreases even more, to 0.816 V in **IVd**. The difference between the first two potentials is determined by the intensity of the electron withdrawing power of the

aryl group linked to the keto group attached at position 3. The substituent connected to the benzoyl fragment from R_3, denoted R, can intensify the polarization of neutral molecules, decreasing their aromatic character. In fact, the ionic structures are anti-aromatic, having only 8 π electrons, as is shown in Scheme 3. Consequentially, the oxidation potentials are influenced by the nature of R and decrease when substituted in the order Cl > F. The successive oxidation steps for **IVb** are shown in Scheme 4.

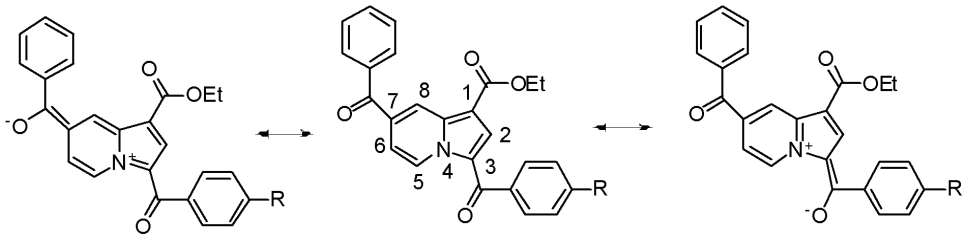

Scheme 3. Limit structures for **IVc** (R = F).

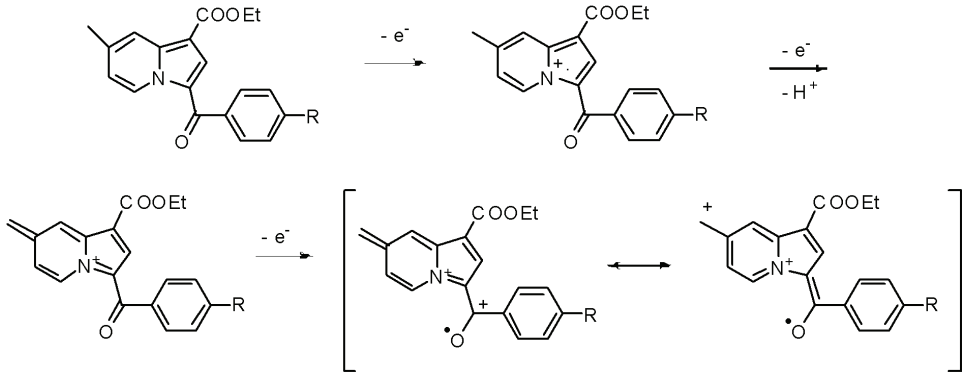

Scheme 4. Successive electron transfers in the oxidation of **IVb** (R = F).

If the PhCO electron withdrawing group is linked to the 7-position, the oxidation potential of the indolizine aromatic system increases to 1.095 V (in **IVc**) and to 1.084 V (in **IVe**). These modifications can also be easily explained by the change in the polarization of the molecule and by conjugation, which decrease the charge density on the indolizine moiety. However, in this case, the ketone group is farther in space from the nitrogen atom and, therefore, the destabilization of the aromatic character of the molecule is lower (Scheme 3).

A subsequent oxidation process of these substituted indolizines is the oxidation of the ketone linked at position 3. The successive oxidation electron transfers neglecting, for the sake of clarity, the chemical steps are shown in Scheme 5. It occurs at an oxidation potential of 1.733 V in **IVf**. The presence of alkyl groups on the pyridinic moiety of indolizine decreases this potential. Their influence,

corroborated with that of the R substituent (Cl, F, NO_2), explains the variation in the oxidation potential: 1.673 V for **IVa** (R = Cl), 1.681 V for **IVb** (R = F), 1.721 for **IVd** (R = NO_2). Simultaneously, the presence of a benzoyl group at the 7-position increases this potential to 1.768 V. It is interesting that the 7-benzoyl group is oxidized at 2.126 V, a potential value much higher than that of the ketones linked to the five-member cycle. It seems that the methyl oxidation is even more influenced by the nature of the R radical. This oxidation potential increases from 1.081 to 1.294 and 1.542 V, respectively, for R = F, Cl and NO_2, these groups having different effects: +E, –I in case of F, almost only –I in case of Cl, and –E, –I in case of NO_2.

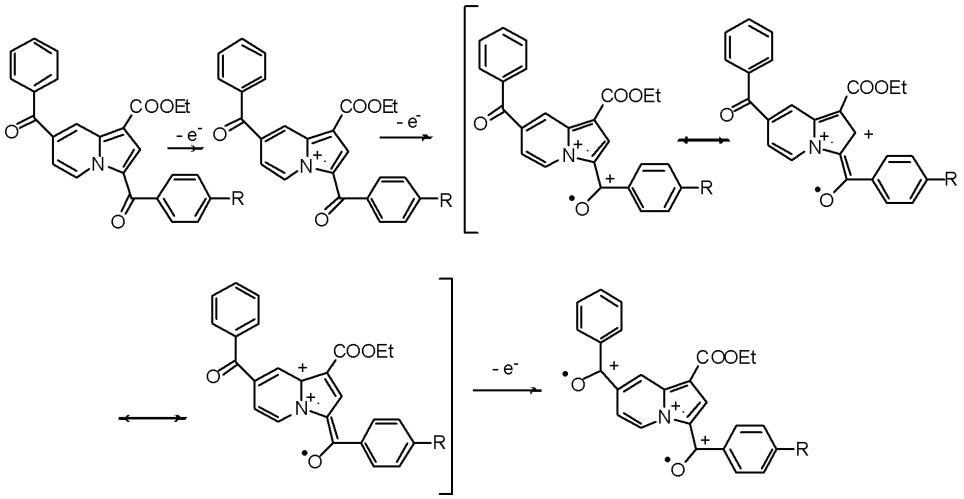

Scheme 5. Successive electron transfers in the oxidation of **IVc** (R = F).

The indolizine reduction potentials are more difficult to be rationalized because other groups are reduced faster and these redox processes affect the reduction of indolizine. Generally, the first reduction occurs at the keto group, which is reduced at –2.065 V in **IVf**. If the methyl group is linked to the 5- or 7-position, the absolute value of the reduction potential increases: –2.086 (**IVa**), –2.183 (**IVb**) and –2.258 V (**IVd**) (in this last case. the potential is also increased by the 8-Et radical). The successive reduction steps in a complex substituted indolizine, such as **IVd** (having NO_2, CO and COOEt as reducible substituents) are shown in Scheme 6. There is an initial reduction of the nitro group to hydroxylamine, followed by the reduction of the ketone group (it is possible that this step leads directly to alcohol in the presence of traces of water). The ester reductions occur at –2.395 V for **IVf**. The presence of a Me group in the 7-position increases the absolute value of this reduction potential to –2.444 (**IVa**) and –2.531 V (**IVb**).

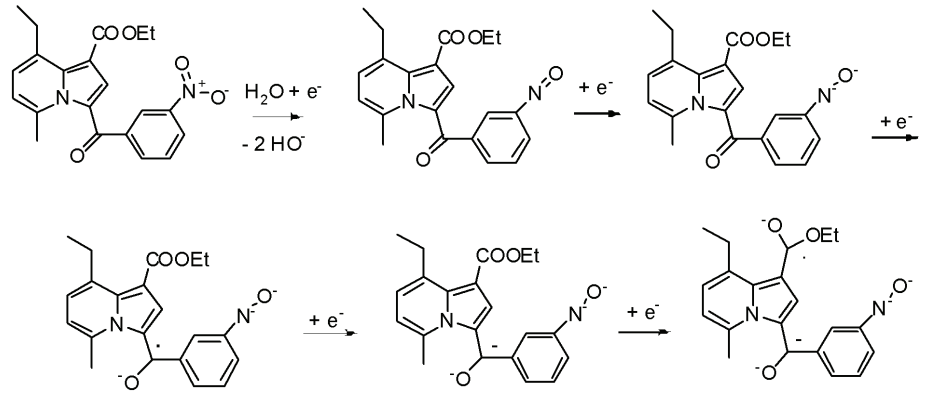

Scheme 6. Successive electron transfers in the reduction of **IVd**.

When two keto groups are present (such as in **IVc**), they are both reduced. The 7-benzoyl group is reduced easier (at –1.685 V) than that in position 3 (at –2.211 V).

The halo groups are reductively cleaved at –2.181 (**IVa**) and –2.164 V (**IVf**).

At the most negative potentials, the reduction of the indolizine system takes place, which occurs, for instance, at –2.852 V in **IVf**, while in **IVa**, **IVb** and **IVd** at –2.897, –2.941 and –2.953 V, respectively, due to the formation of negatively charged species of these compounds before reduction of the indolizine system. The same explanation is valid for **IVc** and **IVe**. The indolizine system is normally reduced at the pyrrole moiety leading to pyridinium salts (Scheme 7).

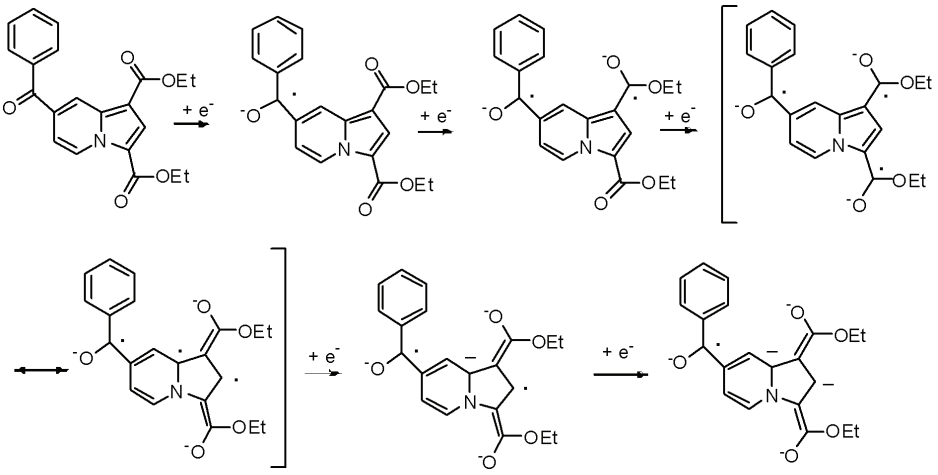

Scheme 7. Successive electron transfers in the reduction of **IVe**.

CONCLUSIONS

The investigated indolizine carboxylates presented similar electrochemical characteristics. The electron transfers of the common functional groups occurred at potentials that varied according to the substituent effect. A detailed investigation was performed to assess the processes responsible for each peak. The differences in their CV and DPV curves could be explained according to the differences in their structures. The electrochemical data helped to characterize and assess their redox processes.

SUPPLEMENTARY MATERIAL

Physical, analytic and spectral data of the compounds, as well as DPV and CV curves of glassy carbon, are available electronically from http://www.shd.org.rs/JSCS/, or from the corresponding author on request.

Acknowledgements. The work has been funded by the Sectoral Operational Programme Human Resources Development 2007–2013 of the Romanian Ministry of Labour, Family and Social Protection through the Financial Agreement POSDRU/88/1.5/S/61178.

И З В О Д

СИНТЕЗА И ЕЛЕКТРОХЕМИЈСКА КАРАКТЕРИЗАЦИЈА СУПСТИТУИСАНИХ ИНДОЛИЗИН-КАРБОКСИЛАТА

MARIA-LAURA SOARE[1], ELEONORA-MIHAELA UNGUREANU[1], EMILIAN GEORGESCU[2] и LIVIU BIRZAN[3]

[1]*Faculty of Applied Chemistry and Material Sciences, University „Politehnica“ of Bucharest, 1–7 Polizu Str., 011061, Bucharest, Romania,* [2]*Research Center Oltchim, Uzinei Street, 1, 240050, Ramnicu Valcea, Romania u* [3]*Institute of Organic Chemistry “C.D. Nenitzescu” of Romanian Academy, Splaiul Independentei 202B, P. O. Box 15-258, 71141 Bucharest, Romania*

У раду је описана синтеза и карактеризација нових деривата индолизина. Посебна пажња је посвећена електрохемијским испитивањима цикличном волтаметријом и диференцијалном пулсном волтаметријом. За свако једињење су утврђени и анализирани редокс процеси који се одигравају у појединим функционалним групама. Оваква анализа је заснована на детаљном поређењу електрохемијског понашања једињења, сличности у њиховој структури и ефектима супституената.

(Примљено 10. августа, ревидирано 15 октобра 2012)

REFERENCES

1. J. B. Henry, R. J. MacDonald, H. S. Gibbad, H. McNab, A. R. Mount, *Phys. Chem. Chem. Phys.* **13** (2011) 5235
2. V. V. Yanilkin, V. A. Mamedov, N. V. Nastapova, A. A. Kalinin, V. I. Morozov, O. G. Isaikina, *Russ. J. Electrochem.* **43** (2007) 1127
3. L.-L. Gundersen, C. Charnock, A. H. Negussie, F. Rise, S. Teklu, *Eur. J. Pharm. Sci.* **30** (2007) 26
4. S. Teklu, L.-L. Gundersen, F. Rise, M. Tilset, *Tetrahedron* **61** (2005) 4643
5. H. Li, K. Koya, L. Sun, M. Ono, US Patent No. A61K 31/437 (2006)
6. J. Gubin, J. Lucchetti, J. Mahaux, D. Nisato, G. Rosseels, M. Clinet, P. Polster, P. Chatelain, *J. Med. Chem.* **35** (1992) 981

7. K. A. Smith, A. Streitwieser Jr., *J. Org. Chem.* **48** (1983) 2629
8. E. I. Kostik, A. Abiko, A. Oku, *J. Org. Chem.* **66** (2001) 2618
9. X. Fang, Y.-M. Wu, J. Deng, S.-W. Wang, *Tetrahedron* **60** (2004) 5487
10. B. Furdui, R. Dinică, M. Demeunynck, I. Druță, *Rom. J. Phys.* **53** (2008) 369
11. J. Barluenga, G. Lonzi, L. Riesgo, L. A. López, M. Tomás, *J. Am. Chem. Soc.* **132** (2010) 13200
12. D. A. Lerner, E. M. Evleth, *Chem. Phys. Lett.* **15** (1972) 260
13. M. Becuwe, D. Landy, F. Delattre, F. Cazier, S. Fourmentin, *Sensors* **8** (2008) 3689
14. M. K. Bayazit, K. S. Coleman, *J. Am. Chem. Soc.* **131** (2009) 10670
15. V. A. Mamedov, A. A. Kalinin, V. V. Yanilkin, N. V. Nastapova, V. I. Morozov, A. A. Balandina, A. T. Gubaidullin, O. G. Isaikina, A. V. Chernova, Sh. K. Latypov, I. A. Litvinov, *Russ. Chem. Bull.* **56** (2007) 2060
16. M.-L. Soare, M.-R. Bujduveanu, E.-M. Ungureanu, E. Georgescu, L. Birzan, *Rev. Roum. Chim.* **56** (2011) 1011
17. E. Georgescu, M. R. Caira, F. Georgescu, B. Draghici, M. M. Popa, F. Dumitrascu, *Synlett* (2009) 1795
18. E. Georgescu, F. Georgescu, F. Dumitrascu, M. M. Popa, B. Draghici, *ACS Comb. Sci.* **14** (2012) 101
19. N. L. Weinberg, *Technique of Electroorganic Synthesis*, Part II, Wiley, New York, USA, 1975, p.p. 175, 721, 773, 843
20. E.-M. Ungureanu, *Electrochimia organica de la fundamente la aplicatii*, Ed. Politehnica Press, Bucuresti, 2011, p. 81 (in Romanian)
21. H. Lund, O. Hammerick, *Organic Electrochemistry*, Marcel Dekker, New York, 2001, p. 207
22. A. J. Bard, L. R. Faulkner, *Electrochemical Methods: Fundamentals and Applications*, 2nd Ed., Wiley, New York, 2001, p. 236.

Journal of the Serbian Chemical Society
JSCS@tmf.bg.ac.rs • www.shd.org.rs/JSCS

J. Serb. Chem. Soc. 78 (6) S75–S80 (2013) *Supplementary material*

SUPPLEMENTARY MATERIAL TO

Synthesis and electrochemical characterization of substituted indolizine carboxylates

MARIA-LAURA SOARE[1], ELEONORA-MIHAELA UNGUREANU[1]*, EMILIAN GEORGESCU[2] and LIVIU BIRZAN[3]**

[1]*Faculty of Applied Chemistry and Material Sciences, University "Politehnica" of Bucharest, 1–7 Polizu Str., 011061, Bucharest, Romania,* [2]*Research Center Oltchim, Uzinei Street 1, 240050, Ramnicu Valcea, Romania and* [3]*Institute of Organic Chemistry "C. D. Nenitzescu" of the Romanian Academy, Splaiul Independentei 202B, P. O. Box 15-258, 71141 Bucharest, Romania*

J. Serb. Chem. Soc. 78 (6) (2013) 827–838

PHYSICAL, ANALYTIC AND SPECTRAL DATA OF THE COMPOUNDS AND DPV AND CV CURVES OF GLASSY CARBON

*Methyl 3-(4-chlorobenzoyl)-7-methylindolizine-1-carboxylate (**IVa**)*. Yellow crystals; yield: 52 %; m.p.: 175–176 °C; Anal. Calcd. for $C_{18}H_{14}ClNO_3$ (FW: 327.76): C, 65.96; H, 4.3; N, 4.27 %. Found: C, 65.72; H, 4.45; N, 4.21 %; IR (KBr, cm^{-1}): 1711, 1643, 1612, 1526, 1478, 1462, 1344, 1227; ^{1}H-NMR (300 MHZ, $CDCl_3$, δ / ppm): 2.50 (3H, *s*, CH_3-7), 3.89 (3H, *s*, CH_3-ester), 6.94 (1H, *dd*, *J* = 1.9, 7.1 Hz, H-6), 7.48 (2H, *d*, *J* = 8.4 Hz, H-3′+H-5′), 7.73 (1H, *s*, H-2), 7.75 (2H, *d*, *J* = 8.4 Hz, H-2′+H-6′), 8.18 (1H, *dd*, *J* = 1.0, 2.0 Hz, H-8), 9.81 (1H, *d*, *J* = 7.1 Hz, H-5); ^{13}C-NMR (75 MHZ, $CDCl_3$, δ / ppm): 21.61 (CH_3), 51.21 (CH_3), 104.97, 117.91, 118.21, 121.86, 128.49, 128.61 (2C), 129.13, 130.25 (2C), 137.58, 138.25, 139.81, 140.48, 164.40 (CO_2), 183.71 (C=O); MS-ESI (*m*/*z*): 328/330 [M+1].

*Ethyl 3-(4-fluorobenzoyl)-7-methylindolizine-1-carboxylate (**IVb**)*. Yellow crystals; yield: 69 %; m.p.: 146–148 °C; Anal. Calcd. for $C_{19}H_{16}FNO_3$ (FW: 325.34): C, 70.14; H, 4.96; N, 4.30 %. Found: C, 70.33; H, 5.10; N, 4.14 %; IR (KBr, cm^{-1}): 1710, 1643, 1610, 1526, 1477, 1462, 1343, 1227, 1176; ^{1}H-NMR (300 MHZ, $CDCl_3$, δ / ppm): 1.40 (3H, *t*, *J* = 7.1 Hz, CH_3-ester), 2.50 (3H, *s*, CH_3-7), 4.38 (2H, *q*, *J* = 7.1 Hz, CH_2-ester), 6.93 (1H, *dd*, *J* = 2.0, 7.2 Hz, H-6), 7.19 (2H, *t*, *J* = 8.7 Hz, H-3′+H-5′), 7.73 (1H, *s*, H-2), 7.84 (2H, *dd*, *J* = 5.4, 8.8 Hz, H-2′+H-6′), 8.19 (1H, *dd*, *J* = 1.0, 2.0 Hz, H-8), 9.81 (1H, *d*, *J* = 7.2 Hz, H-5); ^{13}C-NMR (75 MHZ, $CDCl_3$, δ / ppm): 14.53 (CH_3), 21.61 (CH_3), 60.01

Corresponding authors. E-mail: (*)em_ungureanu2000@yahoo.com; (**)lbirzan@yahoo.com

(CH_2), 105.23, 115.27, 115.56, 117.76, 118.26, 121.68, 131.15, 131.26, 136.12, 136.17, 140.43, 163.55 (J = 252.2 Hz), 166.34 (CO_2), 183.69 (C=O); MS-ESI (m/z): 326 [M+1].

Ethyl 7-benzoyl-3-(4-fluorobenzoyl)indolizine-1-carboxylate ***(IVc)***. Yellow crystals; yield: 63 %; m.p.: 178–179 °C; Anal. Calcd. for $C_{25}H_{18}FNO_4$ (FW: 415.41): C, 72.28; H, 4.37; N, 3.37 %. Found: C, 72.43; H, 4.51; N, 3.19 %; IR (KBr, cm^{-1}): 1696, 1658, 1629, 1597, 1528, 1474, 1349, 1290, 1231, 1211; ^{1}H-NMR (300 MHZ, $CDCl_3$, δ / ppm): 1.33 (3H, *t*, J = 7.1 Hz, CH_3-ester), 4.35 (2H, *q*, J = 7.1 Hz, CH_2-ester), 7.22 (2H, *d*, J = 8.6 Hz, H-3′+5′), 7.53–7.65 (3H, *m*, Ph+H-6), 7.64–7.69 (1H, *m*, Ph), 7.87 (1H, *s*, H-2), 7.90–7.92 (4H, *m*, Ph), 8.77 (1H, *s*, H-8), 9.94 (1H, *d*, J = 7.4 Hz, H-5); ^{13}C-NMR (75 MHZ, $CDCl_3$, δ / ppm): 14.34 (CH_3), 60.47 (CH_2), 109.45, 114.56, 115.55, 115.83, 122.66, 123.44, 128.60 (2C), 128.79, 129.91 (2C), 131.44, 131.56 (2C), 133.06, 134.86, 136.53, 137.89, 163.45 (J = 251.92 Hz), 166.74 (CO_2), 184.37 (C=O), 194.00 (C=O); MS-ESI (m/z): 416 [M+1].

Ethyl 8-ethyl-5-methyl-3-(3-nitrobenzoyl)indolizine-1-carboxylate ***(IVd)***. Yellow crystals; Yield: 55 %; m.p.: 129–131 °C; Anal. Calcd. for $C_{21}H_{20}N_2O_5$ (FW: 380.39): C, 66.31; H, 5.30; N, 7.36 %. Found: C, 66.49; H, 5.16; N, 7.21 %; IR (KBr, cm^{-1}): 1702, 1615, 1528, 1471, 1348, 1220; ^{1}H-NMR (300 MHZ, $CDCl_3$, δ / ppm): 1.27 (3H, *t*, J = 7.4 Hz, CH_3 from C_2H_5-8), 1.35 (3H, *t*, J = 7.1 Hz, CH_3-ester), 2.56 (3H, *s*, CH_3-5), 3.33 (2H, *q*, J = 7.4 Hz, CH_2 from C_2H_5-8), 4.32 (2H, *q*, J = 7.1 Hz, CH_2-ester), 6.96 (1H, *d*, J = 7.3 Hz, H-6), 7.33 (1H, *d*, J = 7.3 Hz, H-7), 7.71 (1H, *s*, H-2), 7.75 (1H, *t*, J = 8.0 Hz, H-5′), 8.38 (1H, *dt*, J = 1.4, 7.7 Hz, H-6′), 8.47–8.49 (1H, *m*, H-4′), 8.87 (1H, *t*, J = 1.9 Hz, H-2′); ^{13}C-NMR (75 MHZ, $CDCl_3$, δ / ppm): 14.41 (CH_3), 15.03 (CH_3), 23.22 (CH_3), 26.75 (CH_2), 60.53 (CH_2), 108.13, 117.52, 123.81, 124.78, 126.67, 128.14, 129.62, 131.72, 133.69, 135.56, 137.60, 140.25, 140.56, 148.13, 163.87 (CO_2), 179.07 (*C*=O); MS-ESI (m/z): 381 [M+1].

Diethyl 7-benzoylindolizine-1,3-dicarboxylate ***(IVe)***. Pale yellow crystals; yield: 57 %; m.p.: 136–138 °C; Anal. Calcd. for $C_{21}H_{19}NO_5$ (FW: 365.38): C, 69.03; H, 5.24; N, 3.83 %. Found: C, 69.31; H, 5.09; N, 3.68 %; IR (KBr, cm^{-1}): 1721, 1693, 1658, 1597, 1528, 1474, 1349, 1231, 1198; ^{1}H-NMR (300 MHZ, $CDCl_3$, δ / ppm): 1.27 (3H, *t*, J = 7.1 Hz, CH_3-ester), 1.36 (3H, *t*, J = 7.1 Hz, CH_3-ester), 4.27 (2H, *q*, J = 7.1 Hz, CH_2-ester), 4.46 (2H, *q*, J = 7.1 Hz, CH_2-ester), 7.41–7.49 (3H, *m*, H-3′, H-4′, H-5′), 7.54–7.59 (1H, *m*, H-6), 7.77––7.81 (2H, *m*, H-2′, H-6′), 7.98 (1H, *s*, H-2), 8.65 (1H, *dd*, J = 1.0, 2.0 Hz, H-8), 9.51 (1H, *dd*, J = 1.0, 7.3 Hz, H-5); ^{13}C-NMR (75 MHZ, $CDCl_3$, δ / ppm): 14.34 (CH_3), 14.40 (CH_3), 60.25 (CH_2), 60.73 (CH_2), 108.85, 113.60, 116.53, 123.13, 124.84, 127.65, 128.54 (2C), 129.84 (2C), 132.84, 132.91, 136.77, 136.85, 160.87 (CO_2), 163.67 (CO_2), 194.25 (C=O); MS-ESI (m/z): 366 [M+1].

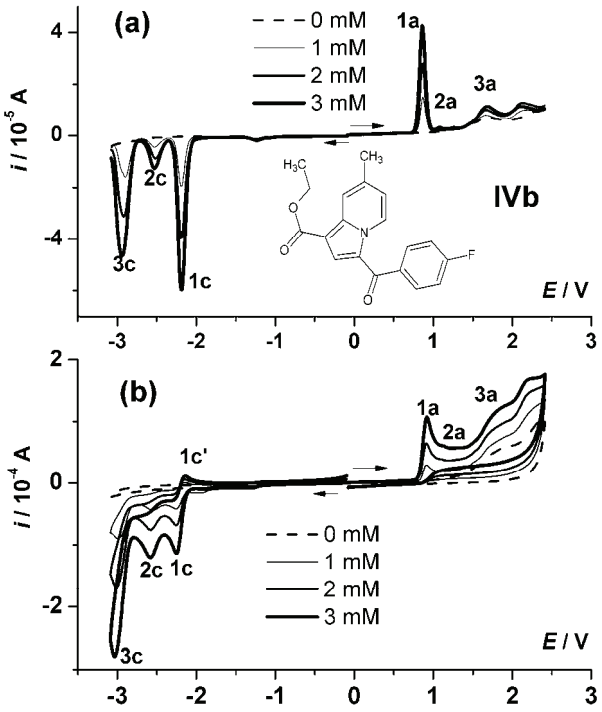

Fig. 1S. a) DPV and b) CV curves for different concentrations of **IVb** in 0.1 M TBAP, CH_3CN.

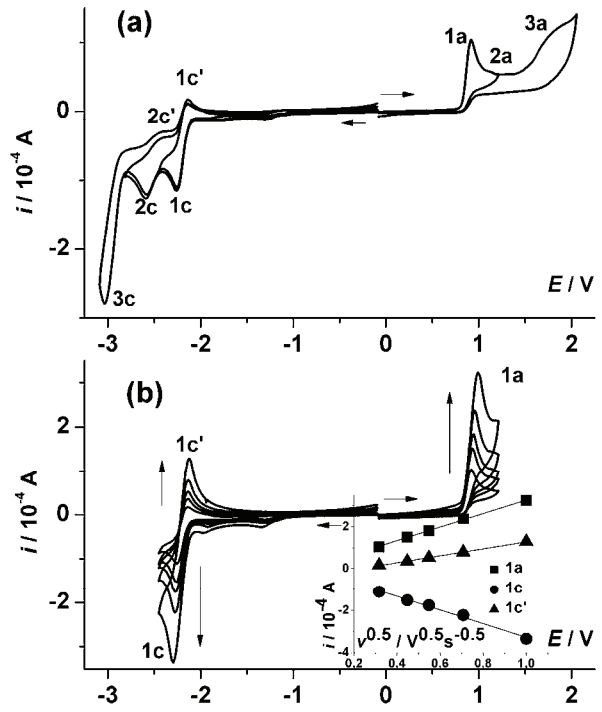

Fig. 2S. CV curves for various scan domains at 0.1 V s^{-1} (a) and different scan rates: 0.1, 0.2, 0.3, 0.5 and 1 V s^{-1} in the domains of peaks 1c and 1a (b) for **IVb** (3 mM) in 0.1 M TBAP, CH_3CN.

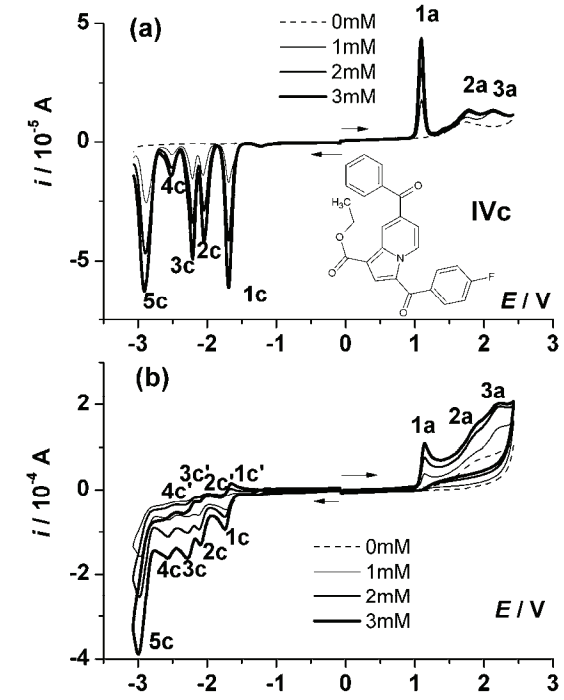

Fig. 3S. a) DPV and b) CV curves for different concentrations of **IVc** in 0.1 M TBAP, CH_3CN.

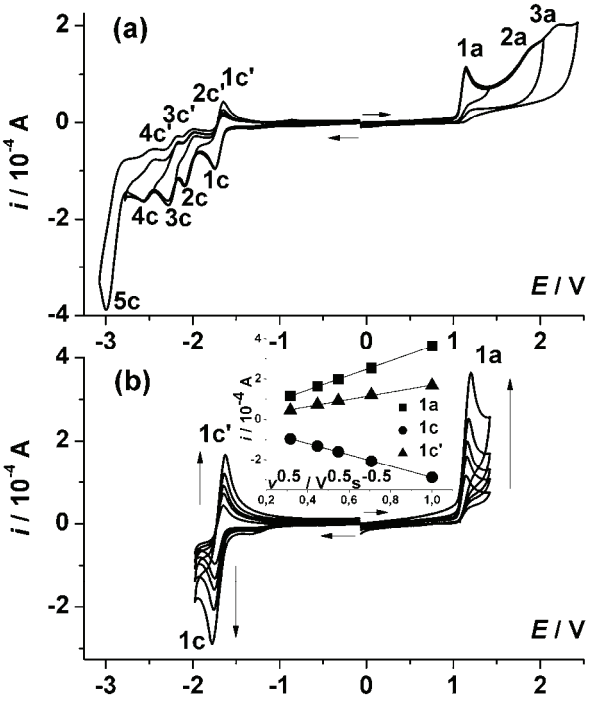

Fig. 4S. CV curves for various scan domains at 0.1 V s^{-1} (a) and at different scan rates: 0.1, 0.2, 0.3, 0.5 and 1 V s^{-1} (b) in the domain of peaks 1c and 1a for **IVc** (3 mM) in 0.1 M TBAP, CH_3CN.

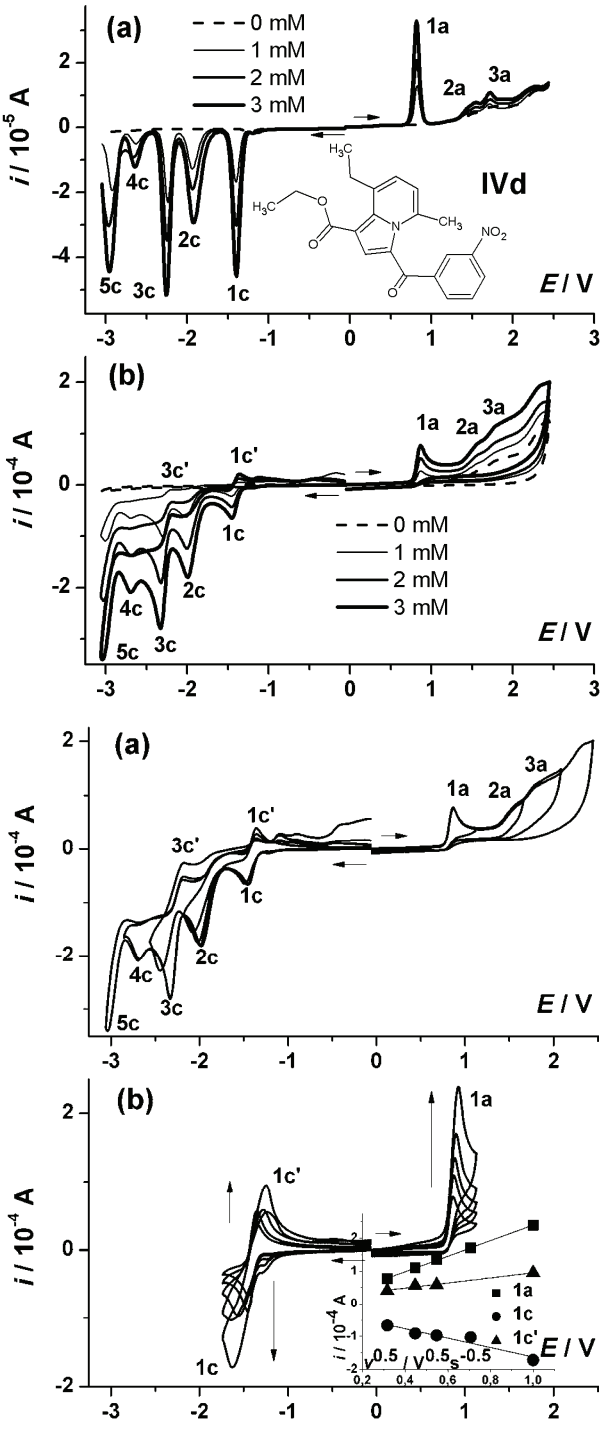

Fig. 5S. a) DPV and b) CV curves for different concentrations of **IVd** in 0.1 M TBAP, CH_3CN.

Fig. 6S. CV curves for various scan domains at 0.1 V s^{-1} (a) and at different scan rates: 0.1, 0.2, 0.3, 0.5 and 1 V s^{-1} (b) in the domain of peaks 1c and 1a for **IVd** (3 mM) in 0.1 M TBAP, CH_3CN.

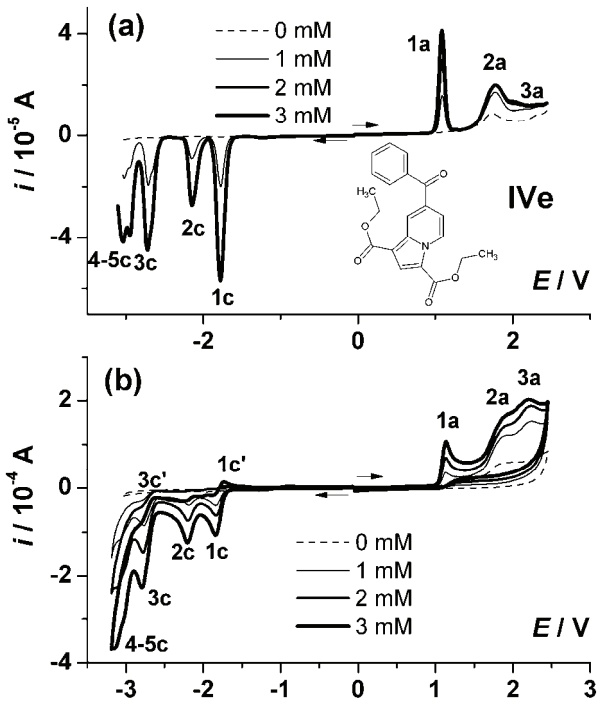

Fig. 7S. a) DPV and b) CV curves for different concentrations of **IVe** in 0.1 M TBAP, CH_3CN.

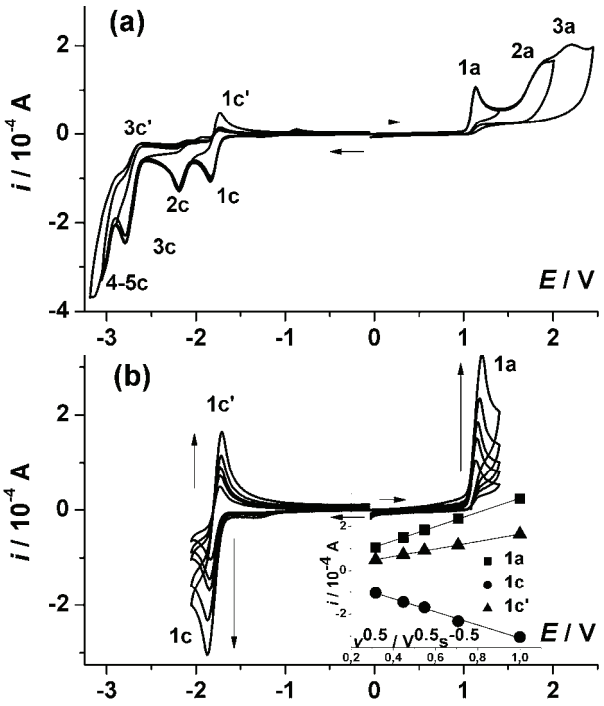

Fig. 8S. CV curves for various scan domains at 0.1 V s^{-1} (a) and different scan rates: 0.1, 0.2, 0.3, 0.5 and 1 V s^{-1} (b) in the domain of peaks 1c and 1a for **IVe** (3 mM) in 0.1 M TBAP, CH_3CN.

Journal of the Serbian Chemical Society
JSCS-info@shd.org.rs • www.shd.org.rs/JSCS
J. Serb. Chem. Soc. 78 (6) 839–850 (2013)
JSCS–4462
UDC 547.466+543.544.5.068.7:641.3.002.2
Original scientific paper

Validation of an HPLC method for the determination of amino acids in feed

IGOR JAJIĆ[1], SAŠA KRSTOVIĆ[1], DRAGAN GLAMOČIĆ[1], SANDRA JAKŠIĆ[2] and BILJANA ABRAMOVIĆ[3*#]

[1]*Faculty of Agriculture, University of Novi Sad, Trg D. Obradovića 8, 21000 Novi Sad, Serbia,* [2]*Scientific Veterinary Institute, Rumenački put 20, 21000 Novi Sad, Serbia and* [3]*Faculty of Sciences, University of Novi Sad, Trg D. Obradovića 3, 21000 Novi Sad, Serbia*

(Received 12 July, revised 17 October 2012)

Abstract: The subject of this study was the validation of a high-performance liquid chromatography method for the analysis of amino acids in fodder. The contents of amino acids were determined in maize, soybean, soybean meal, as well as in their mixtures enriched with different amounts of methionine, threonine and lysine. The method involved the acid hydrolysis of the sample (6 h at 150 °C), automated derivatisation of the amino acids with the aid of *o*-phthaldialdehyde and 9-fluorenylmethyl chloroformate reagents, separation on a ZORBAX Eclipse-AAA column and detection using a diode-array detector. The method is characterized by high specificity (the difference between the retention times of the fodder samples and standard mixtures were below 1.7 %), wide linear range (from 10 to 1000 nmol cm^{-3}, r^2 = 0.9999), high accuracy (recovery 93.3–109.4 %), and the precision of the results (*RSD* below 4.14 % in the case of repeatability and below 4.57 % in the case of intermediate precision). The limit of detection and the limit of quantification were in the ranges 0.004–1.258 μg cm^{-3} and 0.011–5.272 μg cm^{-3}, respectively. The results demonstrated that the procedure could be used as a method for the determination of the composition of primary amino acids of fodder proteins.

Keywords: amino acids; feed; liquid chromatography; method validation.

INTRODUCTION

The determination of the amino acid composition of the proteins in food is of great importance.[1] Namely, the amino acid level is an indicator of the nutritional value of food and fodder proteins.[2] As a laboratory technique, the analysis of amino acid plays an important role in biochemical, pharmaceutical and biomedical fields.[3] Hitherto, several different methods have been developed for the

* Corresponding author. E-mail: biljana.abramovic@dh.uns.ac.rs
# Serbian Chemical Society member.
doi: 10.2298/JSC120712144J

determination of amino acids.[4–26] Mostly, the methods were based on the technology developed by Moore and Stein,[4] which includes post-column derivatisation and detection in the visible region on an amino acid analyser. These analyses are reliable, but costly and time-consuming.[9] The HPLC technique, combined with pre-column derivatisation of amino acids, has become a very important method for the analysis of amino acids.[9] It should be emphasized that pre-column derivatisation has gained wide acceptance and a number of different derivatisation reagents have been used.[10–18] One of the most popular derivatisation reagents is *o*-phthaldialdehyde (OPA), which ensures relatively easy derivatisation and rapid reaction in aqueous solution at room temperature.[3,18–20] Nevertheless, during the manual procedure of derivatisation by OPA reagent, due to the time differences between the reaction and injection, significant errors in quantification may occur. By applying an automated procedure with an autosampler, the exact time and sample volume of each step can be controlled according to the injector program, which prevents human error inherent in the manual procedure.[21] Furthermore, OPA derivatisation is suitable for the analysis of primary amines only; hence, secondary amino acids need to be derivatised by another reagent.[22] 9-Fluorenylmethyl chloroformate (FMOC) is such a reagent used for the derivatisation of secondary amino acids, including hydroxyproline, sarcosine and proline.[23] Liu[3] managed to bring together OPA and FMOC in an automated derivatisation procedure to enable the simultaneous detection of both primary and secondary amino acids. In addition to derivatisation, protein hydrolysis is also a very important procedure in the analysis of amino acids.[8] The first acid hydrolysis was performed in 1820 by Baconnot, who used sulphuric acid to hydrolyse gelatine, wool and muscle fibres.[8] This was demonstrated in a collaborative study performed by the Association of Biomolecular Resource Facilities,[7] which indicated that many laboratories obtained satisfactory results by performing the hydrolysis in 6 mol dm^{-3} HCl at 150 °C under vacuum for 1 h. The traditional hydrolysis with 6 mol dm^{-3} HCl for 20–24 h at 110 °C under vacuum may lead to losses of serine, threonine, and tyrosine. On the other hand, during the acid hydrolysis, some amide bonds between aliphatic amino acids are more difficult to cleave. The Ala–Ala, Ile–Ile, Val–Val, Val–Ile, Ile–Val, and Ala–Val linkages are resistant to the hydrolysis, and may require a longer hydrolysis time of 48 or 72 h at 110 °C.[24]

The present paper compares two methods of sample hydrolysis for the determination of the amino acid composition of proteins in maize. In the first procedure, the samples were hydrolyzed traditionally with 6 mol dm^{-3} HCl at 110 °C for 24 h, and in the other with 6 mol dm^{-3} HCl (containing 0.1 % phenol) under vacuum at 150 °C for 6 h. In both cases, the samples were automatically derivatised with OPA and FMOC, and analyzed inline by HPLC with DAD detection, according to the method published in an Agilent application note.[25] Since

the second procedure appeared to be more suitable, it was applied for the determination of amino acids in maize, soybean, soybean meal, as well as in their mixture enriched with different amounts of methionine, threonine and lysine. The procedure was validated based on the specificity, linearity, accuracy, precision, limit of detection and limit of quantification for different fodder samples.

EXPERIMENTAL

Materials

Acetonitrile (LC grade), methanol (LC grade), and phenol (*p.a*. grade), were purchased from Sigma-Aldrich (St. Louis, MO). Borate buffer, OPA and FMOC reagents and standard solutions of mixture of 15 amino acids (10, 25, 100, 250 and 1000 nmol cm^{-3}) were obtained from Agilent Technologies (Waldbronn, Germany). Hydrochloric acid, used for the preparation of 6 mol dm^{-3} and 0.1 mol dm^{-3} HCl, was obtained from Lach-Ner (Neratovice, Czech Republic). Sodium phosphate monobasic was purchased from Acros Organics (New Jersey, USA). Nitrogen gas was purchased from Messer Technogas (Belgrade, Serbia). LC grade water was produced by a Heming ID-3 system (Belgrade, Serbia). The reference material of a complete fodder mixture for piglets was purchased from the National Reference Laboratory of the Central Institute for Supervising and Testing in Agriculture (Brno, Czech Republic).

Apparatus

Vacuum hydrolysis tubes (19 mm×100 mm) were obtained from Pierce (Rockfors, IL). Cellulose membrane syringe filter (0.22 μm pore size), screw cap vials and screw caps were purchased from Agilent Technologies (Waldbronn, Germany). Blue-labelled filter discs (quant.) grade: 391 were obtained from Munktell (Bärenstein, Germany).

The hydrolysis was performed using a Reacti-Therm™ heating/stirring module (Thermo Scientific, Rockford, IL), while the evaporation procedure also included a Reacti-Vap™ Evaporator (Thermo Scientific, Rockford, IL).

The analysis was performed on an Agilent 1260 Infinity liquid chromatography system, equipped with a μ-degasser (G1379B), 1260 binary pump (G1312B), 1260 standard autosampler (G1329B), 1260 thermostated column compartment (G1316A), 1260 diode array and multiple wavelength detector (G1315C), and a Zorbax Eclipse-AAA column (150 mm× 4.6 mm, i.d., particle size 5 μm) (Agilent Technologies, Santa Clara, CA).

Procedure

Samples. Maize, soybean, and soybean meal were analyzed for their amino acid content. Then, a mixture of maize, soybean, and soybean meal was made in the mass ratio 70:15:15. The mixture was divided into four parts, and one part, marked as “zero”, was used as such, while the other three parts were supplemented with methionine, threonine and lysine in different concentrations. The mixtures “one”, “two” and “five” contained 0.1, 0.2 and 0.5 % of each added amino acids, respectively.

Preparation of protein hydrolysates. The fodder samples and the mixtures were finely ground to pass through a 0.5 mm sieve. The samples were then hydrolyzed by two different procedures. First, 0.1–1.0 g was weighed (equivalent to 10 mg nitrogen content) into a screw-capped test tube and 2 cm^3 of 6 mol dm^{-3} HCl was added. The tubes were capped and the samples were hydrolyzed for 24 h at 110 °C. After the hydrolysis, the mixtures were evaporated to dryness under vacuum. The hydrolysates were reconstituted in 2 cm^3 of 0.1 mol dm^{-3} HCl.[27]

In the second procedure, samples of the same mass were weighed into vacuum hydrolysis tubes and 7 cm^3 of 6 mol dm^{-3} HCl with 0.1 % of phenol were added and mixed gently. The hydrolysis was realised in a Reacti-Therm™ heating/stirring module for 6 h at 150 °C. After the hydrolysis, the samples were cooled to room temperature and evaporated to dryness using a Reacti-Therm™ heating/stirring module and Reacti-Vap™ Evaporator, at 70 °C under a stream of nitrogen. The residues were quantitatively transferred into 50 cm^3 volumetric flasks using 0.1 mol dm^{-3} HCl. The solutions were filtered through quantitative filter paper into glass tubes and the filtrates were purified using 0.22 μm pore size, cellulose membrane syringe filters.[27]

HPLC Determination. The chromatographic conditions employed were in accordance with the Agilent method,[25] except for mobile phase A, which consisted of 5.678 g of Na_2HPO_4 per 1 dm^3 water, adjusted to the pH 7.8 with a 6 mol dm^{-3} HCl solution (buffer strength 40 mmol dm^{-3}). The mobile phase B was acetonitrile–methanol–water (45:45:10, vol. %). Briefly, the hydrolyzed samples or the solutions the standard amino acid mixture were automatically derivatised with OPA and FMOC by programming the autosampler (1. draw 2.5 μl from vial 1 (borate buffer), 2. draw 0.5 μl from sample (position X), 3. mix 3 μl in air, max. speed, 2×, 4. wait 0.5 min, 5. draw 0 μl from vial 2 (water, uncapped vial), 6. draw 0.5 μl from vial 3 (OPA), 7. mix 3.5 μl in air, max speed, 6×, 8. draw 0 μl from vial 2 (water, uncapped vial), 9. draw 0.5 μl from vial 4 (FMOC), 10. mix 4 μl in air, max speed, 6×, 11. draw 32 μl from vial 5 (water), 12. mix 18 μl in air, max speed, 2× and 13. inject). After derivatisation, 0.5 μl of each sample was injected into a Zorbax Eclipse-AAA column at 40 °C, with detection at λ_1 = 338 nm and λ_2 = 262 nm. The separation was performed at a flow rate of 2 cm^3 min^{-1} employing a solvent gradient (vol. %,) as follows: 0 min, 0 % B, 1.9 min, 0 % B, 18.1 min, 57 % B, 18.6 min, 100 % B, 22.3 min, 100 % B, 23.2 min, 0 % B and 26 min, 0 % B.

RESULTS AND DISCUSSION

The hydrolysis is an extremely important step in amino acid analysis because it significantly affects the amino acid recovery.[28] During traditional acid hydrolysis, cysteine and tryptophan are destroyed,[29] and losses of serine, threonine and tyrosine are observed.[7] Besides the losses of some amino acids, their quantification after traditional hydrolysis is quite hard and insufficiently precise. As can be seen in Fig. 1, the peaks of all amino acids are unsuitable for quantification. On the other hand, when the samples were hydrolyzed according to the second procedure, with a shorter hydrolysis time and hydrolysate evaporation under a stream of nitrogen, amino acid quantification was very good (Fig. 2). This is also supported by the chromatogram obtained for the standard amino acid mixture (Fig. 3). The shorter period of hydrolysis and better quantification clearly confirmed the advantage of the second hydrolysis procedure, which was then used for all samples.

Hence, the validation parameters were estimated for the amino acids that gave satisfactory results at the recovery level, which included aspartate (ASP), glutamate (GLU), serine (SER), glycine (GLY), threonine (THR), arginine (ARG), alanine (ALA), tyrosine (TYR), valine (VAL), methionine (MET), phenylalanine (PHE), isoleucine (ILE), leucine (LEU) and lysine (LYS). Unfortunately, none of

the secondary amino acids, derivatised by FMOC reagent, gave satisfactory results. In order to achieve a complete assessment of the validation parameters of the method, both the amino acid standard mixtures and fodder samples were analysed. This provided the validation of all steps in the amino acid analysis of the fodders.

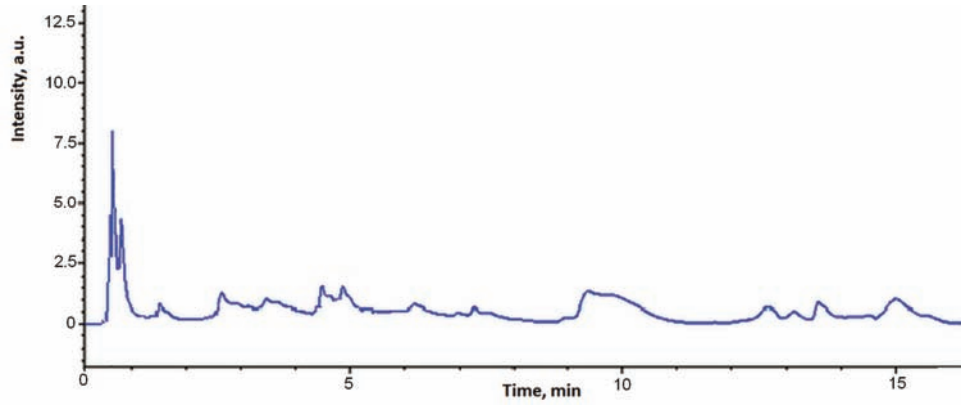

Fig. 1. Chromatogram of the maize hydrolysate obtained at 110 °C during 24 h.

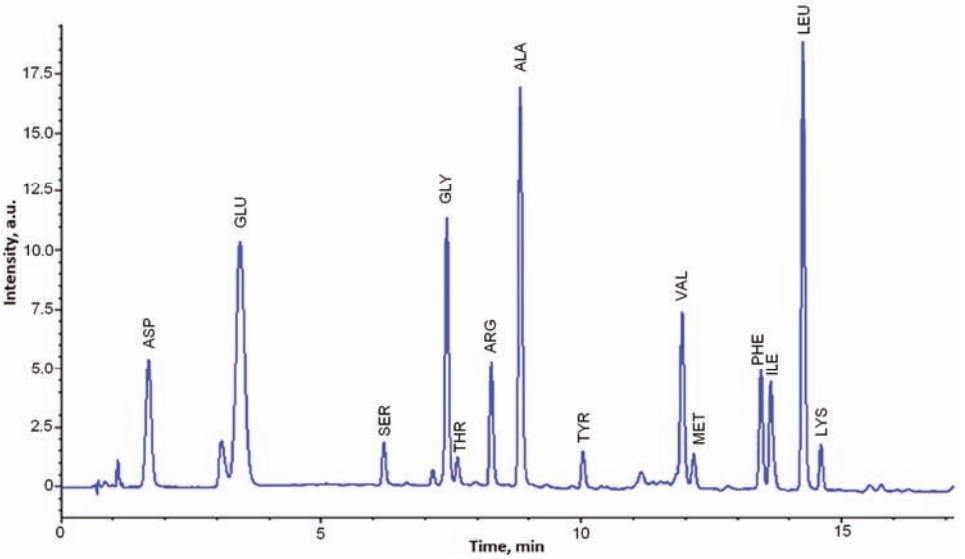

Fig. 2. Chromatogram of the maize hydrolysate obtained at 150 °C during 6 h.

Specificity. With the aim of studying the specificity of the method, a comparison was made of the retention times (t_R) of five different concentrations of standard solutions of the amino acid mixture (Table I) and seven different fodder samples (Table II). As can be seen from the Tables, the t_R values were not

significantly influenced either by the concentration of amino acids, or by the matrix. Namely, the relative standard deviation (*RSD*) of the t_R values of the standard amino acid mixtures was in the range from 0.02 to 0.52 % (Table I), and for the fodder samples, in the range from 0.02 to 0.46 % (Table II). As can be seen from the mean values of t_R for the standard amino acid mixtures and fodder samples, presented in Table III, there were slight variations between the t_R values, ranging from 0 to 1.7 %. According to Reason,[30] for specific methods, the difference between t_R values should be within ±3 %.

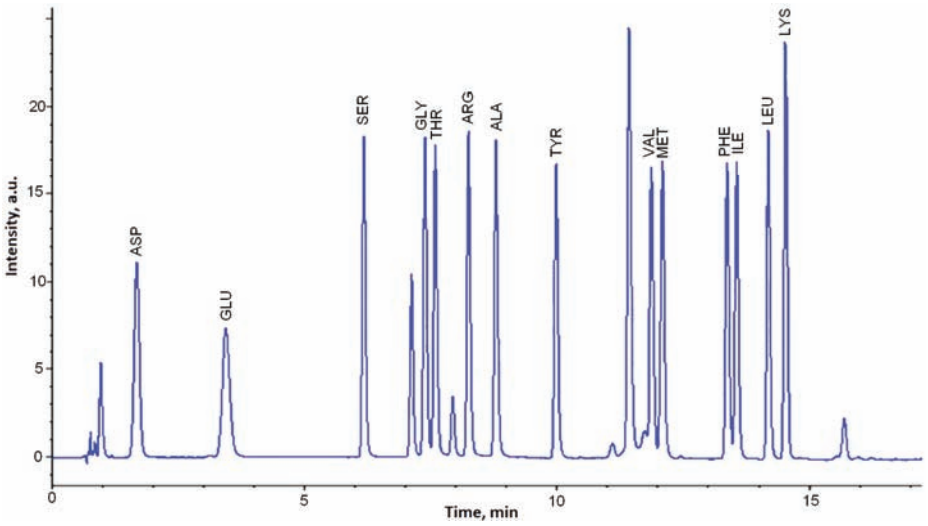

Fig. 3. Chromatogram of the standard amino acid mixture (1000 nmol cm^{-3}).

TABLE I. Specificity evaluation comparing retention times; retention times of the standard amino acid mixture (n = 3)

Amino acid	Concentration, nmol cm^{-3}					Average	*RSD* / %
	10	25	100	250	1000		
ASP	1.669	1.667	1.666	1.670	1.673	1.669	0.16
GLU	3.433	3.431	3.428	3.435	3.436	3.433	0.09
SER	6.170	6.165	6.166	6.166	6.167	6.167	0.03
GLY	7.384	7.373	7.374	7.373	7.378	7.376	0.06
THR	7.574	7.577	7.579	7.576	7.582	7.578	0.04
ARG	8.250	8.232	8.231	8.235	8.241	8.238	0.10
ALA	8.787	8.772	8.774	8.778	8.782	8.779	0.07
TYR	9.981	9.967	9.970	9.973	9.974	9.973	0.05
VAL	11.863	11.862	11.863	11.864	11.725	11.835	0.52
MET	12.084	12.078	12.079	12.080	12.078	12.080	0.02
PHE	13.367	13.370	13.365	13.367	13.362	13.366	0.02
ILE	13.558	13.554	13.553	13.544	13.549	13.552	0.04
LEU	14.180	14.184	14.179	14.179	14.175	14.179	0.02
LYS	14.512	14.513	14.509	14.521	14.519	14.515	0.03

TABLE II. Specificity evaluation comparing retention times; retention times of the amino acids in the fodder samples (n = 3)

Amino acid	Concentration, nmol cm^{-3}							Average	*RSD* %
	Maize soybean	Soybean Meal		Mixture 0	Mixture 1	Mixture 2	Mixture 5		
ASP	1.675	1.671	1.673	1.674	1.673	1.673	1.671	1.673	0.09
GLU	3.410	3.410	3.413	3.445	3.442	3.411	3.415	3.421	0.46
SER	6.168	6.161	6.164	6.168	6.170	6.170	6.167	6.167	0.05
GLY	7.370	7.367	7.372	7.374	7.370	7.373	7.375	7.372	0.04
THR	7.576	7.573	7.577	7.579	7.573	7.576	7.579	7.576	0.03
ARG	8.239	8.238	8.241	8.238	8.236	8.246	8.255	8.242	0.08
ALA	8.772	8.774	8.774	8.777	8.772	8.772	8.780	8.774	0.03
TYR	9.972	9.971	9.971	9.967	9.970	9.970	9.972	9.970	0.02
VAL	11.857	11.855	11.855	11.851	11.852	11.848	11.849	11.852	0.03
MET	12.076	12.075	12.073	12.069	12.071	12.068	12.067	12.071	0.03
PHE	13.359	13.357	13.355	13.351	13.351	13.345	13.342	13.351	0.05
ILE	13.548	13.544	13.544	13.539	13.538	13.531	13.530	13.539	0.05
LEU	14.171	14.168	14.170	14.163	14.160	14.152	14.152	14.162	0.06
LYS	14.520	14.515	14.517	14.511	14.509	14.499	14.500	14.510	0.06

TABLE III. The differences among the average retention times of the fodder samples and of the standard amino acids mixture

Amino acid	Average retention time, min		Difference, %
	Fodder samples	Standard mixtures	
ASP	1.673	1.669	0.4
GLU	3.421	3.433	–1.2
SER	6.167	6.167	0.0
GLY	7.372	7.376	–0.4
THR	7.576	7.578	–0.2
ARG	8.242	8.238	0.4
ALA	8.774	8.779	–0.5
TYR	9.970	9.973	–0.3
VAL	11.852	11.835	1.7
MET	12.071	12.080	–0.9
PHE	13.351	13.366	–1.5
ILE	13.539	13.552	–1.3
LEU	14.162	14.179	–1.7
LYS	14.510	14.515	–0.5

Linearity. The linearity was established using five standard solutions containing 10, 25, 100, 250 and 1000 nmol cm^{-3} of each amino acid. The data of peak area *vs.* amino acid concentration were treated by linear least squares regression analysis. The values of the slope, intercept and the coefficient of determination of the calibration curve for amino acids are given in Table IV. The linearity data obtained should obey the equation $y = bx + a$, where a is zero within the 95 % confidence limits, and the coefficient of determination (R^2) is greater

than 0.98.[30] In the present study, the area response obeyed the equation $y = bx + a$. The high value of the coefficient of determination indicates a good linearity, *i.e.*, R^2 in all cases was 0.9999 except for phenylalanine, where R^2 was 0.9986.

TABLE IV. Linearity data for the standard amino acids mixture

Amino acid	Slope×10^3	Intercept×10^4	R^2
ASP	1.584	0.60	0.9999
GLU	0.503	5.03	0.9999
SER	1.216	–0.11	0.9999
GLY	0.871	–0.12	0.9999
THR	1.393	–0.59	0.9999
ARG	1.997	–1.03	0.9999
ALA	1.004	–2.61	0.9999
TYR	2.195	–0.89	0.9999
VAL	1.226	0.28	0.9999
MET	1.676	0.99	0.9999
PHE	1.942	12.29	0.9986
ILE	1.533	1.19	0.9999
LEU	1.499	0.91	0.9999
LYS	1.585	17.32	0.9999

Accuracy. Accuracy may be defined as the agreement between the found value and the true value of the reference material provided by a reference laboratory, and can be presented as the percent recovery. This validation parameter was estimated by analyzing the reference material of the complete fodder mixture for piglets. The analysis was performed three times on three different days, by repeating the whole analytical procedure. After the analysis, the percent recovery was calculated for every well-recovered amino acid and the results are presented in Table V. As can be seen, the best percent recovery was obtained in the case of serine (99.4 %), while lysine had the highest (109.4 %) and methionine the lowest (93.3 %) percent recovery. The average percent recovery, considering all amino acids, was 104.6 %, which is within the range of 90–110 %, which can be considered acceptable.[30] Only in case of cystine and proline was no satisfactory recovery obtained.

*Precision***.** In this work, the precision was estimated by measuring the repeatability and intermediate precision. In the case of repeatability, the same sample of maize was derivatised and injected 6 times in a row and then the *RSD* was calculated for each amino acid. The obtained *RSD* values were in the range of 1.82–4.14 % (Table VI), which, being less than 5 %, could be considered acceptable.[30]

The intermediate precision was estimated by repeating the whole analytical procedure on three different days. The same maize sample was hydrolyzed three times, derivatised, and injected, separately on three different days. As can be seen

from Table VII, the *RSD* was less than 4.57 %, and, being below 10 %, it could be considered acceptable.[30]

TABLE V. Recovery for each amino acid in the reference material

Amino acid	Reference value, %	Found value, %				Recovery, %
		1	2	3	Average	
ASP	1.100	1.153	1.189	1.147	1.163	105.7
GLU	2.931	3.219	3.186	3.206	3.204	109.3
SER	0.654	0.634	0.650	0.666	0.650	99.4
GLY	0.592	0.634	0.642	0.652	0.643	108.6
THR	0.489	0.491	0.498	0.611	0.533	109.0
ARG	0.860	0.873	0.891	0.926	0.897	104.3
ALA	0.614	0.638	0.645	0.658	0.647	105.4
TYR	0.437	0.412	0.402	0.415	0.410	93.8
VAL	0.654	0.655	0.662	0.755	0.691	105.7
MET	0.326	0.298	0.305	0.308	0.304	93.3
PHE	0.697	0.732	0.742	0.796	0.757	108.6
ILE	0.517	0.541	0.553	0.548	0.547	105.8
LEU	1.044	1.097	1.111	1.127	1.112	106.5
LYS	0.790	0.853	0.877	0.862	0.864	109.4

TABLE VI. Repeatability of the determination of the amino acids in maize

Amino acid	Content of amino acids, %							*RSD* %
	1	2	3	4	5	6	Average	
ASP	0.629	0.614	0.661	0.602	0.620	0.603	0.625	3.56
GLU	1.998	1.944	2.099	1.914	1.958	1.946	1.983	3.62
SER	0.394	0.389	0.378	0.382	0.364	0.437	0.381	3.02
GLY	0.368	0.349	0.343	0.344	0.332	0.35	0.347	3.80
THR	0.350	0.324	0.350	0.332	0.341	0.335	0.339	3.36
ARG	0.414	0.402	0.398	0.396	0.375	0.398	0.397	3.56
ALA	0.701	0.694	0.687	0.671	0.635	0.682	0.678	3.88
TYR	0.224	0.217	0.215	0.210	0.201	0.214	0.213	4.01
VAL	0.463	0.449	0.438	0.438	0.420	0.426	0.442	3.59
MET	0.147	0.145	0.142	0.141	0.134	0.134	0.142	3.50
PHE	0.478	0.476	0.465	0.447	0.434	0.467	0.460	4.14
ILE	0.365	0.352	0.364	0.339	0.347	0.331	0.353	3.15
LEU	1.167	1.150	1.172	1.122	1.136	1.121	1.149	1.82
LYS	0.274	0.289	0.274	0.284	0.277	0.235	0.280	2.38

Limit of detection and limit of quantification. The limit of detection (*LOD*) and the limit of quantification (*LOQ*) were determined based on the standard deviation of the response and the slope of the linearity plot. The *LOD* is calculated as 3.3α/b and *LOQ* as 10α/*b*, where α is the standard deviation of the *y*-intercept and *b* is the slope of the calibration curve.[30] The *LOD* and *LOQ* values calculated for each well-recovered amino acid are presented in Table VIII. The lowest *LOD* level was observed for arginine (0.004 μg cm^{-3}) and the highest

for leucine (1.707 μg cm^{-3}). The same observation was valid for the *LOQ* values, with the lowest (0.011 μg cm^{-3}) and the highest (5.172 μg cm^{-3}) values being obtained for arginine and leucine, respectively.

TABLE VII. Intermediate precision of the determination of the amino acids in maize

Amino acid	Content of amino acids, %				*RSD*
	1	2	3	Average	%
ASP	0.635	0.605	0.663	0.634	4.57
GLU	1.965	1.915	1.802	1.894	4.41
SER	0.412	0.398	0.385	0.398	3.39
GLY	0.365	0.353	0.368	0.362	2.19
THR	0.350	0.324	0.325	0.333	4.42
ARG	0.402	0.372	0.388	0.387	3.88
ALA	0.668	0.683	0.675	0.675	1.11
TYR	0.219	0.221	0.213	0.218	1.91
VAL	0.440	0.447	0.456	0.448	1.79
MET	0.139	0.143	0.135	0.139	2.88
PHE	0.431	0.458	0.442	0.444	3.06
ILE	0.361	0.349	0.358	0.356	1.75
LEU	1.162	1.148	1.131	1.147	1.35
LYS	0.286	0.298	0.305	0.296	3.24

TABLE VIII. *LOD* and *LOQ* values

Amino acid	*LOD*[a] μg cm^{-3}	*LOD*[b] mg g^{-1}	*LOQ*[a] μg cm^{-3}	*LOQ*[b] mg g^{-1}
ASP	0.118	0.0590	0.357	0.1785
GLU	0.150	0.0750	0.455	0.2275
SER	0.088	0.0440	0.267	0.1335
GLY	0.024	0.0120	0.074	0.0370
THR	0.069	0.0345	0.210	0.1050
ARG	0.004	0.0020	0.011	0.0055
ALA	0.028	0.0140	0.085	0.0425
TYR	0.023	0.0115	0.071	0.0355
VAL	0.044	0.0220	0.133	0.0665
MET	0.043	0.0215	0.129	0.0645
PHE	1.258	0.6290	3.812	1.9060
ILE	0.041	0.0205	0.123	0.0615
LEU	1.707	0.8535	5.172	2.5860
LYS	0.698	0.3490	2.115	1.0575

[a]μg of amino acid in cm^3 of solution injected into the HPLC; [b]mg of amino acid in g of fodder sample

CONCLUSIONS

The achievement of the study is a reliable and high throughput method for the separation and quantification of amino acids in the routine analysis of fodder. The method is based on the automated pre-column derivatisation of fodder samples using a combined OPA/FMOC reaction, which guarantees highly repro-

ducible reaction times and lack of degradation, and provides an important contribution to the results. The method appeared to be highly specific, accurate, precise, and linear across the analytical range. The *LOD* and *LOQ* values were in the range of 0.004–1.258 μg cm^{-3} and 0.011–5.272 μg cm^{-3}, respectively. The acid hydrolysis with 6 mol dm^{-3} HCl at 150 °C lasting 6 h, not only shortened the analysis time by 3 to 4 times, but also resulted in the chromatograms that were significantly more suitable the quantification of amino acids in fodder.

Acknowledgment. The work was financially supported by the Ministry of Education, Science and Technological Development of the Republic of Serbia (Project No. 31081).

И З В О Д

ВАЛИДАЦИЈА HPLC МЕТОДЕ ЗА ОДРЕЂИВАЊЕ АМИНОКИСЕЛИНА У ХРАНИ ЗА ЖИВОТИЊЕ

ИГОР ЈАЈИЋ[1], САША КРСТОВИЋ[1], ДРАГАН ГЛАМОЧИЋ[1], САНДРА ЈАКШИЋ[2] и БИЉАНА АБРАМОВИЋ[3]

[1]Пољопривредни факултет, Универзитет у Новом Саду, Трг Д. Обрадовића 8, 21000 Нови Сад, [2]Научни институт за ветеринарство, Руменачки пут 20, 21000 Нови Сад и [3]Природно–математички факултет, Универзитет у Новом Саду, Трг Д. Обрадовића 3, 21000 Нови Сад

Предмет овог истраживања је валидација методе за анализу аминокиселина у храни за животиње течном хроматографијом високе ефикасности. Одређен је аминокиселински састав кукуруза, соје и сојине сачме, као и њихове смеше, обогаћене различитим количинама метионина, треонина и лизина. Метода укључује киселинску хидролизу узорака (6 h на 150 °C), аутоматску дериватизацију аминокиселина помоћу реагенаса *о*-фталдиалдехида и 9-флуоренил-метил-хлороформата, раздвајање на колони ZORBAX Eclipse-AAA, и детектовање детектором са низом диода. Нађено је да је метода високо специфична (разлике између ретенционих времена узорака хранива и стандардних смеша су ниже од 1,7 %), са широким линеарним опсегом (од 10 до 1000 nmol cm^{-3}, r^2 = = 0,9999), високом тачношћу (ефикасност 93,3–109,4 %), и прецизношћу резултата (*RSD* испод 4,14% у случају поновљивости и испод 4,57 % у случају просечне прецизности). Граница детекције је у опсегу од 0,004 до 1,258 μg cm^{-3}, а граница одређивања од 0,011 до 5,272 μg cm^{-3}. На основу постигнутих резултата се може закључити да се метода може користити за квантитативно одређивање примарних аминокиселина протеина у храни за животиње.

(Примљено 12 јула, ревидирано 17. октобра 2012)

REFERENCES

1. B. Wathelet, *Biotechnol. Agron. Soc. Environ.* **3** (1999) 197
2. D. Heems, G. Luck, C. Fraudeau, E. Verette, *J. Chromatogr., A* **798** (1998) 9
3. H. Liu, *Methods Mol. Biol.* **159** (2000) 123
4. S. Moore, W. H. Stein, *Methods Enzymol.* **6** (1963) 819
5. H. Edelhoch, *Biochemistry* **6** (1967) 1948
6. J. L. Young, M. Yamamoto, *J. Chromatogr.* **78** (1973) 349
7. K. U. Yuksel, T. T. Andersen, I. Apostol, J. W. Fox, J. W. Crabb, R. J. Paxton, D. J. Strydom, in *Techniques in Protein Chemistry VI*, J. W. Crabb, Ed., Academic Press, San Diego, CA, 1994, p. 185
8. M. I. Tyler, *Methods Mol. Biol*. **159** (2000) 1

9. G. Sarwar, H. G. Botting, *J. Chromatogr*. **615** (1993) 1
10. C. Bruton, *Int. Lab*. (1986) 30
11. P. Fürst, L. Pollack, T. Graser, H. Godel, *J. Chromatogr*. **499** (1990) 557
12. M. Simmaco, D. de Biase, D. Barra, F. Bossa, *J. Chromatogr*. **504** (1990) 129
13. P. Haynes, D. Sheumack, L. Greig, J. Kibby, J. Redmond, *J. Chromatogr*. **588** (1991) 107
14. K. Ou, M. Wilkins, J. Yan, A. Gooley, Y. Fung, D. Sheumack, K. Williams, *J. Chromatogr.* **723** (1996) 219
15. A. Gratsfeld-Huesgen, Hewlett Packard Technical Note 12-5966-3110E (1998)
16. R. Gatti, M. G. Gioia, P. Andreatta, G. Pentassuglia, *J. Pharmaceut. Biomed. Anal*. **35** (2004) 339
17. L. Bosch, A. Alegría, R. Farré, *J. Chromatogr., B* **831** (2006) 176
18. X. Li, R. Rezaei, P. Li, G. Wu, *Amino Acids* **40** (2011) 1159
19. G. Paramás, G. Bárez, C. C. Marcos, R. J. García-Villanova, S. Sánchez, *Food Chem*. 95 (2006) 148
20. R. Hanczkó, A. Jámbor, A. Perl, I. Molnár-Perl, *J Chromatogr., A* **1163** (2007) 25
21. G. Ogden, P. Foldi, *LC-GC* **5** (1984) 28
22. D. C. Turnell, J. D. Cooper, *Clin. Chem*. **28** (1982) 527
23. S. Einarsson, *J. Chromatogr*. **348** (1985) 213
24. J. Ozols, *Methods Enzymol*. **182** (1990) 587
25. J. W. Henderson, R. D. Ricker, B. A. Bidlingmeyer, C. Woodward, *Agilent Technical Note 5980-1193E*, 2000
26. V. Gökmen, A. Serpen, B. A. Mogol, *Anal. Bioanal. Chem*. **403** (2012) 2915
27. *Thermo Scientific Pierce GC and HPLC Technical Handbook*, 2008
28. M. P. Bartolomeo, F. Maisano, *J. Biomol. Tech*. **17** (2006) 131
29. J. C. Anders, *Biopharm. Int*. **4** (2002) 32
30. A. J. Reason, *Methods Mol. Biol*. **211** (2003) 181.

Journal of the Serbian Chemical Society
JSCS-info@shd.org.rs • www.shd.org.rs/JSCS
J. Serb. Chem. Soc. 78 (6) 851–863 (2013) UDC 66.095.26:55:66.046.59:544.032.1:539.4
JSCS–4463 *Original scientific paper*

Compressive strength and hydrolytic stability of fly ash-based geopolymers

IRENA NIKOLIĆ[1]*, DIJANA ĐUROVIĆ[2], RADOMIR ZEJAK[3], LJILJANA KARANOVIĆ[4], MILENA TADIĆ[1], DRAGOLJUB BLEČIĆ[1] and VELIMIR R. RADMILOVIĆ[5]

[1] University of Montenegro, Faculty of Metallurgy and Technology, Džordža Vašingtona bb, 81000 Podgorica, Montenegro, [2] Institute of Public Health of Montenegro, Džona Džeksona bb, 81000 Podgorica, Montenegro, [3] University of Montenegro, Faculty of Civil Engineering, Džordža Vašingtona bb, 81000 Podgorica, Montenegro, [4] Laboratory of Crystallography, Faculty of Mining and Geology, University of Belgrade, Đušina 7, 11000 Belgrade, Serbia and [5] Faculty of Technology and Metallurgy, University of Belgrade, Karnegijeva 4, 11120 Belgrade, Serbia

(Received 24 October 2012, revised 1 January 2013)

Abstract: The process of geopolymerization involves the reaction of a solid aluminosilicate material with a highly alkaline silicate solution that yields an aluminosilicate inorganic polymer named a geopolymer, which may be successfully applied in civil engineering as a replacement for cement. In this study, the influence of the synthesis parameters: solid to liquid ratio, NaOH concentration and the ratio of Na_2SiO_3/NaOH, on the mechanical properties and hydrolytic stability of fly ash-based geopolymers in distilled water, sea water and simulated acid rain, were investigated. The highest value of compressive strength was obtained using 10 mol dm^{-3} NaOH and at a Na_2SiO_3/ /NaOH ratio of 1.5. Moreover, the obtained results showed that the mechanical properties of fly ash-based geopolymers are in correlation with their hydrolytic stability, *i.e.*, factors that increase the compressive strength also increase the hydrolytic stability of fly ash-based geopolymers. The best hydrolytic stability of the fly ash-based geopolymers was shown in seawater while the lowest stability was recorded in simulated acid rain.

Keywords: geopolymerization; fly ash; compressive strength; hydrolytic stability.

INTRODUCTION

Geopolymerization is a relatively new, environmentally friendly technology that is based on the reaction of aluminosilicate materials with strongly alkali silicate solutions yielding three dimensional aluminosilicate structures known as

* Corresponding author. E-mail: irena@ac.me
doi: 10.2298/JSC121024001N

geopolymers. Geopolymers are inorganic polymeric materials with Si–O–Al and Si–O–Si bonds. Depending on the reaction parameters, three types of geopolymers are considered: poly(sialate) (–Si–O–Al–O–), poly(sialate–siloxo) (–Si–O–Al–O–Si–O–) and poly(sialate–disiloxo), (–Si–O–Al–O– Si–O–S–O–), in which the ratios of Si:Al are 1, 2 and 3, respectively. Geopolymers with the poly(sialate) structure are mainly investigated and their structure is composed of tetrahedral $[SiO_4]^{4-}$ and $[AlO_4]^{5-}$.[1] The oxygen is sheared between two adjacent tetrahedral. Reaction mechanism of its formation may be presented as follows:[2]

$$(Si_2O_5,Al_2O_2)_n + 3nH_2O \xrightarrow{\text{NaOH, KOH}} n(OH)_3 - Si - O - Al^{(-)} - (OH)_3 \quad (1)$$

$$n(OH)_3 - Si - O - Al^{(-)} - (OH)_3 \xrightarrow{\text{NaOH, KOH}} (Na,K) - \left(Si(O)_2 - O - Al^{(-)}(O)_2 - O\right)_n + 3nH_2O \quad (2)$$

In recent years, geopolymers have attracted much attention primarily due to their good mechanical properties and therefore are considered as a possible replacement for Portland cement. Moreover, they are characterized by good thermal stability,[3] fire resistance[4,5] and resistance to aggressive environments, especially under acid conditions,[6] even better than those of cement-based materials. In addition, replacement of cement with geopolymers would have an environmental benefit, since cement plants contribute 5–10 % to the global emissions of CO_2.[7]

Properties of geopolymers primarily depend on the choice of raw materials. Geopolymerization process may use a variety of raw materials, but the main advantage of geopolymerization is the possibility to utilize the waste materials. The essential requirement, regardless of the raw materials selection, is the high content of aluminum and silica oxides. Fly ash, metakaolin and blast furnace slag are mainly used for geopolymerization processes. Moreover, processing conditions, type and concentration of alkaline solution and solid to liquid ratio determine the characteristics of geopolymers, because they define the ratio between Na_2O/Al_2O_3 and SiO_2/Al_2O_3. In addition, temperature and time of curing affect the geopolymer properties.

The geopolymerization mechanism has not yet been fully understood and it is assumed that it consists of several steps. The first step is dissolution of the solid aluminosilicate materials in the alkaline medium. The next step is condensation of the oligomeric species, leading to the formation of aluminosilicate gel.

The final step consists of hardening of the gel and bonding of non-dissolved solid particles in the final geopolymeric structure.[8]

The aim of this work was to investigate the effect of the synthesis parameters on the compressive strength of fly ash-based geopolymers and their hydrolytic stability in different aquatic environments.

EXPERIMENTAL

The fly ash used for the synthesis of the geopolymers was supplied from the coal-fired power station Pljevlja. The chemical composition of the fly ash is given in Table I.

TABLE I. Chemical composition of the employed fly ash

Compound	Content, %
SiO_2	49.45
Fe_2O_3	5.23
Al_2O_3	21.77
TiO_2	0.66
CaO	13.34
Na_2O	0.46
ZnO	$4.5 \cdot 10^{-3}$
MgO	1.29
MnO	0.02
P_2O_5	0.24
K_2O	1.4
Loss on ignition (LOI)	4.35

The fly ash was activated with alkali solutions made by mixing Na_2SiO_3 and NaOH solutions in the mass ratios 1, 1.5 and 2. A commercial sodium silicate solution (Na_2O = 8.5 %, SiO_2 = 28.5 %, density of 1.4 kg m^{-3}) was used. The concentration of the NaOH solution was 7, 10 or 13 mol dm^{-3}. Geopolymer pastes were prepared by mixing fly ash with an alkali solution in solid to liquid (S/L) ratios of 0.75, 1 and 1.25. The pastes were cast in closed plastic cylindrical moulds of dimensions 28 mm×60 mm and cured for 48 h at 65 °C. After the curing process, the samples were removed from the moulds after cooling and then left to rest for an additional 28 days at ambient temperature before any testing was performed. The samples were tested after 28 days because in most cases the strength requirements for cement-based materials were attained after aging for this time.

Three control geopolymer samples of each series were tested for compressive strength on an HP-400 hydraulic press at room temperature in air (standard test conditions). Before testing, the surfaces of the sample were polished flat and parallel to a height / diameter ratio of approximately 2.

Mineralogical investigations were realized by X-ray powder diffraction (XRPD) analysis employing a PHILIPS PW 1710 diffractometer operating in the step-scan mode (2θ range 4–|–90°, step 0.02°, time 0.8 s) using monochromatized Cu K_α radiation (λ = 1.54178 Å) The crystalline phases were identified from the obtained XRPD patterns by comparing the intensities and positions of the Bragg peaks with JCPDS (Joint Committee on Powder Diffraction Standards) data files.

The microstructural investigations were performed by scanning electron microscopy (SEM) in tandem using an FEI 235DB dual beam focused ion beam (FIB) system equipped

with an EDAX Genesis energy dispersive spectrometer (EDS).[9] Cross sectioning of the porous microconstituents was performed using a 1000 pA gallium ion beam with an operating voltage of 5 kV. In order to minimize electron charging effects, a through lens back scattered electron detector (TLD-B) was used for image recording.

The hydrolytic stability of the geopolymers was investigated through dissolution tests in deionized water, seawater and simulated acid rain (H_2SO_4:HNO_3 = 40:60, pH 3). For this purpose, 2 g of geopolymer, granulation smaller than 90 μm, was mixed with 100 cm^3 distilled water, sea water or acid rain and left in contact for 24 h. After the test, the leachates were separated by filtration and analyzed for their Al and Si content by ICP–OES (Spectro Arcos). The pH of the suspensions was recorded before and after the hydrolytic stability test.

RESULTS AND DISCUSSION

Compressive strength

The results obtained in the investigation of the influence of the solid to liquid ratio, alkalinity and silicate dosage on the compressive strength of the geopolymers are summarized in Table II.

TABLE II. Changes in the compressive strength of the geopolymers in dependence on the reaction parameters

Sample	S/L	c(NaOH) / mol dm^{-3}	$m(Na_2SiO_3)/m$(NaOH)	Compressive strength, MPa
FA1	0.5	10	1.5	–
FA2	0.75	10	1.5	12.18
FA3	1	10	1.5	15.43
FA4	1.25	10	1.5	18.27
FA5	1	7	1.5	13.35
FA6	1	13	1.5	14.71
FA7	1	10	1	14.62
FA8	1	10	2	11.7

It is evident that with increasing S/L ratio, the value of compressive strength of fly ash-based geopolymers (samples FA1–4) increased. The highest value of compressive strength was attained for the mixture FA4 prepared at an S/L ratio of 1.25, which is attributed to the lowest water content in the geopolymer mixture. Water is necessary for the dissolution of solid fly ash particles and the hydrolysis of the dissolved Al^{3+} and Si^{4+}, providing the aluminate and silicate monomers according to Eqs. (3)–(5).[10] Al is present in the form of $[Al(OH)_4]^-$ and Si may be present as $[SiO(OH)_3]^-$ and/or $[SiO_2(OH)_2]^{2-}$. Depending on the pH of alkaline solution, the $[SiO_2(OH)_2]^{2-}/[SiO(OH)_3]^-$ ratio changes. In highly alkaline solutions, $[SiO_2(OH)_2]^{2-}$ species are dominant while in dilute solutions, the $[SiO(OH)_3]^-$ species predominate.[10,11]

$$Al_2O_3 + 3H_2O + 2OH^- \rightarrow 2[Al(OH)_4]^- \quad (3)$$

$$SiO_2 + H_2O + OH^- \rightarrow [SiO(OH)_3]^- \quad (4)$$

$$SiO_2 + 2OH^- \rightarrow [SiO_2(OH)_2]^{2-} \quad (5)$$

The increase of water content is favorable from a standpoint of dissolution and the hydrolysis process because it accelerates the dissolution of Al and Si from the starting material. Simultaneously with dissolution and hydrolysis processes, the condensation process occurs between aluminate and silicate monomers, yielding to the formation of aluminosilicate network–aluminosilicate gel. However, contrary to the dissolution and hydrolysis process, water is being released during the condensation process according to the Eqs. (6) and (7).[10]

$$[Al(OH)_4]^- + [SiO(OH)_3]^- \rightarrow [(OH)_3\ \overset{HO}{\underset{}{Al}} - \overset{H}{\underset{}{O}} - SiO(OH)_2]^{2-} \rightarrow \quad (6)$$

$$[(OH)_3 Al - O - SiO(OH)_2]^{2-} + H_2O$$

$$[Al(OH)_4]^- + [SiO_2(OH)_2]^{2-} \rightarrow [(OH)_3\ \overset{HO}{\underset{}{Al}} - \overset{H}{\underset{}{O}} - SiO_2(OH)]^{3-} \rightarrow \quad (7)$$

$$[(OH)_3 Al - O - SiO_2(OH)]^{3-} + H_2O$$

The content of excess water suppresses the condensation process, which results in a weakening of the geopolymer structure. This means that an increase in the S/L ratio leads to a lower water content in the geopolymer mixture and enhances the condensation process,[12] which results in an increase of the compressive strength. Moreover, an excess of water greatly affects the porosity of the samples, because the water evaporates leaving behind pores in the geopolymer structure. The systems with higher water contents had a higher porosity and a weaker structure.

The presence of water is also important from the standpoint of the workability of the geopolymer paste, which enables its molding. The highest value of compressive strength was achieved at S/L ratio of 1.25 but this mixture was also extremely difficult to mould and additional pressure had to be applied in order to provide molding. On the other hand, water excess (mixture FA1) resulted in shrinkage during the curing period, negatively affecting the compactness of the geopolymer samples. Therefore, the influence of NaOH concentration and composition of alkali silicate solution on the compressive strength and hydrolytic stability of fly ash-based geopolymers were limited to an S/L ratio of 1 (mixture FA3, FA5–8), when molding without additional pressure was possible.

The fly ash-based geopolymers were strengthened by increasing the NaOH concentration when keeping the Na_2SiO_3/NaOH and S/L ratios constant (samples FA3, 5 and 6). However, the positive influence of a higher NaOH concentration strengthening the geopolymer structure is limited. The fly ash-based geopolymers reached a maximum compressive strength at 10 mol dm^{-3} NaOH, at a constant

Na_2SiO_3/NaOH ratio. Further increases of the NaOH concentration reduced the compressive strength. A similar effect of alkaline dosage on the strength of fly ash-based geopolymers was also observed previously.[8,13]

The influence of the NaOH concentration on the compressive strength of fly ash-based geopolymers may be considered through two aspects of the geopolymerization process: from a standpoint of the dissolution process and from a standpoint of the role of alkali metal in the geopolymerization process.

The function of NaOH in a geopolymerization process is twofold. The task of OH^- is to provide dissolution of Al and Si from the vitreous fly ash while the Na^+ ions balance the negative charge on the tetrahedral AlO_4^- group in the geopolymer structure.

The increase of compressive strength of the fly ash-based geopolymers with increasing NaOH concentration is affected by the enhanced formation of an aluminosilicate gel.[13] An increase of the concentration of OH^- promotes the dissolution of Al^{3+} and Si^{4+} from the fly ash[14,15] leading to the formation of reactive monomeric species (Eqs. (3)–(5)), which accumulate during the induction period of the geopolymerization.[16] These monomeric species condense and form oligomeric Si and/or Si–Al species,[17] which continue further to condense leading to the formation of a gelatinous aluminosilicate network, *i.e.*, a geopolymer. An increase in the OH^- concentration leads to a reduction of the induction period of the geopolymerization process and faster aluminosilicate gel formation.[18] As more gel is formed, it overwhelms the remaining fly ash particles and forms a continuous mass of gel, resulting in a denser geopolymer matrix[13] and higher compressive strength of the geopolymers. However, on the other hand, an increase in the quantity of gel with increasing NaOH concentration above 10 mol dm^{-3} leads to a thickening of the solution, which results in lower mobility of the solution and ions and, hence, reduced dissolution of the fly ash[13] and lower compressive strength.

Moreover, Al is easier to dissolve in NaOH solutions of concentrations below 10 mol dm^{-3} compared to Si[19] and condensation between aluminate and silicate species is more probable. Increasing the NaOH concentration above 10 M accelerates Si dissolution giving more dissolved Si^{4+} when compared to the dissolved Al^{3+} and thus promoting condensation between silicate species,[11] which results in decreasing compressive strength.

In addition, increasing the NaOH concentration also leads to increasing concentrations of Na^+ and thus, the effect of Na^+ on the condensation process must be taken in consideration. Increasing the Na^+ concentration causes a decrease in the rate of silica condensation[20] and hence, slightly decreases the compressive strength of the fly ash-based geopolymers. The NaOH concentration is also greatly influenced by the water content in the geopolymer system, which is essential for the hydrolysis process, according to Eqs. (3)–(5). An increase of the

NaOH concentration leads to a decrease in the water content available for the hydrolysis process, which may influence negatively the formation of dissolved Al and Si species in the aquatic phase of the geopolymer systems and thus, reduces the compressive strength.

The results of the investigation of the influence of the silicate dosage on the compressive strength of fly ash-based geopolymers showed that an increase in the silicate dosage, *i.e.*, an increase of the Na_2SiO_3/NaOH ratio from 1 to 1.5 led to increases in compressive strength of the geopolymers (FA 3, 7 and 8). A further increase in the silicate/hydroxide ratio to 2 led to slight reductions in the strength of the geopolymers. The data presented here are in general agreement with earlier observations.[13,21]

As Al is easier to dissolve in a highly alkaline solution compared to Si, the role of silicate solution in a geopolymer mixture is to provide a sufficient concentration of silicate species to condense with Al species and produce an aluminosilicate gel. The increase of silicate dosage has as a result a gradually shift in the chemical system from monosilicate, chains and cyclic trimers to species with larger rings and then to complex structures and polymers, leading consequentially, to increases in the mechanical properties of the resulting geopolymeric materials.[8]

The presence of soluble silicates affects an increase in the degree of geopolymerization and the evolution of mechanical strength.[13] The decrease in the compressive strength of the fly ash-based geopolymers synthesized at a Na_2SiO_3/ /NaOH mass ratio higher than 1.5 was influenced by inefficient workability of the geopolymer pastes.

Moreover, the silicate dosage influences the concentration of free hydroxide ions in solution, which are essential for the dissolution of the starting materials. An increase of the silicate dosage in alkali solution decreases the free hydroxide ions concentration because it is consumed during the polymerization of silica.[22] This results in a decrease in the compressive strength.

Mineralogical and microstructural analysis

Mineralogical and microstructural analysis was restricted to FA3, the geopolymer with the highest compressive strength. The X-ray powder diffraction patterns of the fly ash and fly ash-based geopolymer are shown in Fig. 1.

The XRPD pattern of fly ash shows the presence of a non-crystallized, *i.e.*, amorphous, phase. The dominant crystalline phase was identified as quartz SiO_2. It seemed possible that one member of a melilite solid solution (the two end members are gehlenite, $Ca_2Al_2SiO_7$ and akermanite, $Ca_2MgSi_2O_7$), as well as calcite, $CaCO_3$, and anothrite, $CaAl_2Si_2O_8$, were present in very small quantities. However, because of their very small amount and low crystallinity their unambiguous identification based on XRPD measurements was not possible.

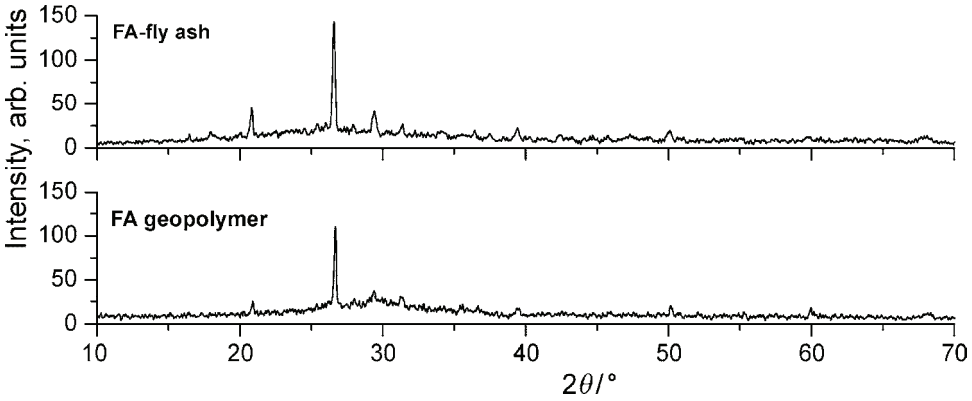

Fig.1. XRPD Pattern of the fly ash (FA) and fly ash-based geopolymer (FA geopolymer).

The XRPD pattern of FA3 geopolymer showed that it was mainly X-ray amorphous, as was expected. Some non-dissolved components, quartz, and probably very small quantities of calcite, anothrite and melilite remained from the non-reacted fly ash but no new crystalline phase was formed because of the geopolymerization reaction.

A cross-sectional SEM microphotograph of the same sample of fly ash-based geopolymer is shown in Fig. 2a. The microstructure of the fly ash-based geopolymer consisted of flat regions, amorphous phase – gel (point 1) and porous regions, which represent partially reacted or non-reacted fly ash (point 2). Micro-cracks connecting the porous regions were formed during the compression testing. Typical EDS spectra from the porous and flat regions are shown in Figs. 2b and 2c, respectively. Silica, aluminum, oxygen and sodium are the main constituents of the aluminosilicate gel phase. The average Si/Al ratio in the gel phase was two, which is in agreement with previous observations that geopolymers with the Si/Al ratios of 1, 2 or 3 show the best mechanical properties.[2]

Hydrolytic stability of the fly ash-based geopolymers

The geopolymers in contact with distilled water and acid rain generated a highly alkaline suspension with pH of 11.1 and 10.9, respectively. The excess of Na^+ ions that remained non-reacted after the geopolymerization process were deposited in the pores of the geopolymer.[23] In contact with aquatic media, these ions were dissolved, which led to the increase of the pH values of the suspensions. In addition, presence of water caused hydrolysis of gel and the leaching of a part of the incorporated sodium,[17] which also contributed to the increase of the pH values of the suspensions.

On the other hand, the pH of geopolymer suspension with seawater before testing was 9.3 but it had decreased to a value of 8.4 after the test.

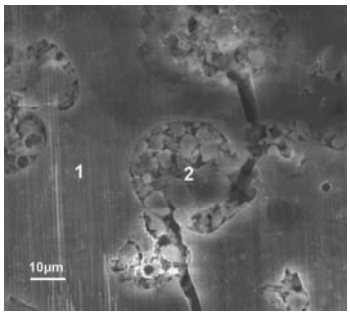

(a)

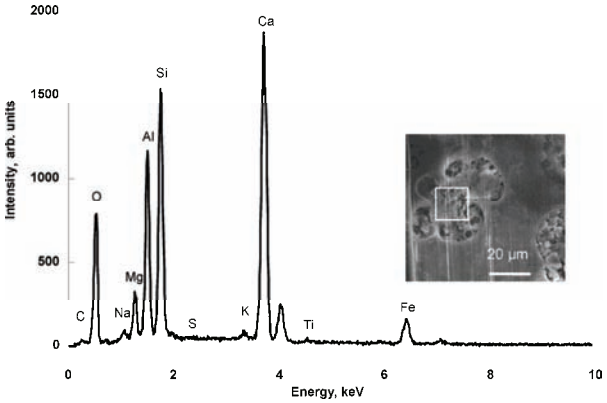

(b)

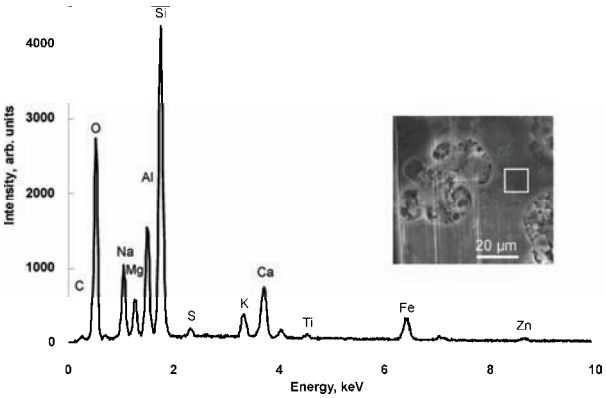

(c)

Fig. 2. a) Cross-sectional view of fly ash-based geopolymer; note the presence of the continuous flat regions and porous islands; b) EDS spectrum taken from the porous region and c) EDS spectrum taken from the flat region.

The results of the investigation of the hydrolytic stability of the geopolymers are given in Fig. 3. The hydrolytic stability of the geopolymers is reflected in the stability of the aluminosilicate gel in different aquatic conditions. Under the influence of water, scission of Si–O–Si bonds in the gel with the release of Si occurs,[24] which forms silicic acid in an aqueous environment (mono or poly).[25] In addition, the presence of Al ions in the leachate indicates a certain degree of dealumination due to the degradation of Al–O–Si bonds. However, Al is dissolved in lower quantities compared to Si, which is consistent with the considerably higher quantities of Si in geopolymer mixtures due to the higher Si content in the fly ash and addition of soluble silicates. Geopolymers are hydrolytically stable if smaller amounts of Si and Al are released into the aquatic environment. Fly ash-based geopolymers are almost insoluble in seawater, *i.e.* the highest hydrolytic stability the geopolymers were shown in seawater, given that the lowest concentrations of Si were evidenced, while the Al concentrations were below the detection limit. On the other hand, the lowest hydrolytic stability of geopolymers was

observed in acid rain. The geopolymers exhibited somewhat higher hydrolytic stability in distilled water than in acid rain. The similar behavior of the geopolymers in distilled water and acid rain is probably influenced by the similar pH values of the suspensions (Table III).

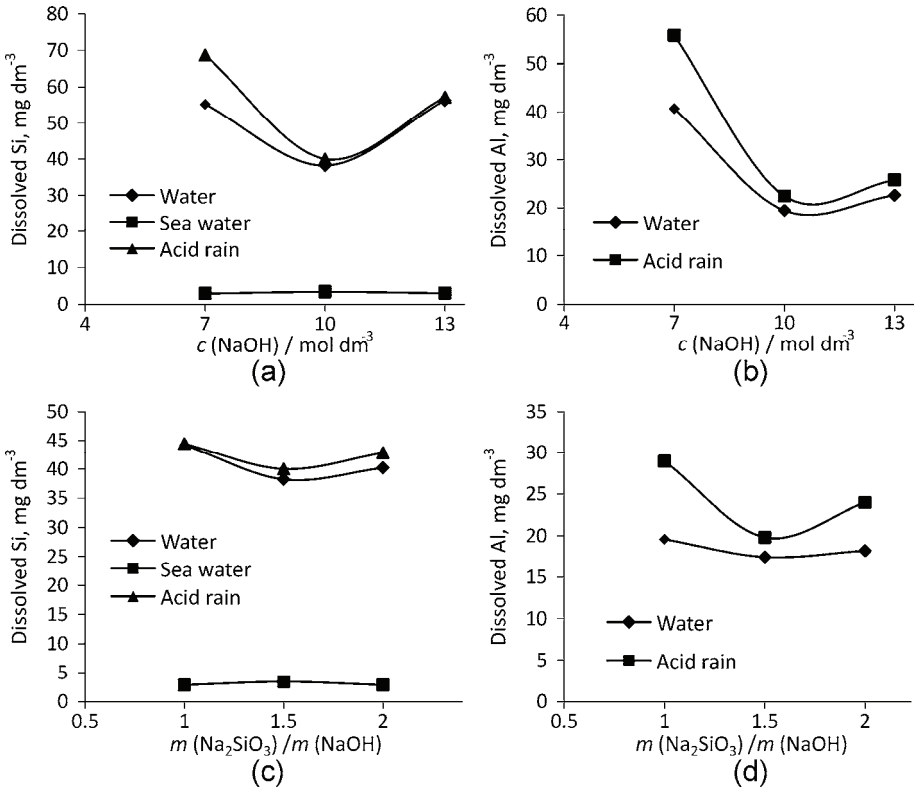

Fig. 3. Hydrolytic stability of the examined geopolymers according to the dissolved amount of Al and Si as functions of the investigated parameters (NaOH concentration, Na_2SiO_3/NaOH mass ratio and type of the aquatic medium).

Experimental investigations on the influence of the NaOH concentration and Na_2SiO_3/NaOH ratio showed that the hydrolytic stability of geopolymers in distilled water and acid rain correlates with the mechanical properties, *i.e.*, the factors that increase the compressive strength also improve the hydrolytic stability (Fig. 3).

Increasing the NaOH concentration from 7 to 10 mol dm^{-3} decreased the dissolution of Si and Al in water and acid rain. A further increase in the concentration to 13 mol dm^{-3} led to increased solubility of Si and Al. Similarly, an increase of the Na_2SiO_3/NaOH ratio from 1 to 1.5 led to reduced degradation of the aluminosilicate gel, *i.e.*, decreases in the Si and Al concentrations in the

leachates, while a further increase of this ratio led to increased solubility of Si and Al, *i.e.*, to a decrease in the hydrolytic stability. The lowest concentrations of Si and Al in the leachate after the hydrolytic test, *i.e.* the highest hydrolytic stability of the geopolymers, was recorded at a concentration of 10 mol dm^{-3} NaOH and a Na_2SiO_3/NaOH ratio of 1.50, under which conditions, the highest value of compressive strength was observed.

TABLE III. pH values of geopolymer suspension in distilled water, seawater and acid rain before and after the hydrolytic test

Medium	pH before test	pH after test
Distilled water	11.1	10.9
Seawater	9.3	8.4
Acid rain	10.9	10.6

The presence of aluminum in an aluminosilicate gel is very important from the standpoint of hydrolytic stability of the gel in an aqueous environment. Previous studies demonstrated that the hydrolytic stability of a sodium silicate gel may be improved by aluminum incorporation.[17,26] From this point of view, the availability of Al to participate in the geopolymerization reaction is of great importance for the stabilization of the resulting gel in different aquatic environments.

In this sense, factors that increase the dissolution of fly ash are of primary importance for the hydrolytic stability of fly ash-based geopolymers.

As an increase in the concentration of NaOH to a value of 10 mol dm^{-3} enhanced the dissolution of fly ash[19], a greater quantity of Al participated in gel formation, which improved the hydrolytic stability of the geopolymers in distilled water and acid rain environments. The resulting decrease in the hydrolytic stability on increasing the NaOH concentration to 13 mol dm^{-3} was the consequence of a lower participation of Al in the gel phase due to a decrease in Al dissolution from fly ash.[19] Besides, the decrease in hydrolytic stability of the geopolymers when the NaOH concentration was increased to above the 10 mol dm^{-3} was reflected in a considerably higher dissolution of Si into distilled water and acid rain in comparison to Al dissolution, which is in agreement with the higher participation of Si in the gel due to the enhanced dissolution of Si from the fly ash.[19]

On the other hand, the hydrolytic stability of the fly ash-based geopolymers did not change considerably on changing the silicate dosage. Some significant dissolution of Al and a slight dissolution of Si from the geopolymer matrix in distilled water and acid rain were observed when changing the Na_2SiO_3/NaOH ratio from 1 to 1.5. A further increase in this ratio slightly increased the hydrolytic stability.

CONCLUSIONS

The microstructure of fly ash-based geopolymers consists of a porous phase (non-reacted or partially reacted fly ash) and a flat alumninosilicate gel. The main constituents of the gel are Si, Al, O and Na.

Analysis of influence of the synthesis parameters on the compressive strength of the fly ash-based geopolymers showed that the strength might be increased by increasing the S/L ratio due to a reduction in the water content of the geopolymer mixture and by increasing the NaOH concentration and the Na_2SiO_3/NaOH ratio. However, the increase in strength with increasing NaOH concentration and Na_2SiO_3/NaOH ratio reaches a maximum and then decreases. The highest value of compressive strength was attained using 10 mol dm^{-3} NaOH and a Na_2SiO_3/ /NaOH ratio of 1.5.

The change in the hydrolytic stability of the fly ash-based geopolymers with change of the investigated parameters followed the change in the mechanical properties, *i.e.*, the conditions that increased the compressive strength also improved the hydrolytic stability. The hydrolytic stability of fly ash-based geopolymers was the best in seawater and the lowest in acid rain. The geopolymers exhibited a somewhat higher hydrolytic stability in distilled water than in acid rain.

Acknowledgements. The authors gratefully acknowledge the financial support from the Ministry of Science of Montenegro within the framework of Project No. 01-460. The FIB analysis was performed at the National Center for Electron Microscopy at Lawrence Berkeley National Laboratory, funded by the U.S. Department of Energy under Contract DE-AC02-05CH11231. VRR acknowledges the support of the Nanotechnology and Functional Materials Center, funded by the European FP7 Project No. 245916 and from the Ministry of Education, Science and Technological Development of the Republic of Serbia, Project No. 172054.

ИЗВОД

ПРИТИСНА ЧВРСТОЋА И ХИДРОЛИТИЧКА СТАБИЛНОСТ ГЕОПОЛИМЕРА НА БАЗИ ПЕПЕЛА

ИРЕНА НИКОЛИЋ[1], ДИЈАНА ЂУРОВИЋ[2], РАДОМИР ЗЕЈАК[3], ЉИЉАНА КАРАНОВИЋ[4], МИЛЕНА ТАДИЋ[1], ДРАГОЉУБ БЛЕЧИЋ[1] и ВЕЛИМИР Р. РАДМИЛОВИЋ[5]

[1]Металуршко–технолошки факултет, Универзитет Црне Горе, Цорца Вашингтона бб, 81000 Подгорица, Црна Гора, [2]Институт за јавно здравље Црне Горе, Џона Џексона бб, 81000 Подгорица, Црна Гора, [3]Грађевински факултет, Универзитет Црне Горе, Цорца Вашингтона бб, 81000 Подгорица, Црна Гора, [4]Лабораторија за кристалографију, Рударско–геолошки факултет, Универзитет у Београду, Ђушина 7, 11000 Београд и [5]Технолошко–меалуршки факултет, Универзитет у Београду, Карнегијева 4, 11120 Београд

Процес геополимеризације укључује реакцију чврстих алумосиликата са јаким алкалносиликатним раствором при чему настаје алумосиликатни полимер назван геополимер, који се успешно може користити у грађевинарству као замена за цемент. У овом раду испитиван је утицај параметара синтезе: односа чврсто-течно, концентрације NaOH и односа Na_2SiO_3/NaOH на механичке особине и хидролитичку стабилност геополимера на бази пепела у дестилованој води, морској води и симулираној киселој киши. Највеће вредности пртисне чврстоће су добијене коришћењем 10 mol dm^{-3} NaOH

при односу Na_2SiO_3/NaOH од 1,5. Осим тога, резултати су показали да су механичке особине геополимера на бази пепела у колерацији са њиховом хидролитичком стабилношћу. Фактори који повећавају притисну чврстоћу повећавају и хидролитичку стабилност геополимера на бази пепела. Најбољу хидролитичку стабилност геополимери показују у морској води док је најслабија стабилност забележена у киселој киши.

(Примљено 24. октобра 2012, ревидирано 1. јануара 2013)

REFERENCES

1. F. Pacheco-Torgal, J. Castro-Gomes, S. Jalali, *Constr. Build. Mater.* **22** (2008) 1305
2. J. Davidovits, *J. Therm. Anal.* **37** (1991) 163
3. D. L. Y. Kong, J. G. Sanjayan, *Cem. Concr. Compos.* **30** (2008) 986
4. T. W. Cheng, J. P. Chiu, *Miner. Eng.* **16** (2003) 205
5. R. E. Lyon, P. N. Balaguru, A. Foden, U. Sorathia, J. Davidovits, M. Davidovics, *Fire Mater.* **21** (1997) 67
6. T. Bakharev, *Cem. Concr. Res.* **35** (2005) 658
7. E. Gartner, *Cem. Concr. Res.* **34** (2004) 1489
8. D. Panias, I. P. Giannopoulou, T. Perraki, *Colloids Surf., A* **301** (2007) 246
9. http://ncem.lbl.gov/frames/FIB.html (October 15, 2012)
10. L. Weng, K. Sagoe-Crentsil, *J. Mater. Sci.* **42** (2007) 2997
11. K. Sagoe-Crentsil, L. Weng, *J. Mater. Sci.* **42** (2007) 3007
12. Z. Zuhua, Y. Xiao, Z. Huajun, C. Yue, *Appl. Clay Sci.* **43** (2009) 218
13. U. Rattanasak, P. Chindaprasirt, *Min. Eng.* **22** (2009) 1073
14. C. Panagiotopoulou, E. Kontori, T. Perraki, G. Kakali, *J. Mater. Sci.* **42** (2007) 2967
15. A. Hajimohammadi, J. L. Provis, J. S. J. van Deventer, *Chem. Mater.* **22** (2010) 5199
16. A. Palomo, M. W. Grutzeck, M. T. Blanco, *Cem. Concr. Res.* **29** (1999) 1323
17. D. Dimas, I. Giannopoulou, D. Panias, *J. Mater. Sci.* **44** (2009) 3719
18. C. A. Rees, *PhD Thesis*, University of Melbourne, Australia, 2007
19. C. Li, Y. Li, H. Sun, L. Li, *J. Am. Ceram. Soc.* **94** (2011) 1773
20. L. Kobera, R. Slavík, D. Koloušek, M. Urbanová, J. Kotek, J. Brus, *Ceram. Silik.* **55** (2011) 343
21. S. Songpiriyakij, T. Kubprasit, C. Jaturapitakkul, P. Chindaprasirt, *Constr. Build. Mater.* **24** (2010) 236
22. I. L. Svensson, S. Sjöberg, L. O. Öhman, *J. Chem. Soc., Faraday Trans.* **82** (1986) 3635
23. P. Duxson, G. C. Lukey, F. Separovic, J. S. J. van Deventer, *Ind. Eng. Chem. Res.* **44** (2005) 832
24. T. Skorina, I. Tikhomirova, *J. Mater. Sci.* **47** (2012) 5050
25. M. Dietzel, *Geochim. Cosmochim. Acta* **64** (2000) 3275
26. I. Giannopoulou, D. Panias, *J. Mater. Sci.* **45** (2010) 5370.

Journal of the Serbian Chemical Society
JSCS-info@shd.org.rs • www.shd.org.rs/JSCS
J. Serb. Chem. Soc. 78 (6) 865–872 (2013)
JSCS–4464
UDC 536.247+532.2:66.011:544.275–128:544.032.4
Original scientific paper

Correlation of liquid–liquid equilibria of non-ideal binary systems using the non-random, two-liquid model

NIKOLA D. GROZDANIĆ[1#], MIRJANA LJ. KIJEVČANIN[1*#], ZORAN P. VIŠAK[2], DUŠAN K. GROZDANIĆ[1] and SLOBODAN P. ŠERBANOVIĆ[1#]

[1]*Faculty of Technology and Metallurgy, University of Belgrade, Karnegijeva 4, 11120 Belgrade, Serbia and* [2]*Centro de Química Estrutural, Instituto Superior Tecnico, Universidade Técnica de Lisboa, Av. Rovisco Pais 1, 1049-001 Lisboa, Portugal*

(Received 2 October 2012, revised 30 January 2013)

Abstract: The non-random, two-liquid (NRTL) model with three different forms of temperature dependant parameters was used to correlate the liquid–liquid equilibrium data for systems of alcohols with alkanes, and alcohols with two ionic liquids: 1–butyl-2,3-dimethylimidazolium tetrafluoroborate ([bmmim][BF4]) and 1-butyl-3-ethylimidazolium tetrafluoroborate ([beim][BF4]). Different temperature dependences of the NRTL parameters were tested on thirteen literature experimental liquid–liquid equilibrium data for binary systems.

Keywords: liquid – liquid equilibria, NRTL model, optimization, ionic liquids, modeling.

INTRODUCTION

The liquid–liquid equilibria (LLE) established in non-ideal mixtures with strong positive deviations from the Raoult Law is essential for the design and development of separation processes. Liquid–liquid solubility data are valuable in studies of the applicability of activity coefficient models. For accurate process and equipment modeling, development and design, it is important to have a reliable thermodynamic model for a good system description. Ionic liquids (ILs) have become popular in recent years as possible "green" replacements for conventional organic, volatile and toxic solvents. Their unique thermophysical properties, mainly a very low vapor pressure, assign them in the group of "green" solvents. Ionic liquids are liquid salts based on large organic cations and small anions that determine their physicochemical properties. Potential applications that

* Corresponding author. E-mail: mirjana@tmf.bg.ac.rs
# Serbian Chemical Society member.
doi: 10.2298/JSC121002012G

have been reported in the literature,[1] which include using ILs as reaction media, heat transfer fluids, and potential solvents for liquid extraction processes, *etc*.

Activity coefficient models, such as UNIQUAC,[2] UNIFAC[3] and NRTL[4] models, have already been successfully used for the correlation and prediction of the vapor–liquid equilibria (VLE), liquid–liquid equilibria (LLE) and other thermodynamic properties of very complex systems.[5–7]

In this paper, the applicability of the NRTL model on selected mixtures of alcohols with alkanes,[8] and two ionic liquids, *i.e*., 1-butyl-2,3-dimethylimidazolium tetrafluoroborate [bmmim][BF4][9] and 1-butyl-3-ethylimidazolium tetrafluoroborate [beim][BF4],[10] were examined. NRTL (non-random two-liquid model) is an activity coefficient model that correlates the activity coefficients γ_i of a component i with its mole fractions x_i in the liquid phase. It is applicable to soluble and partially soluble liquids, multicomponent vapor–liquid, liquid–liquid, and vapor–liquid–liquid equilibria.

MODELING OF LIQUID–LIQUID EQUILIBRIA

Thermodynamic criteria for liquid–liquid equilibria could be given as:

$$\gamma_i^{\mathrm{I}} x_i^{\mathrm{I}} = \gamma_i^{\mathrm{II}} x_i^{\mathrm{II}} \quad , \quad i = 1, 2, \cdots, m \tag{1}$$

where γ_i^{I} is the activity coefficient of component i in phase I, γ_i^{II} is the activity coefficient of component i in phase II, x_i^{I} is a mole fraction of component i in phase I, x_i^{II} is the mole fraction of component i in phase II and m is the number of components in a mixture.

Since the NRTL model[4] has already been tested mainly on non-ideal mixtures with alkanes,[11] in this paper, the applicability of this model was extended to alcohol + ionic liquids binary systems. The NRTL model is defined as follow:

$$\frac{G^{\mathrm{E}}}{RT} = x_1 x_2 \left(\frac{\tau_{12} G_{12}}{x_2 + G_{12} x_1} + \frac{\tau_{21} G_{21}}{x_1 + G_{21} x_2} \right) \tag{2}$$

The activity coefficients γ for binary systems are expressed with following equations:

$$\ln \gamma_1 = x_2^2 \left[\frac{\tau_{12} G_{12}}{\left(x_2 + G_{12} x_1 \right)^2} + \tau_{21} \left(\frac{G_{21}}{x_1 + G_{21} x_2} \right)^2 \right] \tag{3}$$

$$\ln \gamma_2 = x_1^2 \left[\frac{\tau_{21} G_{21}}{\left(x_1 + G_{21} x_2 \right)^2} + \tau_{12} \left(\frac{G_{12}}{x_2 + G_{12} x_1} \right)^2 \right] \tag{4}$$

The binary interaction parameters are defined as follows:

$$G_{12} = \exp\left(-\alpha_{12} \tau_{12}\right) ; \ \tau_{12} = \frac{\Delta g_{12}}{RT} \tag{5}$$

$$G_{21} = \exp\left(-\alpha_{21} \tau_{21}\right) ; \ \tau_{21} = \frac{\Delta g_{21}}{RT} \tag{6}$$

$$G_{12} \neq G_{21}, \ \alpha_{12} = \alpha_{21}$$

where α is the NRTL excess free energy non-randomness parameter, T is the temperature and R is the gas constant. Parameters Δg_{12} and Δg_{21} are NRTL excess free energy model binary interaction temperature dependent parameters.

Since, as shown previously,[12-14] temperature has strong influence on excess properties or equilibria calculations, thus several different forms of temperature dependence for the parameters Δg_{12} and Δg_{21} were introduced:

Form I

$$\begin{aligned} \Delta g_{12} &= A_{12} + B_{12}T \\ \Delta g_{21} &= A_{21} + B_{21}T \end{aligned} \tag{7}$$

Form II

$$\begin{aligned} \Delta g_{12} &= A_{12} + B_{12}T + C_{12}T^2 \\ \Delta g_{21} &= A_{21} + B_{21}T + C_{21}T^2 \end{aligned} \tag{8}$$

Form III

$$\begin{aligned} \Delta g_{12} &= A_{12} + B_{12}T + C_{12}/T^2 \\ \Delta g_{21} &= A_{21} + B_{21}T + C_{21}/T^2 \end{aligned} \tag{9}$$

The corresponding sets of binary interaction parameters (A_{ij}, B_{ij} and C_{ij} in Eq. (7)–(9)) were determined by minimizing the objective function (Eq. (10)) using the Monte Carlo method with a linear congruent generator of pseudorandom numbers:[15]

$$F_{obj} = \sum_{i=1}^{n}\sum_{j=1}^{m}\left(\gamma_{j,i}^{\mathrm{I}} x_{j,i}^{\mathrm{I}} - \gamma_{j,i}^{\mathrm{II}} x_{j,i}^{\mathrm{II}}\right)^2 \rightarrow \min \tag{10}$$

where n is the number of experimental data.

With the obtained optimized parameters, using Eq. (1), the mole fractions $x'_{1,\mathrm{cal}}$ and $x''_{1,\mathrm{cal}}$ were calculated by the Wegstein method[16] over the entire range of investigated temperatures T.

RESULTS AND DISCUSSION

Experimental data at different temperatures were taken from the literature.[8–10] According to the results of preliminary investigations, the non-randomness parameter α_{12} was set as the constant value of 0.3 for all the selected binary systems.

A deviation of the calculated liquid composition in both liquid phases from the experimental values, $x_{1,i,\mathrm{exp}}^{\mathrm{I}}$ and $x_{1,i,\mathrm{exp}}^{\mathrm{II}}$, is expressed as an absolute average deviations $\Delta(x)$, and an absolute average percent deviation $PD(x)$, for each binary system:

$$\Delta(x) = \left(\frac{100}{2n}\right)\sum\left[\left|\left(x_{1,i,\mathrm{exp}}^{\mathrm{I}} - x_{1,i,\mathrm{cal}}^{\mathrm{I}}\right)\right| + \left|\left(x_{1,i,\mathrm{exp}}^{\mathrm{II}} - x_{1,i,\mathrm{cal}}^{\mathrm{II}}\right)\right|\right] \tag{11}$$

$$\begin{aligned} PD(x),\ \% = \left(\frac{100}{2n}\right)\sum_{i=1}^{n} \{&\left|\left(x_{1,i,\mathrm{exp}}^{\mathrm{I}} - x_{1,i,\mathrm{cal}}^{\mathrm{I}}\right)/x_{1,i,\mathrm{exp}}^{\mathrm{I}}\right| + \\ &+ \left|\left(x_{1,i,\mathrm{exp}}^{\mathrm{II}} - x_{1,i,\mathrm{cal}}^{\mathrm{II}}\right)/x_{1,i,\mathrm{exp}}^{\mathrm{II}}\right|\} \end{aligned} \tag{12}$$

TABLE I. Results of LLE correlation of selected binary systems

System	Form	A_{12}	B_{12} / K	C_{12} / K^2	A_{21}	B_{21} / K	C_{21} / K^2	Δx	$PD(x)$ / %
methanol(1)+	I	5087.152	–0.4564683	–	19068.33	–51.82681	–	1.1	2.1
heptane(2)	II	5373.153	–11.85111	3.44×10^{-2}	17946.13	–37.81441	-3.41×10^{-2}	1.0	1.9
	III	6582.356	–5.347746	8.63×10^{-5}	17504.41	–46.74835	-5.84×10^{-2}	1.4	2.5
methanol(1)+	I	9741.815	–8.631523	–	17998.42	–45.65529	–	0.9	1.7
decane(2)	II	10398.24	–12.24016	4.71×10^{-3}	17612.17	–43.87271	-1.80×10^{-3}	1.0	1.9
	III	10653.80	–11.54547	3.06×10^{-4}	17418.83	–43.77454	-9.46×10^{-2}	1.0	1.9
methanol(1)+	I	9819.706	–10.32724	–	17513.98	–45.01369	–	0.8	1.8
nonane(2)	II	10649.05	–15.72755	8.61×10^{-3}	17674.68	–44.15396	-4.23×10^{-3}	1.1	2.1
	III	9869.354	–10.53669	4.10×10^{-2}	17492.56	–44.91943	-7.95×10^{-2}	1.2	2.3
methanol(1)+	I	6089.4	–1.358492	–	19274.21	–51.37226	–	0.4	0.7
octane(2)	II	7095.347	–6.992282	7.21×10^{-3}	16934.27	–38.08940	-1.80×10^{-2}	0.9	1.7
	III	6647.037	–3.251477	2.42×10^{-4}	17732.54	–46.33763	7.07×10^{-5}	1.2	2.3
1-propanol(1)+	I	30157.50	–59.87851	–	27303.17	–92.20162	–	1.5	1.8
bmmimBF4(2)	II	32523.29	–74.07758	2.04×10^{-2}	27863.01	–95.27888	4.48×10^{-3}	1.4	1.7
	III	31043.13	–62.86951	4.77×10^{-1}	26275.95	–88.77695	5.25×10^{-2}	1.7	2.1
2-propanol(1)+	I	32575.63	–62.92048	–	32172.99	–109.8133	–	1.5	1.8
bmmimBF4(2)	II	34798.18	–73.84294	1.17×10^{-2}	31146.13	–106.5383	4.03×10^{-4}	1.7	1.9
	III	33149.74	–64.75449	-7.39×10^{-2}	31826.74	–108.7165	3.63×10^{-1}	1.6	1.8
1-butanol(1)+	I	34239.07	–69.87634	–	37660.18	–117.7754	–	1.8	2.3
bmmimBF4(2)	II	35268.58	–73.24624	7.59×10^{-4}	36517.72	–114.4179	1.45×10^{-4}	1.6	2.0
	III	35934.61	–75.05195	3.81×10^{-4}	35839.66	–112.2911	-7.64×10^{-2}	1.7	2.1
1-pentanol(1)+	I	53557.86	–126.0032	–	26890.21	–78.81150	–	1.5	2.2
bmmimBF4(2)	II	51991.45	–121.2727	6.38×10^{-4}	37356.00	–140.2646	8.97×10^{-2}	1.6	2.2
	III	53454.68	–125.7185	5.62×10^{-5}	26914.41	–78.82802	3.22×10^{-4}	1.6	2.3

TABLE I. Continued

System	Form	A_{12}	B_{12} / K	C_{12} / K^2	A_{21}	B_{21} / K	C_{21} / K^2	Δx	$PD(x)$ / %
1-hexanol(1)+	I	49936.84	−107.3189	–	28338.00	−78.08791	–	7.0	9.1
bmmimBF4(2)	II	51858.6	−112.6044	7.46×10^{-5}	29127.44	−80.50168	1.37×10^{-4}	7.7	9.8
	III	51096.18	−110.7159	1.16×10^{-2}	29527.43	−81.41587	8.71×10^{-2}	7.8	10.0
1-propanol(1)+	I	59010.53	−159.9736	–	131588.5	−45.58663	–	9.3	12.7
[beim][BF4](2)	II	44997.4	−115.0678	9.47×10^{-5}	76522.65	24.14385	1.92×10^{-4}	9.8	13.2
	III	55920.75	−149.9795	8.98×10^{-4}	60180.19	61.61889	2.86×10^{-4}	9.6	13.0
1-butanol(1)+	I	48474.45	−119.7651	–	69304.97	−32.84957	–	6.8	9.3
[beim][BF4](2)	II	48229.33	−119..1960	8.00×10^{-4}	69885.73	−31.36758	3.02×10^{-4}	6.9	9.5
	III	49631.26	−123.4535	5.36×10^{-4}	69835.64	−43.50067	8.09×10^{-4}	6.4	8.9
1-pentanol(1)+	I	63974.78	−159.6538	–	99311.70	−39.39230	–	4.5	6.4
[beim][BF4](2)	II	77238.06	−199.6191	1.20×10^{-3}	116575.8	−32.10275	6.07×10^{-3}	5.5	7.8
	III	77454.04	−199.9958	3.77×10^{-3}	12815.49	−31.30017	7.97×10^{-3}	5.6	7.9
1-hexanol(1)+	I	45819.51	−101.8396	–	28302.13	−80.91595	–	2.1	2.8
[beim][BF4](2)	II	44934.4	−103.5405	1.20×10^{-2}	34551.99	−108.6523	2.78×10^{-2}	1.4	1.9
	III	41762.36	−89.93496	6.12×10^{-2}	31163.7	−89.36466	2.70×10^{-2}	1.5	2.1

The results for the applied models are presented in Table I. The obtained results are given as the absolute average deviations $\Delta(x)$ and the absolute average percent deviations $PD(x)$. The results are in good agreement with the selected experimental data. Graphical representations of the experimental data and the calculated results for all the suggested temperature forms of parameters Δg_{12} and

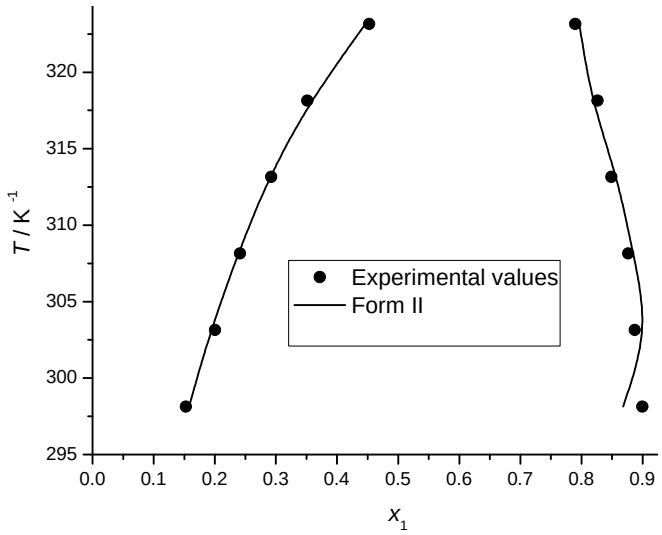

Fig. 1. Phase diagram – Experimental and calculated values of the LLE binary system methanol (1) + heptane (2).

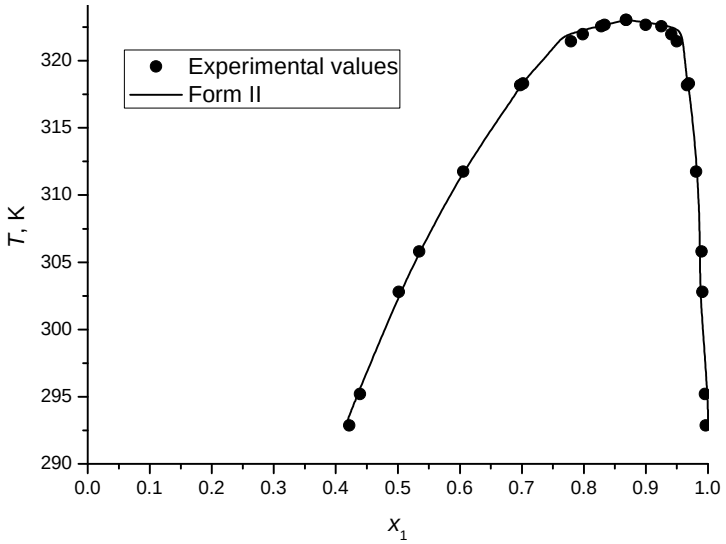

Fig. 2. Phase diagram – Experimental and calculated values of the LLE binary system 1-propanol (1) + bmmim[BF4] (2).

Δg_{21} for the methanol + heptane, 1-propanol + [bmmim][BF4] and 1-pentanol + + [bmmim][BF4] binary systems are shown in Figs. 1–3, respectively. For the binary systems of alcohols with alkanes, all the applied forms of temperature dependent parameters gave very good results, with deviations of about 2 %, as is given in Table I. For the binary systems of alcohols with the ionic liquid 1-butyl-2,3-dimethylimidazolium tetrafluoroborate [bmmim][BF4], as could be seen from Table I, the deviations in the composition calculations are very good, up to 2 %, except for the system with 1-hexanol for which the deviation is higher, up to 10 %, for all forms. The presented deviations rise for all suggested temperature forms with increasing number of carbon atoms. The best result obtained for the alcohol and ionic liquids mixtures was $\Delta(x) = 1.4$ for system 1-propanol + + bmimm[BF4]. For binary systems of alcohols with ionic liquid 1-butyl-3-ethyl-imidazolium tetrafluoroborate [beim][BF4], the deviations were higher, up to 13 % and decrease for all the investigated temperature relationships with increasing number of carbon atoms.

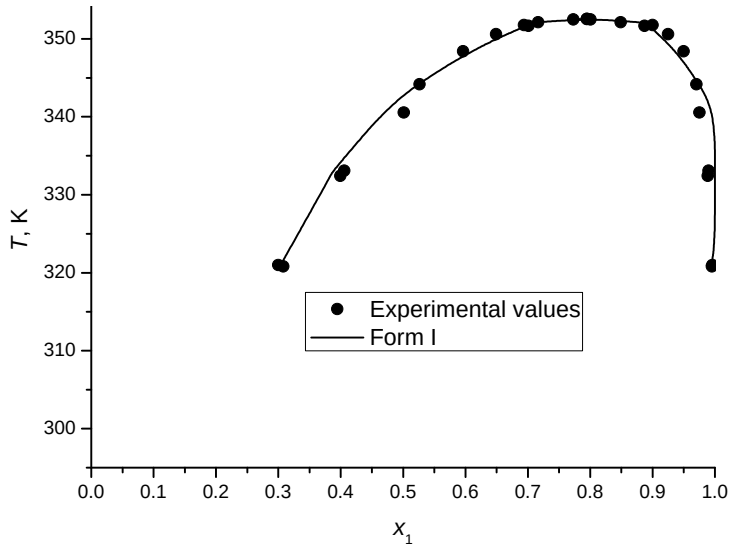

Fig. 3. Phase diagram – Experimental and calculated values of the LLE binary system 1-pentanol (1) + bmmim[BF4] (2).

CONCLUSIONS

Liquid–liquid equilibrium data for thirteen binary systems including alcohols, alkanes, and two ionic liquids at different temperatures were correlated by the NRTL model with three different temperature dependences of the parameters Δg_{12} and Δg_{21}. All three forms of temperature dependent parameters could reproduce most accurately the experimental mutual solubility for all mixtures, with similar results and overall deviations less than 3 %.

Acknowledgements. The authors gratefully acknowledge the financial support received from the Research Fund of the Ministry of Education, Science and Technological Development of the Republic of Serbia (Project No. 172063) and the Faculty of Technology and Metallurgy of the University of Belgrade.

И З В О Д

КОРЕЛИСАЊЕ РАВНОТЕЖЕ ТЕЧНО–ТЕЧНО НЕИДЕАЛНИХ БИНАРНИХ СИСТЕМА ПОМОЋУ NRTL МОДЕЛА

НИКОЛА Д. ГРОЗДАНИЋ[1], МИРЈАНА Љ. КИЈЕВЧАНИН[1], ЗОРАН П. ВИШАК[2], ДУШАН К. ГРОЗДАНИЋ[1] и СЛОБОДАН П. ШЕРБАНОВИЋ[1]

[1] *Технолошко–металуршки факултет, Универзитет у Београду, Карнегијева 4, 11120 Београд и* [2] *Centro de Química Estrutural, Instituto Superior Tecnico, Universidade Técnica de Lisboa, Av. Rovisco Pais 1, 1049-001 Lisboa, Portugal*

NRTL модел са три различита температурно зависна параметра коришћен је за корелисање равнотеже течно–течно за бинарне системе алкохола са алканима, као и алкохола са две јонске течности: 1–butyl-2,3-dimethylimidazolium tetrafluoroborate ([bmmim][BF4]) и 1-butyl-3-ethylimidazolium tetrafluoroborate ([beim][BF4]). У раду су тестиране три различите форме температурне зависности параметара NRTL модела. Равнотежа течност–течност је моделована на тринаест бинарних система. Код свих система су добијени веома задовољавајући резултати са средњим грешкама око 3 %, коришћењем све три форме температурне зависности.

(Примљено 2. октобра 2012, ревидирано 30. јануара 2013)

REFERENCES

1. N. Grozdanić, V. Najdanović-Višak, M. Kijevčanin, S. Šerbanović, M. Nunes da Ponte, Z. Višak, *Fluid Phase Equilib.* **310** (2011) 198
2. D. S. Abrams, J. M. Prausnitz, *AIChE J.* **21** (1975) 116
3. A. Fredenslund, R. L. Jones, J. M. Prausnitz, *AIChE J.* **21** (1975) 1086
4. H. Renon, J. M. Prausnitz, *Ind. Eng. Chem. Process Design Develop.* **8** (1969) 413
5. H. Radfarnia, C. Ghotbi, V. Taghikhani, G. Kontogeorgis, *J. Chem. Thermodyn.* **38** (2006) 923
6. E. Tritopoulou, G. Pappa, E. Voutsas, I. Economou, D. Tassios, *Ind. Eng. Chem. Res.* **42** (2003) 5399
7. H. Matsuda, K. Ochi, K. Kojima, *J. Chem. Eng. Data* **48** (2003) 184
8. H. Higashiuchi, Y. Sakuragi, *Fluid Phase Equilib.* **36** (1987) 35
9. X. Li, K. Tamura, *J. Chem. Thermodyn.* **42** (2010) 1478
10. C. Chokradjaroen, X. Li, K. Tamura, *J. Chem. Thermodyn.* **46** (2012) 72
11. L. Casas, A. Tourino, B. Orge, G. Marino, M. Iglesias, J. Tojo, *J. Chem. Eng. Data* **47** (2002) 887
12. B. Djordjević, M. Kijevčanin, S. Šerbanović, *Fluid Phase Equilib.* **155** (1999) 205
13. B. Djordjević, M. Kijevčanin, A. Tasić, S. Šerbanović, *J. Serb. Chem. Soc.* **64** (1999) 801
14. S. P. Šerbanović, I. R. Grgurić, M. Lj. Kijevčanin, A. Ž. Tasić, B. D. Djordjević, *The Korean J. Chem. Eng.* **21** (2004) 858
15. S. Kuo, *Computer Applications of Numerical Methods*, Addison-Wesley, Reading, MA, 1972
16. L. Lapidus, *Digital Computation for Chemical Engineers*, McGraw-Hill, New York, 1962.

Journal of the Serbian Chemical Society
JSCS-info@shd.org.rs • www.shd.org.rs/JSCS
J. Serb. Chem. Soc. 78 (6) 873–881 (2013)
JSCS–4465
UDC 66.021.3+66.021.4+542.9:621.3.013.1
Original scientific paper

An analytical solution to the problem of radiative heat and mass transfer over an inclined plate at a prescribed heat flux with chemical reaction

HITESH KUMAR*

Department of Information Technology, IBRI College of Technology, Ibri, P. O. Box 466, Oman

(Received 9 July, revised 24 September 2012)

Abstract: A steady laminar flow of viscous electrically conducting incompressible fluid over a semi-infinite inclined porous plate, which was at a prescribed heat flux, with radiation, heat generation and chemical reaction is presented in this manuscript. The analytical solutions for velocity, concentration and temperature were found in terms of an exponential function. The effects of various parameters, such chemical reaction, thermal Grashof number, radiation parameter, angle of inclination, *etc*., on the velocity and temperature are presented graphically.

Keywords: heat transfer; mass transfer; heat flux; heat generation; concentration; inclined wall; chemical reaction.

INTRODUCTION

Convection flow driven by temperature and concentration differences has been the objective of extensive research because such processes exist in nature and has engineering applications. The process occurring in nature includes the photosynthetic mechanism, calm-day evaporation and vaporization of mist and fog, while the engineering applications include chemical reaction in a reactor chamber consisting of rectangular ducts, chemical vapor deposition on surfaces and cooling of electronic equipment. The study of natural convection flow for an incompressible viscous fluid past a heated surface has important applications, such as the cooling of nuclear reactors, the boundary layer control in aerodynamics, crystal growth and food processing and cooling towers.

Moreover, when the temperature of the surrounding fluid is high, radiation effects play an important role that cannot be ignored.[1,2] The effects of radiation on temperature have become more important industrially. Many processes in engineering areas occur at high temperatures and in such cases radiative heat

* E-mail: hiteshrsharma@gmail.com
doi: 10.2298/JSC120709100K

transfer become important for the design of pertinent equipment. Nuclear power plants, gas turbines and the various propulsion devices for aircraft, missiles, satellites and space vehicles are examples of such engineering areas. In such cases, the effects of radiation and free convection have to be taken into consideration. For an impulsively started infinite vertical isothermal plate, Ganesan *et al.*[3] studied the effects of radiation and free convection by using Rosseland approximation.[4] The problem of radiative heat transfer with hydromagnetic flow and viscous dissipation over a stretching surface in the presence of variable heat flux was solved analytically by Kumar.[5]

The problems of free convection and mass transfer of an electrically conducting fluid past an inclined surface with the effect of a magnetic field has vast applications in geophysics, astrophysics and many other engineering areas. Chen[6] studied the analysis of natural convection flow over a permeable inclined surface with variable wall temperatures and concentration. Hossain *et al.*[7] studied free convection flow from an isothermal plate at a small angle to the horizontal. Anghel *et al.*[8] presented a numerical solution of free convection flow past an inclined surface. Bhuvaneswari *et al.*[9] studied an exact analysis of radiation convective heat and mass transfer flow over an inclined plate in a porous medium. Sivasankaran *et al.*[10] presented a Lie group analysis of natural convection heat and mass transfer in an inclined surface. In many engineering and physical problems in which a fluid undergoes exothermic or endothermic reaction, it is highly important to study the effect of heat generation and absorption. Therefore, the study of heat generation or absorption of a moving fluid is important in chemical reactions and those concerned with dissociating fluids. Chamkha and Khalid[11] introduced similarity solutions for hydromagnetic simultaneous heat and mass transfer with heat generation and absorption in natural convection from an inclined plate. Vajravelu and Hadjinicolaou[12] studied the heat transfer boundary layer of a viscous fluid over a stretching sheet with internal heat generation. Kumar[13] investigated heat transfer over a stretching porous sheet subjected to a power law heat flux in the presence of a heat source.

Diffusion rates can be altered tremendously by chemical reactions. The effect of a chemical reaction depends on whether the reaction is homogeneous or heterogeneous. This depends on whether they occur in an interface or as a single-phase volume reaction. In a well-mixed system, the reaction is heterogeneous if the reactants are in multiple phases and homogeneous if the reactants are in the same phase. In most cases of chemical reactions, the reaction rate depends on the concentration of the species itself. Kandasamy *et al.*[14] studied thermophoresis and variable viscosity effects on the magnetohydrodynamics of mixed convective heat and mass transfer past a porous wedge in the presence of a chemical reaction. Kandasamy and Devi[15] studied the effects of chemical reaction, heat and

mass transfer on non-linear laminar boundary-layer flow over a wedge with suction or injection.

In the present work, radiative heat and mass transfer over an inclined plate in the presence of a chemical reaction was studied when the wall is at prescribed heat flux. The effects of the chemical reaction, radiation parameters, the thermal Grashof number and the angle of inclination on the velocity and temperature fields were studied.

MATHEMATICAL ANALYSIS

Consider a steady laminar flow of an incompressible viscous electrically conducting fluid past a semi-infinite inclined porous wall with an acute angle ϕ from the vertical in the presence of a chemical reaction and radiation. The wall is at the prescribed heat flux. The flow is assumed to be in the *x*-direction, which is taken along the semi-infinite inclined porous plate with the *y*-axis normal to it. A magnetic field of uniform strength B_0 is introduced normal to the flow direction. In the analysis, it is assumed that the magnetic Reynolds number is much lower than unity so that the induced magnetic field can be neglected in comparison to the applied magnetic field. It is also assumed that all fluid properties are constant. Then, under the usual Boussinesq and boundary layer approximations, the governing equations of the mass, momentum, energy and concentration for steady flow can be written as:

$$\frac{\partial v}{\partial y} = 0 \tag{1}$$

$$v\frac{\partial u}{\partial y} = \vartheta\frac{\partial^2 u}{\partial y^2} + g\,\beta_T\,(T - T_\infty)\cos\varphi + g\,\beta_C\,(c - c_\infty)\cos\varphi - \frac{\vartheta}{K'}u - \frac{\sigma B_0^2 u}{\rho} \tag{2}$$

$$v\frac{\partial T}{\partial y} = \alpha\frac{\partial^2 T}{\partial y^2} - \frac{1}{\rho c_p}\frac{\partial q_r}{\partial y} + \frac{Q}{\rho c_p}\left(T - T_\infty\right) \tag{3}$$

$$v\frac{\partial c}{\partial y} = D\frac{\partial^2 c}{\partial y^2} - K_l\left(c - c_\infty\right) \tag{4}$$

with the boundary conditions:

$$\begin{gathered} u = 0\,,\ v = -v_{\mathrm{w}}\,,\ \frac{\partial T}{\partial y} = -\frac{q}{k}\,,\ c = c_{\mathrm{w}}\,,\ \text{at}\ \ y = 0 \\ u \to 0\,,\ T \to T_\infty\,,\ c \to c_\infty\,,\ \text{as}\ \ y \to \infty \\ v_{\mathrm{w}} > 0 \end{gathered} \tag{5}$$

The equation of continuity (1) with the boundary condition (5) changes to:

$$v = -v_{\mathrm{w}} \tag{6}$$

here, $v_{\mathrm{w}} > 0$.

Assuming the Rosseland approximation[4] for the radiative heat flux leads to:

$$q_r = -\frac{4\sigma'}{3\kappa^*}\frac{\partial T^4}{\partial y}$$

If the temperature differences within the flow are sufficiently small such that T^4 may be expressed as a linear function of the temperature, then the Taylor series for T^4 about T_∞, after ignoring higher order terms, is given by:

$$T^4 = 4T_\infty^3 T - 3T_\infty^4$$

Assuming the non-dimensional variables are as follows:

$$Y = \frac{y v_w}{\vartheta},\ U = \frac{u}{u_w},\ \theta = \frac{k v_w (T - T_\infty)}{q\vartheta},\ C = \frac{c - c_\infty}{c_w - c_\infty},\ Gr_T = \frac{g\beta_T q\vartheta^2}{k u_w v_w^3},$$
$$Gr_c = \frac{g\beta_c (c_w - c_\infty)\,\vartheta}{u_w v_w^2},\ K = \frac{K' v_w^2}{\vartheta^2},\ M^2 = \frac{B_0^2 \vartheta\sigma}{v_w^2 \rho},\ \mathrm{Pr} = \frac{\rho\vartheta c_p}{k} = \frac{\vartheta}{\alpha},$$
$$N = \frac{\kappa^* k}{4\sigma' T_\infty^3},\ S = \frac{Q\vartheta}{\rho c_p v_w^2},\ Sc = \frac{\vartheta}{D} \text{ and } K_c = \frac{\vartheta K_l}{v_w^2}$$

and using these non-dimensional parameters, Eqs. (2)–(4) are reduced to:

$$\frac{\mathrm{d}^2 U}{\mathrm{d}Y^2} + \frac{\mathrm{d}U}{\mathrm{d}Y} + Gr_T\,\theta\cos\varphi + Gr_c\,C\cos\varphi - \frac{1}{K}U - M^2 U = 0 \tag{7}$$

$$\left(1 + \frac{4}{3N}\right)\frac{\mathrm{d}^2\theta}{\mathrm{d}Y^2} + \mathrm{Pr}\frac{\mathrm{d}\theta}{\mathrm{d}Y} + \mathrm{Pr}\,S\,\theta = 0 \tag{8}$$

$$\frac{\mathrm{d}^2 C}{\mathrm{d}Y^2} + Sc\frac{\mathrm{d}C}{\mathrm{d}Y} - K_c\,Sc\,C = 0 \tag{9}$$

With the corresponding boundary conditions:

$$\begin{aligned} &U = 0,\ \frac{\partial\theta}{\partial Y} = -1,\ C = 1,\ \text{at}\ \ Y = 0 \\ &U \to 0,\ \theta \to 0,\ C \to 0,\ \text{as}\ \ Y \to \infty \end{aligned} \tag{10}$$

the solutions of Eqs. (7)–(9) with boundary condition (10) are as follows:

$$C = \mathrm{e}^{-aY} \tag{11}$$

$$\theta = d\,\mathrm{e}^{-bY} \tag{12}$$

$$U = p_1\mathrm{e}^{-fY} - p_2\mathrm{e}^{-bY} - p_3\mathrm{e}^{-aY} \tag{13}$$

where:

$$a = \frac{Sc + \sqrt{Sc^2 + 4K_c Sc}}{2},\ L^2 = M^2 + \frac{1}{K},\ \omega = 1 + 4/(3N),\ b = \frac{Pr + \sqrt{Pr^2 - 4Pr\,S\omega}}{2\omega},$$
$$d = \frac{1}{b},\ f = \frac{1 + \sqrt{1 + 4L^2}}{2},\ p_2 = \frac{Gr_T\,d\cos\varphi}{b^2 - b - L^2},\ p_3 = \frac{Gr_c\cos\varphi}{a^2 - a - L^2} \text{ and } p_1 = p_2 + p_3$$

The wall shear stress is given by:

$$\tau_f = \mu\left(\frac{\mathrm{d}u}{\mathrm{d}y}\right)_{y=0} \tag{14}$$

and the skin friction coefficient is defined as:

$$C_f = \frac{\tau_f}{\rho u_w v_w} = \left(\frac{\mathrm{d}U}{\mathrm{d}Y}\right)_{Y=0} = -fp_1 + bp_2 + ap_3 \tag{15}$$

The recovery factor can be written as:

$$R_f = \theta(0) = d \tag{16}$$

the wall mass transfer rate is:

$$J_w = -D\left(\frac{\partial C}{\partial Y}\right)_{Y=0} \tag{17}$$

and the Sherwood number is defined as:

$$Sh = \frac{J_w \vartheta}{(C_w - C_\infty) D v_w} = -\frac{\mathrm{d}C}{\mathrm{d}Y}(0) = a \tag{18}$$

RESULTS AND DISCUSSION

A study of the velocity, temperature, concentration, skin friction, recovery factor and Sherwood number of the steady laminar flow of an incompressible viscous electrically conducting fluid past a semi-infinite inclined wall was performed in the present research.

The velocity as a function of K_c. is plotted Fig. 1 and the obtained results were compared with those of Kandasamy and Devi[15] and good agreement was found. It can be seen from Fig. 1 that the velocity the fluid decreased with increasing chemical reaction, which was considered to be a homogeneous first-order chemical reaction. The diffusing species can either be destroyed or generated in the homogeneous reaction. The chemical reaction parameter can be adjusted to meet these circumstances if one takes $K_c > 0$ for a destructive reac-

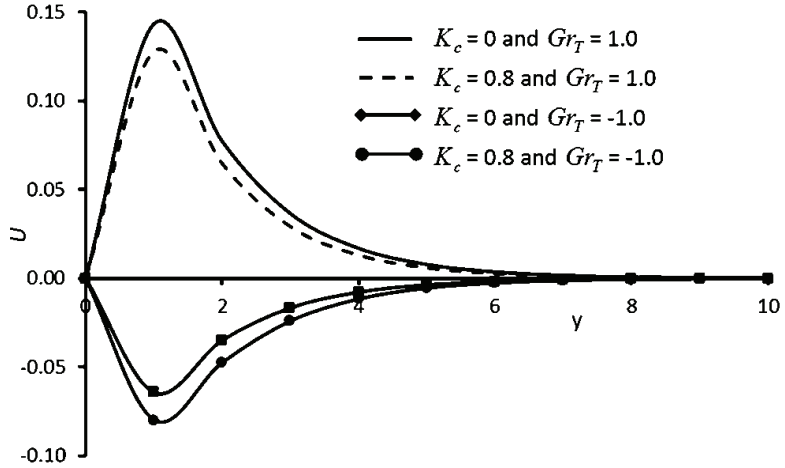

Fig. 1. Dimensionless velocity against non-dimensional y for different values of K_c and Gr_T when Sc = 0.78, Pr = 1.0, S = 0.1, ω = 1.13, K = 1.0, M = 1.73, ϕ = 30° and Gr_c = 0.5.

tion, $K_c < 0$ for a generative reaction and $K_c = 0$ for no reaction. A destructive chemical reaction was assumed herein.

The effect of the angle of inclination (ϕ) on the velocity is shown in Fig. 2. The velocity decreases as ϕ increases. The fluid has a higher velocity when the surface is vertical than when it is inclined because the buoyancy effect decreases due to gravity components ($g\cos\phi$) as the plate is inclined. In the case of $Gr_T < 0$, it can be seen that ϕ increases the velocity. This is because a negative Gr_T makes the rate of heat transfer also negative and at wall, the heat flux becomes positive, which accelerates the convection effect at the wall; the stream function for lower values of the thermal Grashof number become thinner (diluted) due to stronger convection, hence the velocity decreases.

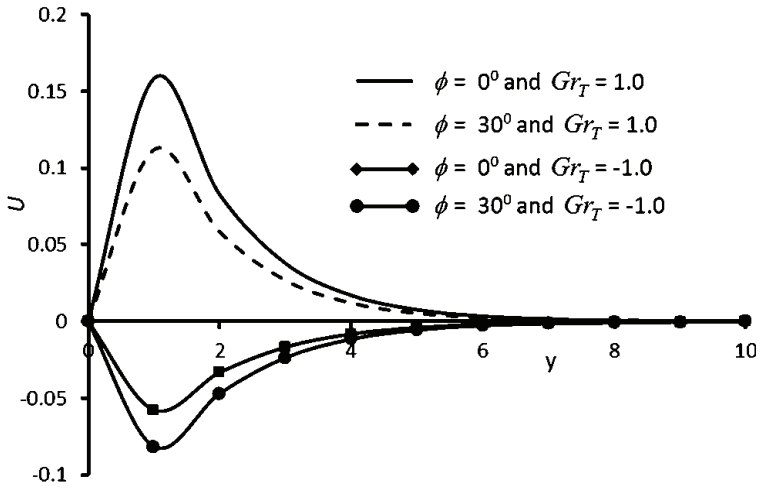

Fig. 2. Dimensionless velocity against non-dimensional y for different values of ϕ and Gr_T when Sc = 0.78, K_c = 0.2, Pr = 1.0, S = 0.1, ω = 1.13, K = 1.0, M = 1.73 and Gr_c = 0.5.

The effects of ω on temperature is presented in Fig. 3, from which it can be seen that θ increases as ω increases or N decreases (because $\omega = 1 + 4/3N$). Numerically, increasing the radiation parameter reduces the radiation effect; physically, increasing the radiation parameter leads to a decrease in the thickness of the thermal boundary layer.

CONCLUSIONS

In the present study, an analytical solution of steady hydromagnetic boundary-layer flow over a semi infinite inclined plate, which is at prescribed heat flux, in the presence of chemical reaction, buoyancy, heat generation and thermal radiation. The flow equations were solved analytically and the obtained results were compared with earlier published work and found to be in good agreement. The velocity of the fluid decreases as the chemical reaction or angle of incli-

nation increases. Radiation (increasing with 1/N) extends the thermal boundary layer and decreases the heat transfer from the surface to the fluid.

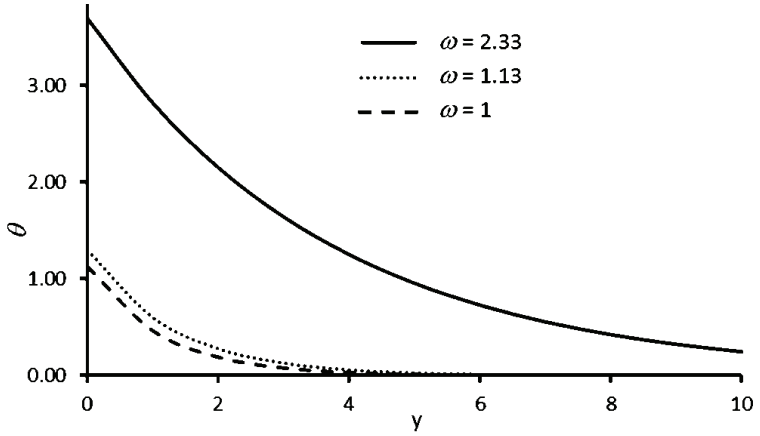

Fig. 4. Dimensionless temperature against non-dimensional y for different values of ω when Pr = 1.0 and S = 0.1.

NOMENCLATURE

y horizontal coordinate (m)
u axial velocity (m s^{-1})
v transverse velocity (m s^{-1})
T temperature of the fluid (K)
T_∞ far field temperature (K)
c species concentration (mol m^{-3})
c_∞ far field concentration (mol m^{-3})
c_w concentration on the surface (mol m^{-3})
g acceleration due to gravity (m s^{-2})
β_T coefficient of thermal expansion (K^{-1})
β_C coefficient of concentration expansion (m^3 mol^{-1})
ϕ angle of inclination (°)
ϑ kinematic viscosity (m^2 s^{-1})
K' permeability of porous medium (m^2)
σ electrical conductivity (S m^{-1})
B_0 magnetic field coefficient (T)
α thermal diffusivity (m^2 s^{-1})
Q heat generation coefficient (W m^{-3} K^{-1})
ρ density (kg m^{-3})
c_p specific heat (J Kg^{-1} K^{-1})
q radiative heat flux in the y-direction (W m^{-2})
D mass diffusion coefficient (m^2 s^{-1})
K_l rate of chemical reaction (s^{-1})
q rate of heat transfer (W m^{-2})

k thermal conductivity (W m^{-1} K^{-1})
u_w surface velocity (m s^{-1})
v_w suction velocity (m s^{-1})
σ' Stefan–Boltzmann constant (W m^{-2} K^{-4})
K^* mean absorption coefficient (m^{-1})
Gr_T thermal Grashof number
Gr_c solutal Grashof number
K dimensionless permeability parameter
M^2 magnetic field parameter
Pr Prandtl number
N radiation parameter
S heat generation parameter
Sc Schmidt number
K_c chemical reaction parameter
Y dimensionless horizontal coordinate
U dimensionless axial velocity
Θ dimensionless temperature
C dimensionless species concentration
Constants: a, b, d, ω, f, p_1, p_2, p_3 and L^2.

Acknowledgment. The author is very much thankful to Prof. (Dr.) S. S. Tak, Jai Narain Vyas University, Jodhpur (India) for offering his valuable suggestions and assistance to improve this paper.

И З В О Д

АНАЛИТИЧКО РЕШЕЊЕ ПРОБЛЕМА ПРЕНОСА ТОПЛОТЕ ЗРАЧЕЊЕМ И ПРЕНОСА МАСЕ СА ХЕМИЈСКОМ РЕАКЦИЈОМ НА КОСОЈ ПЛОЧИ ПРИ ЗАДАТОМ ФЛУКСУ ТОПЛОТЕ

HITESH KUMAR

Department of Information Technology, IBRI College of Technology, Ibri, P. O. BOX 466, Oman

Математички модел стационарног ламинарног тока вискозног, електропроводног, нестишљивог флуида, преко полу-бесконачне косе порозне плоче, са задатим флуксом топлоте, са зрачењем, генерисањем топлоте и хемијском реакцијом, је приказан у раду. Аналитичка решења за брзину, концентрацију и температуру су добијена у облику експоненцијалних функција. Утицаји различитих параметара, као што су хемијска реакција, топлотни Грасхофов број, параметар зрачења, угао нагиба плоче, итд., на брзину и температуру су приказани графички.

(Примљено 9. јула, ревидирано 24. септембра 2012)

REFERENCES

1. M. F. Modest, *Radiative Heat Transfer*, 2nd ed., Academic Press, New York, USA, 2003, p. 281
2. R. Siegel, J. R. Howell, *Thermal Radiation Heat Transfer*, 4th ed., Taylor & Francis, New York, USA, 2002, p. 2
3. P. Ganesan, P. Loganathan, V. M. Soundalgekar, *Int. J. Appl. Mech. Eng.* **6** (2001) 719

4. M. N. Özisik, *Radiative Transfer and Interaction with Conduction and Convection*, Wiley, New York, USA, 1972, 318
5. H. Kumar, *Thermal Sci.* **13** (2009) 163
6. C. H. Chen, *Acta Mech.* **172** (2004) 219
7. M. A. Hossain, I. Pop, M. Ahmad, *Int. J. Theor. Appl. Fluid Mech.* **1** (1996) 194
8. M. Anghel, M. A. Hossain, S. Zeb, I. Pop, *Int. J. Appl. Mech. Eng.* **8** (2001) 473
9. M. Bhuvaneswari, S. Sivasankaran, Y. J. Kim, *World Appl. Sci. J.* **10** (2010) 774
10. S. Sivasankaran, M. Bhuvaneswari, P. Kandaswamy, E. K. Ramasami, *Nonlinear Anal. Model. Control* **11** (2006) 201
11. A. J. Chamkha, A. A. Khalid, *Heat Mass Transfer* **37** (2001) 117
12. K. Vajravelu, A. Hadjinicolaou, *Int. Commun. Heat Mass Transfer* **20** (1993) 417
13. H. Kumar, *Thermal Sci.***5**(Suppl.2) (2011) S187
14. R. Kandasamy, I. Muhaimin, A. B. Khamis, *Heat Mass Transfer* **45** (2009) 703
15. R. Kandasamy, S. P. A. Devi, *J. Comput. Appl. Mech.* **5** (2004) 21.

Journal of the Serbian Chemical Society
JSCS-info@shd.org.rs • www.shd.org.rs/JSCS
J. Serb. Chem. Soc. 78 (6) 883–895 (2013)
JSCS–4466
UDC 552.5:631.872+547.992:
544.722.132+547.1
Original scientific paper

Lindane sorption and desorption behaviour on sediment organic matter

JELENA S. TRIČKOVIĆ[1*#], IVANA I. IVANČEV-TUMBAS[1#], MARIJANA M. KRAGULJ[1], MILJANA Đ. PRICA[2], DEJAN M. KRČMAR[1#], ALEKSANDAR D. NIKOLIĆ[1] and BOŽO D. DALMACIJA[1#]

[1]*University of Novi Sad, Faculty of Sciences, Department of Chemistry, Biochemistry and Environmental Protection, Trg Dositeja Obradovića 3, 21000 Novi Sad, Serbia and* [2]*University of Novi Sad, Faculty of Technical Sciences, Trg Dositeja Obradovića 6, 21000 Novi Sad, Serbia*

(Received 6 July, revised 8 October 2012)

Abstract: The work is concerned with the sorption and desorption behaviours of lindane on four humic acid fractions (HAs) and two humin fractions, sequentially extracted from Ludas Lake sediment. All sorption isotherms fitted to the Freundlich model were nonlinear. The isotherm linearity increased from 0.757 for the first extracted HA to 0.944 for the ninth HA, showing a positive correlation with the atomic H/C ratio, while a negative correlation between the sorption coefficient and aliphaticity of the isolated HAs was observed. It was shown that the sorption processes may be strongly influenced by the physical conformation of and accessibility to sediment organic matter (SOM), as demonstrated by the high K_{oc} and low n values of the humin samples. Despite exhibiting the most nonlinear sorption isotherms, humin samples did not show a pronounced sorption–desorption hysteresis, while the most significant hysteresis was observed for the three HA samples. These results support the hypothesis that the aromatic domains in SOM influence strongly the sorption and desorption behaviour of lindane. The findings obtained in this study may be helpful in understanding the distribution, transport and fate of lindane in soils and sediments.

Keywords: sediments; humic acid; humin; hydrophobic organic compounds; hysteresis.

INTRODUCTION

Sorption is a major process determining the fate and behaviour of hydrophobic organic compounds (HOCs) in sediments and soils. It is widely recognized that soil and sedimentary organic matter (SOM) is the dominant cons-

* Corresponding author. E-mail: jelena.trickovic@dh.uns.ac.rs
# Serbian Chemical Society member.
doi: 10.2298/JSC120706104T

tituent for sorption, sequestration and attenuation of HOCs.[1,2] Since the humic substances (HSs) represent a significant portion of the SOM,[3,4] knowledge of the physical and chemical properties of these substances and the nature of their interactions with HOCs represent aspects relevant to risk assessment and remediation of contaminated sediments. Hence, the identification and comparison of the sorption and desorption behaviour of HOCs by different humic matter fractions are essential to predict the fate and bioavailability of HOCs in soils and sediments.

Many previous papers emphasized the importance of SOM heterogeneity in establishing the nature of the sorption–desorption behaviour and the equilibrium isotherm character of HOCs.[1,5] The concept of amorphous (flexible, rubbery-like) and condensed (rigid, glassy-like) domains of SOM were employed to operationally describe the chemical heterogeneity of SOM having two domains with distinctly different degrees of physicochemical condensation and markedly different HOC sorption behaviour.[6,7] The sorption process is presumed to occur by dissolution of HOCs within the amorphous domains, generating linear, low capacity, non-competitive, and rapid behaviour in the sorption and desorption phases. On the other hand, nonlinear isotherms were observed for the sorption to the condensed domains due to hole-filling (adsorption) process. A number of studies showed the differences of the sorption behaviour of HOCs on HSs.[8–12] The inconsistency of observations may also be attributed to the fact that the HA structural function associated with HOC binding may be more affected by HA sources than by the apparent physicochemical properties.[13] In an earlier paper,[14] which investigated the sorption of pentachlorobenzene on sequentially extracted humic substances from a single sediment sample, it was shown that sorption affinity and mode of sorption to aliphatic and aromatic structures within the SOM differed.

Despite the fact that bioavailability is mostly affected by the desorption process, considerable less information is available in the literature about the effects of structural variations of SOM on the desorption behaviour of HOCs. Therefore, sorption and desorption studies on chemically and structurally different HAs extracted from a single sediment sample could provide more detailed information on the importance of certain structural characteristics of HSs in the sorption mechanism.

Therefore, the objectives of the present study were: *i*) to examine both the sorption and desorption of lindane as a model HOC on four sequentially extracted HA fractions and two humin fractions and *ii*) to find relationships between the structural descriptors of these HSs, lindane sorption and desorption parameters, and sorption–desorption hysteresis.

Hexachlorocyclohexanes (HCHs) were applied globally as pest control from the 1940s.[15] Technical HCH, a mixture of α-, β- and γ-isomer, was banned from

use in North America in the 1970s, but was still used in China until the 1980s and in India and the former Soviet Union until the 1990s.[15] Lindane, purified γ-isomer, was in use in Serbia up to 2006. Due to its persistence in the environment for longer periods, lindane has been detected worldwide.[15,16]

The results of the present study may contribute to a better understanding the effects of structural variations of SOM on the fate of lindane in sediments and soils.

EXPERIMENTAL

Isolation and characterisation of humic acids and humins

The sediment sample was collected from the Ludas Lake, one of the protected areas in the northern province of Serbia, Vojvodina. Ten fractions of HAs and two of humins were isolated by progressive sequential extraction, which involved eight successive extractions with 0.1 M $Na_4P_2O_7$ followed by two extractions with 0.1 M NaOH. Details of the employed extraction procedure and the results of elemental analysis and diffuse reflectance Fourier transform infrared spectroscopy (FTIR) characterization were given in a previous work.[14] The four HA fractions (depicted as HA1, HA3, HA6 and HA9) and two humin samples (depicted as LOHu and HOHu), employed in this study to perform sorption and desorption experiments of lindane, were chemically and structurally different (Table I).

TABLE I. Elemental compositions, atomic *H*/*C* ratios, aliphatic to aromatic peak height ratio and ash content of the four sequentially extracted HA fractions and the two humin fractions used as sorbents in this study[14]

Sample[a]	Composition[b], %				*H/C*	Aliphatic to aromatic peak height ratio	Ash, %
	C	H	N	S			
HA1	52.3	6.44	5.89	3.07	1.47	1.27	15.0
HA3	52.6	6.71	5.66	3.02	1.52	1.28	16.2
HA6	52.8	7.21	5.54	2.38	1.63	1.43	27.3
HA9	55.3	7.93	5.37	2.87	1.71	1.68	18.3
HOHu	54.0	8.46	4.79	6.03	1.87	1.87	65.4
LOHu	23.6	9.38	1.47	4.69	4.74	–	92.5

[a]Number represents the extraction sequence; [b]Values are expressed on an ash-free and moisture-free basis. H/C: atomic ratio of hydrogen to carbon

The atomic H/C ratio, as a descriptor for the degree of aromaticity,[17] increased gradually from 1.47 for HA1 to 1.71 for HA9, showing that the later-extracted HAs had higher contents of aliphatic carbons. Similar conclusions were derived from the results of FTIR analysis. The aliphatic to aromatic peak height ratios increased from 1.27 for HA1 to 1.68 for HA9, showing that aliphaticity increased with increasing sequence of the extraction. HOHu also showed a high degree of aliphaticity, with an *H*/*C* value of 1.87, while LOHu had an extremely high *H*/*C* value of 4.74, probably due to the high ash content (92.5 %), which could have resulted in strong adsorption of water molecules or hydroxyl groups on the edges of broken minerals. This effect, in combination with the relatively low carbon content (23.6 %), led to uncertainties in the *H*/*C* determination for the LOHu sample.

The mild purification procedure of the sequentially alkali-extracted HAs resulted in an expected higher ash content, which ranged from 15 % for HA1 to 27 % for HA6. The results

of a previous study showed that the higher ash contents did not cause differences in the sorption behaviour of pentachlorobenzene on the set of humic acids isolated from the same sediment sample.[14]

Sorption and desorption experiments

All sorption and desorption isotherms were run in duplicate at room temperature in 40 mL glass vials with a screw cap having a Teflon-lined silicon septum covered with aluminium foil. The background solution was 0.01 M $CaCl_2$ in double-distilled water with 200 mg L^{-1} $HgCl_2$ as a biocide. The pH of the background solution was adjusted to 3.90±0.05 for all sorption and desorption experiments, to prevent any potential dissolution of the HAs.[11] The volume of background solution in the sorption and desorption experiments was 35 mL in order to keep the volume of head-space in the vials to a minimal and avoid losses of sorbate during experiments due to volatilisation. The initial volume of background solution in each vial was determined by weighing each vial before and after filling. Lindane (99.8 %) was obtained from Sigma-Aldrich. Due to the low water solubility, before spiking the background solution, stock solutions of lindane were prepared in MeOH. The initial lindane concentrations ranged from 0.030 to 2.7 mg L^{-1}. The volume of lindane stock solution used for background solution spiking was < 0.1 %, which was shown to have no measurable influence on the sorption behaviour of HOCs.[5] The amount of HA and humin samples in each experiment corresponded to a sample/solution ratio that resulted in 20–80 % uptake of lindane. The equilibration period of 24 h was based on a preliminary kinetics experiment performed over 168 h. The solids were separated from the aqueous solutions by centrifugation at 6000 rpm for 20 min. Then, 25 mL of supernatant was removed using a glass pipette and replaced with the same volume of fresh solute-free background solution to start the desorption step by the conventional decant-refill method. The weights of each vial were determined before and after refilling. The vials were further agitated under the same conditions. At the end of the desorption step, the solids were removed by centrifugation under the same conditions and an aliquot of supernatant was withdrawn for lindane determination. Solid-phase solute concentrations before and after desorption were calculated from the mass balance of solute between the solid and aqueous phases.

Supernatants collected after each of the sorption and desorption steps were analyzed after liquid–liquid extraction with hexane, using gas chromatography-electron capture detection (GC/ECD; Agilent Technologies 6890 with ^{63}Ni ECD) on a DB-608 column (J & W Scientific) and quantified according to external standard calibration. Recovery from the liquid–liquid extraction and GC/ECD determination of lindane was 84.9 %, giving an *RSD* of 3.32 % for seven measurements at the 100 μg L^{-1} level. Accordingly, corrections were made for the analytically determined lindane concentrations. To determine the initial concentration of lindane for each isotherm point and to account for lindane losses other than sorption to the sorbent, two control flasks without any sorbent were prepared and treated in the same way. The recoveries of the initial concentrations of lindane from control flasks ranged from 82.5 to 85.2 % and were in the range of recoveries of lindane from solutions without the shaking procedure, indicating no losses of lindane due to processes other than sorption to the sorbents (*e.g.*, volatilisation, degradation).

Data analysis

All sets of equilibrium sorption and desorption data were fitted using the Freundlich model:

$$q_e = K_F c_e^n \quad (1)$$

where q_e and c_e are the solid phase and aqueous phase equilibrium concentrations (in μg g^{-1} and mg L^{-1}, respectively); K_F and the exponent n are the Freundlich sorption capacity coefficient (expressed as (μg g^{-1})/(mg L^{-1})^n) and the site energy heterogeneity factor indicating isotherm nonlinearity (dimensionless), respectively. K_F and n were obtained from direct nonlinear curve fitting of the sorption and desorption data using Origin version 6.1. Statistical analysis was performed using One-Way Analysis of Variance (One-Way ANOVA) at the 0.05 significance level. This analysis is appropriate when making a single test to determine whether two or more populations have the same mean.

Sorption–desorption hysteresis was explored using the Hysteresis Index (*HI*) as proposed by Huang *et al.*[18]:

$$HI = \left.\frac{q_e^d - q_e^s}{q_e^s}\right|_{T,c_e} \quad (2)$$

where q_e^s and q_e^d are the solid-phase solute concentrations for the single cycle sorption and desorption experiments, respectively, and the subscripts T and c_e specify constant temperature and residual aqueous phase concentration, respectively.

RESULTS AND DISCUSSION

Sorption and desorption isotherms

All sorbents exhibited nonlinear isotherms (Figure 1, Table II), meaning that the sorption affinity of the HA fractions and both humin samples decreased as lindane concentration increased. For the HA fractions, n increased in the order of HA1 (0.757) < HA3 (0.806) < HA6 (0.852) < HA9 (0.944), while both humin samples exhibited greater nonlinearity compared to HAs (0.619 for HOHu and 0.638 for LOHu). One-Way ANOVA at the 0.05 significance level was employed to explore whether the obtained variation of n between different samples was statistically significant or not. This analysis was applied separately for HA fractions and humin samples because of their different structural characteristics and sorption behaviour. The statistical analysis was applied to the following pairs of HAs: HA1/HA3, HA3/HA6 and HA6/HA9. The results showed that the variations of the n values were significantly different for all pairs of HAs, as well as for the two humin samples.

The n values for sorption isotherms for HAs increased proportionally with increasing atomic H/C ratio (Fig. 2, open circles), indicating that the isotherm nonlinearity of HAs increased with aromaticity. The same order of nonlinearity was obtained for the n values obtained from the desorption data (Fig. 2, solid circles). The results for lindane sorption are in good agreement with the results obtained for the sorption of pentachlorobenzene,[14] and also with other sorption studies.[8,11,19–22] These studies concluded that HOC sorption in soil is strongly influenced by the aromatic moieties of the SOM. Furthermore, a recent spectroscopic study showed that the condensed domain is mainly attributed to aromatic

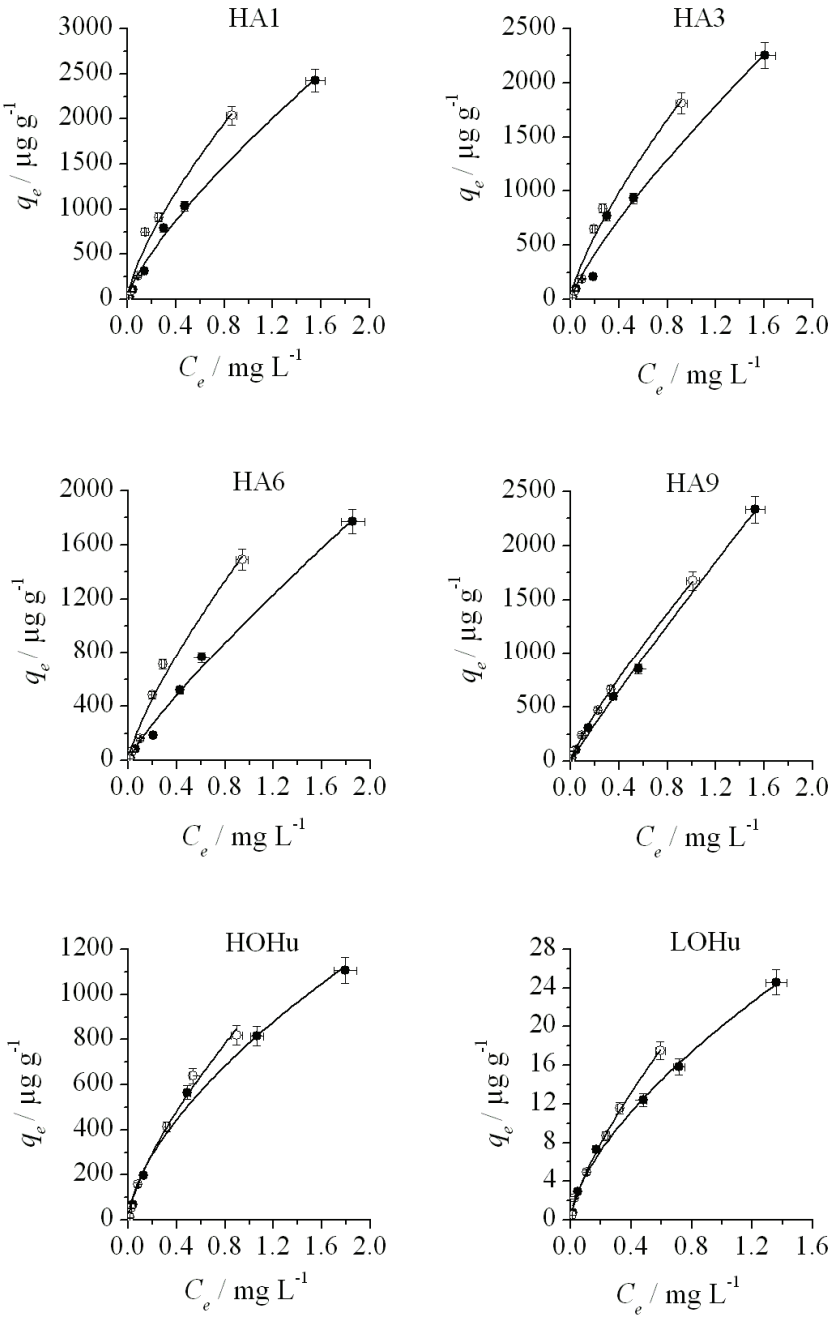

Fig. 1. Sorption and desorption isotherms for lindane by four HA fractions and two humin fractions. Solid line (—) represents the best nonlinear model fit to the Freundlich model. The error bars represent the standard deviation for two measurements.

TABLE II. Freundlich sorption and desorption model parameters and hysteresis indices (*HI*) for four HA fractions and two humin fractions; $K_F OC = K_F/F_{OC}$. $K_{OC} = (q_e/C_e)/F_{OC}$. F_{OC} represents organic carbon fraction

Sample	Process	R^2	n	K_F / (μg/g)/(mg/L)^n	K_FOC	log K_{OC}			*HI*		
						c_e / mg L^{-1}					
						0.05	0.5	5	0.05	0.5	5
HA1	Sorption	0.994	0.757 (±0.004[a])	1752 (±51.2[a])	3941	3.91	3.67	3.43	0.47	0.34	0.23
	Desorption	0.980	0.718 (±0.007)	2293 (±146)	5157	4.08	3.80	3.52			
HA3	Sorption	0.989	0.806 (±0.008)	1548 (±84.6)	3512	3.80	3.60	3.41	0.49	0.32	0.16
	Desorption	0.979	0.752 (±0.008)	1967 (±123)	4462	3.97	3.72	3.48			
HA6	Sorption	0.994	0.852 (±0.005)	1057 (±36.1)	2753	3.63	3.48	3.34	0.89	0.58	0.33
	Desorption	0.982	0.776 (±0.008)	1589 (±90.5)	4139	3.91	3.68	3.46			
HA9	Sorption	0.998	0.944 (±0.003)	1560 (±25.4)	3453	3.61	3.56	3.50	0.47	0.15	–[b]
	Desorption	1.00	0.835 (±0.001)	1658 (±11.7)	3670	3.78	3.61	3.45			
LOHu	Sorption	0.996	0.638 (±0.003)	20.07 (±0.37)	1140	3.53	3.17	2.80	–	0.20	0.50
	Desorption	0.998	0.733 (±0.002)	25.79 (±0.72)	1465	3.51	3.25	2.98			
HOHu	Sorption	0.991	0.619 (±0.005)	784.7 (±25.4)	4192	4.12	3.74	3.36	–	0.10	0.33
	Desorption	0.992	0.699 (±0.005)	915.2 (±35.2)	4889	4.08	3.78	3.48			

[a]Standard deviation; [b]negative value

structures.[23] Therefore, the obtained order of nonlinearity is in line with the degree of condensed character of the organic matter, as suggested by Weber *et al.*,[6,24] who hypothesized that the SOM is comprised of two principal domain types: amorphous (flexible, rubbery-like) and condensed (rigid, glassy-like) domains. The linear and nonlinear sorption behaviours of different SOM domains are attributed respectively to non-specific partitioning in an amorphous domain and to site-specific and capacity-limited adsorption at the surface of a condensed domain. In a previous study, the results of elemental analysis and FTIR characterisation showed that the aliphatic character of HA fractions increased with increasing number of extractions.[14] Consequently, the later-extracted HAs, with relatively higher aliphatic carbon content, should exhibit more linear isotherms than the earlier-extracted ones. Although the number of data points is limited, it is evident that the *n* values for HAs increased proportionally with increasing atomic *H*/*C* ratio, suggesting that sorption becomes more of a partitioning process with increasing aliphaticity. Thus, the obtained order of nonlinearity among HAs supports the role of aromatic moieties in the sorption of HOCs.

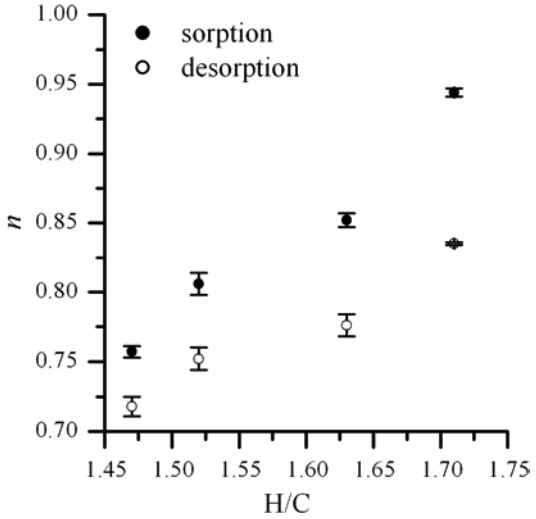

Fig. 2. Relationship between the *n* values for lindane sorption (●) and desorption (○) and atomic *H/C* ratios of four HA fractions and HOHu. The error bars represent the standard deviation for two measurements.

Although both the elemental data and FTIR analysis showed an increased content of amorphous aliphatic domains in HOHu, this sample, as well as LOHu, exhibited greater nonlinearity than the HAs (Table II). Considering the significantly higher mineral phase content in these samples compared to the HAs (LOHu 92.5 %, HOHu 65.4 %), it might be that the mineral matter plays an important indirect role in HOCs sorption in these samples. This is in line with the mechanism suggested by Gunasekara and Xing,[25] who proposed that in the interaction of the crystalline–amorphous complex with mineral surfaces, the first few

molecular layers of the amorphous aliphatic region rearrange to a more condensed form, which enhances nonlinear sorption. However, the higher content of mineral matter in LOHu (92.5 %, n = 0.638) did not cause greater nonlinearity in comparison with HOHu (65.4 %, n = 0.619), implying that other factors might affect the sorption behaviour of the humin samples, *e.g.*, the presence of small amounts of carbonaceous materials. The presence of high-surface area carbonaceous materials in sediments and soils cause nonlinearity of the isotherms due to physical adsorption into the microporous domains, especially at low concentrations.[26,27]

The organic carbon-normalized sorption coefficient (K_FOC) ranged from 1140 for LOHu to 4192 for HOHu, while K_FOC values for HAs varied from 2753 for HA6 to 3941 for HA1 (Table II). However, a direct comparison of the K_FOC values could not be made because of their different units as a result of the nonlinearity of the sorption isotherms obtained for all sorbents. To enable a direct comparison of the sorption affinities among the HA fractions and humin samples, organic carbon-normalized single point distribution coefficients (K_{oc}) at three selected concentrations (c_e = 0.05, 0.5 and 5 mg L^{-1}) were calculated. This was realized by calculating the q_e values corresponding to these three c_e values from the respective best fit Freundlich isotherms, the parameters for which are given in Table II. Lindane sorption (K_{oc}) decreased from HA1 to HA6 at each c_e, showing a slightly increase for HA9, except in the low concentration range. Humic acid fraction HA9 was isolated from the sediment by NaOH extraction, which could have caused alkaline oxidation and slightly different sorption behaviour compared to $Na_4P_2O_7$ isolates.[28] The highest K_{oc} values were obtained for the humin sample HOHu, while the organic matter in the low-organic carbon humin, LOHu, showed the lowest affinity towards lindane.

In the present study, the atomic *H*/*C* ratios correlated with the sorption affinity of lindane, showing a positive trend between aromaticity of the HAs and log K_{oc} (Fig. 3), thus supporting the role of aromatic moieties in HOC sorption. Due to uncertainties linked to the *H*/*C* determination for LOHu, this sample was excluded from the correlation. It can be noticed that the changes of log K_{oc} with changes in the atomic *H*/*C* ratio were especially pronounced in the range of low equilibrium concentrations, which could be expected because the overall sorption under these conditions was dominated by an adsorption mechanism. With increasing equilibrium concentrations, the sorption mechanism shifted towards the distribution and, at concentrations close to solubility of lindane, it became the dominant mechanism in the overall sorption. These results are in line with the observations of several researchers who found a significant positive correlation between the sorption affinity of polycyclic aromatic hydrocarbons and aromaticity.[8,22,29–31] However, the results of a previous study of the sorption of pentachlorobenzene onto a set of HAs isolated from the same sediment sample showed

that the sorption affinity correlated positively with aliphaticity, indicating that the non-polar poly(methylene) domains in the SOM were appropriate sorption domains for the more hydrophobic compound pentachlorobenzene.[14] These results suggest that the properties of both the SOM and the HOCs have to be taken into consideration when explaining the sorption behaviour of HOCs onto the SOM.

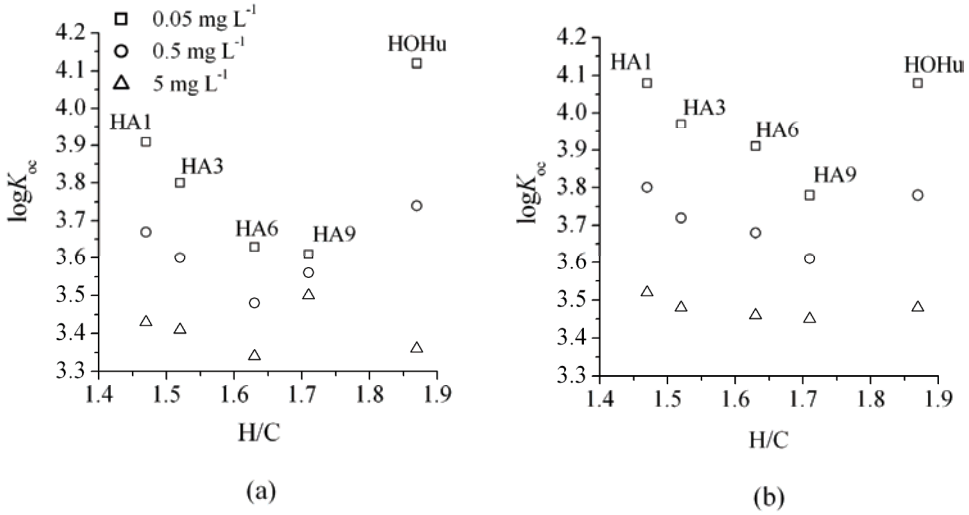

Fig. 3. Relationship between log K_{oc} values for lindane sorption (a) and desorption (b), and the atomic *H/C* ratiosof four HA fractions and HOHu.

Humin has been reported to be an important sink for organic contaminants.[32,33] This was supported by the present study, which showed higher K_{OC} values for HOHu than for HAs (Fig. 3). The increased capacities of humin samples for HOCs could be explained by special physical properties of humin caused by the increased contents of mineral matter. Although mineral surfaces do not contribute to HOC sorption directly, their interaction with organic matter may play an indirect role in the sorption behaviour of humins.[25,34] In addition, the removal of smaller organic fractions could decreased the surface roughness and increased the surface area and porosity of the humin, exposing additional binding sites on its surface.[35] These reports, and the data presented here, demonstrate the increased affinity of HOCs for humin and suggest that the sorption process may be strongly influenced by the changes in the physical conformation of the organic matter, making it more accessible for participation in the sorption.

Sorption–desorption hysteresis

Sorption reversibility provides an additional insight into the sorption mechanisms, as well as structural properties of the sorbent governing the specific sorptive behaviour of the sorbate.

The apparent sorption–desorption hysteresis was quantified for each of the sorption and desorption isotherms using the hysteresis index (*HI*) (Eq. (2)). Hysteresis indices at three concentration levels, c_e = 0.05, 0.5 and 5 mg L^{-1}, were calculated for each sorbent using the sorption and desorption parameters of the Freundlich model. The calculated *HI* values are included in Table II. Sorption––desorption hysteresis exists if *HI* has a positive value and is more pronounced as the value of *HI* increases.

The most significant hysteresis for all HAs was observed at low sorbate concentration, while the desorption increased with increasing lindane loading resulting in lower *HI* values at high sorbate concentration. At high solute concentrations, the sorbed lindane molecules were more readily desorbed compared to molecules sorbed at lower concentrations. It is proposed that at low solute concentrations, sorption sites within the condensed domain are occupied more readily than the sorption sites within the amorphous aliphatic domains, causing a greater extent of sorption–desorption hysteresis in the low concentration range. This mechanism cannot explain the desorption from the two aliphatic-rich humin samples, where the opposite trend was observed: lindane molecules were readily desorbed at low sorbate concentrations, while desorption decreased with increasing lindane loading, resulting in an increase in the *HI* values at high sorbate concentration. It is assumed that at high solute concentrations, the sorbed molecules are forced by a concentration gradient to partition in the amorphous aliphatic domains, causing the increased hysteresis.

In addition, lindane exhibited pronounced desorption hysteresis for three HA fractions, which was significantly greater than for the humin samples and HA9. This is suggested to be caused by a more condensed structure of the SOM in the former samples attributed to aromatic domains.

It is interesting to note that the humin samples, despite exhibiting the most nonlinear sorption isotherms, showed a desorption hysteresis for lindane that was less pronounced than expected based on the results found in the literature.[36] Similar observations on nonlinear sorption and low desorption hysteresis were observed by Ran *et al*.[37] for phenathrene with peat. This observation suggests that the nonlinear sorption obtained with the humin samples does not necessarily result from a hole-filling mechanism, especially in the lower concentration ranges, and could result from a surface interaction. The surface-sorbed molecules probably desorb more readily. However, as the lindane concentration increases, the increased concentration gradient will cause molecules to penetrate deeper into the SOM matrix generating “tenant” pores in which they then reside,[38] resulting in increased hysteresis.

CONCLUSIONS

Sorption/desorption behaviour should be seriously considered as an essential tool in evaluating compound behaviour in sediment risk assessment analysis. Positive correlations of log K_{OC} values at three lindane concentrations and the *H*/*C* ratio in HAs extracted from a single sediment sample, a positive correlation between *n* values and aromatic carbon and greater sorption–desorption hysteresis for three HA fractions compared to humin samples were found, indicating the dominance of aromatic domains in sorption nonlinearity, sorption affinity and irreversibility of lindane sorption on SOM. The above results will help to understand the sorption behaviour of lindane in SOM and provide a theoretical basis for risk assessment and remediation of contaminated sediments.

Aknowledgments. This research was supported under the funding scheme of the Ministry of Education, Science and Technological Development of the Republic of Serbia (Project Nos. III43005 and TR37004).

И З В О Д

СТРУКТУРНЕ ОБЛАСТИ ОРГАНСКЕ МАТЕРИЈЕ СЕДИМЕНТА КОЈЕ УТИЧУ НА СОРПЦИОНО И ДЕСОРПЦИОНО ПОНАШАЊЕ ЛИНДАНА

ЈЕЛЕНА С. ТРИЧКОВИЋ[1], ИВАНА И. ИВАНЧЕВ-ТУМБАС[1], МАРИЈАНА М. КРАГУЉ[1], МИЉАНА Ђ. ПРИЦА[2], ДЕЈАН М. КРЧМАР[1], АЛЕКСАНДАР Д. НИКОЛИЋ[1] и БОЖО Д. ДАЛМАЦИЈА[1]

[1] Универзитет у Новом Саду, Природно-математички факултет, Департман за хемију, биохемију и заштиту животне средине, Трг Доситеја Обрадовића 3, 21000 Нови Сад и [2] Универзитет у Новом Саду, Факултет техничких наука, Трг Доситеја Обрадовића 6, 21000 Нови Сад

У раду је испитивано сорпционо и десорционо понашање линдана на четири хуминске киселине (ХК) и два хумина секвенцијално екстрахованих из седимента језера Лудаш. Све сорпционе изотерме, фитоване према Фројндлиховом моделу, су биле нелинеарне. Линеарност изотерми је расла од 0,757 за прву екстраховану ХК до 0,944 за девету ХК показујући позитивну корелацију са H/C атомским односом, док је између коефицијента сорпције и алифатичности изолованих ХК уочена негативна корелација. Показано је да сорпциони процес може бити снажно условљен физичком конформацијом и доступношћу органске материје седимента (СОМ) на шта указују високе K_{OC} и ниске *n* вредности добијене за узорке хумина. Упркос томе што су узорци хумина дали сорпционе изотерме највеће нелинеарности, они нису показали изражену сорпционо–десорпциону хистерезу, док је најизраженија хистереза уочена за три узорка ХК. Ови резултати подржавају претпоставку да ароматичне области СОМ снажно утичу на сорпционо и десорпционо понашање линдана. Наша запажања могу бити корисна за разумевање расподеле, транспорта и судбине линдана у земљиштима и седиментима.

(Примљено 6. јула, ревидирано 8.октобра 2012)

REFERENCES

1. J. J. Pignatello, B. Xing, *Environ. Sci. Technol.* **30** (1996) 1
2. J. J. Pignatello, *Adv. Colloid Interface Sci.* **76/77** (1998) 445
3. M. Haitzer, S. Höss, W. Traunspurger, C. Steinberg, *Aquat. Toxicol.* **45** (1999) 147
4. M. A. Schlautman, J. J. Morgan, *Environ. Sci. Technol.* **27** (1993) 961

5. W. J. Weber Jr., W. Huang, *Environ. Sci. Technol.* **30** (1996) 881
6. W. J. Weber Jr., P. M. McGinley, L. E. Katz, *Environ. Sci. Technol.* **26** (1992) 1955
7. B. Xing, J. J. Pignatello, *Environ. Sci. Technol.* **31** (1997) 792
8. V. Perminova, N. Y. Grechishcheva, D. V. Kovalevskii, A. V. Kudryavtsev, V. S. Petrosyan, D. N. Matorin, *Environ. Sci. Technol.* **35** (2001) 3841
9. J. D. Mao, L. S. Hundal, M. L. Thompson, K. Schmidt-Rohr, *Environ. Sci. Technol.* **36** (2002) 929
10. J. M. Simpson, B. Chefetz, P. G. Hatcher, *J. Environ. Qual.* **32** (2003) 1750
11. S. Kang, B. Xing, *Environ. Sci. Technol.* **39** (2005) 134
12. J. Zhang, M. He, Y. Shi, *J. Hazard. Mater.* **166** (2009) 802
13. J. Hur, D.-H. Lee, H.-S. Shin, *Org. Geochem.* **40** (2009) 1091
14. J. Tričković, I. Ivančev-Tumbas, B. Dalmacija, A. Nikolić, S. Trifunović, *Org. Geochem.* **38** (2007) 1757
15. Y. F. Li, *Sci. Total Environ.* **232** (1999) 121
16. M. Ricking, J. Schwarzbauer, *Environ. Chem. Lett.* **6** (2008) 83
17. M. Thomsen, P. Lassen, S. Dobel, P. E. Hansen, L. Carlsen, B. B. Mogensenm, *Chemosphere* **49** (2002) 1327
18. W. Huang, H. Yu, W. J. Weber Jr., *J. Contam. Hydrol.* **31** (1998) 129
19. J. Zhang, M. He, *J. Colloid Interface Sci.* **337** (2009) 338
20. M. J. Salloum, B. Chefetz, P. G. Hatcher, *Environ. Sci. Technol.* **36** (2002) 1953
21. B. Xing, *Environ. Pollut.* **111** (2001) 303
22. Y.-P. Chin, G. R. Aiken, K. M. Danielsen, *Environ. Sci. Technol.* **31** (1997) 1630
23. M. D. Johnson, W. Huang, W. J. Weber Jr., *Environ. Sci. Technol.* **35** (2001) 1680
24. W. J. Weber Jr., W. Huang, E. J. Le Boeuf, *Colloids Surf., A* **151** (1999) 167
25. S. Gunasekara, B. Xing, *J. Environ. Qual.* **32** (2003) 240
26. R. M. Allen-King, P. Grathwohl, W. P. Ball, *Adv. Water Resour.* **25** (2002) 985
27. G. Cornelissen, O. Gustafsson, T. D. Bucheli, M. T. O. Jonker, A. A. Koelmans, P. C. M. Van Noort, *Environ. Sci. Technol.* **39** (2005) 6881
28. L. S. K. Pang, A. M. Vassallo, M. A. Wilson, *Org. Geochem.* **16** (1990) 853
29. T. D. Gauthier, W. R. Seitz, C. L. Grant, *Environ. Sci. Technol.* **21** (1987) 243
30. J. Kukkonen, A. Oikari, *Water Res.* **25** (1991) 455
31. V. Perminova, N. Y. Grechishcheva, V. S. Petrosyan, *Environ. Sci. Technol.* **33** (1999) 3781
32. E. A. Guthrie, F. K. Pfaender, *Environ. Sci. Technol.* **32** (1998) 501
33. K. Nam, J. Y. Kim, *Environ. Pollut.* **118** (2002) 427
34. M. J. Salloum, M. J. Dudas, W. B. McGill, *Org. Geochem.* **32** (2001) 709
35. K. Malekani, J. A. Rice, J.-S. Lin, *J. Soil Sci.* **162** (1997) 333
36. B. Pan, B. S. Xing, W. X. Liu, S. Tao, X. M. Lin, X. M. Zhang, Y. X. Zhang, Y. Xiao, H. C. Dai, H. S. Yuan, *Environ. Pollut.* **143** (2006) 24
37. Y. Ran, W. Huang, P. S. C. Rao, D. Liu, G. Sheng, J. Fu, *J. Environ. Qual.* **31** (2002) 1953
38. W. Huang, W. J. Weber Jr., *Environ. Sci. Technol.* **32** (1998) 3549.

Journal of the Serbian Chemical Society
JSCS-info@shd.org.rs • www.shd.org.rs/JSCS
J. Serb. Chem. Soc. 78 (6) 897–905 (2013)
JSCS–4467
UDC 547.972.1+544.526.5+542.92+544.526.5+546.47'221.1
Original scientific paper

Photocatalytic degradation of Rose Bengal using semiconducting zinc sulphide as the photocatalyst

SHWETA SHARMA[1], RAKSHIT AMETA[2], R. K. MALKANI[1] and SURESH C. AMETA[2]*

[1]*Department of Chemistry, M. L. Sukhadia University, Udaipur-313002 (Rajasthan), India and* [2]*Department of Chemistry, Pacific College of Basic & Applied Sciences, PAHER University, Udaipur-313001 (Rajasthan), India*

(Received 16 July, revised 6 December 2012)

Abstract: Various semiconductors have been used as photocatalysts for the removal of different dyes from their aqueous solutions. Zinc sulphide semiconductor was used in the present investigation as a photocatalyst for the removal of Rose Bengal dye. Effect of different parameters that affect the rate of reaction, such as pH, concentration of dye, amount of semiconductor and light intensity were studied. A mechanism is proposed in which hydroxyl radicals are shown as the active oxidizing species.

Keywords: semiconductor; photocatalyst; Rose Bengal; zinc sulphide; hydroxyl radical.

INTRODUCTION

Today the entire world is facing a major problem of water pollution, which is caused in different manners. Dyes from different textile, dyeing and printing industries are one type of pollutant as these industries discharge their effluent into near-by natural water resources without any treatment. Many researchers have developed different methods to overcome this problem. Photochemistry may play an important role in solving this problem. Its different methods are now proven green and benign in nature. Various semiconductors have been used as photocatalysts for the removal of different dyes from their aqueous solutions. Photocatalytic and oxidative degradation of wastewater pollutants in the presence of TiO_2 was observed by Das *et al.*[1] It was observed that certain organic molecules adsorbed on TiO_2 could be reduced with the concomitant oxidation of water. The photoreduction of CO_2 and water into formaldehyde and methanol in aqueous suspensions of $SrTiO_3$ and TiO_2 was investigated by Blajeni *et al.*[2] Photocatalytic degradation of an H-acid over a novel TiO_2 thin film fixed in a

* Corresponding author. E-mails: ameta_sc@yahoo.com; rakshit_ameta@yahoo.in
doi: 10.2298/JSC120716141S

reactor was studied by Noorjahan *et al.*[3] Ameta *et al.*[4] performed the photo-degradation of Naphthol Green B in the presence of semiconducting antimony trisulphide. The photo-oxidation of oxalate ions in aqueous dispersion of ZnO under UV illumination was investigated by Domenech and Costa[5] in order to determine the efficiency of oxalate ions as hole scavengers. Mansilla and Villas-nov[6] investigated the ZnO-catalysed photodegradation of Kraft-black liquor, which is an effluent from the pulp and paper industries. Platinum impregnated ZnO yielded 100 % decolourisation after 60 min.

ZnS was used for the photoreduction of carbon dioxide by Kanemoto *et al.*[7] Anpo *et al.*[8] gave direct evidence for the participation of extrinsic surface sites in the enhancement of the photocatalytic activity of luminescent ZnS catalyst. Boarh *et al.*[9] studied the structural and optical properties of ZnS nanoparticles, while Hu *et al.*[10] studied the mass production and high photocatalytic activity of ZnS nanoporous nanoparticles. ZnS–montmorillonite nanocomposites were used for the degradation of Eosin B by Miao *et al.*[11]

The photocatalytic activity of antimony(III) sulphide in the bleaching of Azure-B was studied by Ameta *et al.*[12] Rufus *et al.*[13] observed the decomposition of aqueous sulphide in presence of CdS with iridium sulphide and platinum sulphate as photocatalysts. Borgarello *et al.*[14] observed the oxidation of H_2S to sulphur at CdS semiconductor surface while the photocatalytic oxidation of propan-2-ol over a zeolite composite and CdS was carried out by Green and Rud-ham.[15] Kinetic monitoring of the photocatalytic degradation of amaranth by semiconducting ammonium phosphomolybdate was realized by Bansal *et al.*[16] The photocatalytic oxidation of benzydrol over CdS was investigated by Gu *et al.*[17] Chittora *et al.*[18] studied the photoreduction of CO_2 in presence of some photocatalyst such ZnO, Fe_2O_3, *etc*. Darwent and Mills[19] observed the photo-oxidation of water sensitized by WO_3 powder. The bleaching products of Rose Bengal under reducing condition was studied by Zakrzewski *et al.*[20] On the other hand, Sharma *et al.*[21] used semi-conducting bismuth sulphide as a photocatalyst for degradation of Rose Bengal.

EXPERIMENTAL

A 1.0×10^{-3} M solution of Rose Bengal was prepared as a stock solution, which was diluted further as and when required. The optical density of the Rose Bengal solution was determined using a spectrophotometer (Systronics model 106) at λ_{max} = 550 nm.

Zinc sulphide (Reidel), 8.0 μm with a band gap is 3.5 eV, was used as a photocatalyst in the present investigation. Its dispersion was quite stable during illumination, the ZnS powder neither degrading nor dissolving under the employed experimental conditions.

First, the feasibility of using the semiconductor zinc sulphide as a photocatalyst was confirmed. Thus, four sample solutions were made. using 50 mL of 1.20×10^{-5} M Rose Bengal in four beaker.s The first and second solutions contained only Rose Bengal; the first solution was kept in the dark while the second was exposed to light. The third and fourth samples

contained in addition to Rose Bengal, 0.10 g zinc sulphide; the third sample was kept in dark, while the fourth was exposed to light.

After 4 h, the optical densities of the four solutions were measured using a spectrophotometer. It was found that the optical densities of solutions 1–3 remained almost constant, while that of the fourth solution had decreased from its initial value. From these observations, it was clear that this reaction requires presence of both light and zinc sulphide, *i.e.*, it was a photocatalytic reaction.

A solution of 1.20×10^{-5} M of R. Bengal was prepared in doubly distilled water and 0.10 g of zinc sulphide was added to it. The pH of the reaction mixture was adjusted to 8.5 with previously standardized sodium hydroxide and sulphuric acid solutions. Then the solution was exposed to a 200 W tungsten lamp. An aliquot of 2.0 mL was taken out from the reaction mixture and its optical density was observed at 550 nm at regular time intervals.

It was observed that the optical density of R. Bengal solution decreased with increasing time of exposure and that the degradation of R. Bengal was almost completed after 8 h of illumination. This was confirmed experimentally in additional experiments.

A plot of log *OD* against time was found to be linear. The rate constant was determined as $k = 2.303\times$slope). A typical run is presented in Table I.

TABLE I. A typical run; [Rose Bengal] = 1.20×10^{-5} M, m(ZnS) = 0.10 g, light intensity = = 70.0 mW cm^{-2}, pH 8.5. Rate constant, $k = 4.51\times10^{-5}$ s^{-1}

Time, min	Optical density (*OD*)	1 + log *OD*
0.0	0.361	0.5575
15.0	0.345	0.5378
30.0	0.335	0.5250
45.0	0.322	0.5078
60.0	0.304	0.4829
75.0	0.288	0.4594
90.0	0.282	0.4502
105.0	0.266	0.4249
120.0	0.258	0.4116
135.0	0.250	0.3979
150.0	0.237	0.3747
165.0	0.230	0.3617
180.0	0.220	0.3424

RESULTS AND DISCUSSION

In the present investigation, four rate affecting factors. *i.e.*, pH, concentration of dye, amount of semiconductor and light intensity were studied.

Effect of pH

The pH of the solution is likely to affect the degradation of Rose Bengal and hence, the effect of pH on the rate of degradation of Rose Bengal was investigated in the pH range 5.0–10.0, as the degradation was found to be reasonably fast in this range. The results are reported in Table II.

It is evident from these data that the rate of photocatalytic degradation of Rose Bengal increased with increasing pH. The increase in the rate of photoca-

talytic degradation may be due to greater availability of OH^- at higher pH values. The OH^- will generate more OH radicals by combining with the photogenerated holes in the semiconductor and these hydroxyl radicals are considered responsible for this photocatalytic degradation.

TABLE II. Effect of pH; [Rose Bengal] = 1.20×10^{-5} M, *m*(ZnS) = 0.10 g, light intensity = = 70.0 mW cm^{-2}

pH	$k\times10^5$ / s^{-1}
5.0	2.57
5.5	2.85
6.0	3.16
6.5	3.41
7.0	3.78
7.5	4.00
8.0	4.26
8.5	4.51
9.0	4.16
9.5	3.89
10.0	3.54

However, after a certain pH value, *i.e.*, 8.5, a further increase in pH of the medium decreased the rate of photocatalytic degradation. This may be due to the fact that Rose Bengal does not remain in its cationic form because of the larger concentration of OH^- and, as such, the force of attraction between the dye and negatively charged semiconductor surface decreases. As a consequence, the reaction rate decreases. It means that for an efficient photocatalytic degradation of Rose Bengal, it should remain either in its neutral form or partially in cationic form.

Alkaline conditions provide more OH^- and, as a consequence, more hydroxyl radicals were generated and therefore the reaction proceeded more smoothly in alkaline medium. Moreover, the formation of hydroxyl radicals may be efficient on the surface of metal oxides or sulphides.

Effect of dye concentration

Effect of variation of dye concentration was studied by taking different concentrations of Rose Bengal. The results are tabulated in Table III.

It was observed that the rate of photocatalytic degradation first increased with increasing concentration of Rose Bengal. This may be due to the fact that as the concentration of Rose Bengal was increased, more dye molecules were available for excitation and energy transfer and hence, an increase in the rate was observed. However, on further increase in the dye concentration, the rate of photocatalytic degradation decreased. This may be attributed to the fact that the dye started acting as a filter for the incident light that did not permit the desired light

intensity to reach the semiconductor particles; thus, the rate of photocatalytic degradation of Rose Bengal decreased.

TABLE III. Effect of Rose Bengal concentration; light intensity = 70.0 mW cm^{-2}, *m*(ZnS) = = 0.10 g, pH 8.5

[Rose Bengal]×10^5 M	$k \times 10^5$ / s^{-1}
0.4	2.20
0.6	2.78
0.8	3.29
1.0	4.02
1.2	4.51
1.4	4.22
1.6	3.97
1.8	3.66
2.0	3.28

Effect of amount of semiconductor

The amount of semiconductor is also likely to affect the process of dye degradation and hence, different amounts of photocatalyst were used. The results are reported in Table IV.

TABLE IV. Effect of amount of semiconductor; [Rose Bengal] = 1.20×10^{-5} M, pH 8.5, light intensity = 70.0 mW cm^{-2}

Zinc sulphide amount, g	$k \times 10^5$ / s^{-1}
0.02	2.44
0.04	2.81
0.06	3.20
0.08	3.84
0.10	4.51
0.12	4.52
0.14	4.51
0.16	4.50

It has been observed that the rate of photodegradation of Rose Bengal initially increased with increasing amount of semiconductor but ultimately, it becomes almost constant after a certain amount. This may be attributed to the fact that as the amount of semiconductor was increased, the amount of exposed surface area also increases, but after a certain limit, *i.e.*, 0.10 g, if the amount of semiconductor was further increased, there would be no increase in the exposed surface area of the photocatalyst. This may be considered like a saturation point; above which, any increase in the amount of semiconductor had negligible or no effect on the rate of photocatalytic degradation of Rose Bengal, as any increase in the amount of semiconductor after this saturation point would only increase the thickness of the layer at the bottom of the reaction vessel. This was confirmed by

taking reaction vessels of different dimensions. The saturation point shifted to higher range for larger vessels, while the reverse was true for smaller vessels.

Effect of light intensity

To investigate the effect of light intensity on the photocatalytic degradation of Rose Bengal, the distance between the light source and the exposed surface area was varied. The intensity of light at each distance was measured by Suryamapi (CEL Model SM201). The results are summarized in Table V.

TABLE V. Effect of light intensity; [Rose Bengal] = 1.20×10^{-5} M, m(ZnS) = 0.08 g, pH 8.5

Intensity of light, mW cm^{-2}	$k\times10^5$ / s^{-1}
10.0	1.12
20.0	1.76
30.0	2.50
40.0	3.11
50.0	3.62
60.0	4.05
70.0	4.51
80.0	4.06

The results indicate that degradation of Rose Bengal was accelerated as the intensity of light was increased, because any increase in the light intensity will increase the number of photons striking per unit area of semiconductor powder. An almost linear behaviour between light intensity and rate of reaction was observed. However, on increasing the intensity above 70.0 mW cm^{-2}, there was a decrease in the rate. This may be due to some side reactions.

The effect of different parameters on rate constant was studied and it was observed that it was changed from 4.51×10^{-5} to 2.57×10^{-5} s^{-1} (in case of pH), to 2.20×10^{-5} (in case of dye concentration), to 2.44×10^{-5} s^{-1} (in case of amount of semiconductor) and to 1.12×10^{-5} s^{-1} (in case of light intensity). *i.e.*, by 1.75; 2.05; 1.85 and 4.02 times, respectively, that is approximately 100–200 % increases. This amount of change is significant as far as the rate is concerned.

Mechanism

Based on these observations, a tentative mechanism for the photocatalytic degradation of Rose Bengal (RB) is proposed:

$$^1RB_o \xrightarrow{h\nu} {}^1RB_1 \quad (1)$$

$$^1RB_1 \xrightarrow{ISC} {}^3RB_1 \quad (2)$$

$$SC \xrightarrow{h\nu} e^-(CB)+h^+(VB) \quad (3)$$

$$h^+ + OH^- \longrightarrow {}^\bullet OH \quad (4)$$

$$^3RB_1 + {}^\bullet OH \longrightarrow \text{Leuco RB} \quad (5)$$

$$\text{Leuco RB} \longrightarrow \text{Products} \quad (6)$$

A molecule of Rose Bengal absorbs radiations of a suitable wavelength giving gives rise to its excited singlet state, which then undergoes intersystem crossing (ISC) to give the triplet state of the dye. On the other hand, the semiconducting zinc sulphide (SC) also utilizes the radiant energy to excite its electron from the valence band to the conduction band; thus, leaving behind a hole. This hole abstracts an electron from OH^- to generate OH radicals. These radicals oxidize the dye to its leuco form, which may ultimately degrade to harmless products.

The proposed mechanism involves the oxidation of Rose Bengal to smaller fragments involving hydroxyl radicals which was confirmed by using a hydroxyl radical scavenger. *i.e.*, 2-propanol, when the rate of degradation was drastically reduced in presence of the scavenger. Secondly, the degradation of Rose Bengal to less toxic or harmless products is a green chemical approach to waste water treatment (Advanced Oxidation Processes).

CONCLUSION

Photocatalytic degradation of Rose Bengal was performed in the presence of the semiconductor zinc sulphide. The degradation rate increased with increasing pH because more hydroxyl ions were present (generating more hydroxyl radicals). It attains maximum rate at pH 8.5; a further increase in pH above 8.5 results in a decrease in the rate of the reaction, because of decreasing attraction between the neutral form of the dye and the negatively charged semiconductor surface. Increasing the concentration of Rose Bengal also increased the rate up to a certain value due to the increase in the number of dye molecules, but it shows a declining behaviour on further increase of the concentration of dye. This decrease may be attributed to the fact that at higher concentration, the dye may acts as an internal filter for the incident radiations, which decreases the intensity of the incident radiation on the semiconductor particles.

The results indicate that initially the rate increases with increasing amount of semiconductor but after 0.10 g, the rate becomes virtually constant (saturation behaviour). This may be due to the complete coverage of the bottom of the reaction vessel by the semiconductor. Any further increase will not add to an increase in the exposed surface area but only increases the thickness of the layer. An increase in the light intensity will increase the number of photons striking semiconductor zinc sulphide powder per unit area per second and as a consequence, the reaction rate increases almost linearly with the increase in light intensity. The optimum reaction conditions were obtained as: pH = 8.5; [Rose Bengal] = = 1.20×10^{-5} M; ZnS = 0.10 g; light intensity = 70.0 mW cm^{-2}.

Scavengers trap the active species by reducing their activity in the solution and as a result reaction rate becomes quite low or reaction almost stops. Here, the participation of $^{\bullet}OH$ as an active oxidizing species was confirmed by using 1 mL of M/10 2-propanol, which is a specific scavenger of $^{\bullet}OH$. It was observed that the rate of dye degradation was reduced drastically from 4.51×10^{-5} to 2.05×10^{-7} s^{-1}.

И З В О Д

ФОТОКАТАЛИТИЧКА РАЗГРАДЊА БОЈЕ *ROSE BENGAL* ПОМОЋУ ПОЛУПРОВОДНОГ ЦИНК ОКСИДА КАО ФОТОКАТАЛИЗАТОРА

SHWETA SHARMA[1], RAKSHIT AMETA[2], R. K. MALKANI[1] и SURESH C. AMETA[2]

[1]*Department of Chemistry, M. L. Sukhadia University, Udaipur-313002 (Rajasthan), India* и [2]*Department of Chemistry, Pacific College of Basic & Applied Sciences, PAHER University, Udaipur-313001 (Rajasthan), India*

Различити полупроводници се користе као фотокатализатори у поступцима уклањања боја из водених раствора. Плупроводни цинк-оксид је у овом истраживању коришћен као фотокатализатор за процес разградње боје *Rose Bengal*. Анализирани су утицаји различитих параметара који могу утицати на брзину реакциије, као што су pH, концентрација боје, количина фотокатализатора и интензитет светла. Предложен је механизам реакције, који показује да је хидроксилни радикал активна оксидујућа врста.

(Примљено 16. јула, ревидирано 6. децембра 2012)

REFERENCES

1. S. Das, M. Munner, K. R. G. Das, *J. Photochem. Photobiol.*, *A* **77** (1994) 83
2. B. A. Blajeni, M. Halmann, J. Mannasen, *Sol. Energy* **25** (1980) 165
3. M. Noorjahan, M. P. Reddy, V. D. Kumari, B. Levendrine, P. Boule, M. Subrahmanyam, *J. Photochem. Photobiol.*, *A* **156** (2003) 179
4. R. Ameta, P. B. Punjabi, S. C. Ameta, *J. Serb. Chem. Soc.* **76** (2011) 1049
5. J. Domenech, J. M. Costa, *J. Photochem. Photobiol.* **44** (1986) 675
6. H. D. Mansilla, J. Villasnov, *J. Photochem. Photobiol.*, *A* **78** (1994) 267
7. K. Kanemoto, J. Shiragoni, C. Pac, S. Yanagida, *J. Phys. Chem.* **96** (1992) 3521
8. M. Anpo, A. Malsumoto, S. Kodama, *J. Chem. Soc., Chem. Commun.* (1987) 1038
9. J. P. Borah, J. Barman, K. C. Sarma, *Chalcogenide Lett.* **5** (2008) 201
10. J. S. Hu, L. L. Ren, Y. G. Guo, H. P. Liang, A. M. Cao, L. J. Wan, C. L. Bai, *Angew. Chem. Int. Ed.* **44** (2005) 1269
11. S. Miao, Z. Li, B. Han, H. Yang, Z. Miao, Z. Sun, *J. Colloid Interface Sci.* **201** (2006) 116
12. R. Ameta, A. Pandey, P. B. Punjabi, S. C. Ameta, *Chem. Environ. Res.* **14** (2005) 255
13. I. B. Rufus, B. Viswanathan, V. Ramakrishnan, J. C. Kuriacose, *J. Phys. Chem.* **99** (1995) 1540
14. F. Borgarello, K. Kalyansundaram, M. Gratzel, E. Pelizzetti, *Helv. Chim. Acta* **65** (1982) 243
15. K. G. Green, R. Rudham, *J. Chem. Soc.* **89** (1993) 1867
16. A. Bansal, D. Sharma, R. Ameta, H. S. Sharma, *Malaysian J. Chem.* **13** (2011) 18
17. K. J. Gu, Y. Cao, B. W. Zhang, *Acta. Chim. Sinica* **47** (1989) 668

18. A. K. Chittora, B. Sharma, M. Bala, S. C. Ameta, *Natl. Conv. Solar Energy, Udaipur (India)* (1990) 169
19. J. R. Darwent, A. Mills, *J. Chem. Soc., Faraday Trans.* **78** (1982) 359
20. A. Zakrzewski, D. C. Neckers, *Tetrahedron* **43** (1987) 4507
21. S. Sharma, R. Ameta, R. K. Malkani, S. C. Ameta, *Maced. J. Chem. Chem. Eng.* **30** (2011) 229.

Journal of the Serbian Chemical Society
JSCS-info@shd.org.rs • www.shd.org.rs/JSCS

J. Serb. Chem. Soc. 78 (6) 907 (2013)

Erratum (printed version only)

Issue No. 5 (2013), Vol. 78, paper No. *JSCS-4442*:

– page 611, line 6 from above should read:

(Received 20 May, revised 8 July 2012)